Dissertation

submitted to the
Combined Faculties for the Natural Sciences and for Mathematics
of the Ruperto–Carola University of Heidelberg, Germany
for the degree of
Doctor of Natural Sciences

presented by

Dipl.-Phys. Jens Braun

born in Tübingen, Germany

Oral examination: December 18, 2006

Functional Renormalization Group Methods in Quantum Chromodynamics

Referees: Prof. Dr. Hans-Jürgen Pirner
Dr. habil. Holger Gies

Funktionale Renormierungsgruppenmethoden in der Quantenchromodynamik

Zusammenfassung

Wir wenden funktionale Renormierungsgruppenmethoden auf die Quantenchromodynamik (QCD) an. Zunächst berechnen wir die Massenänderung des Pions in einem endlichen Volumen mit Hilfe des Quark-Meson-Modells. Dabei untersuchen wir insbesondere die Bedeutung von Quarkeffekten. Im Einklang mit Gitter-QCD Rechnungen finden wir, daß die Wahl der Randbedingungen für die Quarkfelder einen wesentlichen Einfluß hat. Ein Vergleich unserer Ergebnisse mit entsprechenden Resultaten von chiraler Störungstheorie und Gitter-QCD-Rechnungen legt nahe, daß die Grösse der heutzutage verwendeten Gitter noch nicht ausreichend ist, als daß chirale Störungstheorie zur Extrapolation der Resultate für Niederenergie-Observablen angewendet werden könnte.
Phasenübergänge in der QCD bei endlicher Temperatur und Dichte sind Gegenstand aktueller Forschung. Einerseits untersuchen wir den chiralen Phasenübergang bei endlicher Temperatur in endlichem und unendlichem Volumen mit Hilfe des Quark-Meson-Modells. Obwohl qualitativ richtig, legen unsere Ergebnisse nahe, daß das Modell die Dynamik der QCD in der Nähe des Phasenübergangs nicht vollständig erfaßt. Andererseits beschreiben wir chirale Symmetriebrechung durch Quarks und Gluonen. Hierzu berechnen wie die laufende QCD-Kopplung für alle Skalen und Temperaturen. Damit bestimmen wir dann quantitativ die chirale Phasengrenze in der Ebene von Temperatur und Quarkanzahl und finden gute Übereinstimmung mit Gitter-QCD-Rechnungen.

Functional Renormalization Group Methods in Quantum Chromodynamics

Abstract

We apply functional Renormalization Group methods to Quantum Chromodynamics (QCD).
First we calculate the mass shift for the pion in a finite volume in the framework of the quark-meson model. In particular, we investigate the importance of quark effects. As in lattice gauge theory, we find that the choice of quark boundary conditions has a noticeable effect on the pion mass shift in small volumes. A comparison of our results to chiral perturbation theory and lattice QCD suggests that lattice QCD has not yet reached volume sizes for which chiral perturbation theory can be applied to extrapolate lattice results for low-energy observables.
Phase transitions in QCD at finite temperature and density are currently very actively researched. We study the chiral phase transition at finite temperature with two approaches. First, we compute the phase transition temperature in infinite and in finite volume with the quark-meson model. Though qualitatively correct, our results suggest that the model does not describe the dynamics of QCD near the finite-temperature phase boundary accurately. Second, we study the approach to chiral symmetry breaking in terms of quarks and gluons. We compute the running QCD coupling for all temperatures and scales. We use this result to determine quantitatively the phase boundary in the plane of temperature and number of quark flavors and find good agreement with lattice results.

Contents

Chapter 1

Challenges of Quantum Chromodynamics

At the beginning of the 20th century, there was to a large degree consent among physicists that nuclei are not fundamental particles, but built up from protons and neutrons. This realization raised the question which force kept these building blocks together. However, this question about the nature of the strong force remained unanswered for several years.

After the discovery of other strongly interacting particles, the so-called *hadrons*, in the first large collision experiments, in 1964 Gell-Mann proposed a new theory for the description of the properties of these particles, cf. Refs. [1, 2]. The original quark model introduced by Gell-Mann was able to explain the existence of some but not all of the newly discovered particles. For example, it was not possible to reconcile the existence of the baryonic resonance $\Delta^{++}(\frac{3}{2}^+)$ which is made up of three up-quarks in a spin-up state, without violating the Pauli Principle. In the seventies, it was then shown that the shortcomings of the original quark model could be resolved by assigning a so-called color charge to the quarks [3, 4, 5, 6]. Considering the problems of the original quark model with the baryonic resonance $\Delta^{++}(\frac{3}{2}^+)$, it was reasonable to assume the existence of three colors. Due to the principle of gauge invariance the existence of gauge bosons which carry various combinations of color and anti-color, so-called *gluons*, was postulated as well. Gauge invariance is a fundamental property of physical theories. For example, in electrodynamics it implies that the photons are massless and the electric charge is conserved. The gluons should be massless and mediate the interaction between the quarks, as the photons do in Quantum Electrodynamics (QED). In contrast to QED, however, the gauge bosons of the strong interaction interact with each other, which explains the short range of the strong force[1].

This new theory, which was called *Quantum Chromodynamics* (QCD), was not

[1]We add that the gauge bosons of the *weak force* interact also**,** but only weakly. In contrast to QCD, however, they are not massless, which in this instance explains the short range of the weak force.

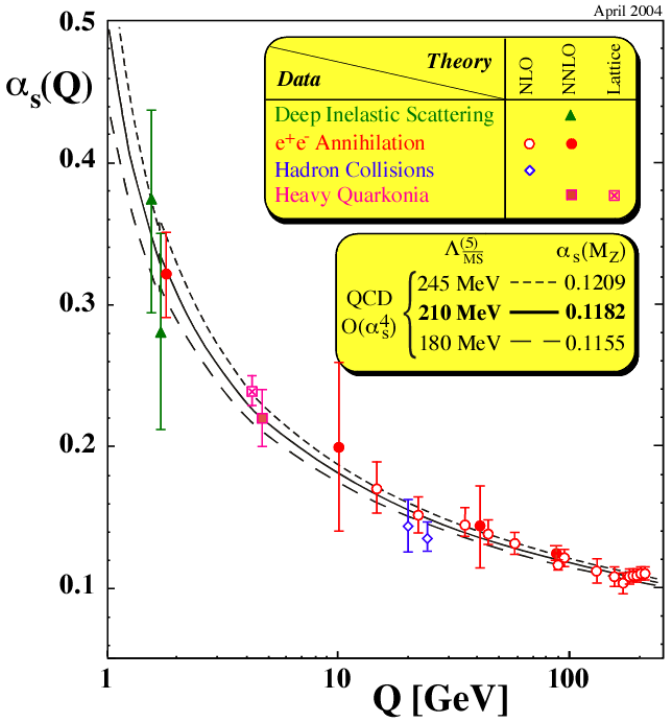

Figure 1.1: Running coupling of QCD: Comparison of theoretical predicted and experimentally determined values of the coupling as a function of momentum transfer Q [9].

immediately accepted in the physical community, since there were no experimental hints for the existence of either quarks or gluons. In QCD, the hadrons are explained as color-neutral objects of quarks and gluons, in which the color charges are *confined*. By definition, *confinement* means that only colorless objects, so-called color-singlets, can be observed, and that color charges remain unobservable, inside these composite objects. This confinement of color charges arises ultimately due to the fact that the energy, which is needed to separate two quarks, rises proportional to their distance. Therefore the low-energy regime of QCD is characterized by the confinement of quarks and gluons. The confinement property by itself, however, is not sufficient to explain the observed mass spectrum in this regime, which is distinguished by the existence of light pions. The mass of these pions, $m_\pi \approx 140\,\mathrm{MeV}$, is much smaller than the masses of the other hadrons, $m_\mathrm{H} \gtrsim 1000\,\mathrm{MeV}$. This characteristic property of the mass spectrum can be explained by the spontaneous breakdown of the *chiral symmetry* in QCD at low energies. It is this large mass gap due to the broken chiral symmetry, together with the fact that the pions interact only weakly, which allows for a successful description of low-energy QCD through effective theories in terms of the pion fields. Famous candidates of such effective theories are chiral perturbation theory [7] and the Gell-Mann-Levy model [8].

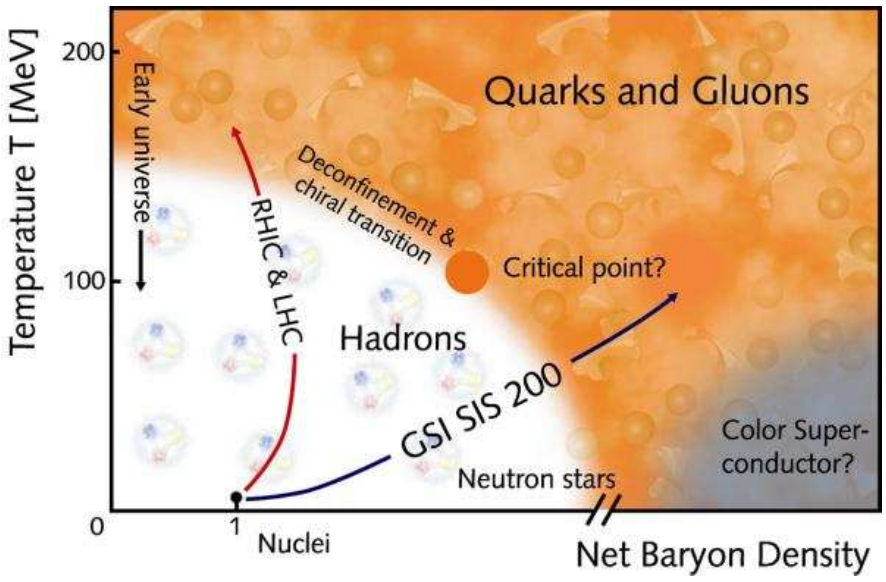

Figure 1.2: Sketch of the phase diagram of QCD [12].

Beside its confining property at low energies, QCD is governed by *asymptotic freedom* at high energies, as has been shown by Gross, Wilczek and Politzer [10, 11] in 1973. Asymptotic freedom means that the strength of the QCD coupling becomes smaller and smaller at high energies, corresponding to small distances. In Fig. 1.1, we show the running QCD coupling α_s as a function of momentum transfer Q. At high momentum transfers, where perturbation theory is applicable, we find coincidence of the experimentally determined values of α_s with their theoretical predictions. At small momentum transfers, however, the running coupling approaches a Landau pole in perturbation theory. Here perturbation theory predicts its own breakdown.

Although the high- as well as the low-energy limits of QCD are essentially well-understood, the connection of both limits is still a challenge. The aspects of dynamical mass generation, namely chiral symmetry breaking and confinement, in the intermediate-momentum regime cannot be addressed within a perturbative framework. Here, non-perturbative methods are indispensable.

So far we have considered the zero temperature limit of QCD. At finite temperature, the description of QCD becomes even more involved. Here a deconfinement phase transition has been observed in lattice QCD simulations. Below the deconfinement phase transition temperature T_d, there are only color-singlet states. However, above T_d, we encounter a rich spectrum of color-singlet as well as colored states, as suggested by recent discussions on the existence of a strongly interacting high-temperature phase in QCD [13, 14]. The existence of such a strongly interacting phase spoils a perturbative description of QCD at finite temperature and makes the theoretical description more difficult, in particular with regard to the dynamics in the vicinity of the finite-

temperature and finite-density phase boundary of QCD.

In Fig. 1.2, we show a sketch of the phase diagram of QCD. Most of the quantitative information that we have about this phase diagram comes from lattice QCD simulations. We will give a brief introduction to lattice simualtions in Sec. 2.2 and also discuss its limitations critically. QCD lattice simulations find a chiral phase transition temperature of $T_\chi \approx 175\,\mathrm{MeV}$ for two light quark flavors at vanishing baryon density [15] and a decrease of this temperature for increasing baryon density [16, 17, 18]. Lattice results indicate that the chiral and the deconfinement phase transition take place at the same temperature for vanishing and small baryon densities. But so far, it has not been established that this must be the case for all densities. Following the phase boundary to higher densities, it is commonly expected to reach a critical point [19, 16, 20, 21]. Even though the existence of such a critical point is likely, it is not yet conclusively confirmed. Besides this uncertainty, even the order of the phase transitions at small and vanishing baryon density is highly debated. For finite current quark masses, a crossover is observed, but in case of two massless quark flavors, the predictions from different lattice collaborations are not in agreement [15, 22].

The structure of the QCD phase diagram is of great importance for many different research fields. The high temperatures and baryon densities that are reached in current heavy-ion collider experiments at CERN SPS and RHIC make a penetration of the phase boundary possible and open the door for a study of the strongly interacting high-temperature phase, the so-called *quark-gluon plasma* phase [23, 24, 25, 26, 27]. The aim of GSI experiments is to probe the phase diagram for smaller temperatures but higher baryon densities. In the early universe the phase boundary was crossed parallel to the temperature axis of the phase diagram. In contrast, the properties of the phase diagram for large densities and small temperatures are of particular interest in astrophysics. For example, one can estimate that the density in neutron stars is a about six times larger than the density typically encountered in nuclear physics. Finally, it is likely that a regime in the phase diagram exists at very high densities where effects such as color-superonductivity and color-flavor-locking become important [28].

As already this brief history of QCD shows, there are still a lot of challenging questions in QCD, even more than 30 years after this theory has been introduced. Our discussion also shows that most of these questions are theoretically accessible only within a non-perturbative framework. In this work, we focus mainly on the dynamics near the phase boundary of QCD in finite volumes as well as at finite temperature. In this context, we also present a study of the running QCD coupling at finite temperature and show that there is an intriguing relation between its running and the quark and gluon dynamics near the phase boundary. Since phase transitions are inherently non-perturbative phenomena, we need non-perturbative methods to study them. There are many different approaches to choose from: lattice simulations, Dyson-Schwinger equations (DSE), functional Renormalization Group (RG) methods, ... In this work, we remain solely within a functional RG framework. However, in Chap. 2, we will briefly introduce the underlying concepts of lattice simulations and DSE as well. Before we

give a detailed derivation and discussion of functional RG equations, we will introduce the basic ideas of the renormalization group. Moreover, we will argue why we have chosen this approach and why we think that this approach can shed more light on the challenging questions of QCD mentioned above. In Chap. 3, we will discuss how low-energy observables in QCD are affected by the presence of a four-dimensional Euclidean volume. For this purpose we study a phenomenological low-energy QCD model in terms of quarks and mesons coupled via an Yukawa-type interaction. We will show that there exists a fascinating relation between the choice of the fermionic boundary conditions in spatial directions and the volume dependence of low-energy observables of QCD, such as the pion mass and the pion decay constant. Our results obtained from the non-perturbative RG study are qualitatively in accordance with results from lattice simulations, provided we apply periodic boundary conditions for the quarks. Choosing anti-periodic boundary conditions, we find agreement with chiral perturbation theory. These observations will finally lead us to the conclusion that lattice simulations have not yet reached volume sizes for which chiral perturbation can be applied to extrapolate results from the lattice. In Chap. 4, we show then that non-perturbative RG methods are well-suited for studying gauge theories. After a discussion of the technical aspects of such an approach, we compute the strong running coupling for Yang-Mills theory as well as for QCD for a wide range of temperatures and scales. After that, we will discuss how four-fermion interactions can be treated within the RG framework. In this context, we will show that an interesting interplay exists between gluodynamics and (induced) quark dynamics in the vicinity of the chiral phase boundary of QCD. These findings will allow us to compute the critical temperature of QCD from a first-principle study in terms of quarks and gluons. An extension of our study to an arbitrary number of massless quark flavors will then result in a determination of the QCD phase boundary in the plane of temperature and number of quark flavors. A brief summary of our main results and an outlook are found in Chap. 5.

Chapter 2

Non-perturbative Methods in Quantum Field Theory

In this chapter, we discuss several non-perturbative approaches to quantum field theories. First, we address the question why we need non-perturbative methods at all for the study of quantum field theories. Since we compare our results, obtained with non-perturbative RG methods, with results from lattice simulations and Dyson-Schwinger equations, we briefly discuss these two non-perturbative approaches in Sec. 2.2 and 2.3. Non-perturbative RG methods are then extensively discussed in Sec. 2.4.

2.1 Why do we need non-perturbative methods?

In QCD, the need for non-perturbative methods follows immediately from the fact that the coupling α_s increases strongly for small momentum transfers $Q \lesssim 1\,\mathrm{GeV}$, see Fig. 1.1. At high momentum scales, the predictions of perturbation theory for the running coupling are in accordance with experiment. At low momentum scales, however, the perturbative results for the coupling approach a Landau pole in perturbation theory. In this regime, Feynman graphs with many loops become as relevant as graphs with only a few loops. Since perturbation theory relies on the fact that the coupling is small, i. e. $\alpha_s \ll 1$, it predicts its own breakdown in the low-momentum regime.

The increase of the coupling and its behavior on small momentum scales are deeply related to the question of quark confinement in this momentum regime and cannot be addressed with perturbative methods. Although there are various effective low-energy theories (e. g. chiral perturbation theory) which describe the low-energy limit of QCD in terms of hadronic degrees of freedom well, these theories are not able to bridge the gap between the high-energy regime of QCD, dominated by quarks and gluons, and the low-momentum limit. Thus, non-perturbative methods are essential for the prediction of the hadronic mass spectrum and the understanding of dynamical mass generation in QCD.

Another example for the need for non-perturbative methods in QCD is given by

collision experiments, where one faces the problem of hadronization in deep inelastic scattering and jet formation.

In this work, we will mostly concentrate on strongly interacting systems at finite temperature and their phase transitions. Phase transitions in QCD are currently very actively researched and can only be addressed by non-perturbative methods. We emphasize that this is not particular to QCD, as it is also the case for a description of the phase transition in a simple one-component scalar field theory [29].

But non-perturbative methods are not only needed to describe phase transitions at finite temperature and density, they are also essential for a determination of bulk thermodynamic quantities of QCD, such as the pressure or the energy density, even at temperatures much higher than the transition temperature. Again, we rush to add that the necessity of non-perturbative methods in this case is not a property inherent in QCD, it belongs to all quantum field theories.

We finally note that there is also a particular interest in non-perturbative methods in topics beyond QCD. An example for such a research field is the determination of the validity limits of the *standard model*.

These examples of unsolved problems in quantum field theories serve as a motivation for the use of the non-perturbative approaches discussed in the following sections.

2.2 Lattice simulations

Lattice simulations are an example of a non-perturbative method. Since we compare our results with results from lattice simulations throughout this work, we briefly introduce and discuss this method in the context of QCD; for reviews see Ref. [30, 31].

In order to simulate QCD on a computer, one has to reduce the infinite number of degrees of freedom to a finite set. This is done by discretizing the 4-dimensional space-time in form of a lattice cube[1] with lattice spacing a and side length L. In a more field theoretical language, the discretization of space-time by the finite lattice spacing amounts to an ultraviolet regularization, whereas the infrared is regularized by the finite volume of the box.

Wilson's approach [32] is based on the path-integral formalism, where the expectation value of an observable $\hat{O}$ can be calculated by evaluating the integral

$$\langle \hat{O} \rangle = \frac{\int \mathcal{D}\mathcal{A}\, \hat{O} \left(\det G_F^{-1}[\mathcal{A}]\right) \mathrm{e}^{-S[\mathcal{A}]}}{\int \mathcal{D}\mathcal{A} \left(\det G_F^{-1}[\mathcal{A}]\right) \mathrm{e}^{-S[\mathcal{A}]}} \overset{\text{finite a}}{=} \frac{\int \mathcal{D}\mathcal{U}\, \hat{O} \left(\det G_F^{-1}[\mathcal{U}]\right) \mathrm{e}^{-S[\mathcal{U}]}}{\int \mathcal{D}\mathcal{U} \left(\det G_F^{-1}[\mathcal{U}]\right) \mathrm{e}^{-S[\mathcal{U}]}}\,, \tag{2.1}$$

where S denotes the QCD action. The expression by means of the integral over the gauge potentials $\mathcal{A}$ is the continuum representation for the expectation value whereas the expression on the RHS is the lattice representation, written by means of an integral

[1] We restrict our discussion to an isotropic lattice, but this does not have to be the case in general. On the contrary, lattices for simulations of QCD at finite temperature are usually anisotropic.

over so-called link-variables $\mathcal{U}$. On the lattice, one exchanges the gauge potentials $\mathcal{A}$ of the continuum formulation for the link variables $\mathcal{U}$ in order to formulate a gauge-invariant action S, which is more convenient for simulations on a computer. The link variables represent the gluonic degrees of freedom on the lattice and describe the color transport between two neighboring lattice points. The determinant in the integrals given above is the famous fermion determinant of the inverse quark propagator, which results from an integration over the quark fields. This integration is necessary because it is not possible to handle Grassmann-valued fields directly in lattice simulations. Since the calculation of the determinant is very time-consuming, one often works in the so-called *quenched* approximation, in which the quark propagator is treated as a constant. We do not specify the various expressions in Eq. (2.1) any further since it is not necessary for what follows[2].

Lattice simulations have the great advantage that they in principle allow for a simulation of full QCD, in contrast to the functional methods discussed in the subsequent sections. Lattice QCD has been quite successful in the study of non-perturbative phenomena: for example, the deconfinement phase transition in Yang-Mills theory as well as the chiral phase transition in QCD have been extensively studied, or bulk thermodynamic quantities, such as the pressure, have been measured. For a review, we refer to Ref. [33].

However, despite their great success, lattice simulations also have drawbacks. The most difficult problem is the incorporation of fermions in the simulation. This is due to the fact that the fermion propagator on the lattice does not have only a single pole, which represents the physical particle, but also additional poles, arising due to the discretization of the fermion fields on the lattice. This is known as the *fermion-doubling* problem. There exist several proposals for the implementation of the quark fields which attempt to cure this problem, e. g. Wilson fermions, staggered fermions or domain-wall fermions, for reviews see Ref. [30, 34]. However, all these implementations have in common that one must pay a price to get rid of the so-called fermion-doublers: for example, Wilson fermions break chiral symmetry explicitly, even in the case of vanishing current quark masses. In case of domain-wall fermions, one has to introduce a five dimensional lattice, which obviously increases the simulation time considerably. In the other case, quarks are treated with large current quark masses in the simulations in order to keep the simulation time short. But the application of large current quark masses requires that lattice results have to be extrapolated to the physical values of the quark masses. For this purpose one mainly uses chiral perturbation theory [7]. This seems to work well for most of the low-energy observables, but for other quantities of interest, e. g. for the chiral phase transition temperature, there is no extrapolation scheme available which provides a complementary approach to the lattice. We will discuss the dependence of the chiral phase transition temperature on the quark mass in Sec. 3.6 and 4.7 within a non-perturbative RG approach, and we will compare our

[2]Physical and mathematical aspects of gauge theories in the continuum are discussed in more detail in Sec. 4.2.

results to lattice predictions.

Besides the complications in connection with the implementation of the fermions, problems in lattice simulations may arise due to the discretization of space-time by the finite lattice spacing and the finite volume. Currently, the lattices used in simulations are coarse-grained, $a \sim 0.1 - 0.2\,\mathrm{fm}$, and the side length of the lattice cubes are still small, $L \sim 2\,\mathrm{fm}$. It is therefore natural to expect that lattice results are still affected by these two scales. To get a physically meaningful numbers out of lattice results, one has to extrapolate to vanishing lattice spacing, $a \to 0$, and infinite volume, $L \to \infty$. The former limit is often explored using RG methods, whereas only chiral perturbation has been used for the latter one so far. The extrapolation to infinite volume is subject of our investigation in Chap. 3, where we review the problem of finite-volume effects in lattice simulations in more detail. In particular, the dependence of the lattice results on the choice of the quark boundary conditions in the Euclidean time directions is discussed in the light of our non-perturbative RG results. In addition, we try to estimate limits for the applicability of chiral perturbation theory to finite-volume extrapolations of lattice results.

2.3 Dyson-Schwinger Equations

In Chap. 4, we connect our results for the running coupling of Yang-Mills theory qualitatively with the results from Dyson-Schwinger equations. Therefore we give a brief introduction to this method in this section.

Dyson-Schwinger equations (DSE) are a non-perturbative functional method for studying quantum field theories [35, 36]. As an illustration, we give the DSE for an Euclidean[3] scalar theory, cf. e. g. Ref. [37, 38]:

$$\int \mathcal{D}\phi \, \frac{\delta}{\delta\phi} \mathrm{e}^{-S[\phi]+\int J\cdot\phi} = 0 \qquad \Leftrightarrow \qquad \left[\frac{\delta S}{\delta\phi}\left[\frac{\delta}{\delta J}\right] - J\right] Z[J] = 0\,, \tag{2.2}$$

where S is the action of the theory, J is a source term and $Z[J]$ is the generating functional of the disconnected correlation functions. In order to derive the DSE in terms of Z, which is given by the expression on the RHS of Eq. (2.2), we have used that the functional integral over a total functional derivative vanishes. From this equation, we can derive an infinite set of integral equations for correlation functions by expanding in powers of the source J. Since it is not possible to solve this infinite tower of equations completely, one has to truncate this infinite set, which is equivalent to a restriction to a finite subset of correlation functions.

The DSE approach has been extensively used to study all kinds of quantum field theories, from scalar field theories to QCD. Especially for the latter, the approach via DSE has been quite successful in the investigation of confinement-scenarios in QCD at

[3] We refer to App. A for our conventions.

zero and finite temperature. For reviews and recent results in this field, we refer to Refs. [39, 40, 41, 42, 43].

At the end of subsection 2.4.1, we will briefly discuss the relation of DSE to non-perturbative RG flow equations.

2.4 Non-perturbative RG methods

In this section we discuss the *Functional Renormalization Group*, which provides the opportunity to study quantum-field theories non-perturbatively. First, we recall the basic ideas of the Renormalization Group, then we discuss the properties of the effective action, derive the Functional RG flow equation and discuss various aspects of this equation in Sec. 2.4.2. Finally, we discuss the sub-class of generalized proper-time RG flow equations in Sec. 2.4.3.

2.4.1 Basic Ideas of the Renormalization Group

In perturbation theory, the correlation functions contain divergencies which can be removed by a renormalization prescription. In any given theory, the renormalized constants (e. g. the coupling constant) are nothing but mathematical parameters which can be arbitrarily changed by changing the renormalization prescription. One should not confuse these renormalized constants with physical observables such as, for example, the *physical* mass of a particle, which is defined as the pole of the propagator. Physical observables are, of course, invariant under a variation of the renormalization prescription, provided we have not truncated the perturbation series[4].

Once we have removed the divergences, we are still free to perform additional finite renormalizations which result in different effective renormalization prescriptions. Therefore we can think of any given renormalization prescription as performing a reordering of the perturbative expansion and expressing it in terms of new, renormalized constants [45]. The transformations from the renormalization prescriptions can usually be parametrized by introducing of a single mass scale μ. A so-called Renormalization Group (RG) equation then describes the changes of the renormalized parameters of the theory (e. g. the coupling constant) induced by a variation of the scale μ. The set of renormalization prescription *transformations* is called the Renormalization Group[5].

In statistical physics, one finds that completely different many-body systems show the same *quantitative* behavior near phase transitions, where long-range fluctuations are important. In the vicinity of these critical points, the behavior of the theory is

[4] If we considered a truncated perturbation series, we would find that there is a residual dependence on the renormalization prescription. Such a dependence can be controlled to some extent by the "Principal of Minimum Sensitivity" [44].

[5] Strictly speaking, the Renormalization Group is not a group in the mathematical sense [45].

independent of the details of the theory and can be described with a (small) set of numbers, the so-called critical exponents, and scaling relations. This phenomenon is called *universality*. For example, the $3d$ Ising model and $SU(2)$ Yang-Mills theory belong to the same universality class. Typical scaling relations near a critical point (e. g. a second order phase transition point) are of the form

$$\xi \sim \left(\frac{T - T_{\rm cr}}{T_{\rm cr}} \right)^{-\nu} \quad \text{and} \quad G(x,0) \sim |x|^{2-d-\eta} \,, \tag{2.3}$$

where ξ is the range of correlated fluctuations (correlation length) and G denotes the two-point correlation function between fluctuations at the origin and at space-time point x. The universal critical exponents are ν and η, whereas d denotes the number of Euclidean space-time dimensions. The temperature is denoted by T and the critical temperature by $T_{\rm cr}$. It is important to stress that such scaling laws cannot be deduced from any fixed order perturbation theory calculation, since there are inherently non-perturbative phenomena underlying these lawss.

Wilson's (basic) idea of the renormalization group is to start with a (renormalized) microscopic theory at large momentum scale Λ (corresponding to a small length scale), defined by a (classical) action S, and then to integrate out successively all fluctuations from high to low momentum scales [46]. This procedure produces a scale-dependent action, where the expressions for the action on the different scales are related by continuous *RG transformations*. The couplings of the action are now scale-dependent; the change under a change of the scale is referred to as RG flow of the couplings. In this picture, we have found universality, if the scale-dependent couplings approach a fixed point. It is this property of capturing even long-range fluctuations which makes the RG to such a powerful tool for studying statistical field theory as well as quantum-field theory.

For our study of QCD in Chap. 3 and 4, we will apply non-perturbative RG flow equations [46, 47, 48, 49, 50, 51] for a so-called "averaged effective action" Γ_k, which depends on a scale k. We will discuss this in detail in Sec. 2.4.2. Here, we only note that these approaches are based on the fact that an infinitesimal RG transformation (RG "step"), performed by an integration over a single momentum shell, is finite. For this reason we are able to integrate out all quantum fluctuations through an infinite sequence of such RG steps. Then the flow equation describes the continuous trajectory from the microscopic theory at large momentum scales to the full quantum action (macroscopic theory) at small momentum scales. It therefore allows to cover physics across different length scales.

Before we derive and discuss non-perturbative RG flow equations in the next section, we relate the RG approach to the non-perturbative methods discussed in the first two sections of this chapter, namely lattice simulations and Dyson-Schwinger equations.

First, it is important to mention that the solutions of the Functional RG in the infrared limit (at long length scales) are also solutions of the DSE, provided the full theory is taken into account [52, 38]. However, since this is impossible in most cases, we briefly discuss some of the technical differences between both approaches: As we will show in the next subsection, the RG approach provides a solution for the effective action itself. In contrast, the DSE approach has not yet been applied to an explicit calculation of the effective action, but primarily for the correlation functions. Since spontaneous symmetry breaking is indicated by the existence of multiple solutions of the effective action, a comparison between the multiple solutions for the correlation functions from DSE has to be performed without knowing the effective action. In this case, a study of spontaneous symmetry breaking with DSE becomes more involved than with the RG approach. Moreover, the RG allows for a flexible construction of approximations of the full theory, see Sec. 2.4.2 and 2.4.3. Finally, a comfortable study of the fixed point structure of a given theory is provided by the RG due to the successive integration of momentum shells in this approach.

Compared to lattice simulations, the RG approach has the advantage that it allows to implement chiral quarks as well as quarks with small finite current quark masses. In addition, we can study quantum field theories in infinite and finite volume with the RG, whereas lattice simulations are restricted to finite volume by definition. On the other hand, the RG approach has the disadvantage that is not possible to take all operators of a theory into account, in contrast to lattice simulations. This brief comparison shows that both approaches are *complementary*: the RG approach can help to gain a better understanding of lattice results and lattice simulations can help to check wether a given RG truncation takes all operators relevant for a particular phenomenon into account. As a result, one could possibly work out the relevant mechanisms for a given phenomenon, say the chiral phase transition of QCD or finite-volume behavior of low-energy observables of QCD. On the other hand, the RG approach may help to bridge gaps between lattice simulations and nature, e. g. through the extrapolation of the chiral phase transition temperature to small current quark masses or the extrapolation to large volumes.

In any case, only with the help of all these non-perturbative approaches will it be possible for us to gain a profound understanding of the non-perturbative aspects of QCD.

2.4.2 The Functional Renormalization Group

Before we derive the non-perturbative RG flow equation for the effective action, we introduce the effective action and discuss its properties, cf. e.g. [53, 54]. We work in Euclidean space-time throughout this work, and we refer to Appendix A for details on our conventions.

The Effective Action

Our starting point is the generating functional

$$Z[J^T] = \langle 0|0\rangle_J \equiv \int \mathcal{D}\phi \, \mathrm{e}^{-S[\phi]+J^T(x)\cdot\phi(x)} \,, \tag{2.4}$$

where S is the (classical) action. The field variable ϕ as well as the source J are regarded as generalized vectors in field space and are defined as

$$\phi = \begin{pmatrix} \psi \\ \bar{\psi}^T \\ \varphi \\ \vdots \end{pmatrix} \quad \text{and} \quad J^T = \left(\bar{\eta},\, \eta^T,\, j,\, \dots\right) \,. \tag{2.5}$$

Here ψ represents a Dirac spinor,and φ denotes a real scalar field. The dots indicate that other types of fields, e. g. gauge-fields, are allowed as well. For convenience, we have introduced a generalized matrix product in d dimensions:

$$M \cdot N = \int d^d y \, \left[M(x_{i_1}, \dots, x_{i_{m-1}}, y)\right]_{\kappa_1\kappa_{n-1}\cdots\lambda} \left[N(y, x_{j_2}, \dots, x_{j_p})\right]_{\lambda\mu_2\cdots\mu_q} \,, \tag{2.6}$$

where M and N are arbitrary operators and the greek letters denote discrete indices.

The generating functional $Z[J]$ denotes the vacuum persistence amplitude, which gives the probability that the ground state does not change under the influence of the source J. Using the functional approach, the Green's functions of the theory can be deduced by taking functional derivatives of the generating functional Z with repsect to the source J:

$$\begin{aligned} \langle 0|\, T\left\{\phi_{i_1}(x_1)\cdots\phi_{i_n}(x_n)\right\}|0\rangle &= \int [\mathcal{D}\phi]\, \phi_{i_1}(x_1)\cdots\phi_{i_n}(x_n)\, \mathrm{e}^{-S[\phi]} \\ &= \left(\frac{\overrightarrow{\delta}}{\delta J^T_{i_1}(x_1)}\right)\cdots\left(\frac{\overrightarrow{\delta}}{\delta J^T_{i_n}(x_n)}\right) Z[J^T]\Big|_{J=0} \,. \end{aligned} \tag{2.7}$$

However, the Green's functions generated by this procedure are the so-called disconnected Green's functions, i. e. these Green's functions are reducible in the sense that they contain completely disjoint pieces. In Fig. 2.1, we illustrate qualitatively how the disconnected graphs can be decomposed into a sum of various connected diagrams. From the physical point of view, it is not convenient to work with the generating functional $Z[J]$, since the disconnected pieces of the generated Green's functions do not contribute to the S-Matrix. For this reason, one introduces a generating functional for the connected Green's functions $W[J]$ as

$$\mathrm{e}^{W[J^T]} = Z[J^T] \,, \tag{2.8}$$

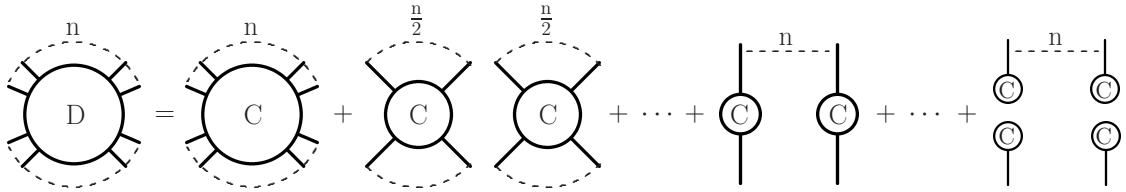

Figure 2.1: Illustration of the relation between disconnected (D) and connected (C) graphs for a disconnected graph with $2n$ external legs.

Here we will not prove rigorously that $W[J^T]$ is the generating functional for the connected Green's function, but the proof can be performed in the following way: Taking the first functional derivative of $W[J^T]$ with respect to J^T yields Φ, the so-called classical field or normalized vacuum expectation value of the field ϕ in the presence of the source J:

$$\frac{\overrightarrow{\delta}}{\delta J_a^T(x)} W[J^T] = \mathrm{x} \bullet\!\!-\!\!\textcircled{C} \quad = \frac{\langle 0|\, \phi_a(x)\, |0\rangle_J}{\langle 0|0\rangle_J} \equiv \Phi_a(x) \tag{2.9}$$

The field Φ is a function of x as well as a functional of J^T. Naively, one would expect that Φ vanishes identically in the limit of vanishing source J. However, as we will see in the following chapters, even in this limit fields can have a non-vanishing vacuum expectation value in case of spontaneous symmetry breaking. Now let us turn to the second derivative of $W[J^T]$:

$$\begin{aligned} G_{ab}(x,y) \;\equiv\; & \frac{\overrightarrow{\delta}}{\delta J_a^T(x)} \frac{\overrightarrow{\delta}}{\delta J_b(y)} W[J^T] = \mathrm{x} \bullet\!\!-\!\!\textcircled{C}\!\!-\!\!\bullet \mathrm{y} \\ = \;& \frac{\langle 0|\, T\{\phi_a(x)\phi_b^T(y)\}\, |0\rangle_J}{\langle 0|0\rangle_J} - \left(\frac{\langle 0|\, \phi_a(x)\, |0\rangle_J}{\langle 0|0\rangle_J}\right)\left(\frac{\langle 0|\, \phi_b^T(y)\, |0\rangle_J}{\langle 0|0\rangle_J}\right) \\ = \;& \mathrm{x} \bullet\!\!-\!\!\textcircled{D}\!\!-\!\!\bullet \mathrm{y} \;-\; \mathrm{x} \bullet\!\!-\!\!\textcircled{C}\;\;\textcircled{C}\!\!-\!\!\bullet \mathrm{y} \;. \end{aligned} \tag{2.10}$$

On the RHS of this equation, we have the full two-point Green's function minus its disconnected part. Therefore the second derivative of $W[J]$ with respect to the source is just the connected two-point function, i. e. the full propagator $G(x,y)$. The proof that the n-th derivative of $W[J]$ yields the connected n-point functions can now be performed straightforwardly by induction.

However, the class of connected Green's functions is still reducible, i. e. this class still contains graphs which can be decomposed into two disjoint graphs by cutting only one internal line. Feynman-graphs which cannot be decomposed into two disjoint graphs by cutting only one internal line are called one-particle irreducible (1PI): The 1PI graphs of a given theory represent a (minimal) basis for the connected Feynman graphs. For this reason it is more practical to calculate only the 1PI graphs and build

up the connectred graphs from these than to compute all connected Green's functions directly from their generating functional $W[J^T]$. Thus we need a generating functional for 1PI graphs.

The vacuum expectation value Φ can be used as a new variable in order to define a new generating functional $\Gamma[\Phi]$ by performing a Legendre transformation on the generating functional $W[J^T]$:

$$\Gamma[\Phi] = -W[J] + J^T \cdot \Phi \,. \tag{2.11}$$

Taking the functional derivative of Γ with respect to the source J, we obtain

$$\frac{\overrightarrow{\delta}}{\delta J_a^T}\Gamma[\Phi] = 0 \,. \tag{2.12}$$

This result proves that the generating functional $\Gamma[\Phi]$ does not depend explicitly on the source J.

The generating functional $\Gamma[\Phi]$ is called the effective action. It depends only on the classical field Φ and all fluctuations have been integrated out. The effective action is the generating functional for which we are looking: Taking functional derivatives of $\Gamma[\Phi]$ with respect to the field Φ yields the 1PI Green's functions. We will not prove this statement here, but we motivate it and show how a rigorous proof can be worked out. For convenience, we suppress continuous as well as discrete indices from now on. By taking the first functional derivative of the effective action $\Gamma[\Phi]$ with respect to Φ, we obtain

$$\Gamma[\Phi]\frac{\overleftarrow{\delta}}{\delta\Phi} = J^T \,. \tag{2.13}$$

Note that this is the quantum-mechanical analogon to the classical field equation. Moreover, in limit of vanishing sources the solutions of Eq. (2.13) represent the stable ground-states of the theory[6]. The second functional derivative of the effective action reads

$$\frac{\overrightarrow{\delta}}{\delta\Phi^T}\Gamma[\Phi]\frac{\overleftarrow{\delta}}{\delta\Phi} = \left(\frac{\overrightarrow{\delta}}{\delta J^T}\frac{\overrightarrow{\delta}}{\delta J}W[J^T]\right)^{-1} \overset{(2.10)}{=} G^{-1} \,. \tag{2.14}$$

This result is of crucial importance: The second functional derivative of the effective action Γ with respect to the field Φ is the inverse of the full propagator. For vanishing source J, Eq. (2.14) relates the full propagator to the curvature of the effective action in the physical ground-state of the theory. We immediately obtain from Eq. (2.14) that

$$G \cdot \frac{\overrightarrow{\delta}}{\delta\Phi^T}\Gamma[\Phi]\frac{\overleftarrow{\delta}}{\delta\Phi} \cdot G = G \,, \tag{2.15}$$

[6]They are stable only if the second functional derivative of the effective action is strictly positive for this solution.

which means that the connected two-point function of a theory can be constructed from the 1PI two-point function by dressing the external legs with the propagator.

Relation (2.15) can be generalized for arbitrary n-point functions. Using Eq. (2.14), we find

$$\frac{\overrightarrow{\delta}}{\delta\Phi^T} = \left(\frac{\overrightarrow{\delta}}{\delta\Phi^T}J^T\right)\frac{\overrightarrow{\delta}}{\delta J^T} = G^{-1}\cdot\frac{\overrightarrow{\delta}}{\delta J^T}\,. \tag{2.16}$$

This relation allows an interpretation of what happens when we take the n-th derivative of the effective action with respect to the classical field Φ: Taking a derivative of the generating functional $W[J]$ with respect to the source J adds an external line to a Green's function. Now, Eq. (2.16) tells us that taking a derivative of the effective action $\Gamma[\Phi]$ with respect to Φ means adding an external line and then removing the propagator from this line. This amputation of the external propagators generates the 1PI Green's functions. Using Eq. (2.16), one can prove inductively that the connected n-point functions can be constructed from the corresponding 1PI functions.

These properties, that the minimum of the effective action with respect to the classical field Φ corresponds to the ground-state of the theory under consideration, that 1PI graphs represent a minimal basis for the connected graphs, and that the second functional derivative of the effective action is equivalent to the inverse propagator, make the effective action into a convenient tool for studying quantum field theories.

Functional Renormalization-Group Equation

Our goal is to derive a non-perturbative RG flow equation for an "effective average action" Γ_k that depends on a scale k. This scale-dependent effective action is a generalization of the effective action discussed above and includes only the effects of fluctuations with momenta $p^2 \gtrsim k^2$. In the literature, Γ_k is often called a "coarse-grained" effective action, since it is averaged over volumes $\sim 1/k^d$, i. e. quantum fluctuations on smaller length scales than $1/k$ are integrated out. The underlying idea is to calculate the generating function of 1PI graphs of a given theory by starting at an UV scale Λ with the microscopic (classical) action S and then successively integrating out quantum fluctuations by lowering the scale k. The 1PI generating functional from the preceding section is then obtained in the limit $k \to 0$. In other words, the coarse-grained effective action interpolates between the classical action S at the UV scale Λ and the 1PI generating functional Γ^{1PI} in the infrared limit $k \to 0$. This is depicted in Fig. 2.2.

In the following, we derive a flow equation for Γ_k. This flow equation describes how the scale-dependent effective action at the scale k changes under a variation of the scale. The starting point for the derivation of the flow equation is a UV- and IR-regularized generating functional for the disconnected Green's functions:

$$Z_k[J^T] = \int_\Lambda \mathcal{D}\phi(p)\mathrm{e}^{-S[\phi]-\Delta S_k[\phi]+J^T\cdot\phi} \equiv \mathrm{e}^{W_k[J]}\,, \tag{2.17}$$

Figure 2.2: The figure illustrates the basic idea of the coarse-grained effective action, which is to connect physics on small length scales (large k) with physics on large length scales (small k).

where a cutoff term has been inserted to regularize the IR regime. It is defined as

$$\Delta S_k[\phi] \;=\; \frac{1}{2}\int \frac{d^dp}{(2\pi)^d}\,\phi_a^T(-p)R_k^{ab}(p^2)\phi_b(p) \equiv \frac{1}{2}\,\phi^T\cdot R_k\cdot\phi\,, \tag{2.18}$$

where R_k is matrix-valued regulator function. Through the insertion of the cutoff term, we have defined a generating functional which now depends on the scale k. Here we tacitly assume that the theory is well-defined by a UV-regularized generating functional, where the index Λ indicates that we only integrate over fields $\phi(p)$ with momenta $p \lesssim \Lambda$, i. e. we implicitly take $\phi(p) = 0$ for $p > \Lambda$.

It is useful to introduce the dimensionless scale variable $t = \ln(k/\Lambda)$. The cutoff function $R_k(p^2)$ and its derivative with respect to t as a function of the squared momenta p^2 are depicted in Fig. 2.3. The cutoff function $R_k(p^2)$ has to fulfill certain conditions: First, $R_k(p^2)$ must fulfill

$$\lim_{\frac{p^2}{k^2}\to 0} R_k(p^2) > 0 \tag{2.19}$$

in order to serve as an IR regularization of the theory. Second, the cutoff function must vanish in the IR-limit $k \to 0$:

$$\lim_{\frac{k^2}{p^2}\to 0} R_k(p^2) = 0\,. \tag{2.20}$$

This is a necessary condition to obtain the 1PI generating functional in the limit $k \to 0$. Finally, we want to recover the initial condition at the UV scale Λ. Therefore the cutoff function should obey

$$\lim_{k\to\Lambda} R_k(p^2) \to \infty \tag{2.21}$$

for fixed p^2. This property ensures that $\Gamma_{k\to\Lambda} = S$. In the following, we will always use linear cutoff functions which can be written in terms of a dimensionless regulator shape function $r(p^2/k^2)$ as

$$R_k(p^2) = Z_k p^2 r\left(\frac{p^2}{k^2}\right) \tag{2.22}$$

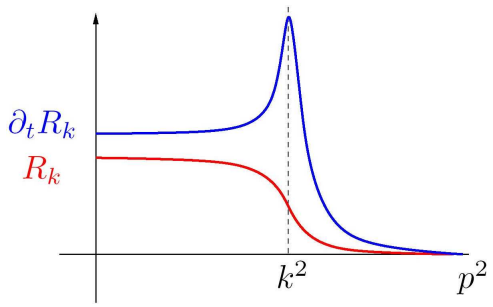

Figure 2.3: The cutoff function and its derivative with respect to t as a function of the squared momenta p^2 for fixed k^2.

for bosonic degrees of freedom. For scalar field theories, the presence of such a cutoff function is in general unproblematic. For gauge theories, however, it causes problems due to condition (2.19) which requires the cutoff function to act like a mass term for small momenta. Therefore the cutoff function breaks gauge symmetry. At first glance this seems to be a severe drawback of the Functional Renormalization Group, but this is not true at all. In order to treat gauge theories perturbatively within a path-integral approach, one always has to fix the gauge. This gauge-fixing procedure necessarily breaks gauge invariance. Gauge-invariant results are then recovered by applying Ward-Takahashi identities. Consequently, we should think of the cutoff function as just an additional source of gauge-symmetry breaking. In analogy to perturbation theory, one then has to deal with *modified* Ward-Takahashi identities in order to recover gauge invariance [55, 52, 56]. However, there are also alternatives: first, one can construct gauge-invariant flows as proposed in [57, 58]. Second, we can apply the background-field method, see Chap. 4 for details. Roughly speaking, this approach allows to construct RG flows that are invariant under transformations of the background field which is finally identified with the physical gauge field. For fermions, the construction of a cutoff function which preserves chiral symmetry is not so involved [59]. An appropriate choice is

$$R_k^{\psi}(\not{p}) = Z_k^{\psi} \not{p}\, r_{\psi}\left(\frac{p^2}{k^2}\right) , \tag{2.23}$$

where $r_{\psi}(p^2/k^2)$ is a dimensionless regulator shape function.

Let us now return to the derivation of the RG flow equation. In order to calculate the coarse-grained effective action from the IR-regularized functional $W_k[J^T]$ defined in Eq. (2.17), we follow the steps along the lines of the calculation of the (standard) effective action. We introduce a new field variable (classical field) by defining

$$\frac{\delta W_k[J]}{\delta J^T(x)} \equiv \Phi(x) . \tag{2.24}$$

Note that Φ is a functional of J^T and depends on k, since the generating functional does depend on it due to the insertion of the cutoff term in Eq. (2.17). Now we employ a modified Legendre transformation and define the scale-dependent effective action[7] as

$$\Gamma_k[\Phi] = -W_k[J] + J^T \cdot \Phi - \Delta S_k[\Phi]\,, \tag{2.25}$$

where the cutoff term depends on the fields Φ. This has two effects: first, it ensures that only fluctuations around the classical field are quenched, and second, it is necessary for the connection of Γ_k with the classical (or "bare") action S at the UV scale. Taking a functional derivative of Eq. (2.25) with respect to the classical field Φ yields[8]

$$\left(\Gamma_k[\Phi] + \Delta S_k[\Phi]\right) \frac{\overleftarrow{\delta}}{\delta\Phi} = J^T\,. \tag{2.26}$$

The full scale-dependent inverse propagator is then obtained by taking a functional derivative of Eq. (2.26) with respect to Φ as

$$G_k^{-1} = \frac{\overrightarrow{\delta}}{\delta J^T}\frac{\overrightarrow{\delta}}{\delta J} W_k[J^T] = \frac{\overrightarrow{\delta}}{\delta \Phi^T}\Gamma_k[\Phi]\frac{\overleftarrow{\delta}}{\delta\Phi} + R_k\,. \tag{2.27}$$

Now we take the derivative of the generating functional $W_k[J]$ with respect to t for a fixed source J:

$$\begin{aligned}
\partial_t W_k[J^T]\Big|_J &= \mathrm{e}^{-W_k[J^T]}\,\partial_t\,\mathrm{e}^{W_k[J^T]} \\
&= -\frac{1}{2}\left[\frac{\langle 0|\phi^T\cdot(\partial_t R_k)\cdot\phi|0\rangle_J}{\langle 0|0\rangle_J}\right] \\
&\overset{(2.27)}{=} -\frac{1}{2}\mathrm{STr}\Big\{G_k^{-1}\cdot(\partial_t R_k)\Big\} - \partial_t\Delta S_k[\Phi].
\end{aligned} \tag{2.28}$$

The super-trace arises due to the fact that ϕ contains both fermionic as well as bosonic degrees of freedom; it provides a minus sign in the fermionic subspace of the matrix. The flow equation for the coarse-grained effective action is obtained by taking the derivative of Eq. (2.25) with respect to t for fixed[9] classical field Φ:

$$\begin{aligned}
\partial_t\Gamma_k[\Phi]\Big|_\Phi &= -\partial_t W_k[J]\Big|_J - \partial_t\Delta S_k[\Phi] \\
&\overset{(2.28)}{=} \frac{1}{2}\mathrm{STr}\left\{\left[\frac{\overrightarrow{\delta}}{\delta\Phi^T}\Gamma_k[\Phi]\frac{\overleftarrow{\delta}}{\delta\Phi} + R_k\right]^{-1}\cdot\left(\partial_t R_k(p^2)\right)\right\}.
\end{aligned} \tag{2.29}$$

[7] A functional obtained by an ordinary Legendre transformations is convex. The coarse-grained effective action Γ_k is not necessarily convex for finite k due to the insertion of the cutoff term, but convexity is recovered in the limit $k \to 0$.

[8] For convenience, we work in momentum space from now on.

[9] It is also possible to study scale-dependent fields Φ. This is a powerful extension of the flow equation discussed here, since it allows for a transition between different types of fields in the RG flow. For example, quark-antiquark pairs can be "bosonized" in the RG flow [60, 61, 62, 63].

This flow equation for the coarse-grained effective action can be written as

$$\partial_t \Gamma_k[\Phi] = \frac{1}{2}\,\mathrm{STr}\,\left[\Gamma_k^{(1,1)}[\Phi] + R_k\right]^{-1} \cdot (\partial_t R_k) = \quad \frac{1}{2}$$

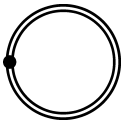

, (2.30)

where we have introduced the $(n+m)$-point functions defined as

$$\Gamma_k^{(n,m)}[\Phi] = \overbrace{\frac{\overrightarrow{\delta}}{\delta\Phi^T}\cdots\frac{\overrightarrow{\delta}}{\delta\Phi^T}}^{n-\text{times}}\,\Gamma_k[\Phi]\,\overbrace{\frac{\overleftarrow{\delta}}{\delta\Phi}\cdots\frac{\overleftarrow{\delta}}{\delta\Phi}}^{m-\text{times}}\,. \tag{2.31}$$

The $(n+m)$-point function defined in this way is a $(n+m)$-dimensional object in field space. The double-line in Eq. (2.30) represents the full propagator of the theory which includes the complete field dependence, and the solid black dot in the loop stands for the insertion of $\partial_t R_k$. This shows that the cutoff function specifies details of the momentum-shell integration, cf. Fig. 2.3 for an example of $\partial_t R_k$. We observe further that this so-called *Functional RG flow equation* is linear in the full propagator, as it should be the case for an exact one loop flow [64]. It is a nonlinear functional differential equation, since it involves the second functional derivative of the effective action. Although the flow equation (2.30) has a simple one-loop structure, we stress that this loop is not an "ordinary" perturbative loop, since it depends on the full propagator. It can be shown that arbitrarily high loop orders are indeed summed up by integrating this flow equation [64]. Finally, we note that the flow equation for Γ_k is *not* equal to the total derivative of a one-loop effective action:

$$\partial_t \Gamma_k[\Phi] \neq \frac{1}{2}\partial_t\,\mathrm{Tr}\,\ln\left(\Gamma_k^{(1,1)}[\Phi] + R_k\right)\,, \tag{2.32}$$

since terms $\propto \partial_t \Gamma_k^{(1,1)}$ are missing in Eq. (2.30).

So far, we have obtained an *exact* renormalization group flow equation for the effective action since we have made no approximations in our derivation. However, this equation is not solvable in its most general form. In the next paragraph, we discuss how an approximate solution can be obtained.

Truncation of RG flows and higher n-Point functions

The RG flows of higher n-point functions are obtained straightforwardly from the flow equation (2.30) by taking the appropriate number of functional derivatives. For simplicity, we restrict the discussion to a single-component scalar field theory. The flow equation for the one-point function reads then

$$\partial_t \Gamma_k^{(1,0)}[\Phi] = -\frac{1}{2}\,\mathrm{STr}\,(\partial_t R_k)\left[\Gamma_k^{(1,1)}[\Phi]+R_k\right]^{-1}\Gamma_k^{(2,1)}[\Phi]\left[\Gamma_k^{(1,1)}[\Phi]+R_k\right]^{-1}\,. \tag{2.33}$$

Its graphical representation is given by

∂_t 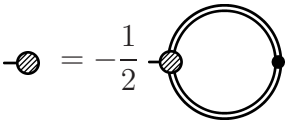 (2.34)

Taking a functional derivative of the flow equation one-point function, we obtain the equation for the two-point function:

$$\begin{aligned}\partial_t \Gamma_k^{(1,1)}[\Phi] &= -\frac{1}{2}\,\mathrm{STr}\left(\partial_t R_k\right)\left[\Gamma_k^{(1,1)}[\Phi]+R_k\right]^{-1}\Gamma_k^{(2,2)}[\Phi]\left[\Gamma_k^{(1,1)}[\Phi]+R_k\right]^{-1} \\ &\quad +\mathrm{STr}\left(\partial_t R_k\right)\left[\Gamma_k^{(1,1)}[\Phi]+R_k\right]^{-1}\Gamma_k^{(2,1)}[\Phi]\left[\Gamma_k^{(1,1)}[\Phi]+R_k\right]^{-1}\Gamma_k^{(1,2)}[\Phi]\left[\Gamma_k^{(1,1)}[\Phi]+R_k\right]^{-1}.\end{aligned} \tag{2.35}$$

Its graphical representation reads

∂_t 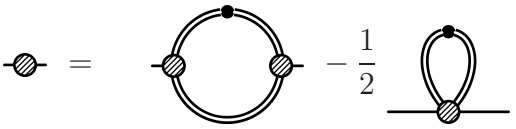 (2.36)

This can be continued to obtain the flow for all n-point functions. For example, we give the graphical representation of the flow for the three-point function:

∂_t 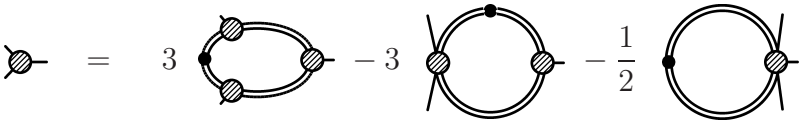 (2.37)

From this, we observe that information about the $(n+1)$- and $(n+2)$-point function is needed in order to solve the flow equation for the n-point function. This means that we obtain an infinite coupled tower of flow equations by taking functional derivatives of the flow equation (2.30). Since we are not able to solve this infinite tower of flow equations, we need to truncate the effective action and restrict it to correlation functions with $N_{\max}$ external fields. However, such a *truncation* poses severe problems: first, the system of flow equations is no longer closed and, second, neglecting higher n-point functions may cause problems in the IR region if one is interested in studying strongly coupled theories, e. g. QCD, where one would expect that contributions from higher n-point functions are of crucial importance. In subsection 2.4.3 and in particular in chapter 4, we discuss a possible method to keep track of the flows of all n-point functions.

In general, the strategy for studying quantum field theories with the functional RG is as follows: One writes down the most general ansatz for the effective action, containing all operators invariant under the symmetries of the theory. Then one truncates the effective action by either reducing n-point functions to a more simplified momentum dependence or just taking them as contact terms. Additionally, one chooses a value for $N_{\max}$ and neglects all n-point functions with $n > N_{\max}$ right from the beginning.

In other words, since it is impossible to study the flow of an effective action containing *all* operators allowed by the symmetries, one has to restrict oneself to a subspace of operators which one expects to be relevant for the physical problem under consideration. This is the most difficult step and it requires a lot of physical insight in order to choose the correct subspace of operators. In this context, it is important to stress that this truncation must not be confused with an expansion in some small parameter as in perturbation theory. The assumption here is that the influence of neglected operators on the operators included in the truncation is small.

Once one has chosen a certain truncation, one needs to check how trustworthy the results are. An obvious sign for an insufficient truncation is an unstable RG flow. For example, RG flows of four-fermion interactions show a divergence at a finite scale $k = k_{\rm cr}$. In this particular case, however, there is a physical reason for the instability. A divergence in the flow of four-fermion interactions indicates the onset of chiral symmetry breaking, see Subsec. 3.4.1 . Adding bosonic operators to the truncation can cure this instability [60, 61, 62]. Thus one possibility to check a given truncation is to extend the truncation by including additional operators and then check if the results obtained from this new truncation are in agreement with the former results. If this is not the case, one must rethink the chosen truncation. However, even if the results are not sensitive to the additional operators added to the truncation, this does not necessarily mean that one has included all relevant operators in the calculation. Moreover, it might also be the case that one physical observable is insensitive to the additional operators but others are not.

Another possibility to assess the reliability of a given truncation is to vary the cutoff function R_k and then to check if the results depend on the choice of the cutoff function. This possibility is based on the fact that physical observables should not depend on the regularization scheme. Since the scheme is specified by the cutoff function, the physical observables should be independent of this choice. If they are not, the truncation should be extended.

But in any case, an approximate solution of the flow equation can also describe non-perturbative physics reliably if the relevant degrees of freedom in the form of RG relevant operators are kept in the ansatz of the effective action.

2.4.3 Generalized Proper-Time Flows

In this section, we discuss a special subclass of *exact* RG flow equations, the class of Proper-Time flow equations, which can be obtained from Eq. (2.30). In order to derive this class of flow equations, we make use of the *background-field method*, which we discuss next.

The Background-Field Method

The background-field method is a very powerful method to study gauge theories, since it allows to construct a gauge-invariant effective action [65, 53]. We discuss this application in detail in Sec. 4.3. Here we introduce this method. The flow equation for the background-field effective action is then discussed in the next paragraph. Our starting point is a modified version of the generating functional for the disconnected Green's functions, which is given by

$$\begin{aligned} \hat{Z}[J^T,\hat{\phi}] &= \int \mathcal{D}\varphi\, \mathrm{e}^{-S[\varphi+\hat{\phi},\hat{\phi}]+J^T\cdot\varphi} \\ &\overset{\varphi=\phi-\hat{\phi}}{=} \int \mathcal{D}\phi\, \mathrm{e}^{-S[\phi,\hat{\phi}]+J^T\cdot(\phi-\hat{\phi})} = Z[J^T,\hat{\phi}]\mathrm{e}^{-J^T\cdot\hat{\phi}} \equiv \mathrm{e}^{\hat{W}[J,\hat{\phi}]}\,, \end{aligned} \tag{2.38}$$

where $\hat{Z}$ is a functional of the sources J^T and the background fields $\hat{\phi}$. On the LHS, we have split the quantum fields in the action S into fluctuation fields φ and background fields $\hat{\phi}$. The source couples only to the fluctuation fields φ. On the RHS, we have shifted the integration variable in such a way that the fluctuation fields are now given by $(\phi-\hat{\phi})$. We also allow for an explicit dependence of the action S on the background fields $\hat{\phi}$. We will encounter such a dependence when we discuss gauge theories in Sec. 4.3. For a scalar theory, we recover the standard generating functional Z for $\hat{\phi}=0$, i. e. $\hat{Z}[J,0]=Z[J,0]$. Beyond this, we observe that $\hat{W}$ and the standard generating functional of connected Green's functions W are related by

$$\hat{W}[J^T,\hat{\phi}] = W[J^T,\hat{\phi}] - J^T\cdot\hat{\phi}\,. \tag{2.39}$$

Note that the standard generating functional W depends explicitly on the background fields, since we allowed for an explicit dependence of the action S on these fields. Now we introduce modified classical fields by

$$\hat{\Phi} \equiv \frac{\overrightarrow{\delta}}{\delta J^T}\hat{W}[J^T,\hat{\phi}] = \Phi - \hat{\phi}\,. \tag{2.40}$$

The background-field effective action is obtained through a Legendre transformation with respect to the classical fields $\hat{\Phi}$ as

$$\hat{\Gamma}[\hat{\Phi},\hat{\phi}] = -\hat{W}[J,\hat{\phi}] + J^T\cdot\hat{\Phi} = -W[J,\hat{\phi}] + J^T\cdot\Phi \overset{(2.11)}{=} \Gamma[\Phi,\hat{\phi}]\,. \tag{2.41}$$

Again, the explicit dependence of the action S on the background fields results in an explicit dependence of the standard effective action Γ on these fields. From this we read off the important relation

$$\hat{\Gamma}[\hat{\Phi},\hat{\phi}] = \Gamma[\hat{\Phi}+\hat{\phi},\hat{\phi}] \overset{(2.40)}{=} \Gamma[\Phi,\hat{\phi}] \tag{2.42}$$

between the background-field effective action $\hat{\Gamma}$ and the standard effective action Γ. Consequently, the background-field effective action is just a convential effective action

computed in the presence of the background fields $\hat{\phi}$. If we consider the limit of vanishing classical fields $\hat{\Phi}$, which is equivalent to setting $\Phi = \hat{\phi}$, we get

$$\hat{\Gamma}[0, \hat{\phi}] = \Gamma[\hat{\phi}, \hat{\phi}] = \Gamma[\Phi, \Phi] \,. \tag{2.43}$$

This result means that the standard effective action can be obtained by evaluating the background-field effective action for $\hat{\Phi} = 0$.

Although it seems a bit awkward to calculate the background-field effective action instead of the standard effective action, it has some important advantages: Usually, the 1PI Green's functions are generated from the modified effective action by differentiating with respect to the classical fields. But in this case, functional derivatives of $\hat{\Gamma}[\hat{\Phi}, \hat{\phi}]$ with respect to $\hat{\Phi}$ generate 1PI graphs in the presence of the background field $\hat{\phi}$. Since $\hat{\Gamma}[0, \hat{\phi}]$ does not depend on $\hat{\Phi}$, it does not generate graphs with external legs. Moreover, we know that $\hat{\Gamma}[0, \hat{\phi}]$ contains all 1PI diagrams without external legs in the presence of the background fields $\hat{\phi} = \Phi$. This circumstance enables us to calculate the standard effective action by summing only graphs without external legs. Due to Eq. (2.43), we obtain the correct standard effective action by using this procedure. The second advantage, which is the most interesting one for our later purposes, is that it makes it possible to derive a gauge-invariant effective action, see Sec. 4.3.

RG Flows in the Background-Field Approach

In order to calculate the flow equation for the background-field effective action, we start once more from a IR- and UV-regularized generating functional for the disconnected Green's functions:

$$\begin{aligned} \hat{Z}_k[J^T, \hat{\phi}] \quad &= \quad \int_\Lambda \mathcal{D}\varphi \, \mathrm{e}^{-S[\varphi+\hat{\phi},\hat{\phi}] - \Delta S_k[\varphi,\hat{\phi}] + J^T \cdot \varphi} \\ &\overset{\varphi=\phi-\hat{\phi}}{=} \int \mathcal{D}\phi \, \mathrm{e}^{-S[\phi,\hat{\phi}] - \Delta S_k[\phi-\hat{\phi},\hat{\phi}] + J^T \cdot (\phi-\hat{\phi})} \equiv \mathrm{e}^{\hat{W}_k[J^T,\hat{\phi}]} \,. \end{aligned} \tag{2.44}$$

In the second line, ϕ represents the full quantum fields, which are a sum of the fluctuation fields $\varphi = \phi - \hat{\phi}$ and the background fields $\hat{\phi}$. In principle we allow for all kinds of fields, but it is important to stress that the generalization to gauge-fields is more involved. It will be discussed in detail in Sec. 4.3. In the cutoff term ΔS_k, we allow for an explicit dependence of the cutoff function on the background field:

$$\Delta S_k[\varphi, \hat{\phi}] \quad = \quad \frac{1}{2} \int \frac{d^d p}{(2\pi)^d} \, \varphi^T(-p) R_k^{\hat{\phi}}(p^2) \varphi(p) \equiv \frac{1}{2} \, \varphi^T \cdot R_k^{\hat{\phi}} \cdot \varphi \,. \tag{2.45}$$

The dependence of the cutoff function on the background field is indicated by the superscript $\hat{\phi}$. As we will see below, it is a generalization necessary to obtain the generalized proper-time form of the flow equation. Note that ΔS_k provides an infrared cutoff for the fluctuation field φ, but not for the full field ϕ.

The flow equation for the background-field effective action $\hat{\Gamma}[\hat{\Phi},\hat{\phi}]$ is worked out in complete analogy to the flow equation of the standard effective action in Sec. 2.4.2. Defining the background-field coarse-grained effective action as

$$\hat{\Gamma}_k[\hat{\Phi},\hat{\phi}] \;=\; -\hat{W}_k[J,\hat{\phi}] + J^T\cdot\hat{\Phi} - \Delta S_k[\hat{\Phi},\hat{\phi}]\,, \tag{2.46}$$

the corresponding flow equation reads

$$\partial_t\,\hat{\Gamma}_k[\hat{\Phi},\hat{\phi}] = \frac{1}{2}\,\mathrm{STr}\,\left\{\left[\hat{\Gamma}_k^{(1,1,0,0)}[\hat{\Phi},\hat{\phi}] + R_k^{\hat{\phi}}\right]^{-1}\left(\partial_t R_k^{\hat{\phi}}\right)\right\}\,, \tag{2.47}$$

where we have introduced the following short-hand notation for the generalized n-point functions:

$$\hat{\Gamma}_k^{(i,j,k,l)}[\hat{\Phi},\hat{\phi}] = \overbrace{\left(\frac{\overrightarrow{\delta}}{\delta\hat{\Phi}^T}\cdots\frac{\overrightarrow{\delta}}{\delta\hat{\Phi}^T}\right)}^{i-\text{times}}\overbrace{\left(\frac{\overrightarrow{\delta}}{\delta\hat{\phi}^T}\cdots\frac{\overrightarrow{\delta}}{\delta\hat{\phi}^T}\right)}^{k-\text{times}}\hat{\Gamma}_k[\hat{\Phi},\hat{\phi}]\overbrace{\left(\frac{\overleftarrow{\delta}}{\delta\hat{\phi}}\cdots\frac{\overleftarrow{\delta}}{\delta\hat{\phi}}\right)}^{l-\text{times}}\overbrace{\left(\frac{\overleftarrow{\delta}}{\delta\hat{\Phi}}\cdots\frac{\overleftarrow{\delta}}{\delta\hat{\Phi}}\right)}^{j-\text{times}}.$$

We stress that the RG flow for the background-field effective action defined by Eq. (2.47) is still complete and consistent, and standard perturbation theory can be reproduced by an integration of the flow equation [66].

Before we continue, we check the dependence of the flow equation (2.47) on the background field $\hat{\phi}$. For this purpose it is convenient to consider the first functional derivative of the coarse-grained effective action (2.46) with respect to the background field $\hat{\phi}$:

$$\hat{\Gamma}_k^{(0,0,0,1)}[\hat{\Phi},\hat{\phi}] = \frac{1}{2}\mathrm{STr}\left\{\left[\hat{\Gamma}_k^{(1,1,0,0)}[\hat{\Phi},\hat{\phi}]+R_k^{\hat{\phi}}\right]^{-1}\left(R_k\frac{\overleftarrow{\delta}}{\delta\hat{\phi}}\right)\right\} + \frac{\langle 0|\,S[\phi,\hat{\phi}]\frac{\overleftarrow{\delta}}{\delta\hat{\phi}}\,|0\rangle_J^{\mathrm{dis.}}}{\langle 0|0\rangle_J}. \tag{2.48}$$

Note that the second term also depends on the scale k. If the action, as well as the cutoff function R_k, is independent of the background field, then the RHS of Eq. (2.48) vanishes. Consequently, the effective action would depend only on the field $\hat{\Phi}$. If we have a cutoff function which depends on the background fields, but an action which is independent of the background field, then the effective action does not depend on the background field for $k\to 0$, since the cutoff function has to vanish in this limit (see Eq. (2.20)). For example, this particular case is on hand when one studies a scalar-field theory or a quark-meson model[10]. In gauge theories, the situation can be even more involved: if one uses background-field dependent gauges[11], the action S also depends on the background field. In this case, the first term on the RHS of Eq. (2.48) still vanishes in the limit $k\to 0$, but the second term does not, cf. Ref. [68, 69, 70].

[10] In Chap. 3, we study a quark-meson model with RG flow equations. There, we use an approximation of the flow equation (2.47) which we discuss below.

[11] If one uses axial gauges, where only the cut-off function R_k depends on the background field, there is no dependence of the action S on the background field [67].

In order to find a representation of the flow equation (2.47) in terms of proper-time integrals, we have to choose a certain class of cutoff functions R_k [69]. This class is obtained by taking R_k as a function of $\hat{\Gamma}_k^{(1,1,0,0)}[0,\hat{\phi}]$. It is important to stress that the we are not allowed to take R_k as a function of $\hat{\Gamma}_k^{(1,1,0,0)}[\hat{\Phi},\hat{\phi}]$ as the cutoff term (2.45) would no longer be bilinear in the fluctuation fields, and therefore we would lose the one-loop structure of the flow equation (2.47).

Writing the cutoff as a function of $\hat{\Gamma}_k^{(1,1,0,0)}[0,\hat{\phi}]$ represents an optimization of the RG flow, since it adjusts the regularization to the spectral flow of the fluctuations [71, 64]. As the discussion in the next paragraph indicates, this implies a significant improvement, since larger classes of diagrams can be resummed in a given truncation. To be specific, we replace the regulator $R_k^{\hat{\phi}}$ in Eq. (2.45) as follows:

$$R_k^{\hat{\phi}}(p^2) \longrightarrow R_k(x) = x\, r(y) \tag{2.49}$$

with $r(y)$ being a dimensionless regulator shape function with a dimensionless argument. The quantities x and y are given by

$$x = \hat{\Gamma}_k^{(1,1,0,0)}[0,\hat{\phi}]\,, \quad y = \frac{x}{\mathcal{Z}_k k^2}\,. \tag{2.50}$$

This is the class of the *spectrally adjusted* cutoff functions. Note that in general both, R_k and $\mathcal{Z}_k$, are matrix-valued in field space. A natural choice for the matrix entries of $\mathcal{Z}_k$ is given by the wave function renormalizations of the corresponding fields, since this establishes manifest RG invariance of the flow equation. So far, we have not specified the type of the fields. However, the definition of y is not appropriate for fermionic degrees of freedom since x is not necessarily positive definite in this case. We discuss the derivation of the flow equation for fermions separately in the next paragraph. For now, we restrict the discussion to bosonic fields.

Using the spectrally adjusted cutoff functions, the flow equation (2.47) can be formally written as

$$\partial_t \hat{\Gamma}_k[\hat{\Phi},\hat{\phi}] = \frac{1}{2}\,\mathrm{STr}\left[\hat{\Gamma}_k^{(1,1,0,0)}[\hat{\Phi},\hat{\phi}] + R_k[x]\right]^{-1} \cdot \Big\{ (\eta_{\mathcal{Z}} - 2)\cdot x \cdot y \cdot r' + (\partial_t x)\cdot\left[r + y\cdot r'\right]\Big\}\Big|_{x=\hat{\Gamma}_k^{(1,1,0,0)}[0,\hat{\phi}]}\,, \tag{2.51}$$

where r' denotes the first derivative of the dimensionless regulator shape function r with respect to its dimensionless argument, and $\eta_{\mathcal{Z}}$ denotes the (matrix-valued) anomalous dimension

$$\eta_{\mathcal{Z}} := -\partial_t \ln \mathcal{Z}_k = -\frac{1}{\mathcal{Z}_k}\partial_t \mathcal{Z}_k\,. \tag{2.52}$$

Note that the completeness and consistency property of the flow equation (2.47) is not spoiled by the improvement in terms of the insertion of $\hat{\Gamma}_k^{(1,1,0,0)}[0,\hat{\phi}]$ in the regulator. The RG flow equation (2.51) represents the starting point for the derivation of the so-called generalized proper-time RG flow equation.

Generalized Proper-Time RG flows for Bosons

Let us now derive and discuss the generalized proper-time RG flow equation for bosonic degrees of freedom. In order to obtain this flow equation, we identify the background field $\hat{\phi}$ with the field Φ. From Eq. (2.42) and (2.46), we read off that the background-field effective action $\hat{\Gamma}_k[\hat{\Phi},\hat{\phi}]$ evaluated for $\hat{\Phi}=0$ is equivalent to the standard effective action $\Gamma[0,\Phi]$ in the IR limit $k\to 0$. This motivates the definition

$$\Gamma_k[\Phi] := \hat{\Gamma}_k[0,\Phi]\,. \tag{2.53}$$

Due to the identification of the background field $\hat{\phi}$ with the classical field Φ, Eq. (2.51) can be written as [71, 66]

$$\begin{aligned}\partial_t\,\Gamma_k[\Phi] \;=\; \frac{1}{2}\,\mathrm{STr}\left\{\frac{\partial_t\hat{\Gamma}_k^{(1,1,0,0)}[0,\Phi]}{\hat{\Gamma}_k^{(1,1,0,0)}[0,\Phi]}\cdot\left[g\left(\frac{\hat{\Gamma}_k^{(1,1,0,0)}[0,\Phi]}{\mathcal{Z}_k k^2}\right)-h\left(\frac{\hat{\Gamma}_k^{(1,1,0,0)}[0,\Phi]}{\mathcal{Z}_k k^2}\right)\right]\right.\\ \left.+\,(2-\eta_{\mathcal{Z}})\cdot h\left(\frac{\hat{\Gamma}_k^{(1,1,0,0)}[0,\Phi]}{\mathcal{Z}_k k^2}\right)\right\}.\end{aligned} \tag{2.54}$$

The auxiliary functions $g(y)$ and $h(y)$ are related to the regulator shape function $r(y)$ by

$$h(y)=\frac{-yr'(y)}{1+r(y)}\,,\quad g(y)=\frac{r(y)}{1+r(y)}\,. \tag{2.55}$$

We observe that the RG flow of the effective action $\Gamma_k[\Phi]$ depends on the propagator of the fluctuation fields $\hat{\Gamma}_k^{(1,1,0,0)}[0,\Phi]$ and its flow[12]. This is an important difference to the flow equation (2.47), where the RHS depends only on the propagator $\hat{\Gamma}_k^{(1,1,0,0)}[\hat{\Phi},\hat{\phi}]$, but not on its flow. This additional dependence on the flow of the propagator is due to the adjustment of the cutoff function to the spectral flow of the fluctuations. But there is also drawback[13]: the flow equation (2.54) is *not* closed, since the propagator of the fluctuation field $\hat{\Gamma}_k^{(1,1,0,0)}[0,\Phi]$ and the propagator $\Gamma_k^{(1,1)}[\Phi]$ are not identical:

$$\Gamma_k^{(1,1)}[\Phi]=\hat{\Gamma}_k^{(1,1,0,0)}[0,\Phi]+\hat{\Gamma}_k^{(1,0,0,1)}[0,\Phi]+\hat{\Gamma}_k^{(0,1,1,0)}[0,\Phi]+\hat{\Gamma}_k^{(0,0,1,1)}[0,\Phi]. \tag{2.56}$$

[12] We emphasize that no admissible cutoff-shape function r exists such that $h(y)=g(y)$. Therefore the term proportional to the flow of the two-point functions is present for all cutoff-shape functions.

[13] This drawback is due to the identification of the background field $\hat{\phi}$ with the field Φ and not due to the insertion of $\hat{\Gamma}_k^{(1,1,0,0)}[0,\hat{\phi}]$ in the cutoff function.

However, we can immediately deduce from Eq. (2.48) that both propagators coincide in the limit $k \to 0$, where the cutoff function R_k vanishes, provided the action S does not depend on the background field. As we already mentioned above, such a background-field dependence is possible for gauge theories. Nevertheless, for the remainder of this thesis we assume that

$$\Gamma_k^{(1,1)}[\Phi] \stackrel{!}{=} \hat{\Gamma}_k^{(1,1,0,0)}[0,\Phi]\,. \tag{2.57}$$

We stress that this assumption suffices to extract perturbative β functions [72], as we will show when we consider gauge theories in Chap. 4. Moreover, the validity of the assumption (2.57) can, in principle, be quantitatively controlled by a check of the following constraint:

$$\hat{\Gamma}_k^{(1,0,0,1)}[0,\Phi] + \hat{\Gamma}_k^{(0,1,1,0)}[0,\Phi] \stackrel{!}{=} -\hat{\Gamma}_k^{(0,0,1,1)}[0,\Phi]\,. \tag{2.58}$$

The insertion of $\hat{\Gamma}_k^{(1,1,0,0)}[0,\hat{\phi}]$ into the cutoff function and the assumption (2.57) enable us to write the flow equation (2.54) in terms of proper-time integrals[14]. For this purpose we make use of the Laplace transforms of the auxiliary functions $h(y)$ and $g(y)$, defined as

$$h(y) = \int_0^\infty ds\, \tilde{h}(s)\mathrm{e}^{-ys} \quad \text{and} \quad g(y) = \int_0^\infty ds\, \tilde{g}(s)\mathrm{e}^{-ys}\,. \tag{2.59}$$

Introducing the functions $\tilde{H}(s)$ and $\tilde{G}(s)$ through the relations

$$\begin{aligned} \frac{d}{ds}\tilde{H}(s) &= \tilde{h}(s)\,, \qquad & \tilde{H}(0) &= 0\,, \\ \frac{d}{ds}\tilde{G}(s) &= \tilde{g}(s)\,, \qquad & \tilde{G}(0) &= 0\,, \end{aligned} \tag{2.60}$$

allows us to write the flow equation in the following useful and convenient form [71]:

$$\partial_t \Gamma_k[\Phi] = \frac{1}{2}\int_0^\infty ds\, \mathrm{STr}\, \hat{f}(s,\eta_{\mathcal{Z}})\, \mathrm{e}^{-\frac{s}{\mathcal{Z}_k k^2}\Gamma_k^{(1,1)}[\Phi]}\,. \tag{2.61}$$

Eq. (2.61) is called the *generalized* proper-time flow equation. It will be applied to gauge theories in Chap. 4. The operator $\hat{f}(s,\eta_{\mathcal{Z}})$ provides the translation of the regulator R_k into Laplace space:

$$\hat{f}(s,\eta_{\mathcal{Z}}) = \tilde{g}(s)(2-\eta_{\mathcal{Z}}) + (\tilde{H}(s) - \tilde{G}(s))\frac{1}{s}\partial_t. \tag{2.62}$$

The big advantage of the generalized proper-time flow equation is that the functional traces in Eq. (2.61) can now be evaluated, for instance, with powerful heat-kernel techniques, and all details of the regularization are encoded in the auxiliary functions $\tilde{h}, \tilde{g}$.

[14] Writing the flow equation in terms of proper-time integrals means nothing else than a Laplace transformation of Eq. (2.54).

Generalized Proper-Time RG flows for Fermions

So far, we have discussed the generalized proper-time form of the RG flow equation for bosons. Quark fields can similarly be treated within this framework. For our purposes in Chap. 4, it is advisable to separate a possible explicit (constant) mass contribution from the fermionic submatrix of $\hat{\Gamma}_k^{(1,1,0,0)}[0,\Phi]$:

$$\hat{\Gamma}_k^{(1,1,0,0)}[0,\Phi]\Big|_\psi = \mathcal{X}_\psi[0,\Phi] + \mathrm{i}M\,. \tag{2.63}$$

Here the index ψ indicates that we focus on the fermionic submatrix of $\hat{\Gamma}_k^{(1,1,0,0)}[0,\Phi]$. The imaginary unit factor multiplying the mass matrix M appears due to our conventions for fermions in Euclidean space-time, see App. A.

As we discussed in the last paragraph, the derivation of the generalized proper-time RG is based on the assumption that we can equate

$$\Gamma_k^{(1,1)}[\Phi] \stackrel{!}{=} \hat{\Gamma}_k^{(1,1,0,0)}[0,\Phi]\,,$$

and on an optimization of the cutoff function. This assumption for the inverse propagator of the fluctuation field is still required for the derivation of the fermionic flow equation. However, the optimization of the regulator that we have proposed for bosons in Eqns. (2.49) and (2.50), is not appropriate for fermions. The reason is that the fermionic submatrix of $\hat{\Gamma}_k^{(1,1,0,0)}[0,\Phi]$ is in general not positive definite[15]. Thus the transformation of the flow equation into Laplace-space is ill-defined. Moreover, $\hat{\Gamma}_k^{(1,1,0,0)}[0,\Phi]|_\psi$ has mass dimension one, and not two as it is the case for bosons. For these reasons we optimize the fermionic part of the RG flow by using the regulator [73]

$$R_k^\psi(x_\psi) = x_\psi r_\psi(y_\psi)\,, \tag{2.64}$$

with $r_\psi(y_\psi)$ being a dimensionless regulator shape function with a dimensionless argument. The operators x_ψ and y_ψ are defined as

$$x_\psi := \Gamma_k^{(1,1)}[\Phi]\Big|_\psi - \mathrm{i}M \quad \text{and} \quad y_\psi := \frac{x_\psi x_\psi^\dagger}{(\mathcal{Z}_k^\psi k)^2}\,, \tag{2.65}$$

where $\mathcal{Z}_k^\psi$ denotes a wave-function renormalization. Note that R_k^ψ and $\mathcal{Z}_k^\psi$ are in general matrix-valued in field space. This form of the fermionic regulator preserves chiral symmetry, provided $\Gamma_k^{(1,1,0,0)}[\Phi]|_\psi$ is symmetric under chiral transformations. If we used $\Gamma_k^{(1,1)}[\Phi]|_\psi$ instead of $\Gamma_k^{(1,1)}[\Phi]|_\psi - \mathrm{i}M$ for the optimization of the cutoff function, then the cutoff function would generate additional symmetry breaking contributions

[15] In the simplest case, $\hat{\Gamma}_k^{(1,1,0,0)}[0,\Phi]|_\psi$ is the Dirac-operator for which the existence of negative eigenvalues is well-known.

in the RG flow beside the contributions that arise due to the truncation. Since this is unwanted, we have separated the explicit mass term in Eq. (2.63).

Following the steps along the lines of the derivation drawn in the last paragraph, we finally obtain the flow equation for fermions:

$$\partial_t \Gamma_k[\Phi]\Big|_\psi = \frac{1}{2}\int_0^\infty ds\, \mathrm{STr}\, \hat{f}_\psi\left(s, \eta_\psi, \tfrac{M_{\bar{\psi}\psi}}{k}\right) \exp\left(-\frac{s\, x_\psi x_\psi^\dagger}{(\mathcal{Z}_k^\psi k)^2}\right)\Bigg|_{x_\psi = \left(\Gamma_k^{(1,1)}[\Phi]\Big|_\psi - \mathrm{i}M\right)} . \quad (2.66)$$

Here we have introduced the anomalous dimension of the fermion field,

$$\eta_\psi := -\partial_t \ln Z_k^\psi . \quad (2.67)$$

The operator $\hat{f}_\psi(s, \eta_\psi, \tilde{m})$ is defined in direct analogy to the definitions for bosons as

$$\hat{f}_\psi(s, \eta_\psi, \tilde{m}) = \tilde{g}^\psi(s, \tilde{m})(1 - \eta_\psi) + (\tilde{H}^\psi(s, \tilde{m}) - \tilde{G}^\psi(s, \tilde{m}))\frac{1}{2s}\partial_t . \quad (2.68)$$

The fermion mass matrix M enters the definition of $\hat{f}_\psi$ through $\tilde{m} = \frac{M}{k}$. The regulator shape function $r_\psi(y)$ is related to the auxiliary functions which appear in the definition of the operator $\hat{f}_\psi(s, \eta_\psi, \tilde{m})$ through

$$h^\psi(y, \tilde{m}) = \frac{-2y^2 r'_\psi(1 + r_\psi)}{y(1 + r_\psi)^2 + \tilde{m}^2}, \quad g^\psi(y, \tilde{m}) = \frac{y r_\psi(1 + r_\psi)}{y(1 + r_\psi)^2 + \tilde{m}^2} \quad (2.69)$$

and

$$h^\psi(y, \tilde{m}) = \int_0^\infty ds\, \tilde{h}^\psi(s, \tilde{m})\mathrm{e}^{-ys}, \quad \frac{d}{ds}\tilde{H}^\psi(s, \tilde{m}) = \tilde{h}^\psi(s, \tilde{m}), \quad \tilde{H}^\psi(0, \tilde{m}) = 0. \quad (2.70)$$

The corresponding functions $g^\psi(y, \tilde{m})$, $\tilde{g}^\psi(s, \tilde{m})$, and $\tilde{G}^\psi(s, \tilde{M})$ are related to each other in a manner analogous to Eq. (2.70). The present construction facilitates a simple inclusion of finite quark masses without complicating the convenient generalized proper-time form of the flow equation.

Truncation of Generalized Proper-Time RG flows and n-point functions

In this paragraph, we discuss the consequences of the insertion of $\hat{\Gamma}_k^{(1,1,0,0)}$ into the cutoff function. As we have already discussed in Sec. 2.4.2, the RG flows of higher n-point functions are obtained by taking the appropriate number of functional derivatives of the flow equation of the effective action. Of course this still holds for generalized proper-time RG flows. First we discuss how the diagrammatic representations of the flow equations of the higher n-point functions change due to the insertion of $\hat{\Gamma}_k^{(1,1,0,0)}$ in the cutoff function, then we discuss why this provides an optimization and how it can be used in order to resum larger classes of diagrams in a given truncation.

For simplicity, we restrict the discussion to a single-component scalar field theory. The flow equation for the one-point function is then given by

$$\begin{aligned}\partial_t \Gamma_k^{(1,0)}[\Phi] &= -\frac{1}{2}\,\mathrm{Tr}\left(\partial_t R_k\right)\left[\Gamma_k^{(1,1)}[\Phi]+R_k\right]^{-1}\Gamma_k^{(2,1)}[\Phi]\left[\Gamma_k^{(1,1)}[\Phi]+R_k\right]^{-1}\\ &\quad -\frac{1}{2}\,\mathrm{Tr}\left(\partial_t R_k\right)\left[\Gamma_k^{(1,1)}[\Phi]+R_k\right]^{-1}\left(\frac{\overrightarrow{\delta}}{\delta\Phi^T}R_k\right)\left[\Gamma_k^{(1,1)}[\Phi]+R_k\right]^{-1}\\ &\quad +\frac{1}{2}\,\mathrm{Tr}\left(\partial_t\frac{\overrightarrow{\delta}}{\delta\Phi^T}R_k\right)\left[\Gamma_k^{(1,1)}[\Phi]+R_k\right]^{-1}. \end{aligned} \tag{2.71}$$

The representation of this flow equation in terms of Feynman-graphs reads

∂_t 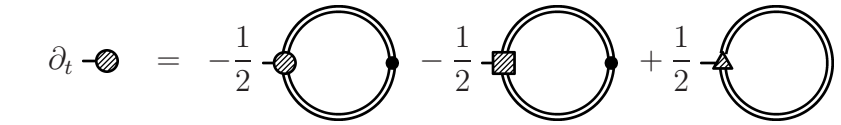 . (2.72)

The meaning of the various vertices is given by

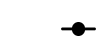 $= \partial_t R_k = \Gamma_k^{(1,1)}[\Phi]\,\partial_t r + \left(\partial_t \Gamma_k^{(1,1)}[\Phi]\right) r\,,$ (2.73)

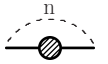 $= \Gamma_k^{(l,m)}[\Phi] \quad \text{with} \quad (l+m \stackrel{!}{=} n)\,,$ (2.74)

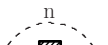 $= \overbrace{\frac{\overrightarrow{\delta}}{\delta\Phi^T}\cdots\frac{\overrightarrow{\delta}}{\delta\Phi^T}}^{l-\text{times}} R_k \overbrace{\frac{\overleftarrow{\delta}}{\delta\Phi}\cdots\frac{\overleftarrow{\delta}}{\delta\Phi}}^{m-\text{times}} \quad \text{with} \quad (l+m \stackrel{!}{=} n-2)\,,$ (2.75)

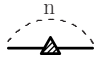 $= \partial_t$  . (2.76)

We observe that the square and triangle vertices are sums of the n-point functions $\Gamma_k^{(i,j)}$ and their t-derivatives. The meaning of the solid black dot is significantly different from its meaning in Sec. 2.4.2, since it now depends on $\Gamma_k^{(1,1)}$. Due to this dependence we integrate over shells of eigenvalues of $\Gamma_k^{(1,1)}$, instead of over naive canonical momentum shells, thereby accounting for the flow of these eigenvalues. The graphical representation of RG flow for the two-point function can be obtained by adding external legs to the Feynman-graphs in Eq. (2.72):

∂_t 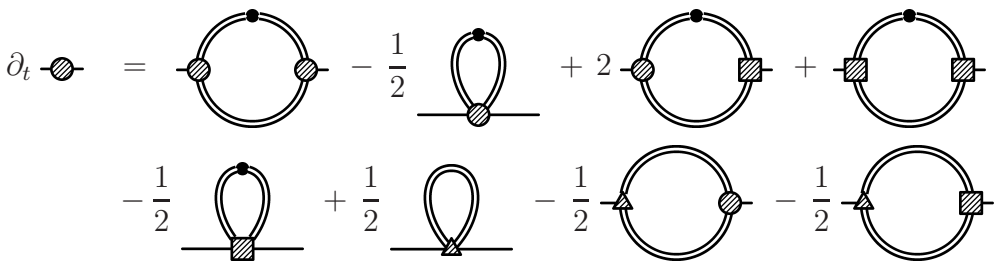 . (2.77)

This can be continued straightforwardly to obtain the RG flow equations for all n-point functions. In order to simplify the following discussion we define $\Gamma_k^{(i+j)} := \Gamma_k^{(i,j)}$.

From the derivation of the flow equations we recognize that we need information about the two-, three-, ..., n-, $(n+1)$- and $(n+2)$-point function in order to solve the flow equation for the n-point function. This is due to the fact that the RHS of the flow equations also depend explicitly on the flows of lower and higher n-point functions, in contrast to the situation discussed in Sec. 2.4.2. The resulting infinite tower of flow equations has the form

$$\partial_t \Gamma_k^{(i)}[\Phi] = X_i\left(\Gamma_k^{(2)}, \Gamma_k^{(3)}, \ldots, \Gamma_k^{(i+2)}\right) + \sum_j^{i+2} Y_{ij}\left(\Gamma_k^{(2)}, \Gamma_k^{(3)}, \ldots, \Gamma_k^{(i+2)}\right) \partial_t \Gamma_k^{(j)}[\Phi]\,, \quad (2.78)$$

with known functions X_i and Y_{ij}. The latter obeys $Y_{ij} = 0$ for $j > i+2$. Note that X_i and Y_{ij} are infinite-dimensional and that Eq. (2.78) is linear in the t derivatives of $\Gamma_k^{(n)}$. Provided the matrix $(1-Y)_{ij}$ is invertible, the solution is formally given by

$$\partial_t \vec{\Gamma}_k = (1-Y)^{-1} \cdot \vec{X}\,, \quad (2.79)$$

where the RHS depends solely on $\Gamma_k^{(2)}, \Gamma_k^{(3)}, \ldots$.

Since we are not able to solve this infinite tower of flow equations completely, we need to truncate the effective action. But in contrast to the situation described in Sec. 2.4.2 there are now several possibilities, two of which are of particular interest: first, we can restrict the effective action to correlation functions with $N_{\max}$ legs and drop all higher correlators, i. e. we can consider the limit $\Gamma_k^{(i)} \to 0$ and $Y_{ij} \to 0$ for $i, j > N_{\max}$. This corresponds to the truncation scheme discussed in Sec. 2.4.2, with all its drawbacks. Second, there is the possibility to set $\Gamma_k^{(i)} = 0$ by hand for $i > N_{\max}$ in Eq. (2.79), but to still keep track of the flows of all $\Gamma_k^{(n)}$. We stress that setting $\Gamma_k^{(i)} = 0$ by hand for $i > N_{\max}$ does not mean that we drop the flows $\partial_t \Gamma_k^{(i)}$ for $i > N_{\max}$, since in general the flow equation for $\Gamma_k^{(n)}$ depends on all correlators with $n \leq N_{\max}$ as well. This is reflected in the existence of nonzero entries in the infinite-dimensional matrix Y_{ij} even for $i, j > N_{\max}$. Since $(1-Y)^{-1}$ is infinite-dimensional as well, the flow equation for any $\Gamma_k^{(n)}$ consists of an infinite number of terms[16]. For this reason, larger classes of diagrams can be resummed by integrating the flow equations even remaining within a given truncation.

We have shown that the spectrally adjusted cutoff provides an efficient reorganization of the RG flow equation [71]. Already a small truncation contains information from the flow of infinitely many n-point functions. The introduction of a background field is a necessary condition in order to obtain such an optimization of the RG flow. Applications of the flow equation (2.61) to gauge theories have been studied in Ref. [72, 74, 75],

[16]Note that setting $\Gamma_k^{(i)} = 0$ by hand for $i > N_{\max}$ in Eq. (2.79) is not equivalent to dropping them right from the beginning.

where the term $\propto \partial_t \Gamma_k^{(2)}$ in Eq. (2.61) has been neglected. The crucial importance of including this term for a study of gauge theories has been shown in Ref. [71, 76, 77]. In Chap. 4, we study the running of the strong coupling and the chiral phase boundary of QCD by means of the flow equation (2.61), incorporating the terms $\propto \partial_t \Gamma_k^{(2)}$.

Proper-Time Renormalization Group

In this final paragraph we discuss a special approximation of the flow equation (2.61), which is called the *proper-time* RG flow equation. The proper-time RG has been successfully applied to study scalar theories, models for low-energy QCD and even gravity, see e. g. Refs. [78, 79, 80, 81, 82, 83, 84, 85, 86]. Although the proper-time RG flow equation is not *exact*, as was proved in [64], it yields quantitatively good results for the critical exponents of $O(N)$-models[17], cf. Refs. [78, 87].

The proper-time RG flow equation for bosons can be deduced from Eq. (2.54) by neglecting the term $\propto \partial_t \hat{\Gamma}_k^{(1,1,0,0)}[0,\Phi]$ and assuming $\Gamma_k^{(1,1)}[\Phi] \stackrel{!}{=} \hat{\Gamma}_k^{(1,1,0,0)}[0,\Phi]$:

$$\begin{aligned} \partial_t \Gamma_k[\Phi] &= \frac{1}{2}\,\mathrm{STr}\,(2-\eta_{\mathcal{Z}})\cdot h\left(\frac{\Gamma_k^{(1,1)}[\Phi]}{\mathcal{Z}_k k^2}\right) \\ &\overset{(2.59)}{=} \frac{1}{2}\,\mathrm{STr}\,(2-\eta_{\mathcal{Z}})\int_0^\infty ds\,\tilde{h}(s)\,\exp\left(-\frac{s}{\mathcal{Z}_k k^2}\Gamma_k^{(1,1)}[\Phi]\right), \end{aligned} \tag{2.80}$$

where the super-trace on the RHS acts only in the bosonic subspace. The corresponding proper-time flow equation for fermions reads

$$\begin{aligned} \partial_t \Gamma_k[\Phi]\Big|_\psi &= \frac{1}{2}\,\mathrm{STr}\,(2-\eta_{\mathcal{Z}})\cdot h^\psi\left(\frac{\Gamma_k^{(1,1)}[\Phi]\left(\Gamma_k^{(1,1)}[\Phi]\right)^\dagger}{(\mathcal{Z}_k^\psi k)^2}\right) \\ &\overset{(2.59)}{=} \frac{1}{2}\,\mathrm{STr}\,(2-\eta_{\mathcal{Z}^\psi})\int_0^\infty ds\,\tilde{h}^\psi(s)\,\exp\left(-\frac{s}{(\mathcal{Z}_k^\psi k)^2}\Gamma_k^{(1,1)}[\Phi]\left(\Gamma_k^{(1,1)}[\Phi]\right)^\dagger\right). \end{aligned} \tag{2.81}$$

In this case, the super-trace on the RHS acts only in the fermionic subspace. Now we switch to the proper-time RG nomenclature for cutoff functions, cf. [78, 79], by *choosing* the functions $\tilde{h}(s)$ and $\tilde{h}^\psi(s)$ to be[18]

$$(2-\eta_{\mathcal{Z}})\,\tau k^2 \tilde{h}\left(\tau k^2\right) = -\partial_t f_a\left(\tau k^2 \mathcal{Z}_k\right) = (2-\eta_{\mathcal{Z}})\,\frac{\left(\tau k^2 \mathcal{Z}_k\right)^{a+1}}{\Gamma(a+1)}\,\mathrm{e}^{-\tau k^2 \mathcal{Z}_k}, \tag{2.82}$$

[17] A rough estimate for the applicability of the proper-time RG to a specific model is given by the anomalous dimension $\eta_{\mathcal{Z}}$ of the fields. If it is small ($\eta_{\mathcal{Z}} \ll 1$), as it is the case for $O(N)$-models or the quark-meson model, the proper-time RG can be applied. If the anomalous dimension becomes large ($\eta_{\mathcal{Z}} \gtrsim 1$) as in QCD, see Chap. 4, this approximation to the Functional RG flow equation should not be applied.

[18] We emphasize that this is a choice which is not necessarily in accordance with the conditions on the cutoff function R_k. In particular, condition (2.21) may be violated by this choice.

and

$$(2-\eta_{\mathcal{Z}})\,\tau k^2\tilde{h}^{\psi}\left(\tau k^2\right) \;=\; (2-\eta_{\mathcal{Z}^{\psi}})\,\frac{\left(\tau k^2\mathcal{Z}_k\right)^{a+1}}{\Gamma(a+1)}\,\mathrm{e}^{-\tau k^2\mathcal{Z}_k}\,. \tag{2.83}$$

The proper-time cutoff function f_a is related to the incomplete Γ-function by

$$f_a\left(\tau k^2\mathcal{Z}_k\right) = \frac{\Gamma(a+1,\tau k^2\mathcal{Z}_k)}{\Gamma(a+1)}\,. \tag{2.84}$$

Here we allow for a free parameter a which must be chosen such that the infrared regime is regularized.

It was found in Ref. [88] that there exists an optimized proper-time cutoff function which corresponds to the optimized cutoff function[19]

$$R_k^{\text{opt.}}(p^2) = (k^2-p^2)\Theta(k^2-p^2) \tag{2.85}$$

within the Functional RG approach[20]. Here $\Theta(x)$ denotes the unit-step function. The optimized proper-time regulator in d dimensions is obtained from Eq. (2.84) by choosing [88]

$$a_{\text{opt.}} = \frac{d}{2}\,. \tag{2.86}$$

We stress that this correspondence is only true in leading order of the derivative expansion (the so-called local potential approximation). In other words, choosing the *optimized* proper-time cutoff function, one finds exactly the same flow equations in leading order of the derivative expansion as in the Functional RG approach with the cutoff function (2.85).

In Chap. 3, we apply the proper-time RG to a quark-meson model in leading order of the derivative expansion in order to study finite-volume effects in low-energy observables of QCD.

[19] We refer to an optimization criterion which is based on the gap induced in the effective propagator $P(y) = p^2(1+r(p^2/k^2))$ by the cutoff function. We denote those regulators to be optimized for which the gap is maximized with respect to the cutoff-scheme. For a detailed discussion of optimization criterions and the properties of optimized flow equations, we refer to Ref. [89, 88, 63].

[20] Here we only give the optimized cutoff $R_k^{\text{opt.}}$ for bosonic degrees of freedom. An optimized cutoff function for fermionic degrees of freedom is given in Ref. [88].

Chapter 3

QCD in Finite Volumes

In this chapter, we study finite-volume effects in QCD. After an introduction to this topic in the first section, we discuss finite-volume effects in chiral perturbation theory in Sec. 3.2. Finite-volume effects in low-energy observables of lattice QCD are briefly reviewed in Sec. 3.3. Our RG approach for the study of finite-volume effects in QCD and the underlying effective low-energy model, namely the quark-meson model, are introduced in Sec. 3.4. We give a general discussion of our results and a comparison with results from chiral perturbation theory and lattice QCD simulations in Sec. 3.5. In Sec. 3.6, we study the chiral phase transition and its dependence on the volume size and on the current quark mass. In the last section of this chapter, we give our conclusion and discuss possible further applications of the RG approach for finite-volume studies.

3.1 Introduction

The study of QCD in a finite volume has been of interest for quite some time. Accurate results of lattice simulations with dynamical fermions necessitate an understanding of finite volume effects. A variety of different methods has been proposed, cf. Refs. [90, 91, 92, 93, 94, 95, 96, 97, 98], to extrapolate reliably from finite lattice volumes to the infinite volume. Finite-volume partition functions for QCD have attracted interest in their own right, because they allow an exact description of QCD at low energies, cf. [99, 100, 101, 102]. The low-energy behavior of QCD is determined by spontaneous chiral symmetry breaking [7], which, however, does not occur in a finite volume. If the current quark mass is set equal to zero, in a finite volume the expectation value for the order parameter of chiral symmetry breaking vanishes, remaining zero even for arbitrary large volumes. The order parameter has a finite expectation value only when the infinite volume limit is taken before the quark mass is set to zero.

The box size L, the pion mass m_π and the pion decay constant f_π are the relevant scales for the transition between the regimes with a strongly broken and with an effectively restored chiral symmetry [99]. As a measure of explicit symmetry breaking, the pion mass is of particular importance. It is primarily the dimensionless product $m_\pi L$

that determines in which regime the system exists for a given pion mass and volume. In order to study chiral symmetry breaking in a finite volume, it is essential to introduce a finite quark mass as a parameter that explicitly breaks the chiral symmetry. Such an explicit symmetry breaking is quite natural in theories which involve effective chiral Lagrangians.

QCD at low energy can be studied by a wide variety of approaches which in essence all rely on the same fact: Due to spontaneous breaking of chiral symmetry, low-energy QCD is dominated by massless Goldstone bosons associated with the broken symmetry. Since these Goldstone bosons interact only weakly, the low-energy limit of QCD can be described in terms of an effective theory of these fields. A description in terms of effective chiral Lagrangians becomes even better if one considers the partition functions in finite Euclidean volume. Compared to the light degrees of freedom, contributions of heavier particles are suppressed by e^{-ML}, where M is the typical separation of the hadronic mass scale from the Goldstone masses. This separation of mass scales is at the origin of the description of QCD with effective theories in terms of the light degrees of freedom only.

A famous method which relies on the fact that low-energy QCD can be described well in terms of an effective theory of the pions is *chiral perturbation theory*. Nowadays, this method represents the most important tool for extrapolations of lattice gauge theory results to small pion masses and to large volumes [99, 101, 94, 103, 104, 93, 91, 98, 97, 105, 106]. In particular for the chiral extrapolation to small pion masses [107, 108, 94, 103, 104], and for the extrapolation to infinite volume for properties of the nucleon [91], chiral perturbation theory describes the lattice results very well.

In contrast to these applications, the finite volume shifts of the meson masses are less well described by chiral perturbation theory [109, 92, 110]. For the pion mass, the shifts predicted by chiral perturbation theory are consistently smaller than those observed in lattice simulations. For volume sizes that are suffciently large so that the internal degrees of freedom such as quarks and gluons are unimportant, one would expect that chiral perturbation theory correctly describes finite volume effects [105]. However, the discrepancies in current systematic investigations of finite volume effects [91, 109, 92, 110, 111] seem to indicate that this range has not yet been reached in lattice simulations.

One issue which cannot be addressed by chiral perturbation theory alone is the influence of the boundary conditions in the spatial directions for the quark fields. While fermionic fields require anti-periodic boundary conditions in the Euclidean time direction, we are free to choose either periodic or anti-periodic boundary conditions in the spatial directions. However, in lattice calculations, this choice changes the finite size effects in low-energy observables significantly, as will be discussed in the following sections. We think that a non-perturbative RG study in terms of an effective low-energy model can shed more light on this interesting finite-size effect, since, in contrast to chiral perturbation theory, it allows to study both types of boundary conditions. To be specific, the underlying model for our investigations is the *quark-meson model*, which

contains a scalar sigma meson and quarks in addition to the pion degrees of freedom. Due to the presence of quarks, the low energy constants of chiral perturbation theory are reproduced [112, 113]. We give a detailed introduction to this model in Sec. 3.4.

Beside this study of finite-size effects in low-energy observables of QCD, the subject of this chapter is to study the dynamics of chiral symmetry breaking in QCD at finite temperature within the quark-meson model. We mainly address the question of the volume dependence of the chiral phase transition temperature, including its dependence on the quark boundary conditions.

In finite volume, strictly speaking no phase transition is possible, since non-analyticities cannot appear in the thermodynamic potential (see e.g. [114]). In general, the investigation of phase transitions and critical behavior from results obtained in a finite volume is difficult and requires an extrapolation to the infinite-volume limit. In addition, if a symmetry is restored across the transition, this usually requires the introduction of an external field which explicitly breaks the symmetry. Even if there is no true order parameter that vanishes strictly in one of the phases, rapid changes over a small temperature range are an indication of a (crossover) transition. Often, peaks in susceptibilities or other higher-order derivatives of the thermodynamic potential are used as criteria to define a pseudo-transition. Here we propose to use the mass of the scalar mode, which corresponds to the inverse correlation length for fluctuations in the quark condensate, to identify the transition point: A distinct minimum of the mass appears at almost the same temperature at which the chiral quark condensate drops rapidly.

Phase transitions in QCD are currently very actively researched. Although most of the attention is focused on the phase transition at finite baryon density and temperature [16, 115, 116, 18, 117, 17, 118, 81], where the existence of a critical point in the phase diagram is not yet conclusively settled [20, 18, 119], there are still challenging questions even at vanishing density: for example, the order of the phase transition is still under discussion [120, 22, 15, 19] or the *weak* dependence of the phase transition temperature on the quark mass [121, 15, 122] which cannot be explained in terms of simple low-energy models [123, 78, 124].

The purpose of our finite-temperature study is twofold: first, we investigate if the weak quark mass dependence of the chiral phase transition temperature can be reproduced by means of the quark-meson model in finite volumes. Even though it was shown that such a weak dependence cannot be explained by means of the quark-meson model in infinite volume [123, 78], there still remains the possibility that this could be a finite-volume effect. Second, should this not be the case, we can conclude that the quark-meson model in its original form without gauge degrees of freedom is definitely not appropriate as an accurate description of the dynamics of chiral symmetry breaking in QCD at finite temperature.

3.2 Chiral Perturbation Theory and Finite Volumes

For finite volume, massless Goldstone bosons dominate the action of a theory with broken chiral symmetry. In chiral perturbation theory (chPT) [7], the pion mass, the pion decay constant and the chiral condensate have been calculated in finite volume [100, 101, 99]. The expansion parameters are the magnitude of the three-momentum $|\vec{p}|$ and the mass of the pion m_π as the lightest degree of freedom, which are small compared to the chiral symmetry breaking scale $4\pi f_\pi$.

Depending on the size L of the volume and the pion mass m_π, chiral perturbation theory distinguishes between two different power counting schemes. If the size of the box is much larger than the Compton wavelength of the pion, $L \gg 1/m_\pi$, the lowest nonzero pion momentum is smaller than the pion mass ($p_{\min} \sim \frac{2\pi}{L} \ll m_\pi$) and the normal power counting scheme applies ("*p-regime*"). In this case, the pions are constrained very little by the presence of the box, and finite size effects are comparatively small [101]. If, on the other hand, the size of the box is smaller than the Compton wavelength of the pion, the normal chiral expansion breaks down, since the smallest momentum $p_{\min} \sim \frac{2\pi}{L} \gg m_\pi$ is now much larger than the pion mass ("*ϵ-regime*"). In this case, the partition function is dominated by the zero modes. After solving the zero-momentum sector of the theory exactly, one expands in corrections due to the finite momentum modes. In Ref. [100], this was done first to one-loop order.

A very useful tool to study the effects of a finite volume on the mass of the pion is Lüscher's formula [125]. It relates the leading finite-volume corrections for the pion mass in Euclidean volume to the $\pi\pi$-scattering amplitude in infinite volume. Corrections to the leading order behavior drop at the least as $\mathcal{O}(e^{-\bar{m}L})$ where $\bar{m} \geq \sqrt{3/2}m_\pi$. For the particular case of the pion mass, the formula for the relative deviation $R[m_\pi(L)]$ of the pion mass $m_\pi(L)$ in the finite volume from the pion mass in the infinite volume $m_\pi(\infty)$ reads

$$\begin{aligned} R[m_\pi(L)] &= \frac{m_\pi(L) - m_\pi(\infty)}{m_\pi(\infty)} \\ &= -\frac{3}{16\pi^2}\frac{1}{m_\pi}\frac{1}{m_\pi L}\int_{-\infty}^{\infty} dy\, F(iy) e^{-\sqrt{m_\pi^2+y^2}L} + \mathcal{O}(e^{-\bar{m}L}). \end{aligned} \tag{3.1}$$

Here, F is the forward $\pi\pi$-scattering amplitude as a function of the energy variable s continued to complex values.

In Ref. [98, 97] the Lüscher's formula was combined with a calculation of the scattering amplitude in chiral perturbation theory in order to study the pion-mass shift in finite volume. A next-to-next-to leading order calculation of F alone does not seem to give a reliable and satisfactory result. For example, a one-loop calculation using Lüscher's formula gives a shift in the pion mass, for example, which is substantially lower than the one expected from the full one-loop calculation in chiral perturbation theory, as performed by Gasser and Leutwyler [100]. This estimate of the finite volume effects can be improved, if one uses the mass correction obtained from Lüscher's formula

with a $\pi\pi$-scattering amplitude including higher orders to correct the full one-loop chiral perturbation theory result [98]. Since Lüscher's formula has sub-leading corrections $\mathcal{O}\left(\exp[-\sqrt{3/2}m_\pi L]\right)$, the corrections to the leading result increase for decreasing pion mass at fixed volume size L with $m_\pi L$. As pointed out by the authors in [98], the Lüscher formula becomes a less reliable approximation exactly for those values of the pion mass for which the chiral expansion converges especially well.

In this thesis, we apply RG flow equations in order to study finite-volume effects. In contrast to chiral perturbation theory, this approach does not rely on either box size or pion mass as an expansion parameter, and does not require to distinguish between two different regimes. The approach remains valid as long as the lowest momenta and the masses of the heaviest particles remain below the ultraviolet cutoff scale. The beauty of the renormalization group method is precisely that the flow equations connect different scales. In the same way as the renormalization group flow equations describe the dependence of the results on the infrared cutoff scale k, they also describe the dependence on the additional scale imposed by the finite volume.

3.3 Finite Volume Effects in Lattice QCD Results

Current Lattice QCD simulations with dynamical fermions are still limited to rather small lattice sizes and in some approaches to quark masses which are still large compared to the physical values. In addition to taking the continuum limit in which the lattice spacing is taken to zero, results from lattice calculations require extrapolation towards the chiral limit and the thermodynamic limit. Thus, in order to compare a result for an observable simulated in a small volume with the physical observable, it is essential to understand the finite volume effects. In an investigation of Aoki et al. [126] of finite volume effects it was found that the choice of the boundary conditions for the quark fields has a direct influence on the size of the observed finite volume shifts [126, 127] and an explanation in terms of quark effects was proposed, for both quenched and unquenched calculations. Such effects cannot be captured by a description in terms of pion fields only. It has been shown by Gasser and Leutwyler that the low-energy constants in the chiral perturbation theory Lagrangian remain unchanged from their values in infinite volume if one considers QCD in a finite Euclidean volume, provided the same anti-periodic boundary conditions as in the temporal direction are chosen as well in the spatial directions for the quark fields [101]. This leaves open the possibility that a change of boundary conditions for the quark fields might in fact lead to a change in the finite volume behavior. If this is the case, then chiral perturbation theory is not an appropriate tool for the extrapolation of lattice results to the infinite-volume limit, at least as long as lattice simulations are constrained to the ϵ-regime ($m_\pi \ll \frac{2\pi}{L}$). We discuss this issue in Subsec. 3.5.3.

To illustrate our interest in the influence of boundary conditions on the volume dependence of low-energy observables, we present an example of a lattice calculation

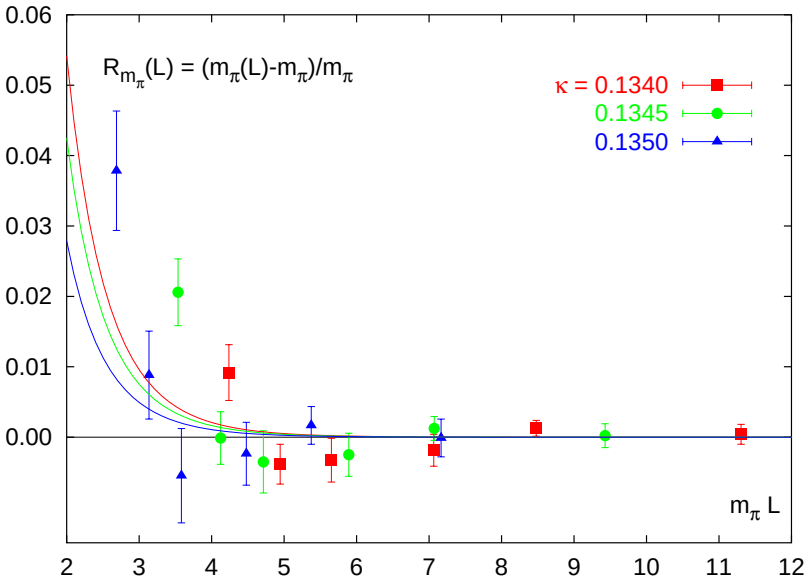

Figure 3.1: The pion mass shift $R[m_\pi(L)] = (m_\pi(L) - m_\pi(\infty))/m_\pi(\infty)$ as a function of $m_\pi(\infty) \cdot L$, obtained in a quenched lattice calculation, from ref. [92]. Shown are results for three different values of the quark mass, determined by κ. The solid lines show the corresponding predictions from chiral perturbation theory.

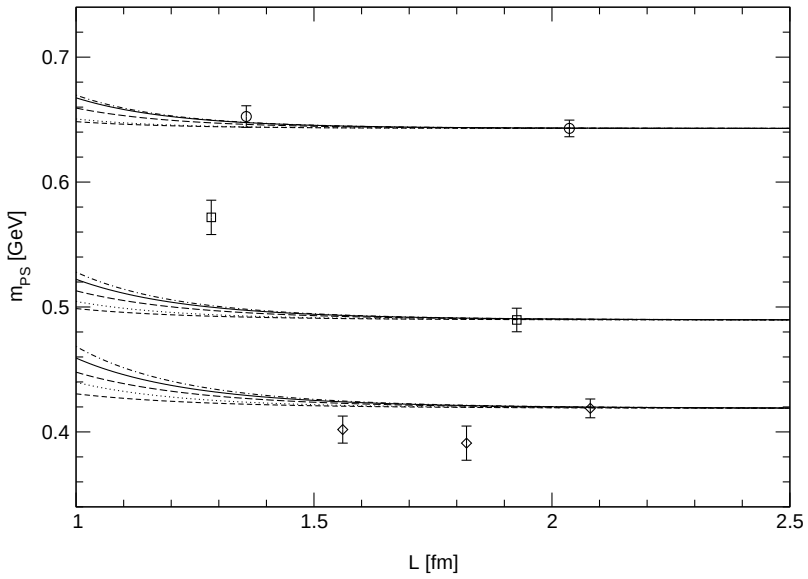

Figure 3.2: The pion mass $m_\pi(L)$ as a function of box size L, obtained in a lattice simulation with two flavors of dynamical Wilson fermions, from ref. [110]. Results for pion masses $m_\pi = 643$ MeV, 490 MeV, 419 MeV (circles, squares, diamonds) are compared to results from Lüscher's formula [125] with input from chPT up to NNLO order [98]. For details, see ref. [110]. For the smallest pion mass, a drop similar to the one in Fig. 3.1 can be observed.

in the quenched approximation from the ZeRo-collaboration [92] in Fig. 3.1. Shown is the shift of the pion mass $m_\pi(L)$ in finite volume relative to the value in infinite volume $m_\pi(\infty)$ as a function of $m_\pi(\infty)\cdot L$ where L is the volume size. Surprisingly, these results show a dropping pion mass for intermediate volume sizes in a region where the standard chiral perturbation theory result (indicated by the solid lines in the figure) predicts only a very weak volume dependence. This behavior would be unexpected from pion effects alone. In addition, finite volume effects from chiral perturbation theory are predicated on the presence of a "pion cloud", which in turn requires the presence of sea quarks [91]. Like chPT, our study is not directly concerned with the quenched approximation, which requires its own low-energy effective theory [128, 129]. Although the quenched calculation in Fig. 3.1 shows the pion mass drop in a very distinct fashion, similar effects for the meson masses are also seen in studies of finite size effects with dynamical quarks [109, 110]. In Fig. 3.2, we show results for the pion mass as a function of the volume size from a lattice calculation with two dynamical flavors of Wilson fermions [110]. Results are given only for few volume sizes, but they also show a decrease of the pseudoscalar mass in small volumes.

Subject of our investigations is the influence of different boundary conditions for the fermionic fields on the finite volume effects in low-energy observables. For this purpose, we apply the proper-time RG formalism to the quark-meson model. This will be the subject of the the next section. Since our model includes dynamical meson fields, and a dynamical breaking of the chiral flavor symmetry according to $SU(N_f) \times SU(N_f) \rightarrow SU(N_f)$ for $N_f = 2$ flavors of quarks, our results are applicable to unquenched lattice calculations with two dynamical quark flavors. The advantage of our approach is that it is complementary to lattice simulations and that it allows for an implementation of different boundary conditions for the fermionic fields, in contrast to chiral perturbation theory. Therefore, we think that our study may be helpful to gain a better understanding of recent lattice results.

3.4 RG Flow Equations for the Quark-Meson Model

This section focuses on the technical aspects of our study of finite-volume effects in QCD within a non-perturbative RG approach. First, we discuss the underlying quark-meson model and its origin. In Subsec. 3.4.2, we set up the RG formalism that allows to incorporate explicit symmetry breaking terms in the RG flow of the quark-meson model. Our strategy for the determination of the initial conditions for the RG flow as well as details on the numerical evaluations are then presented in Subsec. 3.4.3.

3.4.1 The Quark-Meson Model

The quark-meson model, in the form that is used in this work, has its origin in the so-called *Nambu-Jona-Lasinio (NJL)* model [130]. The NJL model is an extremely useful

model for studying dynamical chiral symmetry breaking. The generating functional Z for the disconnected Green's function reads

$$Z[\eta,\bar{\eta},J_0',\vec{J}'] = \int \mathcal{D}\psi\mathcal{D}\bar{\psi}\,\mathrm{e}^{-S[\bar{\psi},\psi]+\bar{\eta}\cdot\psi+\bar{\psi}\cdot\eta+\tilde{J}_0'\cdot(\bar{\psi}\psi)+\vec{J}'\cdot(\bar{\psi}\mathrm{i}\vec{\tau}\gamma_5\psi)} \tag{3.2}$$

with the action

$$S[\bar{\psi},\psi] = \int d^4x \left\{ \bar{\psi}\mathrm{i}\not{\partial}\psi + \frac{\bar{\lambda}_\sigma}{2}\left[(\bar{\psi}\psi)^2 - ((\bar{\psi}\vec{\tau}\gamma_5\psi)^2)\right]\right\}, \tag{3.3}$$

where ψ contains two fermion species and the components of the vector τ are the Pauli-Matrices:

$$\psi = \begin{pmatrix}\psi_1\\ \psi_2\end{pmatrix}, \qquad \vec{\tau} = \begin{pmatrix}\sigma_1\\ \sigma_2\\ \sigma_3\end{pmatrix} \qquad \text{and} \qquad (\bar{\psi}\hat{O}\psi)^2 \equiv (\bar{\psi}_i\hat{O}_k\psi_i)(\bar{\psi}_j\hat{O}_k\psi_j)\,. \tag{3.4}$$

In the generating functional Eq. (3.2), we also introduced source terms for the composite fields $(\bar{\psi}\psi)$ and $(\bar{\psi}\mathrm{i}\vec{\tau}\gamma_5\psi)$. We restrict our considerations to four space-time dimensions for convenience and refer to App. A for our conventions for fermion fields and γ-Matrices in Euclidean space-time. The NJL model is invariant under vector- (T_V) and axial-vector- (T_A) transformations, which are defined as

$$\mathrm{T}_V : \psi \to \mathrm{e}^{\mathrm{i}\vec{\tau}\cdot\vec{\Theta}}\psi \quad \text{and} \quad \mathrm{T}_A : \psi \to \mathrm{e}^{\mathrm{i}\gamma_5\vec{\tau}\cdot\vec{\Theta}}\psi\,. \tag{3.5}$$

Here $\vec{\Theta}$ is a constant vector that specifies the transformation angle. The axial-vector transformations are the so-called *chiral* transformations, which are of particular interest in the following. A necessary condition for this symmetry of the NJL model is that the action does not contain explicit mass terms for the fermion fields. However, the chiral symmetry can be still broken dynamically, if a finite vacuum expectation value $\langle 0|\bar{\psi}\psi|0\rangle$ is generated by loop corrections. This can be seen immediately by calculating the vacuum expectation value of the commutator of the chiral charge Q_5^a and the composite field $\bar{\psi}\mathrm{i}\tau^a\gamma_5\psi$:

$$\langle 0|\left[\mathrm{i}Q_5^a, \bar{\psi}\mathrm{i}\tau^b\gamma_5\psi\right]|0\rangle \propto \delta^{ab}\langle 0|\bar{\psi}\psi|0\rangle \quad \text{with} \quad Q_5^a = \frac{1}{2}\int d^3x\,\bar{\psi}\gamma_\mu\gamma_5\tau^a\psi\,. \tag{3.6}$$

Following the *Nambu-Goldstone theorem*, this implies that there exist three massless pseudo-scalar *Nambu-Goldstone particles* in the channel of the composite field $\bar{\psi}\mathrm{i}\tau^a\gamma_5\psi$. Since the action S does not contain such states, we conclude that the massless states must be bound states.

Formally, we introduce these bound-states by properly writing an exponential factor into the integrand of the generating functional[1]. We use

$$\mathrm{e}^{\int d^4x\left\{\frac{m^2}{g^2}\left(J_0'^2+\vec{J}'^2\right)\right\}} = \mathcal{N}\int \mathcal{D}\sigma\mathcal{D}\vec{\pi}\,\mathrm{e}^{-\int d^4x\left\{\frac{1}{2}m^2\left(\sigma^2+\vec{\pi}^2\right)-\frac{m^2}{g^2}\left(J_0'^2+\vec{J}'^2\right)\right\}}, \tag{3.7}$$

[1]This is known as a *Hubbard-Stratonovich transformation*.

where σ and $\vec{\pi}$ are auxiliary fields, $\mathcal{N}$ is a normalization factor, and g as well as m are constants that remain arbitrary for the moment. Multiplying the integrand of the generating functional with such a factor is allowed, since the additional field-independent terms, which are quadratic in the sources J_0' and $\vec{J}'$, leave the Green's functions of the theory unchanged. Shifting the integration variables in the thus modified generating functional by

$$\sigma \to \sigma - \frac{1}{g} J_0' + \frac{g}{m^2} \left(\bar{\psi}\psi\right) \quad \text{and} \quad \vec{\pi} \to \vec{\pi} - \frac{1}{g} \vec{J}' + \frac{g}{m^2} \left(\bar{\psi} \mathrm{i} \vec{\tau} \gamma_5 \psi\right) , \tag{3.8}$$

we finally obtain the new generating functional

$$Z[\eta, \bar{\eta}, J_0, \vec{J}] = \mathcal{N}' \int \mathcal{D}\sigma \mathcal{D}\vec{\pi} \mathcal{D}\psi \mathcal{D}\bar{\psi}\, \mathrm{e}^{-S[\bar{\psi},\psi,\sigma,\vec{\pi}] + \bar{\eta}\cdot\psi + \bar{\psi}\cdot\eta + J_0\cdot\sigma + \vec{J}\cdot\vec{\pi}} \tag{3.9}$$

with the so-called *bosonized* action

$$S[\bar{\psi}, \psi, \sigma, \vec{\pi}] = \int d^4x \left\{ \bar{\psi} \mathrm{i} \partial\!\!\!/ \psi + \frac{1}{2} m^2 \left(\sigma^2 + \vec{\pi}^2\right) + g \bar{\psi} \left(\sigma + \mathrm{i} \vec{\tau} \vec{\pi} \gamma_5\right) \psi \right\} . \tag{3.10}$$

In order to write the bosonized action in this convenient form, we have used that m^2 and g are arbitrary parameters at our disposal and we have rescaled the source terms J_0 and $\vec{J}$:

$$\bar{\lambda}_\sigma \stackrel{!}{=} -\frac{g^2}{m^2} , \quad J_0 = -\frac{m^2}{g} J_0' , \quad \vec{J} = -\frac{m^2}{g} \vec{J}' . \tag{3.11}$$

Instead of a four-fermion interaction, we now have a Yukawa-interaction and a mass term for the auxiliary fields. The bosonized action Eq. (3.10) is essentially the action of the *quark-meson model*. In hadron physics, however, the auxiliary fields and the arbitrary parameters g and m acquire a physical meaning: the fields σ and $\vec{\pi}$ play the role of the scalar meson and the pseudo-scalar Nambu-Goldstone modes in low-energy QCD, respectively. The Yukawa-coupling g specifies the strength of the quark-meson interaction, whereas m is the mass parameter of the meson fields. Finally, the fermion fields represent constituent quarks. Even the bosonization of the four-fermion interaction contains physics: in the spirit of the RG, the bosonic fields are introduced at a UV scale $\Lambda \sim 1\,\mathrm{GeV}$ that is determined by the validity of a hadronic description of QCD. Below this UV scale, hadronic operators are considered to be the relevant degrees of freedom, since low-energy QCD is dominated by light pions which play the role of the Nambu-Goldstone particles and are associated with the spontaneous breakdown of chiral symmetry. Above this UV scale, a description in terms of quarks and gluons is expected to arise naturally, owing to asymptotic freedom of QCD. It is important to add a comment on the bosonization procedure in the context of the RG: in the remainder of this chapter, we follow the strategy to bosonize the four-fermion interaction at a UV scale Λ. Below this scale, we then consider only operators which arise from the

bosonization at the UV scale Λ. We stress that this is an approximation, since the four-fermion interactions are generated again in the RG flow, already by performing an infinitesimal RG step of size dk. This is problematic, as one now encounters bosonic as well as fermionic operators at the scale $\Lambda - dk$. A so-called "re-bosonization-technique" has been proposed to cure this problem by, to put it sloppily, performing a bosonization of the newly generated four-fermion interactions in each RG step [60]. This method has been successfully applied to QED and one-flavour QCD at zero temperature [60, 62, 61].

Let us make one more point by comparing the NJL model and its bosonized version in more detail. Due to the Yukawa-interaction in Eq. (3.10), spontaneous breakdown of chiral symmetry means that the σ-field acquires a finite expectation value. This, in turn, results in a mass term for the fermionic fields. In the following, we will identify the expectation value of the σ-field with the pion decay constant f_π. This is a consequence of the *Goldberger-Treiman relation*, which results from a detailed study of the axial-vector currents of the bosonized action. Since this is important for our purpose in Chap. 4, we point out that we necessarily encounter broken chiral symmetry if the four-fermion coupling diverges, see e. g. [131]:

$$\frac{1}{\bar{\lambda}_\sigma} \to 0\,. \tag{3.12}$$

This is equivalent to a vanishing coefficient of the term bilinear in the mesonic fields in the bosonized action (3.10).

Since we have now clarified the origin of the quark-meson model, we can discuss it critically. For our RG study in the remainder of this chapter, we use the following effective action

$$\Gamma[\bar{\Psi},\Psi,\phi] = \int d^4x \Big\{ \bar{\Psi}\left(\mathrm{i}\partial\!\!\!/ + m_c\right)\Psi + g\bar{\Psi}(\sigma + i\vec{\tau}\cdot\vec{\pi}\gamma_5)\Psi + \frac{1}{2}(\partial_\mu\phi)^2 + U(\sigma,\vec{\pi}^2)\Big\}, \tag{3.13}$$

where Ψ contains the fields of the up- and down-quark, whereas ϕ contains the fields of the sigma meson and the pions. We have generalized the bosonized NJL model discussed above by including kinetic terms for the mesons as well as higher mesonic self-interaction terms summarized in the potential U. It is not necessary that these additional terms are present at the initial scale Λ, since they arise in the RG flow due to non-vanishing contributions from loop diagrams. Furthermore, we allow for an explicit current quark mass term m_c, but we neglect isospin breaking and assume that the two quark flavors have equal current quark masses. It is also possible to bosonize this term as well, which results in a linear term for the σ-field. As is well known, a linear symmetry breaking term remains unchanged in the RG flow [37]. Therefore the usual strategy is to evolve the potential without a symmetry breaking term. Explicit symmetry breaking is then taken into account after the quantum fluctuations have been integrated out on all scales [123, 59, 78]. In an infinite volume and for small quark masses, this method will yield reasonable results. In a finite-volume study, on which we focus here, the situation is different. Since chiral symmetry is not spontaneously

broken, explicit symmetry breaking has to be included on all scales in the RG flow to obtain a nonzero value for the order parameter. Otherwise, divergences from massless Goldstone bosons would restore the symmetry. Because of this, we implement explicit chiral symmetry breaking by means of an explicit current quark mass term in the action. Due to this current quark mass term, the potential U becomes a functional of σ and $\vec{\pi}^2$, rather than a functional of $\phi^2 = \sigma^2 + \vec{\pi}^2$. The reason for the appearance of $\vec{\pi}^2$ only in addition to σ is that the rotational symmetry of the pion space remains unbroken even in the presence of explicit symmetry breaking terms in the sigma direction. As we will show in the next subsection, the quark mass term generates in the RG flow only contributions to the mesonic operators which are compatible with this ansatz. Therefore we can easily "rebosonize" the contributions arising from this quark mass term in each RG step.

The quark-meson model is an effective model for dynamical spontaneous chiral symmetry breaking at intermediate scales of $k \lesssim \Lambda$. We stress that the quark-meson model cannot predict the volume dependence of pion mass and pion decay constant exactly. It is not a gauge theory, and thus it has neither gluons nor quark confinement. At moderate energies, below the hadronic mass scale Λ, unconfined constituent quarks appear instead of baryonic degrees of freedom. However, the low-energy couplings of the linear sigma-model with quarks are compatible with those of chiral perturbation theory [113, 112]. Despite the shortcomings of this model, we believe that the current approach can shed more light on lattice results regarding the volume dependence of the pion mass. While the actual mechanism in QCD may be different due to the presence of color interactions, the approach employed here gives a possible explanation for the various finite-volume effects in the low-energy observables observed in lattice simulations, as far as they relate to the mechanisms of chiral symmetry breaking in an effective low-energy description of QCD by means of light Nambu-Goldstone particles.

3.4.2 Derivation of the RG Flow Equations

Let us now derive the RG flow equations for the quark-meson model in the proper-time formalism. In the following, we consider the effective action (3.13) in a local potential approximation (LPA), which represents the lowest order in the derivative expansion and which incorporates fermionic as well as bosonic contributions to the potential U. In this approximation, the (classical) fields $\bar{\Psi}$, Ψ and ϕ are considered to be constant over the entire volume. In order to apply the RG flow equations (2.80) and (2.82) to a finite four-dimensional Euclidean volume $L_t \times L^3$, we replace the integrals over the momenta in the evaluation of the trace by sums

$$\int dp_0 \ldots \to \frac{2\pi}{L_t} \sum_{n_0=-\infty}^{\infty} \ldots \qquad \text{and} \qquad \int dp_i \ldots \to \frac{2\pi}{L} \sum_{n_i=-\infty}^{\infty} \ldots . \tag{3.14}$$

The boundary conditions in the Euclidean time direction are fixed by the statistics of the fields. The corresponding Matsubara frequencies take the values

$$\omega_{n_0} = \frac{2\pi}{L_t} n_0 \quad \text{and} \quad \nu_{n_0} = \frac{2\pi}{L_t}\left(n_0 + \frac{1}{2}\right), \tag{3.15}$$

for bosons and for fermions, respectively. When we study chiral symmetry breaking at finite temperate in Sec. 3.6, we will identify the inverse extent of the Euclidean time direction, $1/L_t$, with the temperature T of the system. In contrast to the situation in the Euclidean time direction, we are free in the choice of boundary conditions for the bosons and fermions in the space directions. In the following we use the short-hand notation

$$p_p^2 = \frac{4\pi^2}{L^2}\sum_{i=1}^{3} n_i^2 \quad \text{and} \quad p_{ap}^2 = \frac{4\pi^2}{L^2}\sum_{i=1}^{3}\left(n_i + \frac{1}{2}\right)^2 \tag{3.16}$$

for the three-momenta in the case of periodic (p) and anti-periodic (ap) boundary conditions. We will consider both choices for the quark fields, but employ only periodic boundary conditions for mesonic fields. Then, inserting the effective action (3.13) into Eq. (2.80) and (2.82), the flow equation for the mesonic potential U in finite Euclidean volume reads

$$\begin{aligned} k\frac{\partial}{\partial k} U_k(\sigma, \vec{\pi}^2, L_t, L) \;=\; & \frac{1}{L_t L^3}\frac{(kL)^{2(a+1)}}{(4\pi)^{a+1}\Gamma(a+1)}\Bigg(- 8N_c \Theta_{ap,p}^{(F)}\left(a, (k^2 + M_q^2(\sigma,\vec{\pi}^2))L^2, \frac{L}{L_t}\right) \\ & + \sum_{i=\{\sigma,\vec{\pi}\}} \Theta_p^{(B)}\left(a, (k^2 + M_i^2(\sigma,\vec{\pi}^2))L^2, \frac{L}{L_t}\right)\Bigg), \end{aligned} \tag{3.17}$$

where N_c gives the number of colors and a specifies the proper-time cutoff-function given in Eq. (2.84). The dimensionless threshold functions $\Theta_{ap,p}^{(F)}$ and $\Theta_p^{(B)}$ are discussed in App. D.3. Using the behavior of the these threshold functions in the limit $L \to \infty$ and $L_t \to \infty$, we obtain the corresponding flow equation for infinite Euclidean volume:

$$\begin{aligned} k\frac{\partial}{\partial k} U_k(\sigma, \vec{\pi}^2, L_t \to \infty, L \to \infty) \;=\; & \frac{k^{2(a+1)}}{16a(a-1)\pi^2}\Bigg\{ - \frac{8N_c}{(k^2 + M_q^2(\sigma,\vec{\pi}^2))^{a-1}} \\ & + \frac{1}{(k^2 + M_\sigma^2(\sigma,\vec{\pi}^2))^{a-1}} + \frac{3}{(k^2 + M_\pi^2(\sigma,\vec{\pi}^2))^{a-1}}\Bigg\}. \end{aligned} \tag{3.18}$$

This expression agrees with that in Ref. [78] calculated directly in the infinite-volume case. In order to be able to perform the integration in Laplace-space in Eq. (2.80) and (2.82), we have to choose $a \geq 2$ in infinite volume [78]. As we will discuss in Subsec. 3.4.3, we use the same initial conditions for the flow equation in finite volume as in infinite volume. Therefore we choose the same value for a in finite as well as in infinite volume. To be specific, we choose $a = 2$ for our calculations. This choice for a

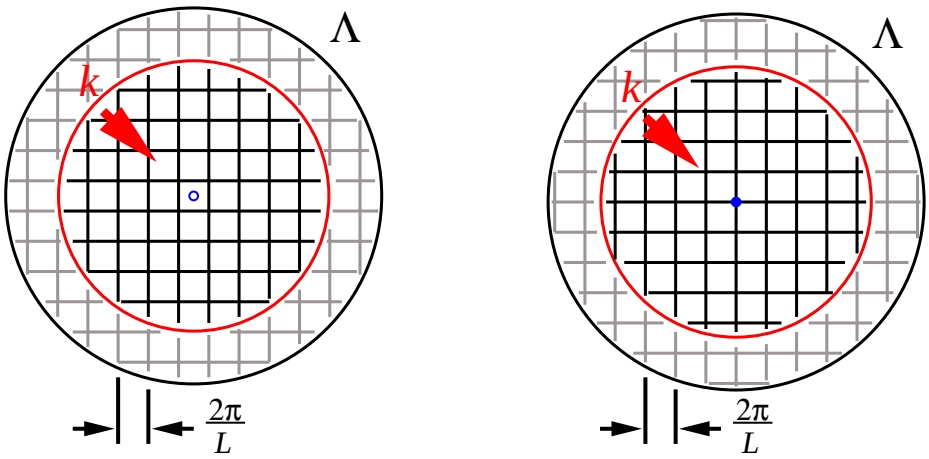

Figure 3.3: Schematic representation of the relation between the momentum summation and the UV and IR cutoff in momentum space, for anti-periodic boundary conditions (left panel) and for periodic boundary conditions (right panel). The UV cutoff is denoted by Λ, while k denotes the variable IR-cutoff of the RG scheme. The arrow indicates the direction of the RG flow from $k = \Lambda$ to $k = 0$. From these figures, one can easily read off that the choice of the boundary condition becomes more and more unimportant for larger volumes.

corresponds in infinite volume to a choice of an optimized regulator in the Functional RG [88], cf. the discussion of the proper-time RG in Subsec. 2.4.3. Integrating the flow equations (3.17) and (3.18) from the UV scale Λ to $k \to 0$, we obtain an effective potential in which quantum corrections from all scales have been systematically included. The relation between the momentum summation resp. integration and the UV and IR cutoff in momentum space as well as the role of the boundary conditions are nicely depicted in Fig. 3.3.

Let us now turn to a discussion of the masses of the quarks, the sigma meson and the pions on the RHS of the flow equations. The constituent quark mass M_q is given by

$$M_q^2 = g^2[(\sigma + m_c)^2 + \vec{\pi}^2]\,. \tag{3.19}$$

The squared meson masses M_i^2, $i \in \{\sigma, \vec{\pi}\}$, are the eigenvalues of the second-order derivative matrix

$$\left(U_k(\sigma, \vec{\pi}^2)\right)^{ij} = \frac{\partial^2 U_k}{\partial\phi_i \partial\phi_j} \tag{3.20}$$

of the meson potential $U_k(\sigma, \vec{\pi}^2)$ with respect to the fields $\phi = (\sigma, \vec{\pi})$. They depend only on the magnitude of the pion fields $\vec{\pi}^2$ and are independent of the direction. We wish to stress the importance of this point, since otherwise the meson contributions

from the flow equations would not be compatible with the ansatz for the potential which we will introduce below. The second derivative matrix is given by

$$\begin{pmatrix} U_{\sigma\sigma} & U_{\vec{\pi}^2\sigma} 2\pi^{(1)} & U_{\vec{\pi}^2\sigma} 2\,\pi^{(2)} & U_{\vec{\pi}^2\sigma} 2\,\pi^{(3)} \\ U_{\sigma\vec{\pi}^2} 2\pi^{(1)} & 2\,U_{\vec{\pi}^2} + U_{\vec{\pi}^2\vec{\pi}^2} 4\,(\pi^{(1)})^2 & U_{\vec{\pi}^2\vec{\pi}^2} 4\,\pi^{(1)}\pi^{(2)} & U_{\vec{\pi}^2\vec{\pi}^2} 4\,\pi^{(1)}\pi^{(3)} \\ U_{\sigma\vec{\pi}^2} 2\,\pi^{(2)} & U_{\vec{\pi}^2\vec{\pi}^2} 4\,\pi^{(2)}\pi^{(1)} & 2\,U_{\vec{\pi}^2} + U_{\vec{\pi}^2\vec{\pi}^2} 4\,(\pi^{(2)})^2 & U_{\vec{\pi}^2\vec{\pi}^2} 4\,\pi^{(2)}\pi^{(3)} \\ U_{\sigma\vec{\pi}^2} 2\,\pi^{(3)} & U_{\vec{\pi}^2\vec{\pi}^2} 4\,\pi^{(3)}\pi^{(1)} & U_{\vec{\pi}^2\vec{\pi}^2} 4\,\pi^{(3)}\pi^{(2)} & 2U_{\vec{\pi}^2} + U_{\vec{\pi}^2\vec{\pi}^2} 4\,(\pi^{(3)})^2 \end{pmatrix}$$

where we have suppressed the scale index k of the potential and use the abbreviations

$$U_\sigma = \frac{\partial U}{\partial \sigma}, \;\; U_{\pi^{(a)}} = \frac{\partial U}{\partial \vec{\pi}^2}\frac{\partial \vec{\pi}^2}{\partial \pi^{(a)}} = U_{\vec{\pi}^2} 2\pi^{(a)}, \;\; U_{\vec{\pi}^2} = \frac{\partial U}{\partial \vec{\pi}^2}, \tag{3.21}$$

and the corresponding expressions for the higher-order derivatives. The eigenvalues of this matrix are given by

$$\begin{aligned} M_1^2 &= \frac{1}{2}\left[2\,U_{\vec{\pi}^2} + 4\,\vec{\pi}^2\,U_{\vec{\pi}^2\vec{\pi}^2} + U_{\sigma\sigma} + \sqrt{(2\,U_{\vec{\pi}^2} + 4\,\vec{\pi}^2 U_{\vec{\pi}^2\vec{\pi}^2} - U_{\sigma\sigma})^2 + 16\,\vec{\pi}^2\,U_{\sigma\vec{\pi}^2}^2}\right], \\ M_2^2 &= 2\,U_{\vec{\pi}^2}, \quad M_3^2 = 2\,U_{\vec{\pi}^2}, \\ M_4^2 &= \frac{1}{2}\left[2\,U_{\vec{\pi}^2} + 4\,\vec{\pi}^2\,U_{\vec{\pi}^2\vec{\pi}^2} + U_{\sigma\sigma} - \sqrt{(2\,U_{\vec{\pi}^2} + 4\,\vec{\pi}^2 U_{\vec{\pi}^2\vec{\pi}^2} - U_{\sigma\sigma})^2 + 16\,\vec{\pi}^2\,U_{\sigma\vec{\pi}^2}^2}\right]. \end{aligned} \tag{3.22}$$

For vanishing cross terms $U_{\sigma\vec{\pi}^2}$, the last eigenvalue reduces to $2\,U_{\vec{\pi}^2} + 4\,\vec{\pi}^2\,U_{\vec{\pi}^2\vec{\pi}^2}$, which corresponds to a derivative in "radial" direction in the pion-subspace. In particular for $\vec{\pi}^2 = 0$, the three pion modes have equal masses. We also note that the pion fields appear only in the combination $\vec{\pi}^2$ in the eigenvalues, despite the fact that the derivative matrix contains terms linear in $\pi^{(a)}$. This is due to the fact that we still have rotation invariance in the pion space even in the presence of explicit symmetry breaking terms in the sigma direction.

In order to solve the flow equations Eq. (2.80) and (2.82), we make a polynomial ansatz for the meson potential U. This ansatz is determined by the following idea: Since the current quark mass is the only source of symmetry breaking, the quark term in the flow equation determines the symmetry breaking terms of the potential. The constituent quark mass can be expanded around a finite expectation value of the mesonic fields, which is chosen in the direction of the field σ,

$$\begin{aligned} M_q^2 &= g^2[(\sigma + m_c)^2 + \vec{\pi}^2] = g^2[(\sigma + \sigma_0 - \sigma_0 + m_c)^2 + \vec{\pi}^2] \\ &= g^2[(\sigma_0 + m_c)^2 + 2m_c(\sigma - \sigma_0) + (\sigma^2 + \vec{\pi}^2 - \sigma_0^2)]. \end{aligned} \tag{3.23}$$

We have rescaled m_c by a factor g for convenience, so that the physical current quark mass is given by gm_c. From this expression, we read off that the contributions to the potential from the fermionic terms in the flow equations can all be expressed in terms of powers of the combinations $(\sigma^2 + \vec{\pi}^2 - \sigma_0^2)$ for the symmetric part and $(\sigma - \sigma_0)$ for

the symmetry-breaking parts. Therefore we make the ansatz

$$U_k(\sigma, \vec{\pi}^2, L_t, L) = \sum_{i=0}^{N_\sigma} \sum_{j=0}^{[\frac{1}{2}(N_\sigma - i)]} a_{ij}(k, L_t, L)(\sigma - \sigma_0)^i (\sigma^2 + \vec{\pi}^2 - \sigma_0^2)^j \quad (3.24)$$

for the meson potential. We show in App. E that this ansatz for the meson potential is indeed sufficient to capture all contributions in the RG flow which arise due to the explicit symmetry breaking through the current quark mass m_c. As we mentioned in the last section, the vacuum expectation value σ_0 is nothing but the pion decay constant. We stress that σ_0 depends on L, L_t, and k as well. The flow equations for the coefficients of the potential are derived by inserting eq. (3.24) into the flow equation for the potential and comparing coefficients on both sides. In principle, such a projection results in an infinite set of coupled first-order differential equations for the coefficients $a_{ij}(k)$. In order to solve this set of equations, we have to truncate the sum in Eq. (3.24) by an appropriate choice for N_σ, where the smallest allowed choice is $N_\sigma = 2$.

It is worthwhile to discuss the calculation of the flow equations for the coefficients a_{ij} and the vacuum expectation value σ_0 in more detail. For this purpose, we define the expansion coefficients of the flow equations (2.80) and (2.82) as

$$\left(k\frac{\partial}{\partial k}U_k\right)^{ij} := \frac{1}{i!}\frac{1}{j!}\left(\frac{\partial}{\partial \sigma}\right)^i \left(\frac{\partial}{\partial \vec{\pi}^2}\right)^j k\frac{\partial}{\partial k}U_k\Bigg|_{\substack{\sigma=\sigma_0 \\ \vec{\pi}^2=0}}, \quad (3.25)$$

where we have suppressed the arguments of U_k. The flow equations for the coefficients a_{ij} in the ansatz for the potential are then given by

$$\begin{aligned}\left(k\frac{\partial}{\partial k}U_k\right)^{ij} = &\left(k\frac{\partial}{\partial k}a_{ij}\right) + a_{i+1,j}\left(-k\frac{\partial \sigma_0}{\partial k}\right)(i+1)(1-\delta_{N_\sigma,i}) \\ &+ a_{i,j+1}(j+1)\left(-2\sigma_0\, k\frac{\partial \sigma_0}{\partial k}\right)(1-\delta_{\frac{1}{2}(N_\sigma-i),j}) \end{aligned} \quad (3.26)$$

with the additional condition that $(1 + 2j) \leq N_\sigma$. From now on, we suppress the arguments of the coefficients a_{ij} for convenience. In order to ensure that the expansion around σ_0 corresponds to an expansion around the minimum of the potential, we have to enforce

$$\frac{\partial}{\partial \sigma}U_k\Big|_{\sigma=\sigma_0} = 0\,. \quad (3.27)$$

For the coefficients a_{10} and a_{01}, this translates into the condition

$$a_{10} + 2a_{01}\sigma_0 \equiv 0. \quad (3.28)$$

Due to this condition, only two of the three variables in the set $\{a_{10}, a_{01}, \sigma_0\}$ are independent, and the third one can be expressed in terms of the other two. Likewise, if we take the derivative of Eq. (3.28) with respect to the renormalization scale k, we get an equation which relates the flow of these three variables:

$$k\frac{\partial}{\partial k}a_{10} + 2a_{01}k\left(\frac{\partial}{\partial k}\sigma_0\right) + 2\sigma_0 k\frac{\partial}{\partial k}a_{01} = 0. \tag{3.29}$$

We can use this equation to replace the flow equation for a_{10} in the tower of equations given by Eq. (3.26). It is desirable to eliminate a_{10}, since σ_0 and a_{01} both correspond to observables we wish to obtain, namely the pion decay constant and the pion mass. In addition, with this replacement the system of differential equations can be solved more easily.

From the general expression for the flow equations Eq. (3.26), we find the particular equations governing a_{10} and a_{01}:

$$\left(k\frac{\partial}{\partial k}U_k\right)^{10} = k\frac{\partial}{\partial k}a_{10} - 2a_{20}\left(k\frac{\partial}{\partial k}\sigma_0\right) - a_{11}\left(2\sigma_0 k\frac{\partial}{\partial k}\sigma_0\right), \tag{3.30}$$

$$\left(k\frac{\partial}{\partial k}U_k\right)^{01} = k\frac{\partial}{\partial k}a_{01} - a_{11}\left(k\frac{\partial}{\partial k}\sigma_0\right) - 2a_{02}\left(2\sigma_0 k\frac{\partial}{\partial k}\sigma_0\right). \tag{3.31}$$

The flow equation for a_{10} is given by the first line in Eq. (3.30). It contains on the LHS only terms that are proportional to the symmetry-breaking current quark mass m_c. Because of this, a_{10} does not evolve in the chiral limit $m_c \to 0$. If it is initially zero at the UV scale, it remains zero on all scales. In this case, the condition (3.29) forces the coefficient a_{01} to vanish as soon as σ_0 acquires a finite expectation value. This corresponds to the appearance of exactly massless Goldstone bosons in case of spontaneous symmetry breaking, in accordance with our expectations for the chiral limit.

In order to derive a flow equation for the minimum of the potential σ_0, we combine the two equations in (3.30) and use eq. (3.29) to eliminate the k-derivatives of a_{10} and a_{01}:

$$\begin{aligned}\left(k\frac{\partial}{\partial k}U_k\right)^{10} &+ 2\sigma_0\left(k\frac{\partial}{\partial k}U_k\right)^{01} \\ &= -\left(k\frac{\partial}{\partial k}\sigma_0\right)\left(2a_{20} + 2a_{01} + 4a_{11}\sigma_0 + 8a_{02}\sigma_0^2\right).\end{aligned} \tag{3.32}$$

From the expressions for the meson masses, evaluated at the minimum of the potential, it can be seen that the expression in brackets, which multiplies the k-derivative of σ_0, is up to a constant factor the square of the σ-mass, M_σ^2. Therefore, this equation is always well-conditioned. The only exception is at the chiral symmetry breaking scale, where M_σ^2 drops sharply, if the explicit symmetry breaking is very small. For reasonably large pion masses, this is not a severe problem.

Finally, we discuss some features of our implementation of explicit symmetry breaking. Incorporating the explicit breaking of the chiral symmetry into the potential and the RG flow from the start has several advantages. The polynomial expansion discussed above evolves automatically from a potential with small symmetry breaking peaked around $\sigma_0 \approx 0$ to a potential with large symmetry breaking peaked at a value $\sigma_0 \approx f_\pi$. Without explicit symmetry breaking, the polynomial expansion in ϕ^2 has to be changed from a parametrization in terms of powers of ϕ^2 to $(\phi^2 - \phi_0^2)$ at the chiral symmetry breaking scale, see e. g. [78].

As we have already discussed in the last subsection, evolving the potential without symmetry breaking and shifting the minimum subsequently by means of a bosonized quark mass term in the effective action is not possible for a study of finite-volume effects in low-energy observables. For our purposes, we have to include explicit symmetry breaking in the RG flow on all scales since, otherwise, divergences from massless Goldstone bosons would restore the symmetry in the limit $k \to 0$, in accordance with the fact that chiral symmetry is not spontaneously broken in finite volumes. In this context, we would like to point out that even in the absence of a symmetry breaking term, the pion decay constant does not remain zero on all renormalization scales k. On some intermediate scale below the chiral symmetry breaking scale, where the quantum fluctuations are only partially integrated out, it acquires a nonzero value, and chiral symmetry is spontaneously broken. However, the emergence of exactly massless Goldstone bosons dominates the infrared evolution of the potential and counteracts the formation of a symmetry breaking quark condensate.

Last but not least, our implementation of symmetry breaking is numerically advantageous. When the potential is expanded in a polynomial in a theory with exactly massless Goldstone bosons, divergences appear in the flow equations for the coefficients of operators of mass dimension higher than four [132]. As an added benefit of including explicit symmetry breaking, the presence of a finite pion mass regulates these IR divergences.

3.4.3 Numerical Evaluation

We have solved the RG flow equations numerically and present the results for the volume dependence of the pion mass and the pion decay constant in the following sections. For the numerical evaluation, we have used the polynomial ansatz for the effective potential given in eq. (3.24), and expanded up to fourth order in the fields:

$$\begin{aligned} U_k(\sigma, \vec{\pi}^2) &= a_{00}(k) + a_{01}(k)(\sigma^2 + \vec{\pi}^2 - \sigma_0^2) + a_{02}(k)(\sigma^2 + \vec{\pi}^2 - \sigma_0^2)^2 \\ &\quad + a_{10}(k)(\sigma - \sigma_0) + a_{20}(k)(\sigma - \sigma_0)^2 + a_{30}(k)(\sigma - \sigma_0)^3 + a_{40}(k)(\sigma - \sigma_0)^4 \\ &\quad + a_{11}(k)(\sigma - \sigma_0)(\sigma^2 + \vec{\pi}^2 - \sigma_0^2) + a_{21}(k)(\sigma - \sigma_0)^2(\sigma^2 + \vec{\pi}^2 - \sigma_0^2)\,. \end{aligned} \tag{3.33}$$

Here, we first discuss our choice of model parameters at the UV scale, and some details of the numerical evaluation.

Λ_{UV} [MeV]	m_{UV} [MeV]	λ_{UV}	gm_c [MeV]	f_π [MeV]	m_π [MeV]
1500	779.0	60	2.10	90.38	100.8
1500	747.7	60	9.85	96.91	200.1
1500	698.0	60	25.70	105.30	300.2

Table 3.1: Values for the parameters at the UV scale used in the numerical evaluation. The parameters are determined in infinite volume by fitting to a particular pion mass and the corresponding value of the pion decay constant, taken from chiral perturbation theory. Note that in our notation, the physical current quark mass corresponds to gm_c.

The UV scale itself is determined from physical considerations as the scale below which a description of QCD with hadronic degrees of freedom is appropriate. Here, we choose $\Lambda = 1.5$ GeV. At the ultraviolet scale Λ, the free parameters of the quark-meson-model are the meson mass m_{UV}, the four-meson-coupling λ_{UV}, and the current quark mass gm_c, which controls the degree of explicit symmetry breaking. The Yukawa coupling g does not evolve in the present approximation [59, 123, 78]. We choose $g = 3.26$, which leads to a reasonable constituent quark mass of $M_q = g(f_\pi + m_c) \approx 310$ MeV for physical values for the pion decay constant $f_\pi = 93$ MeV and the current quark mass $gm_c = 7$ MeV.

In table 3.1, we summarize the three parameter sets which we used in obtaining our results for pion masses of 100, 200 and 300 MeV. We determine these UV parameters by fitting to a particular value for the pion mass $m_\pi(\infty)$ and to the corresponding value for the pion decay constant $f_\pi(\infty)$ in infinite volume. We then evolve the RG equations with these parameters to predict the volume dependence of $f_\pi(L)$ and $m_\pi(L)$.

For any value of the pion mass, the corresponding value of the pion decay constant is taken from chiral perturbation theory [98]. The pion mass is mainly controlled by the value of the current quark mass, which parametrizes the symmetry breaking. The current quark mass gm_c varies from approximately 2 MeV for a pion mass of 100 MeV to about 10 MeV for $m_\pi = 200$ MeV, and it has to be increased to approximately 25 MeV for $m_\pi = 300$ MeV. To achieve the correct corresponding values for the pion decay constant, the meson mass at the UV scale has to be decreased from approximately $m_{UV} = 780$ MeV to $m_{UV} = 700$ MeV, while the pion mass increases from 100 to 300 MeV. The four-meson-coupling λ_{UV} is fixed. We have checked that our results are to a very large degree independent of the particular choice of UV parameters: Different sets of parameters leading to the same values of the low-energy constants in the infinite volume, give the same volume dependence.

Although it facilitates the comparison to chiral perturbation theory, it is not necessary as a matter of principle to use results from chiral perturbation theory for the mass dependence of the pion decay constant. However, as has been found for infinite volume, in order to correctly describe the behavior of the pion decay constant as a function of a single symmetry breaking parameter, it is necessary to go beyond the

approximation of a constant expectation value for the meson field, which we used here, and to include wave function renormalizations in the RG flow. In infinite volume, it was recently shown that the inclusion of the wave function renormalizations in the RG flow makes it possible to recover the correct prefactors of chiral logarithms [112], in agreement with chPT. Such an approach is more powerful than the present one, since in addition to the volume dependence, it predicts the dependence of m_π and f_π on the symmetry breaking parameter m_c. We stress that even in such an approach, it remains necessary to fit the parameters at the UV scale to reproduce the correct values of the low energy constants. Thus, for example the value of the pion decay constant in the chiral limit is not a prediction of the model, but a necessary input to constrain its parameters. The full set of RG-equations, including the wave function renormalization and coupling constant renormalization equations, would reduce the input parameters to the four-fermion coupling and the current quark mass at the UV scale. In connection with the symmetry breaking ansatz Eq. (3.24), these equations are more complicated and have not yet been worked out.

A limit on the possible values of the current quark mass is given by the requirement that all masses, in particular the sigma-mass, must remain substantially smaller than the ultraviolet cutoff $\Lambda_{UV} \approx 1500$ MeV of the model. For a pion mass of $m_\pi = 300$ MeV, we find $m_\sigma \approx 800$ MeV.

With regard to the UV cutoff, we find only a slight dependence of our results for reasonably large volumes, provided we use anti-periodic boundary conditions for the quark fields in spatial directions. When we change the cutoff from $\Lambda_{UV} = 1500$ MeV to $\Lambda_{UV} = 1100$ MeV, our results for the relative shift of the pion mass in the finite volume change little. The change in the pion mass from a variation of the cutoff is of the order of less than 1% for $L > 2$ fm, and approximately 6% at $L = 1$ fm for the largest pion mass we considered here, $m_\pi = 300$ MeV. For smaller pion mass, the dependence on the UV cutoff becomes weaker, for $m_\pi = 100$ MeV it is negligible on the scale of our results. This is due to the fact that a higher degree of explicit symmetry breaking leads to more massive particles for which a smaller value for the UV momentum cutoff becomes more relevant.

For a choice of periodic boundary conditions, however, the cutoff dependence of the results is somewhat more pronounced, in particular for small volumes when the Euclidean time extent is kept large. Varying the cutoff between 1.5 GeV and 1.1 GeV for a pion mass of $m_\pi(\infty) = 300$ MeV, we find that the largest variations are of the order of $5 - 6\%$ of the pion mass, and take place in a volume range of $L = 0.5 - 1.0$ fm, depending on the exact ratio $1/(LL_t)$ of time and space extent. As we argue in the next section, this is mainly due to effects on the quark condensation: for periodic boundary conditions, a larger UV cutoff allows for the build-up of a larger condensate in finite volume, since for any given volume, a larger number of momentum modes $2\pi|\vec{n}|/L$ remain below the cutoff and contribute. In a volume region where the quarks dominate the finite volume effects, a certain cutoff dependence of these effects is therefore expected in this model.

3.5 RG Study of Finite-Volume Effects

3.5.1 RG Flow in a Finite Volume

The results of the RG flow equations for the evolution with the infrared cutoff scale k give a picture of chiral symmetry breaking which reflects the formation of the quark condensate for higher momenta and the effects of pion fluctuations at low scales. Figure 3.4 shows the masses of the pion and sigma, and the pion decay constant as a function of the renormalization scale k, for a value of $m_\pi = 100$ MeV, in the infinite volume limit. Starting at the UV scale Λ_{UV} and proceeding towards smaller values of k, we observe that the pion decay constant f_π grows rapidly around the chiral symmetry breaking scale $k_{\chi SB} \sim 800$ MeV, begins to flatten between $600-400$ MeV, and becomes almost completely flat below 300 MeV. Generally, massive degrees of freedom decouple from the renormalization group flow at a momentum scale given by the value of their mass m, i.e. they do not contribute to the renormalization for $k < m$. This can be seen clearly in the flow of f_π. As soon as the renormalization scale is of the order of the constituent quark mass (approximately 300 MeV), the quarks are no longer dynamical degrees of freedom and f_π becomes essentially constant. The RG flow of the mass of the heaviest meson, the sigma, is in several respects very similar to the flow of f_π. Its slope is also initially large at the chiral symmetry breaking scale and starts to decrease between $600 - 400$ MeV as well. The value of the sigma-mass reaches a maximum at k slightly above 300 MeV. Its decrease below this scale is due to the light pion with a mass of 100 MeV, which remains in the evolution as the only dynamical degree of freedom. When the pion mass is increased, the drop in the sigma-mass below the scale set by the constituent quark mass becomes much less pronounced. For $m_\pi \approx m_q \approx 300$ MeV, $m_\sigma(k)$ is essentially a flat function of k after it has reached its maximum.

In finite spatial volumes, a similar behavior can be observed. For the introductory discussion in this subsection, we restrict ourselves to finite spatial volumes and anti-periodic boundary conditions for the quarks in spatial directions. In the subsequent sections, we will also study the effects of different boundary conditions for the quarks in volumes where we use an anisotropic compactification of space-time in the Euclidean and the spatial directions. In Fig. 3.5 the meson masses and the pion decay constant are shown as a function of the scale $1/L$ set by the finite spatial volume. In these results all quantum fluctuations are integrated out completely, i. e. the scale k is removed. Now let us consider a finite value of k, where the quantum fluctuations are only partially integrated out. The scale $1/L$ introduced by the finite volume is in competition with the renormalization scale k. As soon as k drops below π/L, the renormalization scale no longer controls the renormalization flow. We can interpret the results shown in Fig. 3.5 roughly as an instant picture of the k-flow arrested at a scale $k = \pi/L$. However, this correspondence is not one-to-one: while the cutoff k affects both bosonic and fermionic fields in the same way, this is not true for $1/L$. Since there are no zero modes for fields with anti-periodic boundary conditions, the fermionic

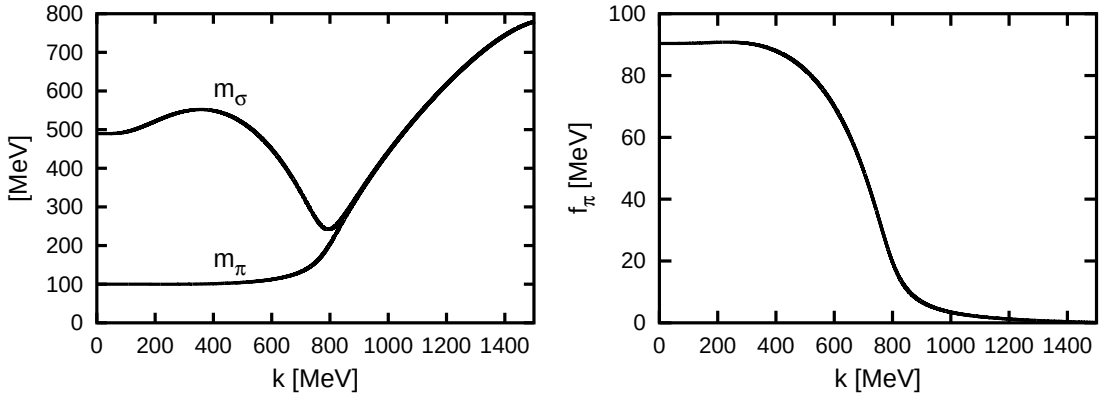

Figure 3.4: degrees of freedom and the pion decay constant as a function of the renormalization scale k in infinite volume. The chiral symmetry breaking scale can be clearly identified as the scale at which the mass of the heaviest meson (the σ) has a minimum. For this figure, we have chosen $m_\pi(\infty) = 100$ MeV and $f_\pi(\infty) = 90.4$ MeV.

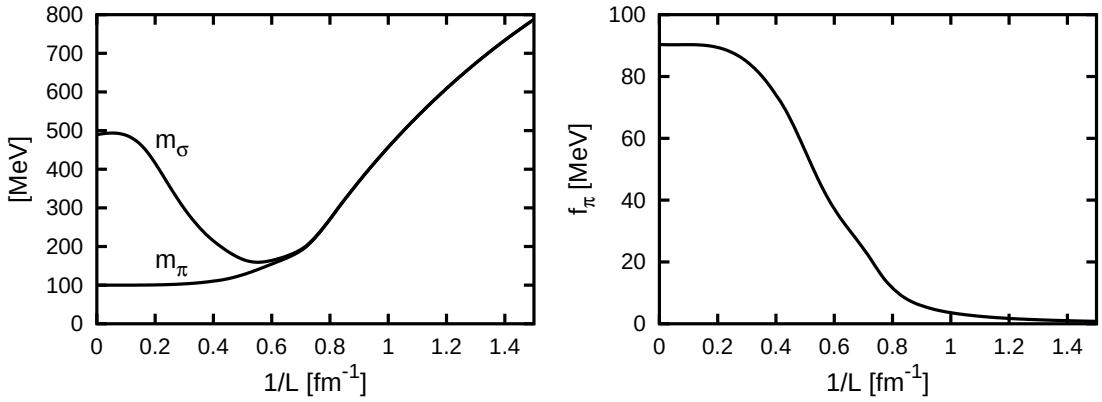

Figure 3.5: Masses of the mesonic degrees of freedom and the pion decay constant as a function of the inverse box size $1/L$. The results are obtained by completely integrating out all quantum fluctuations ($k \to 0$) at fixed L. As soon as $k < 1/L$, the box size becomes the controlling scale, and in the limit $k \to 0$ it is the only scale that remains. As for the preceding figure, we show the results with $m_\pi = 100$ MeV and $f_\pi = 90.4$ MeV for $k \to 0$ and $L \to \infty$.

fields are more strongly affected by this cutoff than the mesons. For the mesons, the scale $\frac{2\pi}{L}$ imposes only a minimum value for the smallest non-zero momentum mode. For the fermionic fields, on the other hand, the lowest momentum mode $\sqrt{3}\pi/L$ can effectively "freeze" the quark fields already above the constituent quark mass scale and no condensation of quarks takes place. For very small volumes $1/L > 0.5$ fm^{-1}, the suppression of quark condensation by the large cutoff becomes the dominating effect, and therefore chiral symmetry is approximately restored. A more subtle effect can also be seen in the behavior of the sigma-mass. While the sigma-mass has a maximum in the k-flow at a value of $m_\sigma \approx 600$ MeV, from which it drops to $m_\sigma \approx 500$ MeV due to the pion fluctuations, there is no corresponding maximum in the $1/L$-dependence. With increasing $1/L$ the pions hardly feel the constraints of the finite volume, but the momentum scale at which the quarks decouple increases consistently. Therefore the pion contributions at low momenta have a greater effect in the RG flow, since the k-region, in which they are the only relevant degrees of freedom, becomes larger. Through this effect, the pions also contribute toward the restoration of chiral symmetry for small volumes.

3.5.2 Influence of the Quark Boundary Conditions

We have calculated the relative pion mass shift

$$R[m_\pi(L)] = \frac{m_\pi(L) - m_\pi(\infty)}{m_\pi(\infty)} \tag{3.34}$$

with both choices for the fermionic boundary conditions for three different pion masses, $m_\pi(\infty) = 100$, 200 and 300 MeV, and for infinite ($L_t/L \to \infty$) as well as for finite extent L_t of the Euclidean time axis with different ratios $L_t/L = 3/1$, $3/2$, $1/1$. Note that L_t is related to the temperature T of the system by $L_t = 1/T$.

In Fig. 3.6, we show the results for the pion mass shift with periodic boundary conditions as a function of the box size L. The three panels show the results for the three different pion masses we investigated, and the curves are labeled with the ratios L_t/L. The main observation is that in this case, for certain volume ranges, the mass of the pion in the finite volume can be *lower* than in infinite volume. In particular, this is the case for pion masses $m_\pi(\infty) \geq 200$ MeV, ratios $L_t/L \geq 3/2$, and volumes smaller than 2 fm: $R[m_\pi(L)]$ takes on negative values and develops a minimum. This can be seen in the lower two panels of Fig. 3.6. Secondly, we note that this minimum in the mass shift becomes deeper for larger pion masses $m_\pi(\infty)$, and the corresponding larger values of $f_\pi(\infty)$. For $m_\pi(\infty) = 300$ MeV, the pion mass shift reaches down to approximately $R[m_\pi] = -0.14$ at $L = 0.7$ fm.

In Fig. 3.7, we compare the results for the pion mass shift with periodic (p) and anti-periodic (ap) boundary conditions for the fermion fields, for the ratios $L_t/L = 3/2$ and $L_t/L = 1/1$. Clearly, employing periodic boundary conditions lowers the relative mass shift $R[m_\pi(L)]$, compared to using anti-periodic boundary conditions. The differences

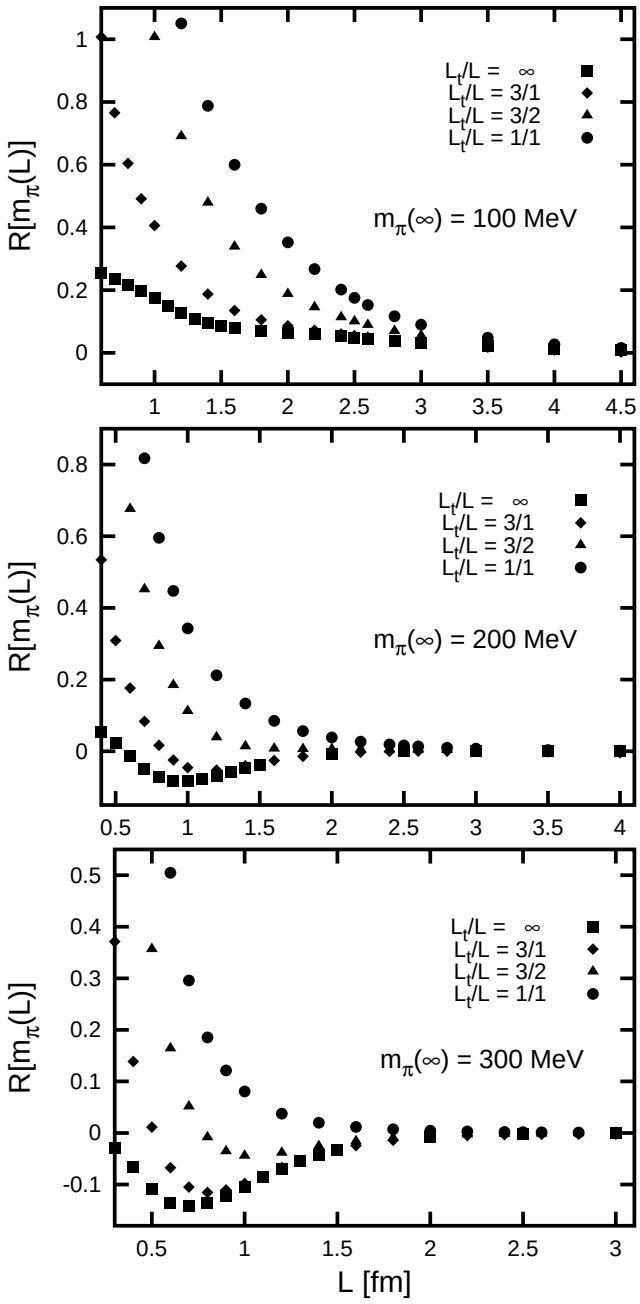

Figure 3.6: Results for the pion mass shift $R[m_\pi(L)] = (m_\pi(L) - m_\pi(\infty))/m_\pi(\infty)$, in a finite Euclidean volume of size $V = L^3 \times L_t$, for periodic boundary conditions. The ratio of L_t/L for the different curves is given in the figure. We show the results for pion masses of $m_\pi(\infty) = 100, 200, 300$ MeV (identified in the figure).

become larger in smaller volumes, for larger pion masses $m_\pi(\infty)$, and with increasing ratios L_t/L. As we have seen in Fig. 3.6 for large pion masses, the pion mass shift becomes negative, if the length of the box in the Euclidean time direction is taken to infinity.

Although at first a surprising result, this shift to smaller pion masses can actually be explained in the framework of the quark-meson model and its mechanism of chiral symmetry breaking. In order to show this, we resort to a version of the model that is simplified compared to our ansatz (3.24), but still contains the same essential structure. In this model, for a fixed symmetry breaking parameter gm_c, the pion mass is completely specified by the scale-dependent order parameter $\sigma_0(k, L)$, and by the values given at the UV scale for the coupling g and the meson mass m^2_{UV}. According to [133, 37], it is

$$M^2_\pi(k, L) = \frac{m_c m^2_{UV}}{\sigma_0(k, L)}. \tag{3.35}$$

For periodic boundary conditions, the "squeezing" of the quark fields in a small finite volume leads to an increase in the chiral quark condensate, before a further decrease of the volume size induces a restoration of chiral symmetry. Following eq. (3.35), the increase in the order parameter leads in turn to the observed decrease in the pion mass. In Fig. 3.8, we show the finite-volume shift $R[f_\pi(L)]$ of the pion decay constant $f_\pi(L) \equiv \sigma_0(L)$ which is defined as

$$R[f_\pi(L)] = \frac{f_\pi(L) - f_\pi(\infty)}{f_\pi(\infty)}\,. \tag{3.36}$$

Indeed, we observe an increasing pion decay constant $f_\pi(L) \equiv \sigma_0(L)$ exactly for those values of L for which the pion mass decreases.

The intermediate increase in the order parameter with the decreasing volume size can be explained more rigorously from the RG flow equations. Since this increase occurs in volumes that are already quite small, the flow is dominated by the zero-momentum modes and it is sufficient to analyze the contributions of these modes.

The zero mode contribution to the flow equation (indicated by the index 0 on the LHS) from quarks and mesons is for purely periodic boundary conditions in spatial directions given by

$$\begin{aligned}\left[k\frac{\partial}{\partial k}U_k(\sigma, \vec{\pi}^2, L, L_t)\right]_0 \;=\; & -\frac{k^{2(a+1)}}{L_t L^3}\left(2 \cdot \frac{4N_c N_f}{(k^2 + \nu_0^2 + M_q(\sigma, \vec{\pi}^2)^2)^{(a+1)}}\right. \\ & \left. -\frac{N_f^2 - 1}{(k^2 + M_\pi(\sigma, \vec{\pi}^2)^2)^{(a+1)}} - \frac{1}{(k^2 + M_\sigma(\sigma, \vec{\pi}^2)^2)^{(a+1)}}\right),\end{aligned} \tag{3.37}$$

where $\nu_0^2 = (\pm\pi/L_t)^2$ corresponds to the value of the two Matsubara frequencies closest to zero and a specifies the proper-time cutoff function given by Eq. (2.84). Note that

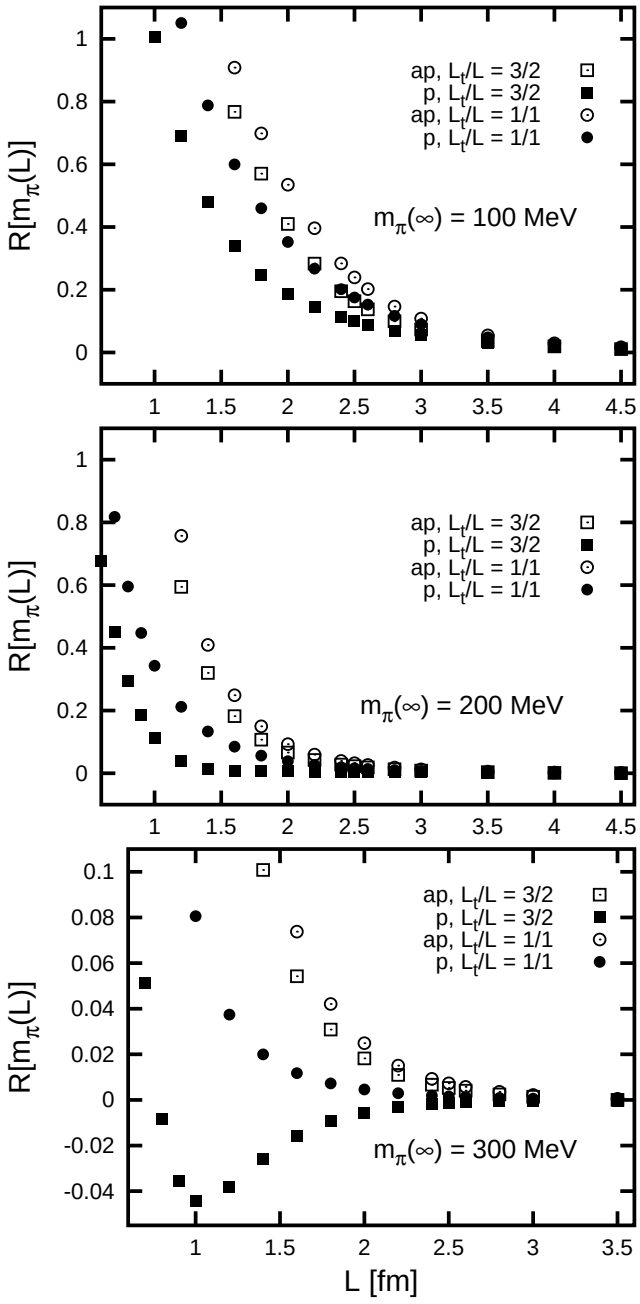

Figure 3.7: Comparison of the pion mass shift in finite volume $R[m_\pi(L)] = (m_\pi(L) - m_\pi(\infty))/m_\pi(\infty)$ for the two choices of fermionic boundary conditions. Open symbols denote results for anti-periodic, solid symbols for periodic boundary condition. The size of the volume is $V = L^3 \times L_t$, the ratios of L_t/L for the different curves are given in the figures. We show results for pion masses of $m_\pi(\infty) = 100, 200, 300$ MeV (identified in the figure).

$M_\pi(\sigma,\vec{\pi}^2)$ and $M_\sigma(\sigma,\vec{\pi}^2)$ depend on the scales k, L and L_t through their dependence on the expansion coefficients of the potential. In contrast, $M_q^2(\sigma,\vec{\pi}^2) = g^2[(\sigma+m_c)^2+\vec{\pi}^2]$ does not depend on these scales, since we are working in the local potential approximation[2]. The prefactor $1/L^3$ diverges for $L\to 0$ for all momentum modes, but enhances only the zero modes: Due to the factors $1/L^2$ of the momentum terms in the denominators, the enhancement is canceled for the non-zero momentum modes, and they are in fact strongly suppressed. If we scale L_t proportional to L, this suppression occurs also for the lowest fermionic terms because of the Matsubara frequencies, although it is much weaker. The result of this competition between suppression and enhancement for the fermions depends on the ratio L_t/L.

We first consider exclusively the contributions of the fermionic zero modes, which exist only for periodic boundary conditions:

$$\left[k\frac{\partial}{\partial k}U_k(\sigma,\vec{\pi}^2,L_t,L)\right]_0^F = -\frac{k^{2(a+1)}}{L_tL^3}\cdot 2\cdot\frac{4N_cN_f}{(k^2+\nu_0^2+M_q^2(\sigma,\vec{\pi}^2))^{a+1}}\,. \tag{3.38}$$

This truncation to the fermionic contributions only is equivalent to the leading term of a large N_c-approximation, as was shown for infinite volume in Ref. [80] and for finite volume in Ref. [134].

In principle, Eq. (3.38) can be integrated analytically, since the constituent quark mass does not depend on any scale-dependent quantities. The result shows that the zero mode contributions to the potential as a function of the expectation value are *repulsive* for small values. Consequently, these contributions increase the expectation value $\sigma_0(k,L,L_t)$ and thus the value of the pion decay constant. Since these zero-momentum contributions are enhanced for small volumes, this explains the increase in the expectation value.

Alternatively, the increase of $\sigma_0(k,L,L_t)$ can be understood in more detail by a direct analysis of the zero mode contributions to the flow equation for the minimum $\sigma_0(k,L,L_t)$ of the potential. Since the flow equation for $\sigma_0(k,L)$ is obtained from the minimum condition

$$\frac{\partial}{\partial\sigma}U_k(\sigma=\sigma_0\,,\vec{\pi}^2=0,L,L_t)=0, \tag{3.39}$$

it is determined by the flow of the potential. As we have seen in our analysis above, the fermionic contributions tend to increase the absolute value of the minimum $\sigma_0(k,L)$, while the mesonic contributions tend to decrease it. Thus, we can perform this analysis entirely by considering the zero mode part of the potential flow given in eq. (3.37).

The renormalization scale k controls the momenta of the quantum fluctuations that are integrated out. As soon as this momentum scale drops below the mass of one of the

[2]We stress that this does not mean that the constituent quark mass is independent of the scales k, $1/L$ and $1/L_t$. The constituent quark mass is obtained by evaluating the expression for $M_q^2(\sigma,\vec{\pi}^2)$ at the minimum of the potential which, of course, depends on k, L and L_t.

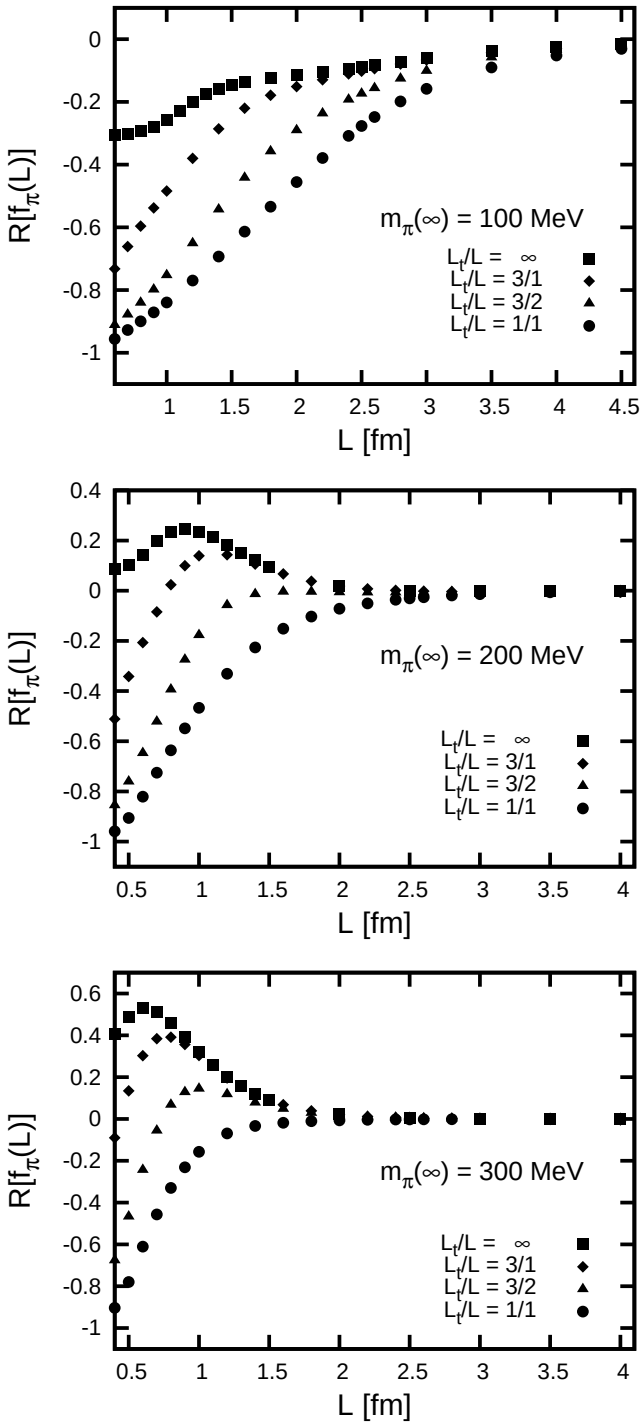

Figure 3.8: Results for the finite-volume shift of the pion decay constant $R[f_\pi(L)] = (f_\pi(L) - f_\pi(\infty))/f_\pi(\infty)$, in a finite Euclidean volume of size $V = L^3 \times L_t$, for periodic boundary conditions. The ratio of L_t/L for the different curves is given in the figure. We show the results for pion masses of $m_\pi(\infty) = 100, 200, 300$ MeV (identified in the figure).

degrees of freedom, that particular field can no longer contribute to the RG evolution of the running couplings: it decouples from the RG flow. We restrict the discussion here to scales $k < m_\sigma$, where the sigma meson has already decoupled.

With periodic boundary conditions, the finite box length in the Euclidean time direction L_t is the only scale which affects the zero modes. The scale π/L_t is in competition with the renormalization scale k, and if k drops below this scale, the lowest Matsubara frequency $\nu_0 = \pi/L_t$ acts as a cutoff and stops that part of the evolution which is driven by the quark fields. If L_t is sufficiently small, this happens already above the scale at which chiral symmetry breaking sets in. In that case, condensation of the quark fields is prevented, and the constituent quark mass remains small. This means that $m_\pi(k \to 0, L, L_t)$ remains large and that $R[m_\pi(L)]$ is large and positive. This is illustrated by the results for $L_t/L = 1/1$ and small L in Fig. 3.6.

The situation is different for large values of $L_t/L > 3/2$. Here, the additional scale set by $1/L_t$ plays a less important role and becomes relevant only for much smaller volumes. In this case, quarks build up a large condensate. According to eq. (3.35), this increase in the chiral condensate leads to a decrease of the pion mass, which is visible in Fig. 3.6 for $L_t/L > 3/2$, $m_\pi(\infty) \geq 200\,\mathrm{MeV}$, and $L \geq 0.8\,\mathrm{fm}$. For large values of L_t/L, the decrease in the condensate for small volumes cannot be explained by the presence of the cutoff π/L_t for the quark fields alone. There is an additional mechanism that decreases σ_0 in such a way that chiral symmetry is broken less strongly. For very small volumes, the pion contributions in Eq. (3.37) dominate the flow of σ_0. Even for a large ratio L_t/L, this leads to a decrease in σ_0 and the observed rise in $R[m_\pi(L)]$ for small L.

For anti-periodic boundary conditions, we do not find any decrease of $R[m_\pi(L)]$ with decreasing finite volume size L for any value of L_t/L, as can be seen in the comparison in Fig. 3.7. In this case, two effects are responsible for the finite volume behavior: effects due to the quark condensation, and effects due to light pions which appear after the chiral condensate has been built up by the quark fields, see also the discussion in Subsec. 3.5.1. In contrast to the case of periodic boundary conditions, for anti-periodic boundary conditions the formation of the quark condensate is strongly suppressed by the existence of a lower bound for the fermionic momenta, which is $\sqrt{3}\pi/L$, see Eq. (3.16), and acts as an infrared cutoff. Consequently, for small L, fewer modes contribute to the chiral condensate. If in addition L_t/L is small, the condensate decreases further and we observe a larger mass shift $R[m_\pi(L)]$.

3.5.3 Comparison to Chiral Perturbation Theory

In this section, we compare our results for the volume dependence of the pion mass to those from chiral perturbation theory.

In Fig. 3.9, we show the pion mass shift as a function of the size L obtained from chPT and from our RG approach. (Note that Fig. 3.9 has a logarithmic scale, whereas Figs. 3.6 and 3.7 have linear scales.) We present results for different pion masses from RG calculations with both periodic and anti-periodic boundary conditions for

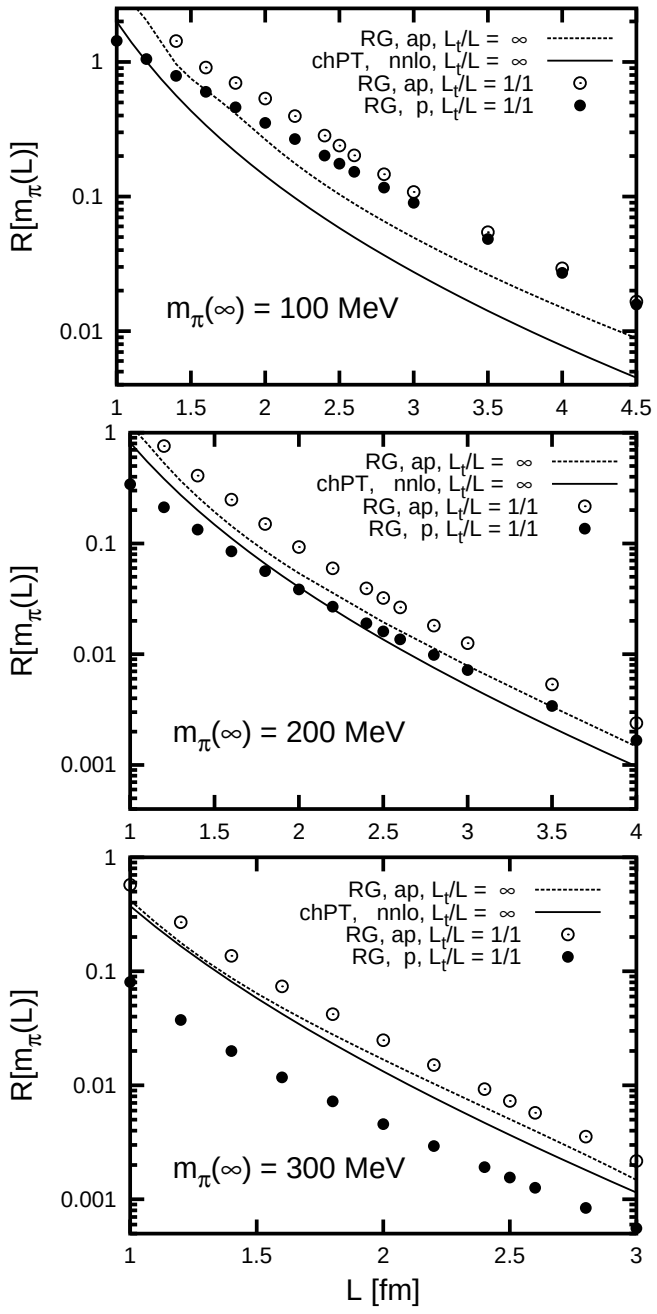

Figure 3.9: Comparison of the pion mass shift $R[m_\pi(L)] = (m_\pi(L) - m_\pi(\infty))/m_\pi(\infty)$ for different boundary conditions with the results of chiral perturbation theory [105] on a logarithmic scale. The ratio of L_t/L for the different curves is given in the figures. We show results for a pion mass of $m_\pi(\infty) = 100, 200, 300$ MeV (identified in the figure).

the fermions, and from chiral perturbation theory [98, 105]. For the chPT results, the pion mass shift is calculated with the help of Lüscher's formula [125]. As discussed in Sec. 3.2, Lüscher's formula relates the leading corrections of the pion mass in finite Euclidean volume to the $\pi\pi$ - scattering amplitude in infinite volume. The sub-leading corrections drop as $\mathcal{O}(e^{-\bar{m}L})$ with $\bar{m} \geq \sqrt{3/2}\, m_\pi$. Using a calculation of the $\pi\pi$-scattering amplitude in chPT to three loops (*nnlo*) as input for Lüscher's formula, the authors of Ref. [98] obtain a correction above the leading order, which is then added to the *exact* one-loop result of Gasser and Leutwyler [100]. In Fig. 3.9, we show the results from Ref. [98]. Lüscher's original approach only considers the periodicity of pion propagators in finite volume as an invariance under a shift by L. More recently, this has been improved to account for the fact that these propagators are actually invariant under shifts by $\vec{n}L$ with arbitrary $\vec{n}$ [105]. The result is a Lüscher formula resummed over $\vec{n}$. In Fig. 3.9, we compare our results to those from chiral perturbation theory for $L_t/L \to \infty$. We find the same slope, provided we impose anti-periodic boundary conditions on the fermionic fields. However, for periodic boundary conditions, our results clearly differ from chPT. This is an interesting result in light of the discussion of finite-volume effects in QCD by Gasser and Leutwyler [101]: They showed that the low-energy constants in the chPT Lagrangian remain unchanged from their values in infinite volume if one considers QCD in a finite Euclidean volume, provided the same anti-periodic boundary conditions as in the temporal direction are chosen as well in the spatial directions for the quark fields. This leaves open the possibility that the finite-volume behavior might change if one uses boundary conditions in spatial directions which differ from the anti-periodic ones in the temporal direction. Applying this argument to our results depicted in Fig. 3.9, we suggest that for anti-periodic boundary conditions the effective low-energy constants, which are relevant for the finite-volume effects in the pion mass, agree in both approaches. The differences observed between the RG results for periodic quark boundary conditions and the chPT results then might imply that the low-energy constants change for periodic boundary conditions.

In Tab. 3.2, we give the values for $R[m_\pi(L)]$ for $L = 2.0,\, 2.5,\, 3.0$ fm, $L_t \to \infty$ and three pion masses $m_\pi(\infty) = 100,\, 200,\, 300\,\mathrm{MeV}$. In addition, the table contains the results of chPT from an exact one-loop calculation for a finite volume [100], and the exact one-loop calculation with corrections in three-loop order obtained from chPT using Lüscher's formula [98]. Moreover, the table contains the results from our RG calculation with anti-periodic boundary conditions for the fermionic fields and the improved results from [105]. We observe that our results are consistently above those from chPT. However, the difference between the RG result and the loop expansion decreases with higher order in loops. In particular, the RG result is closer to the improved calculation [105] than to the "simple" loop calculations in chPT.

For a given volume size, Lüscher's approach becomes an increasingly better approximation with increasing pion mass. The decreasing differences between the chPT results and the RG results with increasing pion mass are compatible with this estimate. For large volumes, the mass shift is completely controlled by pion effects and

		$R[m_\pi(L)]$			
L [fm]	$m_\pi(\infty)$ [MeV]	RG	1L chPT	+(*nnlo-lo*)	resum. chPT
2.0	100	26.6×10^{-2}	8.74×10^{-2}	11.6×10^{-2}	14.2×10^{-2}
	200	5.38×10^{-2}	2.00×10^{-2}	3.31×10^{-2}	4.03×10^{-2}
	300	1.70×10^{-2}	0.56×10^{-2}	1.12×10^{-2}	1.32×10^{-2}
2.5	100	10.37×10^{-2}	3.85×10^{-2}	4.97×10^{-2}	5.84×10^{-2}
	200	1.95×10^{-2}	0.73×10^{-2}	1.17×10^{-2}	1.36×10^{-2}
	300	5.31×10^{-3}	1.65×10^{-3}	3.27×10^{-3}	3.67×10^{-2}
3.0	100	4.94×10^{-2}	1.91×10^{-2}	2.41×10^{-2}	2.75×10^{-2}
	200	7.85×10^{-3}	2.95×10^{-3}	4.65×10^{-3}	5.21×10^{-2}
	300	1.76×10^{-3}	0.54×10^{-3}	1.05×10^{-3}	1.14×10^{-3}

Table 3.2: Values for $R[m_\pi(L)]$, cf. eq. (3.1), the relative shift of the pion mass in finite volumes of $L = 2.0, 2.5, 3.0\,\text{fm}$ and $L_t \to \infty$, compared to the value in infinite volume, for pion masses of $m_\pi(\infty) = 100, 200, 300\,\text{MeV}$. We compare results from our RG calculation with anti-periodic boundary conditions for the fermionic fields to the exact one-loop chPT results of [100] for a finite volume (1L chPT), and the exact one-loop calculation with corrections in three-loop order obtained with chPT using Lüscher's formula [98] (1L chPT + (*nnlo-lo*)). The last column gives the improved results obtained from the resummed Lüscher-formula [105] (resum. chPT).

drops as $e^{-m_\pi L}$, so that both the RG and the chPT results have the same slope in the logarithmic plot. For the entire volume range shown in Fig. 3.9, the RG and chPT results apparently differ only by a factor which is almost independent of the volume size. For $m_\pi(\infty) = 300$ MeV, both agree within errors. For small volumes, however, the RG approach has the advantage that it can be extended to describe the transition into a regime with approximately restored chiral symmetry, where the chiral expansion becomes unreliable.

Compared to the quarks, the mesonic degrees of freedom are less affected by the ratio L_t/L. The upper curve in Fig. 3.9 represents RG calculations with anti-periodic boundary conditions and $L_t/L = 1/1$, which gives a larger $R[m_\pi(L)]$ compared to the lower curve corresponding to $L_t/L = \infty$. Fluctuations due to the light pions yield a decrease of the condensate and explain the increase of $R[m_\pi(L)]$ for larger volumes. In particular for small pion masses ($m_\pi = 100$ MeV) and the ratio $L_t/L = 1/1$, the results with periodic and with anti-periodic boundary conditions overlap over a wide volume range. From our analysis, for sufficiently small values of $m_\pi(\infty)$ this is expected in the region where pion dynamics dominate. Because of this, the slopes of the curves are very similar. The deviations between results at the same, fixed ratio L_t/L that differ only in the choice of boundary conditions become larger for increasing pion masses $m_\pi(\infty)$ and decay constants $f_\pi(\infty)$. This indicates that fermionic effects are increasingly important. Evidence for this is also the observation that the results for the pion mass shift with

periodic boundary conditions have a smaller slope, compared to the results with anti-periodic boundary conditions, and also compared to those of chPT. The reason is that the cutoff scales are different: for periodic boundary conditions, the lowest fermion momentum mode is given by the lowest Matsubara frequency $\nu_0 = \pi/L_t$, and not determined by $\sqrt{3}\pi/L$ as for anti-periodic boundary conditions. In particular for large values of L_t/L, this explains that the finite volume mass shift will be much larger for anti-periodic boundary conditions. For small volumes, we thus find the importance of quark effects confirmed by the dependence on the boundary conditions. But since pion effects dominate for larger volumes, the results of chPT and of our RG approach converge in this volume regime.

3.5.4 Comparison to Lattice QCD results

Apart from the general interest of finite volume effects, the main motivation for our investigation is its possible application to lattice gauge theory. At present, most lattice calculations are performed in volumes of the order of $L = 2-3$ fm. In recent systematic studies of finite volume effects done with Wilson fermions, the lightest pion masses are of the order of $m_\pi = 400 - 500$ MeV [111, 91, 135, 109, 92, 110]. With staggered fermions, pion masses as low as 250 MeV have been realized [136]. Simulations with fermions with good chiral properties such as domain-wall or overlap fermions have been done with pion masses as low as 180 MeV in the quenched approximation [137] and as low as 360 MeV with two fully dynamical flavors [138]. Because the finite volume effects depend on the mass of the lightest field, they become more severe for smaller pion masses. Thus, the better the statistical accuracy of these calculations, the more important it becomes to understand finite size effects and to control the finite size extrapolation.

Our model incorporates chiral symmetry and can still be used in the vicinity of the point where chiral symmetry is restored. Finite volume effects should therefore be captured as far as they relate to chiral symmetry breaking. But our model does not contain gauge degrees of freedom, there are no gluons, and consequently the constituent quarks in this model are not confined. There is no guarantee that the same mechanisms apply as in QCD. Since the model contains dynamical meson fields and chiral symmetry is broken in the usual way, our results can only be compared directly to those of unquenched lattice calculations with two dynamical quark flavors, where normal chPT is also applicable. However, qualitatively our arguments regarding the quark condensate may also have implications for quenched simulations, since a similar mechanism may apply.

For periodic boundary conditions, our results reproduce the qualitative behavior of the lattice results, but clearly differ from chPT, as can be read off from Figs. 3.6 and 3.9, respectively. For anti-periodic boundary conditions, they largely agree with chPT. The issue of finite volume effects has been addressed in several lattice studies [139, 126, 109, 92, 110]. The pion mass shift $R[m_\pi(L)]$ calculated by the ZeRo collaboration [92],

which is shown in Fig. 3.1, actually becomes negative and has a minimum at small volume sizes. Although this negative shift is small, the result seems to be significant. The minimum is most pronounced for small quark masses (at a hopping parameter of $\kappa = 0.1350$). The position of the minimum corresponds to $m_\pi L = 3.5$ or $L = 1.264\,\mathrm{fm}$ with $T/L = 2.25$. The results were obtained in the quenched approximation with periodic boundary conditions for the quark fields. Similar observations have also been made in [109, 110], where the simulations were performed with dynamical Wilson quarks.

In our calculation, such a decrease in the pion mass is reproduced if we choose periodic boundary conditions for the quarks. The minimum appears for large pion mass $m_\pi(\infty) = 300\,\mathrm{MeV}$, $L_t/L \geq 3/2$ and $L = 1\,\mathrm{fm}$, cf. Fig. 3.6. Our model suggests a mechanism for the appearance of this minimum, which may be the same mechanism as on the lattice. In contrast to our findings, however, the decrease of the pion mass in finite volume seems to be larger for smaller infinite-volume pion mass. For lattice calculations, several other mechanisms for finite volume mass shifts have been suggested, from an interaction of hadrons with their mirror states on a periodic lattice [139] to effects on quark propagation related to a breaking of the center symmetry of the gauge group [126].

The influence of boundary conditions for sea and valence quarks in lattice simulations was also studied by Aoki *et al.* [126]. They find that periodic boundary conditions lead to a lower mass shift than anti-periodic boundary conditions (see table III of [126]). This finding is in agreement with our results, as can be seen in Figs. 3.7 and 3.9. The actual pion mass on the lattice is very high ($> 1\,\mathrm{GeV}$). Different choices for the boundary conditions of sea and valence quarks make it possible for the authors to establish a connection between the mass shift and the expectation value that Polyakov loops acquire in the presence of sea quarks. They relate the large increase of the pion mass observed for small lattice size to the restoration of chiral symmetry. This is illustrated by their results for the chiral condensate (Fig. 10 of [126]), which decreases strongly in small volumes. In the same figure, the condensate may increase for intermediate volume size, which would be similar to the behavior of the order parameter seen in our simple model. We agree that the mass shift in small volumes is due to chiral symmetry restoration, and reproduce this result in our calculations.

Our RG approach improves our understanding of the mechanisms of finite volume effects in QCD, but cannot yet give a model independent extrapolation formula to relate finite lattice results to the hadronic world.

3.6 Quark-Meson Model at Finite Temperature

In this section, we use the quark-meson model for a first study of dynamical chiral symmetry breaking at finite temperature in QCD. In particular, we discuss the chiral phase transition in infinite and finite volume and its dependence on the pion mass in

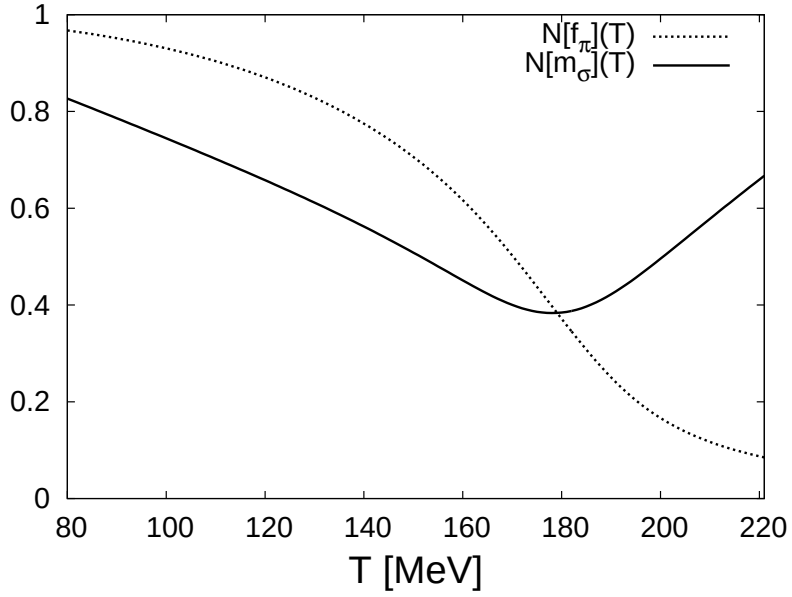

Figure 3.10: Normalized sigma mass $N[m_\sigma](T) = \frac{m_\sigma(T)}{m_\sigma(0)}$ and normalized pion decay constant $N[f_\pi](T) = \frac{f_\pi(T)}{f_\pi(0)}$ as a function of the temperature, in infinite volume for a pion mass $m_\pi^{(0)} = 100\,\mathrm{MeV}$.

Sec. 3.6.1 and 3.6.2, respectively. In Chapter 4, we will discuss this subject again in an approach that incorporates the presence of gluons at high energies.

3.6.1 Chiral Phase Transition Temperature in Infinite Volume

Let us start with a brief discussion of the dependence of the chiral phase transition temperature in infinite volume on the zero-temperature pion mass $m_\pi^{(0)} = m_\pi(T = 0)$. In order to define a chiral phase transition temperature in the presence of explicit symmetry breaking, we use the dependence of the sigma mass on the temperature. We define the phase transition temperature T_c through the minimum of the σ-mass,

$$\left.\frac{\partial m_\sigma(T)}{\partial T}\right|_{T=T_c} = 0 \quad \text{and} \quad \left.\frac{\partial^2 m_\sigma(T)}{\partial T^2}\right|_{T=T_c} > 0\,. \tag{3.40}$$

Alternatively, one can define the phase transition temperature as the turning point of the pion decay constant as a function of temperature[3]. We have checked that

[3]In finite volume, strictly speaking no phase transition is possible, since non-analyticities cannot appear in the thermodynamic potential. For this reason, there is no distinct point that allows for an unique definition for the crossover or the pseudo-critical temperature. For example, the critical temperature T_c can also be defined as the temperature at which f_π reaches half its zero-temperature

m_π [MeV]	0	50	100	150	200	250	300
T_c [MeV]	147.6	163.9	178.1	191.8	208.3	228.0	249.3
$R_c(m_\pi^{(0)})$	0	0.104	0.207	0.300	0.411	0.545	0.689

Table 3.3: Dependence of T_c and $R_c(m_\pi^{(0)}) = \frac{T_c(m_\pi^{(0)}) - T_c(0)}{T_c(0)}$ on $m_\pi^{(0)} = m_\pi(T=0)$.

the values for the chiral phase transition temperature T_c obtained from these two different definitions agree within a few percent. For example, in Fig. 3.10 we compare the normalized σ-mass $N[m_\sigma](T) = \frac{m_\sigma(T)}{m_\sigma(0)}$ and the normalized pion decay constant $N[f_\pi](T) = \frac{f_\pi(T)}{f_\pi(0)}$ for $m_\pi^{(0)} = 100\,\mathrm{MeV}$. One observes that both definitions for the critical temperature yield for practical purposes the same result.

In Tab. 3.3 and Fig. 3.11, we show[4] the chiral phase transition temperature T_c obtained in this way as a function of the pion mass $m_\pi^{(0)}$. We find that the transition temperature T_c depends on the pion mass in the following way,

$$T_c(m_\pi^{(0)}) = a_0 + a_1 m_\pi^{(0)} + a_2 (m_\pi^{(0)})^2 + \mathcal{O}((m_\pi^{(0)})^3), \tag{3.41}$$

where the parameters can be determined from a fit to our numerical results as

$$a_0 = 149.58\,\mathrm{MeV}, \quad a_1 = 0.24258, \quad a_2 = 0.00029\,\mathrm{MeV}^{-1}\,. \tag{3.42}$$

The constant a_0 is then the value for the chiral phase transition temperature in the chiral limit as obtained from the fit. A similar relation was also found in lattice simulations [15, 122] with two or three quark flavors. The corresponding relation is

$$\frac{T_c(N_f,\, m_{PS})}{\sqrt{\bar\sigma}} = \frac{T_c(N_f,\, m_{PS}=0)}{\sqrt{\bar\sigma}} + l_1(N_f)\frac{m_{PS}^{2/\beta\delta}}{\sqrt{\bar\sigma}} + \mathcal{O}(m_{PS}^2)\,, \tag{3.43}$$

where m_{PS} denotes the mass of the pseudoscalar meson, and the string tension $\bar\sigma$ is used to set the scale in the lattice calculation. β and δ are the critical exponents of the $O(4)$-model in three dimensions. The coefficient $l_1(N_f)$ depends only slightly on the number of quark flavors [15].

The analysis in Eq. (3.43) assumes that the transition falls into the $O(4)$ universality class, where the ratio of the critical exponents obeys $1/\beta\delta = 0.55$. Then, the first-order correction term is approximately linear, in agreement with our result. On the lattice, however, the coefficient of the approximately linear term is about one order of magnitude smaller than the result of our calculation. For $N_f = 3$, a lattice QCD

value [140]. The results for T_c obtained with such a definition will in essence agree with our results, as suggested by Fig. 3.10.

[4] We do not show lattice results for comparison in this figure since there is no data available for $m_\pi^{(0)} \leq 300$ MeV in Ref. [15].

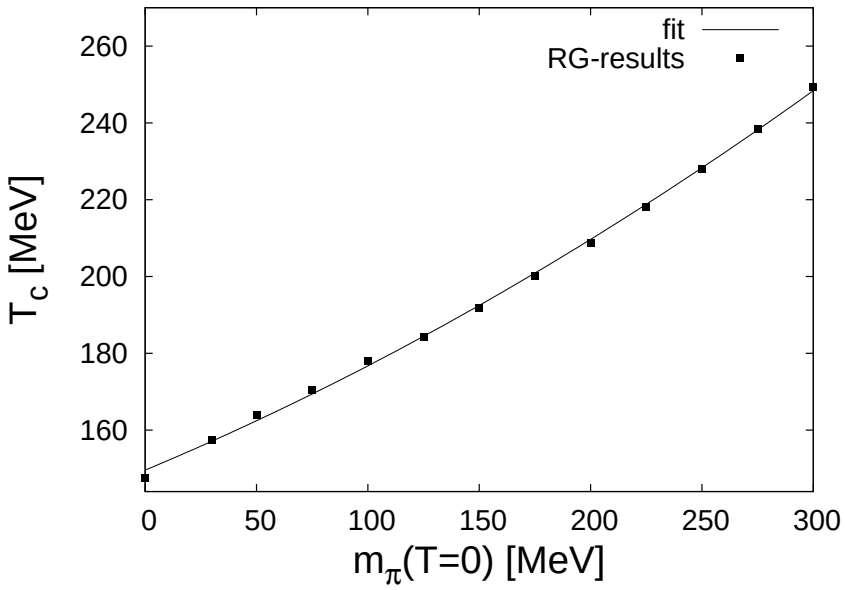

Figure 3.11: Chiral phase transition temperature T_c in infinite volume as a function of $m_\pi(T = 0)$. The dots show the result of our RG-calculation, and the line shows the result of the fit function defined in Eq. (3.41).

calculation [15] gives $l_1(N_f = 3) \approx 0.039$. While the exact value for $l_1(N_f = 2)$ is not given in [15], the authors point out that it is of the same order of magnitude as the value for $N_f = 3$.

As we will see in the next subsection, it is not possible to explain the smaller value of the (approximately) linear term found on the lattice as a finite volume effect: Since a finite volume effect is more severe for smaller pion masses and since it leads to a significantly reduced transition temperature in our model, we expect that the slope of $T_c(m_\pi^{(0)})$ should actually increase in a finite volume, compared to the infinite-volume result. We think that the discrepancy may be a consequence of neglecting the gauge sector in the quark-meson model. In the chiral limit, the chiral phase transition temperature on the lattice is about 30 MeV larger [15] than the value obtained in the quark-meson model[5].

Work on the quark-meson model within the Functional RG suggests that the transition temperature becomes even smaller if one includes wave function renormalizations [123]. This is the case even though the parameters of the model were adjusted in the same way as was done in this calculation[6]. In spite of the difference in the absolute

[5]The absolute values of the phase transition temperature are affected by the way how the scales in the corresponding calculation are fixed. A comparison of dimensionless quantities, such as the coefficient of the linear terms in Eq. (3.41) and Eq. (3.43), is more meaningful.

[6]There is also a dependence on the cutoff-function in the phase transition temperature [132, 134].

Reference	Method	T_c [MeV]
Chapter 3 of this thesis	Proper-time RG, quark-meson model	148
Berges (1997) [123]	Functional RG, quark-meson model	100.7
Schaefer (1999) [78]	Proper-time RG, quark-meson model	149
Braun (2003) [82]	Proper-time RG, quark-meson model	154
Schaefer (2004) [81]	Proper-time RG, quark-meson model	142
Chap. 4 of this thesis	Functional RG, QCD (see caption)	172
Gottlieb (1996) [121]	lattice $16^3 \times 8$ (staggered)	128 ± 9
Karsch (2000) [15]	lattice $16^3 \times 4$ (improved staggered)	173 ± 8
CP-PACS (2000) [141]	lattice $16^3 \times 4$ (improved Wilson)	171 ± 4
Bornyakov (2005) [142]	lattice $16^3 \times 8$ (improved Wilson)	173 ± 3

Table 3.4: Chiral phase transition temperature in the chiral limit ($m_\pi \to 0$) from different RG approaches for the quark-meson model and for QCD, and from lattice simulations. We have restricted our choice of lattice references to the case of $N_f = 2$ flavors that we have treated here. More recent lattice results have been obtained for $N_f = 2 + 1$ flavors, see e.g. [19, 115, 122]. The difference in the RG results arises from a weak dependence of T_c on the initial values at the UV scale and on the choice of the cutoff-function. In Chap. 4, the critical temperature is calculated from a study which incorporates the running QCD coupling and a complete basis of four-fermion interactions.

value, the slope of the function $T_c(m_\pi^{(0)})$ is roughly the same as in our study. This is an additional hint that neglecting the gauge degrees of freedom could indeed be responsible for the difference in the results from the quark-meson model compared to lattice calculations. We discuss this issue further in Sec. 4, where we apply the Functional RG to a study of the chiral phase boundary of QCD, which incorporates gluonic degrees of freedom and four-fermion interactions. As we will see, such a study shows reasonable agreement with results from lattice studies of the chiral phase transition temperature for two and three massless quark-flavors.

Results for T_c in the chiral limit from various lattice and RG approaches are summarized in Tab. 3.4. As can be seen from the table, there is some uncertainty in the value of the chiral phase transition temperature in lattice calculations, which is mainly due to different implementations of the fermions.

3.6.2 Chiral Phase Transition Temperature in Finite Volumes

Now we turn to the investigation of the chiral phase transition temperature in finite spatial volumes. As in section 3.6.1, we define the phase transition temperature T_c via the minimum of the sigma mass. Putting the system in a finite volume introduces an additional scale. Let us first discuss the influence of this additional length scale L

on the sigma- and pion-mass. In Fig. 3.12, we show the sigma- and pion-mass for $m_\pi^{(0)} = 100\,\mathrm{MeV}$ and with periodic boundary conditions for the quarks, as a function of the temperature, for both a small volume $L = 1\,\mathrm{fm}$ and a large volume $L = 4\,\mathrm{fm}$. The minimum of the sigma mass is clearly visible in the plot. Above the transition temperature T_c, where chiral symmetry is restored, the sigma- and pion-mass are degenerate, independent of the size of the volume. In order to gain a better understanding of the meson masses and their dependence on the scales L and T in this temperature regime, we extract the (perturbative) one-loop correction to the meson masses from the corresponding RG flow equation[7]. Since the chiral phase transition is a non-perturbative phenomena, such a one-loop calculation is not trustworthy in the vicinity of the critical temperature: The determination of the critical temperature fails, leading to an unphysical complex temperature [29]. Here, non-perturbative approaches are indispensable, as pointed out by earlier RG flow studies, e. g. Refs. [123, 78, 82], and a study in terms of many-body resummation techniques [124]. Moreover, we neglect the quark contributions in this calculation, since they are suppressed by the appearance of a thermal Matsubara mass. In contrast, the bosonic fields have a vanishing Matsubara mass and therefore their contributions are more important at high temperature. Thus our starting point for the calculation of the mass correction is the RG flow equation for the meson potential (3.17) without the quark contributions. The effective action, from which this "reduced" flow equation can be derived, follows immediately from the effective action (3.13) and reads

$$\Gamma[\phi] = \int d^4x \left\{ \frac{1}{2}(\partial_\mu \phi)^2 + \overbrace{\frac{1}{2}m^2\phi^2 + \frac{\lambda}{4}\phi^4}^{=U(\phi)} \right\}. \tag{3.44}$$

The $O(4)$-vector ϕ is given by $\phi = (\sigma, \vec{\pi})$. Since we have neglected the quark terms in the effective action, the terms in the meson potential (3.33) violating $O(4)$-symmetry drop out. The mass parameter m and the coupling λ in Eq. (3.44) are related to the couplings given in Eq. (3.33) by $m^2 = 2a_{01}$ and $\lambda = 4a_{02}$.

The mass correction $\delta m^2(T, L)$, which is due to finite volume and finite temperature effects, can be decomposed into a sum of two contributions, $\delta m_1^2(T, L \to \infty)$ and $\delta m_2^2(T, L)$. We refer to App. F for details of the calculation.

First, in the regime defined by $0 < \frac{1}{T} \ll L$, the contribution $\delta m_1^2(T, L \to \infty)$ dominates. One can estimate $\delta m_1^2(T, L \to \infty)$ for large temperatures and volumes as

$$\delta m_1^2(T, L \to \infty) \approx \frac{1}{2}\lambda T^2 \text{ for } T \to \infty\,. \tag{3.45}$$

In this case, the meson masses depend linearly on the temperature, in agreement with the result from Ref. [29].

[7] Thermal resummation techniques and their connection to the Functional RG have been recently discussed in Refs. [143, 144].

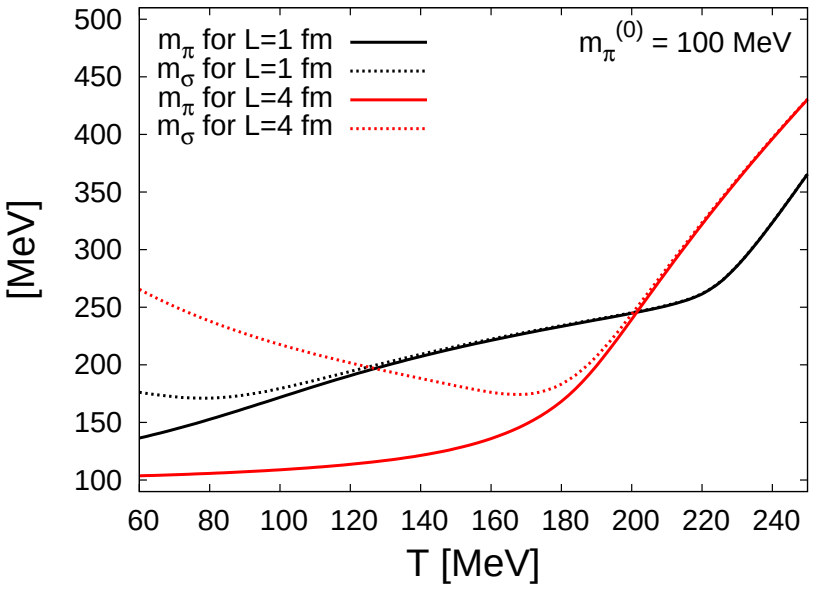

Figure 3.12: Sigma- and pion-mass as functions of the temperature T, with $m_\pi^{(0)} = 100$ MeV and periodic quark boundary conditions, for $L = 1$ fm and $L = 4$ fm. The solid black and the red (gray) lines show the pion mass for $L = 1$fm and $L = 4$ fm, respectively, whereas the dotted black and red (gray) lines show the sigma mass for $L = 1$ fm and for $L = 4$ fm.

Second, if the product $TL \sim \mathcal{O}(1)$, the mass correction is in essence given by

$$\delta m_2^2(T,L) \approx \frac{6\lambda}{(2\pi)^{\frac{3}{2}}}\frac{T}{L}\sum_{n=-\infty}^{\infty}{\sum_{\{l_i\}}}'\Big(\frac{(mL)^2+4\pi^2n^2(TL)^2}{\vec{l}^2}\Big)^{\frac{1}{4}}K_{\frac{1}{2}}\Big(\sqrt{\vec{l}^2((mL)^2+4\pi^2n^2(TL)^2)}\Big), \tag{3.46}$$

where K_n denotes the modified Bessel-functions with index $n = \frac{1}{2}$. The vector $\vec{l}$ is defined as $\vec{l} = \{l_1, l_2, l_3\}$ and the prime indicates that the term with $\vec{l} = 0$ is excluded from the summation. Note that $\delta m_2^2(T,L)$ has a complicated dependence on T and L, but we observe that it scales with $\frac{T}{L}$, rather than with T^2. This explains the difference between the slopes of the meson masses in the regime defined by $\frac{1}{T_c} > \frac{1}{T} \gtrsim L$, and in the regime defined by $0 < \frac{1}{T} \ll L$, which can be seen in Fig. 3.12. In contrast, in the limit $TL \gg 1$ one obtains

$$\delta m_2^2(T,L) \approx \frac{9\lambda}{\sqrt{2}\pi}\frac{T}{L}\sum_{n=-\infty}^{\infty}{\sum_{\{l_i\}}}'\frac{1}{\sqrt{\vec{l}^2}}\exp\Big(-\sqrt{\vec{l}^2((mL)^2+4\pi^2n^2(TL)^2)}\Big). \tag{3.47}$$

The contributions from the non-vanishing thermal Matsubara-modes to $\delta m_2^2(T,L)$ drop exponentially, and $\delta m_2^2(T,L)$ becomes a linear function in the temperature T, due to

the zeroth thermal Matsubara-mode $n = 0$. Therefore, for $TL \gg 1$, $\delta m_2^2(T, L)$ is a sub-leading correction to the meson masses, compared to the contribution $\delta m_1^2(T, L)$. This describes the results for periodic quark boundary conditions well.

The behavior of the meson masses for anti-periodic boundary conditions of the quarks fields in spatial directions is similar to the behavior for periodic boundary conditions depicted in Fig. 3.12 for large volumes. However, there is one essential difference between periodic and anti-periodic boundary conditions: As already discussed in Sec. 3.5, the quark fields have an additional IR cutoff which is given by the minimal spatial momentum

$$p_{ap}^{\min} = \frac{\pi}{L} \,. \tag{3.48}$$

This minimal momentum increases for decreasing volume sizes. The quark fields decouple from the RG flow as soon as the IR-cutoff scale k in Eq. (3.17) drops below $p_{ap}^{\min}$ and the mesons are the only dynamical degrees of freedom in the theory for $k \leq p_{ap}^{\min}$. This additional IR cutoff is responsible for the fact that the quark condensate for a given L is smaller in the case of anti-periodic boundary conditions than for periodic boundary conditions. Therefore the chiral phase transition temperature for anti-periodic boundary conditions is for a given L always smaller than for periodic boundary conditions.

We now present our main results for the volume dependence of the chiral phase transition temperature. Fig. 3.13 contains plots of the transition temperature T_c as a function of the volume size, for different values of the pion mass at zero temperature, $m_\pi^{(0)}$, and for different choices for the quark boundary conditions. For small, realistic pion masses, $m_\pi^{(0)} = 100\,\mathrm{MeV}$, the results for T_c in the upper panel of Fig. 3.13 show a deviation from its infinite volume value of about 6% already for $L = 4\,\mathrm{fm}$ and independent from the choice of boundary conditions. For small volume sizes defined by $m_\pi^{(0)} L < 1$, we observe that the phase transition temperature T_c is strongly affected by the choice of the boundary conditions for the quark fields. For anti-periodic boundary conditions, T_c decreases strongly for small volume sizes. As already discussed above, this is because of the additional infrared cutoff $p_{ap}^{\min}$ for the momenta of the quark fields. For small volumes, it is due to this additional IR-cutoff that the system remains in the phase with approximately restored symmetry.

For periodic quark boundary conditions, we observe a weaker volume dependence of T_c, since the condensation of the quarks is not prevented by the additional IR-cutoff $p_{ap}^{\min}$. For $m_\pi^{(0)} = 100\,\mathrm{MeV}$ and $L \lesssim 1.5\,\mathrm{fm}$, we observe that T_c is almost independent of L, which may be due to the fact that p_p^L approaches Λ_{UV}.

For large pion masses, $m_\pi^{(0)} \gtrsim 300\,\mathrm{MeV}$, and for $L \geq 2\,\mathrm{fm}$, T_c depends only weakly on the box size. The deviation from its infinite volume value is less than 1% already for $L \approx 2.5\,\mathrm{fm}$. We observe only a weak dependence on the choice of the fermionic boundary conditions, as well. The reason is that the length scale set by the pion mass, $L_\pi \sim \frac{1}{m_\pi^{(0)}}$, is much smaller than the box size L. Therefore the volume dependence of T_c is governed by the pion mass scale , rather than the scale set by the spatial box size: pion fluctuations are more strongly suppressed by their large mass than by the

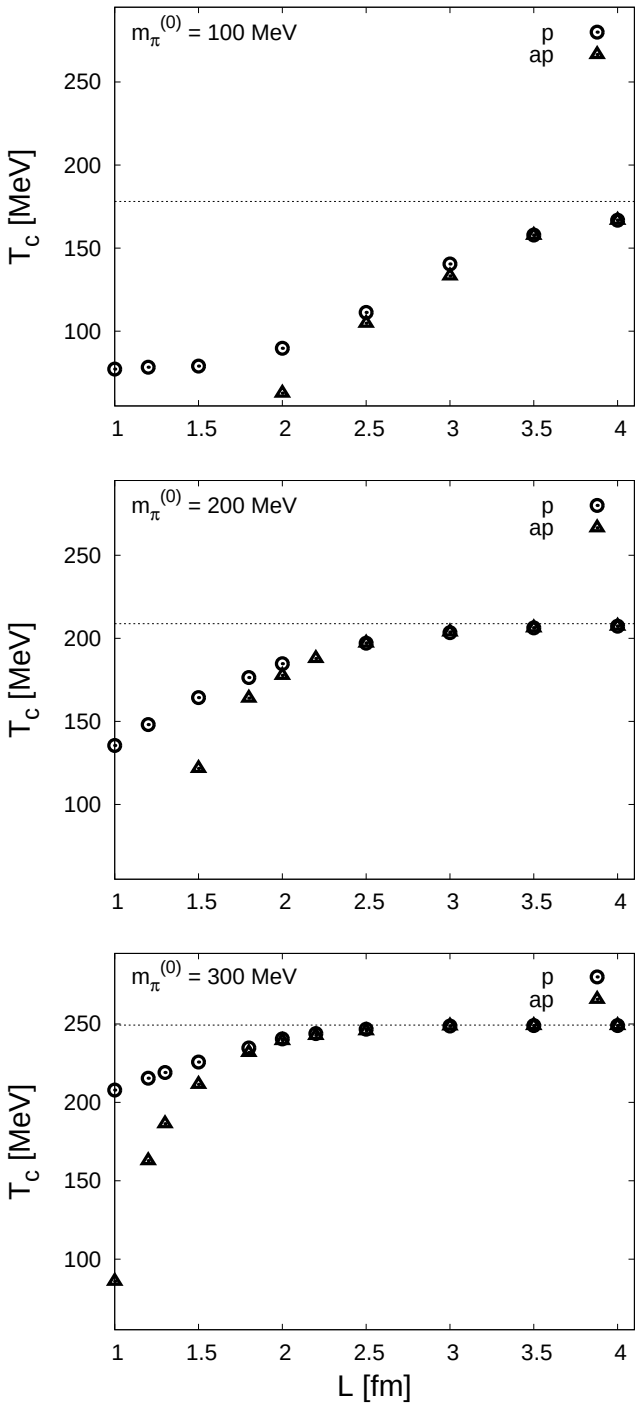

Figure 3.13: The chiral phase transition temperature T_c as a function of the volume size L, for different pion masses $m_\pi^{(0)}$ (identified in the figure), and for periodic (p) as well as anti-periodic (ap) boundary conditions for the quark fields in spatial directions.

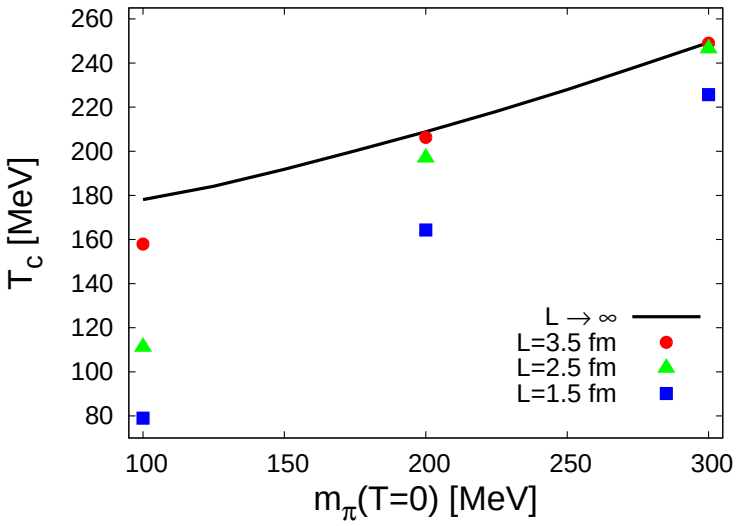

Figure 3.14: Chiral phase transition temperature T_c as a function of $m_\pi(T=0)$ for different box sizes. We show the results for $L = 1.5,\ 2.5,\ 3.5$ fm from bottom to top. For comparison, we also show the results for infinite volume (solid line) from Fig. 3.11.

long-wavelength cutoff from the finite volume. This observation implies that lattice results for T_c are not affected by the finite volume to any considerable degree, provided the pion mass is large, $m_\pi^{(0)} \gtrsim 300\,\mathrm{MeV}$.

Finally, we stress that finite volumes make the coefficient a_1 in Eq. (3.41) bigger for smaller volumes. This can be seen from Tab. 3.5 and Fig. 3.14, where the slope of $T_c(m_\pi^{(0)}, L)$ as a function of $m_\pi^{(0)}$ is even larger at smaller values of L.

3.7 Conclusions

We have presented a new approach to the quark-meson model, which employs the renormalization group method in a finite volume. Central to any such an approach is the inclusion of explicit chiral symmetry breaking. Since chiral symmetry is not broken spontaneously in a finite volume, it is necessary to introduce a finite current quark mass. In this thesis, we have evolved the effective potential with additional symmetry-breaking terms. The form of these terms is constrained by the quark contributions to the renormalization group flow, which introduce the explicit chiral symmetry breaking.

By solving the resulting renormalization group flow equations numerically, we have obtained results for the volume dependence of the meson masses, in particular the pion mass, and the pion decay constant, the order parameter of chiral symmetry breaking.

Comparing our results to those from chiral perturbation theory, we find agreement for larger pion masses, provided we impose anti-periodic boundary conditions on the

L [fm]	$m_\pi^{(0)} = 100\,\mathrm{MeV}$	$m_\pi^{(0)} = 200\,\mathrm{MeV}$	$m_\pi^{(0)} = 300\,\mathrm{MeV}$
1.5	79.0 MeV	164.3 MeV	225.7 MeV
2.5	111.3 MeV	197.1 MeV	246.6 MeV
3.5	157.9 MeV	206.3 MeV	249 MeV
∞	178.1 MeV	208.3 MeV	249.3 MeV

Table 3.5: Chiral phase transition temperatures $T_c(m_\pi^{(0)}, L)$ as function of the pion mass $m_\pi^{(0)}$ and the box size L for periodic boundary conditions for the quark-fields. For comparison, the corresponding values in infinite spatial volume are also given.

fermionic fields. As expected, the differences increase for very small volumes, where chiral symmetry restoration becomes important and chiral perturbation theory unreliable. Moreover, we find that our results for anti-periodic boundary conditions on the fermionic fields show consistently a larger finite volume mass shift for the pion than has been obtained in chiral perturbation theory including up to three loops. The differences between the chiral perturbation theory results which make use of the Lüscher formula and our RG results are consistent with the error estimate for Lüscher's approximation. As one expects, the difference is largest for small values of $m_\pi L$. We have checked that this difference decreases exponentially with an increase in this dimensionless quantity. As shown in Fig. 3.9, our results for anti-periodic boundary conditions and those obtained in chiral perturbation theory with Lüscher's formula [97, 98] converge for large current quark masses. We note that the ratio of the results from chPT and RG does not depend on L, even down to $L = 1.5$ fm.

Extrapolations to infinite volume using chiral perturbation theory are in good agreement with the results from lattice simulations concerning the description of the volume dependence of nucleon properties, such as the nucleon mass [91, 106]. However, it was found that as far as meson masses are concerned, the finite-volume mass-shifts observed on the lattice deviate from the predictions of chiral perturbation theory. This holds also [109] for Lüscher's approach [125], which only takes pion effects into account as well. Generally, the mass shifts predicted from chiral perturbation theory are much smaller than the observed ones [126, 109, 92, 110]. The inclusion of higher orders in the chiral expansion [98] and a summation of additional contributions in Lüscher's expression [105] increase the size of the predicted mass shifts. They also decrease the distance to our RG results, provided we impose anti-periodic boundary conditions on the fermionic fields. In contrast, for periodic boundary conditions, large pion masses, and a large ratio $1/(\beta L)$, we find that our mass shifts in small volumes behave in a substantially different way from those of chPT. In particular, even in volume sizes as large as $L = 2.5$ fm and for $T \to \infty$, the results for the relative shift of the pion mass can do as much as double under a change of the boundary conditions, for example from $R[m_\pi(L)] = 0.0488$ with periodic, to $R[m_\pi(L)] = 0.1037$ with anti-periodic boundary

$m_\pi(\infty)$	Approach	$R[m_\pi(L)] < 0.1$	$R[m_\pi(L)] < 0.01$
100 MeV	RG, ap.	$L > 2.523$ fm	$L > 4.381$ fm
	RG, p.	$L > 1.351$ fm	$L > 4.259$ fm
	chPT	$L > 2.187$ fm	$L > 3.785$ fm
200 MeV	RG, ap.	$L > 1.736$ fm	$L > 2.842$ fm
	RG, p.	$L > 0.5$ fm*	$L > 1.888$ fm
	chPT	$L > 1.639$ fm	$L > 2.653$ fm
300 MeV	RG, ap.	$L > 1.359$ fm	$L > 2.213$ fm
	RG, p.	$L > 1.022$ fm	$L > 1.911$ fm
	chPT	$L > 1.339$ fm	$L > 2.104$ fm

Table 3.6: Bounds on the minimum size of the volume $V = L^3 \times T$ for $T \to \infty$ such that the finite volume pion mass shift $R[m_\pi(L)]$ is < 0.1 or < 0.01, for different values of the pion mass $m_\pi(\infty)$. RG results are given for anti-periodic and for periodic boundary conditions, chPT results are those in NNLO obtained in [105]. Note that for periodic boundary conditions and for $m_\pi = 200$ MeV and $m_\pi = 300$ MeV, the bounds are set by a decrease of the pion mass. *For $m_\pi = 200$ MeV and periodic boundary conditions, the bound $R[m_\pi(L)] < 0.1$ is satisfied in the full volume range described by our model (cf. also Fig. 3.6).

conditions, for a pion mass of $m_\pi = 100$ MeV. In Table 3.6 we give bounds on the minimum size of the volume that are necessary to keep the finite volume mass shift smaller than 10% resp. 1%, calculated for periodic and anti-periodic boundary conditions in the RG approach, and for comparison from the NNLO chPT calculation of Ref. [105]. Compared to anti-periodic boundary conditions, periodic boundary conditions generally allow to achieve the same accuracy with regard to finite volume effects already with a smaller volume size. This is an important conclusion concerning lattice QCD simulations. For the physical values of the pion mass and the pion decay constant, chiral perturbation theory can be applied for volume sizes $L \gg 1$ fm, but, according to Ref. [105], it is a priori impossible to say how large exactly the volume has to be. Ultimately, this question can only be answered by lattice calculations.

The main uncertainty of our RG approach comes from its dependence on the UV cutoff scale Λ_{UV} for large meson masses. The system becomes sensitive to Λ_{UV} for large explicit symmetry breaking, because the mass of the sigma as the heaviest particle approaches the UV cutoff. For a pion mass of $m_\pi = 300$ MeV, the sigma mass is $m_\sigma \approx 800\,\text{MeV}$. In this case, a cutoff variation between $\Lambda_{UV} = 1500$ MeV and 1100 MeV, changes the pion mass for a volume with $L = 1$ fm by approximately 6%, and by less than 1% for $L > 2$ fm. Within this uncertainty, our results agree with those of chPT for $m_\pi = 300$ MeV. In contrast, for $m_\pi = 100$ MeV the cutoff dependence is so weak that it is not noticeable on the scale of the results. The RG and chPT results do not agree within this uncertainty, cf. Table 3.2, for $m_\pi = 100\,\text{MeV}$ and $m_\pi = 200\,\text{MeV}$.

The dependence of our results on the choice of model parameters at the UV scale is much weaker than that on the cutoff. By fitting to the values of the low-energy observables m_π and f_π in infinite volume, we achieve a very high degree of independence from the particular choice of UV parameters.

To summarize our study of finite-size effects in low-energy observables in QCD: The RG approach shows the importance of the fermionic boundary conditions for the pion mass and the pion decay constant. The differences between the results for periodic and anti-periodic boundary conditions increase for increasing pion mass and increasing ratio T/L. Our analysis agrees qualitatively with the observations from lattice QCD, in regards to the dependence on quark boundary conditions as well as in regards to an apparent drop of the pion mass in finite volume. We find convergence of our results to those of chiral perturbation theory calculations for large pion masses and large volumes, where quark effects are not important.

In Sec. 3.6, we have studied dynamical symmetry breaking at finite temperatures by means of the proper-time RG. The underlying model for our study was also the quark-meson model. We have presented results for the volume dependence of the chiral phase transition temperature. In this way, we have obtained non-perturbative results for the transition temperature for various values of the pion mass.

In general, no phase transition can occur in a system of finite volume. The evaluation of lattice results therefore uses a scaling analysis in quark mass and temperature [145, 146, 147, 22], and recently finite-size scaling [22] as an analytical tool. We expect that a Renormalization Group analysis of the critical behavior can complement these approaches. In this work, we have focused on the chiral phase transition temperature, which is not universal and also model-dependent. However, the relative shift of the temperature from infinite to finite volume should depend mainly on the pion mass and the pion decay constant, which are independent of the model and represent an external input to our calculations.

We find that finite volume effects for the transition temperature remain small for large pion masses $m_\pi \gtrsim 300\,\mathrm{MeV}$, as long as the volume is of the order $L \geq 2\,\mathrm{fm}$ in the spatial directions. The scale for the appearance of sizable finite-volume effects is given by the pion mass m_π, and the effects remains small as long as $L \gg \frac{1}{m_\pi}$.

On the other hand, finite size effects are sizable already at a lattice extent of $L \simeq 2\,\mathrm{fm}$ for realistic pion masses of the order of $100\,\mathrm{MeV}$. We expect therefore that finite volume effects will become more relevant in future simulations with realistic pion masses. The strategy for lattice calculations should then be to simulate in volumes where the value $m_\pi L$ is large enough to keep the finite volume effects down to an acceptable size, and to extrapolate to smaller pion masses and the chiral limit.

We note that the choice of periodic boundary conditions in spatial directions for the quark fields, which is commonly employed in lattice simulations, leads to a much smaller finite volume effect on the transition temperature. This conclusion agrees with our results for the volume dependence of the pion mass and pion decay constant.

The dependence of the transition temperature on the pion mass in the quark-meson

model is much stronger than that observed in lattice simulations and becomes even stronger for decreasing volume sizes. Consequently, the puzzle of the weak dependence of the transition temperature on the pion mass in QCD cannot be explained as a finite-volume effect by means of the quark-meson model. Therefore, we conclude that the quark-meson model in its present from is not the appropriate tool for an accurate description of the dynamics of the chiral symmetry breaking at finite temperature. An extension of the quark-meson model with gauge degrees of freedom may cure this deficiency of the model [148, 149, 61, 150, 76]. A new ansatz for studying the dynamics of chiral symmetry breaking at finite temperature within a non-perturbative RG approach is subject of Chap. 4.

Chapter 4

QCD at Finite Temperature

In this chapter, we study QCD at finite temperature from first principles within the RG framework. First, we summarize the state of the art in the study of the QCD phase boundary at finite temperature in Sec. 4.1. This will serve as a motivation for our approach. In Sec. 4.2 to 4.4, we discuss the mathematical background which we need for a careful RG treatment of gauge theories, in particular QCD. Our calculation of the strong running coupling of Yang-Mills theory and QCD is presented in Sec. 4.5. In order to compute the chiral phase boundary of QCD, we have to take quark self-interactions into account. After an explanation of the underlying technical details for a RG study of four-fermion interactions by means of a simple NJL model in Subsec. 4.6.1, we incorporate gluons and show that a simple picture for the chiral quark dynamics in QCD arises from this in Subsec. 4.6.2. We then show in Sec. 4.7 how our approach allows for a determination of the chiral phase boundary of QCD and give a detailed discussion of the phase boundary in the plane spanned by temperature and flavor number. Our conclusions, a critical assessment of our results as well as an outlook are given in Sec. 4.8.

4.1 Introduction

Even more than 30 years after QCD has been theoretically formulated, its phase diagram has been neither qualitatively nor quantitatively determined to any large degree of certainty. The results from various approaches to determine the order of the phase transitions, the transition temperatures themselves as well as the existence of a (tri-)critical point in the phase diagram are not yet fully consistent. By far, this is not only the case at finite density. Even at vanishing density we do not know if the confinement and the chiral phase transition take place at the same temperature and the order of the phase transition for the physically most relevant case of two massless quark flavors is not finally determined. Since lattice QCD simulations have not given final answers to all these questions so far, complementary non-perturbative approaches are indispensable to gain a better understanding of the underlying non-perturbative phenomena.

In Fig. 4.1, we show the so-called "three-flavor phase diagram" for vanishing baryon chemical which has been obtained from lattice QCD simulations [33]: for $N_{\rm f} = 3$ massless quark flavours a first order chiral phase transition has been found at $T_\chi \approx 155$ MeV. For $N_{\rm f} = 2$, the phase transition temperature is shifted to a higher value of $T_\chi \approx 175$ MeV. The deconfinement phase transition temperature in $SU(N_c = 3)$ Yang-Mills theory has been measured at $T_d \approx 270\,\text{MeV}$. However, less is known about the flavour dependence of the chiral phase boundary of QCD at finite temperature from lattice QCD. At zero temperature, the phase structure of QCD has been studied by applying various approaches, from lattice simulations to perturbative calculations, see e. g. Refs. [151, 152, 153, 154, 155, 156]. Nevertheless, there are still challenging questions left, such as a determination of the critical number of quark flavors, $N_{\rm f}^{\rm cr}$, above which QCD remains in the chirally symmetric regime even in the deep IR. Although the value of $N_{\rm f}^{\rm cr}$ varies from $N_{\rm f}^{\rm cr} = 5$ (instanton-liquid model [155]) to $N_{\rm f}^{\rm cr} = 12$ (this work and DSE approach [153]) with a accumulation point around $N_{\rm f}^{\rm cr} = 10$, all these studies confirm the existence of a regime where QCD is chirally symmetric but still asymptotically free. In Fig. 4.2, we give a qualitative many-flavor phase diagram of QCD at zero temperature. A first understanding of this phase diagram can already be gained with the aid of the perturbative two-loop β-function of QCD:

$$\beta(\alpha) = -\overbrace{\frac{1}{6\pi}(11N_c - 2N_f)}^{=b_1}\,\alpha^2 - \overbrace{\frac{1}{24\pi^2}\left(34N_c^2 - 10N_cN_f - 3\frac{N_c^2-1}{N_c}N_f\right)}^{=b_2}\,\alpha^3 - \ldots\,. \quad (4.1)$$

Here α denotes the strong coupling, and the number of colors and massless quark flavors are given by N_c and $N_{\rm f}$, respectively. Considering the first term of the expansion, the demand for asymptotic freedom leads immediately to a constraint for the number of massless quark flavors:

$$N_{\rm f} < N_{\rm f}^{\rm a.f.} = \frac{11}{2}N_c \overset{N_c=3}{=} 16.5\,. \quad (4.2)$$

For $N_{\rm f} > N_{\rm f}^{\rm a.f.}$, QCD is in the so-called *trivial phase* where neither chiral symmetry is broken nor a confining regime emerges in the deep IR. Moreover, a number of quark flavors $N_{\rm f}^{\rm fixed}$, above which the strong coupling approaches a non-trivial fixed point in the IR, follows already from the perturbative two-loop expansion by demanding $b_1 > 0$ and $b_2 < 0$:

$$N_f = N_{\rm f}^{\rm fixed} > \frac{34N_c^3}{13N_c^2 - 3} \overset{N_c=3}{\approx} 8.053\,. \quad (4.3)$$

The regime between $N_{\rm f}^{\rm fixed}$ and $N_{\rm f}^{\rm a.f.}$ is further divided by the existence of the above-mentioned critical number of quark flavors $N_{\rm f}^{\rm cr}$, above which QCD remains in the chirally symmetric regime[1]. Below $N_{\rm f}^{\rm a.f.}$, but above $N_{\rm f}^{\rm cr}$, we have the so-called "*conformal phase*" where the strong coupling approaches an IR fixed point. However, below

[1]Here we tacitly assume that $N_{\rm f}^{\rm cr}$ is larger than $N_{\rm f}^{\rm fixed}$.

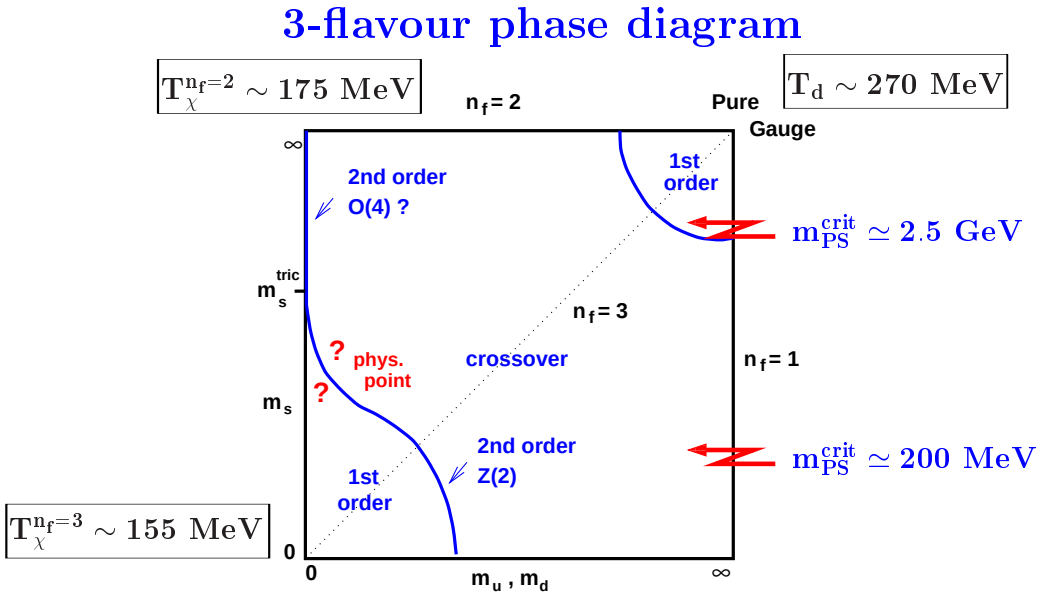

Figure 4.1: The QCD phase diagram of 3-flavor QCD with degenerate up- and down-quark masses and a strange-quark mass m_s for vanishing baryon density taken from Ref. [33].

N_f^{cr}, we find dynamical chiral symmetry breaking in QCD. In this perturbative picture, the emergence of massive quarks in the chiral broken regime would destabilize the IR fixed point of the running coupling. As we will see in the subsequent sections, such a destabilization of the IR fixed point is not confirmed by our non-perturbative RG study of QCD. Finally, QCD is confining and chiral symmetry is broken for values of N_f (much) smaller than N_f^{fixed}.

In this work, we mainly focus on the dependence of the chiral phase transition temperature on the number N_f of massless quark flavours. As explored in heavy-ion collisions, currently at CERN, at RHIC, and in the future at LHC and the FAIR facility at GSI, the properties of strongly interacting matter change distinctly during transitions from low to high temperatures [33]. This makes the theoretical description of QCD by means of effective theories extremely difficult. At low temperature and momentum scales, QCD can be described well by effective field theories in terms of ordinary hadronic states, see e. g. our studies in Chap. 3. But a hadronic picture is eventually bound to fail at higher temperature and momentum scales, where a description in terms of quarks and gluons is expected to arise naturally owing to asymptotic freedom. In the transition region between these asymptotic descriptions, effective degrees of freedom, such as order parameters for the chiral or deconfining phase transition, may characterize the physical properties in simple terms, i.e., with a simple effective action [120].

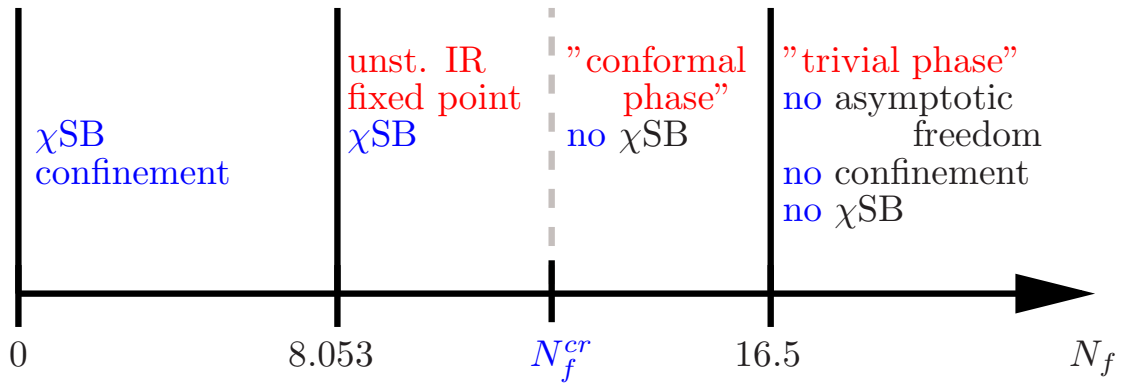

Figure 4.2: Qualitative many-flavor phase diagram of QCD at vanishing temperature.

In lattice simulations, it was found that the QCD pressure function does not approach the Boltzmann-limit of a non-interacting gas of massless quarks and gluons, even at temperatures much higher than the phase transition temperature. This indicates that QCD is strongly interacting even above the phase transition, see Fig. 4.3. This observation has recently attracted much attention [157], implying that any generic choice of degrees of freedom will not lead to a weakly coupled description. In fact, it is natural to expect that the low-energy modes of the thermal spectrum still remain strongly coupled even above the phase transition temperature. If so, a formulation with microscopic degrees of freedom from first principles will serve as the most powerful and flexible approach to bridge wide ranges in parameter space.

In such a microscopic formulation, an expansion in the coupling constant is a natural first step [158]. The structure of this expansion is theoretically involved [159], and exhibits a slow convergence behavior [160] and requires coefficients of nonperturbative origin [161]. Still, with the aid of effective-field theory methods [162], a physically well-understood computational scheme can be constructed . This facilitates a systematic determination of expansion coefficients, and the agreement with lattice simulations is often surprisingly good down to temperatures close to the phase transition temperature [163]. The phase-transition point and the deep IR, however, remain inaccessible with such an expansion.

In this work, we follow a somewhat different strategy to study finite-temperature Yang-Mills theory and QCD in terms of microscopic variables, i.e., in terms of gluons and quarks. Our scheme is based on a systematic and consistent operator expansion of the effective action which is inherently nonperturbative in the coupling. For bridging the scales from weak to strong coupling, we use the functional renormalization group (RG) [47, 50, 164] which has been introduced in Sec. 2.4.

Since we do not expect that microscopic variables will be able to answer all relevant questions in a simple fashion, we concentrate on problems which are more easily accessible to such a formulation in terms of quarks and gluons. First, we focus on the

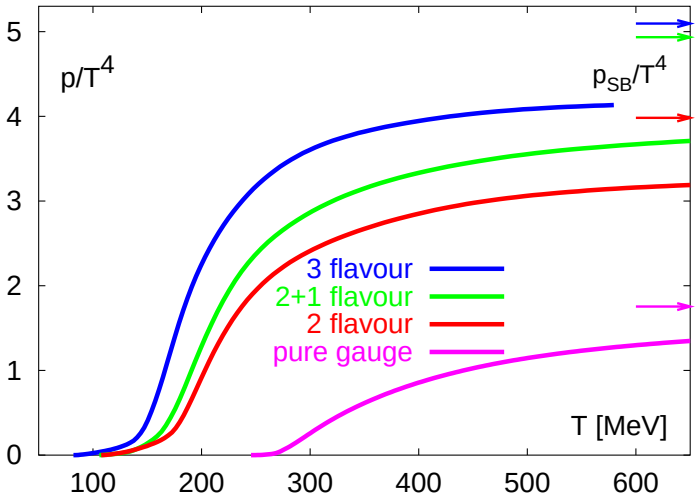

Figure 4.3: The pressure of $SU(3)$-Yang-Mills theory and of QCD with various number of quark flavors as a function of temperature [33].

running of the strong coupling of pure $SU(N_c)$ Yang-Mills theory as well as QCD. Our findings generalize zero-temperature results, obtained previously in a similar study [71], to arbitrary values of the temperature. Second, we use this result in an investigation of the induced quark dynamics, including its back-reactions on gluodynamics, in order to monitor the status of chiral symmetry at finite temperature. It turns out that our approach provides a simple picture for the chiral quark dynamics, which facilitates a computation of the critical temperature above which chiral symmetry is restored. The generalization of our approach to an arbitrary number of quark flavors allows us to explore the phase boundary in the plane of temperature and flavor number N_f. Moreover, we gain a simple analytical understanding of the shape of the chiral phase boundary in the (T, N_f) plane for small as well as large N_f. While fermionic screening is the dominant mechanism for small N_f, we find an intriguing relation between the N_f scaling of the critical temperature near the critical flavor number and the zero-temperature IR critical exponent of the running QCD coupling. This relation is remarkable, since it connects two different universal quantities with each other, and thus represents a generic, testable prediction of the phase-transition scenario.

4.2 Physical and Mathematical Aspects of QCD

We briefly recall some physical and mathematical aspects of QCD. There are several ways to introduce the Lagrangian density of QCD, we give a motivation with the aid of the matter fields, i. e. with the aid of the quarks. The Lagrangian density of N_f

non-interacting quark-flavors reads[2]

$$\mathcal{L} = \bar{\psi}\mathrm{i}\partial\!\!\!/\psi + \mathrm{i}M\bar{\psi}\psi\,, \tag{4.4}$$

where ψ is a column-vector in flavor-space defined as

$$\psi = \begin{pmatrix} \psi_1 \\ \vdots \\ \psi_{N_\mathrm{f}} \end{pmatrix}. \tag{4.5}$$

This theory is invariant under space-time independent transformations of the form

$$\psi(x) \to \mathrm{e}^{-\mathrm{i}\epsilon^a T^a}\psi(x) \tag{4.6}$$

with ϵ^a representing generalized rotating angles and the T^a's being the hermitean generators of the physically underlying (non-abelian) symmetry-group. In QCD, the T^a's are the generators of the Lie-group $SU(3)$ which assigns a so-called *color* quantum number to the quarks. This has been postulated by Fritzsch and Gell-Mann, Nambu, Bardeen and Greenberg [3, 4, 5, 6] in order to reconcile the original quark model introduced by Gell-Mann [1, 2] with the fermionic character of the quarks. For example, it was not possible to reconcile the existence of the baryonic resonance $\Delta^{++}(\frac{3}{2}^+)$ made up of three up-quarks in a spin-up state with the original quark model without violating the anti-symmetry for the wave-function[3]. The fact that the color wave function must be anti-symmetric and that at least three different color states are needed, motivates the appearance $SU(3)$. Later, the existence of three color states was confirmed by the observation of steps in the (normalized) cross-section of e^+e^--collisions. Nevertheless, we do not restrict our calculations in this chapter to three colors only but also derive also results for arbitrary $SU(N_c)$ Lie-groups which obeys

$$\left[T^a, T^b\right] = \mathrm{i}f^{abc}T^c\,, \qquad \mathrm{Tr}\left\{T^aT^b\right\} = \frac{1}{2}\delta^{ab}\,. \tag{4.7}$$

The f^{abc} are the structure constants of the group, and take the values $1, \ldots, N_c^2 - 1$, see also App. B.

Although it is invariant under the transformations (4.6), the Lagrangian density (4.4) is not invariant under local gauge transformations with a space-time dependent ϵ; such a transformation would yield terms proportional to $\partial_\mu\epsilon$. Invariance of the Lagrangian density under under local gauge transformations can be achieved by replacing the ordinary derivative ∂_μ by the so-called covariant derivative D_μ, which depends on auxiliary gauge fields (the so-called *gluons*) and which is defined as

$$D_\mu\psi = [\partial_\mu - \overbrace{\mathrm{i}\bar{g}A_\mu^a T^a}^{\equiv A_\mu}]\psi\,, \tag{4.8}$$

[2]We work in Euclidean space-time, see App. A for our conventions.

[3]The wave-function must be anti-symmetric due to the Pauli Principle.

where $\bar{g}$ is the bare coupling constant. An interaction between the fermions and gluons is introduced by the covariant derivative. The number of gauge fields needed is identical to the number of generators. Gauge invariance is then obtained if the gauge fields transform according to

$$A_\mu \to U A_\mu U^{-1} - [\partial_\mu U]\, U^{-1} \quad \text{with} \quad U = U(x) = \mathrm{e}^{-\mathrm{i}\epsilon(x)^a T^a}\,. \tag{4.9}$$

The corresponding infinitesimal transformation reads

$$\delta A^a_\mu = \frac{1}{\bar{g}}\partial_\mu \epsilon^a - f^{abc}\epsilon^b A^c_\mu = \frac{1}{\bar{g}}[\partial_\mu \delta^{ab} - \bar{g} f^{abc} A^c_\mu]\epsilon^b \equiv \frac{1}{\bar{g}} D^{ab}_\mu \epsilon^b \tag{4.10}$$

in the so-called adjoint representation and

$$\delta A_\mu = \partial_\mu \epsilon + [A_\mu, \epsilon] \quad \text{with} \quad \epsilon = \mathrm{i} T^a \epsilon^a \tag{4.11}$$

in the so-called fundamental representation. From the infinitesimal transformations, we can read off the generators G^a_A of the gauge symmetry,

$$\mathcal{G}^a_A = D^{ab}_\mu \frac{\delta}{\delta A^b_\mu}\,, \tag{4.12}$$

which we apply below for a study of the symmetry properties of the effective action.

So far, the gluons are just auxiliary fields without kinetic terms. However, it is a straightforward task to construct gauge-invariant kinetic terms for the gluons out of the covariant derivatives by repeated application. The simplest kinetic term for the gluons is constructed from the relation

$$[D_\mu, D_\nu]\psi = F_{\mu\nu}\psi \quad \text{with} \quad F_{\mu\nu} = \partial_\mu A_\nu - \partial_\nu A_\mu + [A_\mu, A_\nu]\,, \tag{4.13}$$

yielding the gauge-invariant Lagrangian density

$$\mathcal{L}_{\mathrm{YM}} = \frac{1}{2\bar{g}^2}\mathrm{Tr}\,\{F_{\mu\nu}F_{\mu\nu}\} \equiv \frac{1}{4\bar{g}^2} F^a_{\mu\nu}F^a_{\mu\nu}\,. \tag{4.14}$$

This purely gluonic Lagrangian density is known as the Lagrangian density of *Yang-Mills* theory. Note that this term includes also interactions between three and four gluons, respectively. By adding the fermionic degrees of freedom to the Yang-Mills Lagrangian density, we finally obtain the so-called (classical) QCD action:

$$S_{\mathrm{QCD}} = \int d^d x \left\{ \frac{1}{2\bar{g}^2}\mathrm{Tr}\,\{F_{\mu\nu}F_{\mu\nu}\} + \bar{\psi}\mathrm{i}\not{D}\psi + \mathrm{i}M\bar{\psi}\psi \right\}. \tag{4.15}$$

Note that the QCD action is also invariant under the chiral transformations discussed in Sec. 3.4.1, provided the quarks are massless, $M \equiv 0$.

Let us now discuss briefly the quantization of QCD in the path-integral approach and the problems arising through this. Extensive introductions to this subject can

for example be found in [45, 54]. Since the problems of the path-integral quantization arise in this context from the pure gauge-sector of QCD, it is sufficient to discuss Yang-Mills theory. The straightforward generalization of the generating functional of scalar theories to gauge fields fails, since the expression

$$Z[j] = \int \mathcal{D}A_\mu \mathrm{e}^{-S_{\mathrm{YM}} + j_\mu^T \cdot A_\mu} \tag{4.16}$$

is ill-defined because $\mathcal{D}A_\mu$ is a gauge-invariant integration measure. Here j_μ^T is a row vector, and A_μ is a column vector. The definition (4.16) is problematic since the path-integral runs over all possible gauge-field configurations. This results in a multiple counting of all equivalent gauge configurations which are connected by a gauge transformation. In order to give a meaning to the functional integral (4.16), we divide the space of all gauge configurations into equivalence classes. These so-called orbits contain all configurations which are obtained by applying all possible gauge transformations of the underlying gauge group to an arbitrarily given gauge configuration. For each gauge configuration of a such an orbit the integrand in Eq. (4.16) is constant. A well-defined generating functional is then obtained by defining the integral in such a way that it runs only over physically distinct gauge configurations. Roughly speaking, this means that we pick up only one gauge configuration from each orbit. This can be achieved by inserting the identity

$$1 = \int \mathcal{D}\epsilon \, \delta\left(\mathcal{F}[A_\mu^\epsilon]\right) \det\left(\frac{\delta \mathcal{F}[A_\mu^\epsilon]}{\delta \epsilon}\right) \tag{4.17}$$

in the generating functional (4.16), where the functional $\mathcal{F}$ defines a gauge-fixing condition, $\mathcal{F}[A_\mu^\epsilon] = 0$. The subscript ϵ of the gauge fields indicates that A_μ^ϵ is obtained from an initial configuration A_μ by a finite gauge transformation[4]. This is known as the *Faddeev-Popov* trick. The generating functional (4.16) then reads

$$\begin{aligned} Z[j,\bar{\mu},\mu] &= \mathcal{N} \int \mathcal{D}A_\mu \mathcal{D}c\mathcal{D}\bar{c}\, \mathrm{e}^{-S_{\mathrm{YM}} - \frac{1}{2\xi}\int d^dx \mathcal{F}^\alpha \mathcal{F}^\alpha - \int d^dx \bar{c}^a \frac{\delta F^a}{\delta \epsilon^b} c^b + j_\mu^T \cdot A_\mu + \bar{\mu}\cdot c - \bar{c}\cdot\mu} \\ &\equiv \mathcal{N} \int \mathcal{D}A_\mu \mathcal{D}c\mathcal{D}\bar{c}\, \mathrm{e}^{-S_{\mathrm{YM}} - S_{\mathrm{gf}} - S_{\mathrm{gh}} + j_\mu^T \cdot A_\mu + \bar{\mu}\cdot c - \bar{c}\cdot\mu} \equiv \mathrm{e}^{W[j,\bar{\mu},\mu]} \,. \end{aligned} \tag{4.18}$$

Here Greek letters denote Lorentz indices, whereas Roman letters denote color-indices. The normalization factor $\mathcal{N}$ accounts for the integral over g that has been factored out. In addition, we have used the fact that the determinant is gauge invariant and we have applied an integral representation of the δ functional and of the determinant. We now have the freedom to choose a gauge-fixing parameter ξ . In order to find an integral

[4]We tacitly assume that a solution to the *Gribov* problem [165] within the path-integral approach exists. Therefore we do not discuss problems that arise due to the fact that the argument of the δ functional in Eq. (4.17) does not only have a simple zero and that the determinant is not strictly positive.

representation of the determinant, we have introduced so-called *ghost* fields, which are Grassmann-valued scalar fields. These fields transform as tensors, according to

$$\bar{c}^a \to \bar{c}^a + \bar{g} f^{abc} \omega^b \bar{c}^c \quad \text{and} \quad c^a \to c^a + \bar{g} f^{abc} \omega^b c^c \,, \tag{4.19}$$

where the generators of the underlying symmetry group are given by

$$\mathcal{G}^a_{\rm gh} = -\bar{g} f^{abc} \left(c^c \frac{\delta}{\delta \bar{c}^b} + \bar{c}^c \frac{\delta}{\delta \bar{c}^b} \right) . \tag{4.20}$$

For constructing the effective action Γ_{YM} of Yang-Mills theory, we have also introduced source terms μ and $\bar{\mu}$ for the ghost fields in Eq. (4.18). The effective action is then obtained from Eq. (4.18) in the same way as in Subsec. (2.4.2). The derivation yields

$$\Gamma[\Phi] = -W[J^T] + J^T \cdot \Phi \;\; = -W[j, \bar{\mu}, \mu] + j^T_\mu \cdot \mathbf{A}_\mu + \bar{\mu} \cdot \mathbf{c} - \bar{\mathbf{c}} \cdot \mu \,. \tag{4.21}$$

We have introduced a vector Φ containing the (classical) fields and a corresponding vector for the sources through

$$\Phi = \frac{\overrightarrow{\delta}}{\delta J^T} W[J^T] = \begin{pmatrix} \mathbf{A}_\mu \\ \mathbf{c} \\ \bar{\mathbf{c}}^T \end{pmatrix} \qquad \text{and} \qquad J^T = (j^T_\mu, \bar{\mu}, \mu^T) \,. \tag{4.22}$$

However, the effective action Γ_{YM} is *not* invariant under gauge transformations. This is due to the construction of the well-defined generating functional (4.18). On the other hand, a gauge transformation of the fields in Eq. (4.18) should not change the value of the integral; in other words, physics is unchanged under a gauge transformation of the fields. From this, we conclude that the effective action (4.21) must be invariant under gauge transformations. Applying the generators $\mathcal{G}^a_A$ and $\mathcal{G}^a_{\rm gh}$ simultaneously on both sides of Eq. (4.21) yields the so-called *Ward-Takahashi* identity (WTI), which accounts for the breaking of gauge invariance introduced by the Faddeev-Popov trick:

$$\begin{aligned} \left(\mathcal{G}^a_A + \mathcal{G}^a_{\rm gh}\right) \Gamma[\Phi] \;\; &\overset{(4.21)}{=} \;\; \frac{\langle 0| \left(\mathcal{G}^a_A + \mathcal{G}^a_{\rm gh}\right) (S_{\rm YM} + S_{\rm gf} + S_{\rm gh}) |0\rangle_J}{\langle 0|0\rangle_J} \\ &= \;\; \frac{\langle 0| \left(\mathcal{G}^a_A + \mathcal{G}^a_{\rm gh}\right) (S_{\rm gf} + S_{\rm gh}) |0\rangle_J}{\langle 0|0\rangle_J} \,. \end{aligned} \tag{4.23}$$

In the second line, we have used $\left(\mathcal{G}^a_A + \mathcal{G}^a_{\rm gh}\right) S_{\rm YM} = 0$. We thus establish that the 1PI Green's functions obtained from the effective action Γ must fulfill the constraint imposed by the WTI in order to have a physical meaning.

Note that so far we have not specified the gauge-fixing condition. In the next section, we apply the background-field formalism introduced in Subsec. 2.4.3 to gauge theories and show how a gauge-invariant effective action can be obtained through an appropriate choice of the gauge-fixing condition within this framework.

4.3 The Background-Field Method and Non-Abelian Gauge Theories

The starting point of our discussion is the background-field generating functional $\hat{Z}[J^T, \bar{A}]$, which can be deduced from Eq. (4.18) by splitting the gauge field A_μ into the fluctuation field $a_\mu = A_\mu - \bar{A}_\mu$ and an (auxiliary) non-dynamical background-field $\bar{A}_\mu$:

$$\begin{aligned} \hat{Z}[J^T, \hat{\phi}] &= \mathcal{N} \int \mathcal{D}A_\mu \mathcal{D}c \mathcal{D}\bar{c}\, \mathrm{e}^{-S_{\mathrm{YM}}[a_\mu + \bar{A}] - S_{\mathrm{gf}} - S_{\mathrm{gh}}[a_\mu + \bar{A}] + J^T \cdot \phi} \\ &= Z[J^T] \mathrm{e}^{-J^T \cdot \hat{\phi}} \equiv \mathrm{e}^{\hat{W}[J^T, \hat{\phi}]} \,. \end{aligned} \tag{4.24}$$

We have introduced the following vectors in field space:

$$\phi = \begin{pmatrix} a_\mu \\ c \\ \bar{c}^T \end{pmatrix} \quad \text{and} \quad \hat{\phi} = \begin{pmatrix} \bar{A}_\mu \\ 0 \\ 0 \end{pmatrix} . \tag{4.25}$$

Following the steps along the lines of Subsec. 2.4.3, the background-field effective action becomes (see Eq. (2.42))

$$\hat{\Gamma}[\hat{\Phi}, \hat{\phi}] = -\hat{W}[J^T, \hat{\phi}] + J^T \cdot \hat{\Phi} = \Gamma[\Phi, \hat{\phi}] \quad \text{with} \quad \hat{\Phi} = \frac{\overrightarrow{\delta}}{\delta J^T} \hat{W}[J^T] \,.$$

From the relation between the background-field effective action $\hat{\Gamma}[\hat{\Phi}, \hat{\phi}]$ and the (standard) effective action $\Gamma[\Phi, \Phi]$, which has been derived in Subsec. 2.4.3 for arbitrary fields, we deduce

$$\hat{\Gamma}[\hat{\Phi}, \hat{\phi}] = \Gamma[\Phi, \hat{\phi}] \quad \stackrel{\Phi = \hat{\phi}}{\Longrightarrow} \quad \hat{\Gamma}[0, \hat{\phi}] = \Gamma[\Phi, \Phi] \,, \tag{4.26}$$

where Φ is the conventional classical field defined as

$$\Phi = \frac{\overrightarrow{\delta}}{\delta J^T} W[J^T] \,. \tag{4.27}$$

However, in the case of gauge theories, Eq. (4.26) deserves a comment: if $\hat{\Gamma}[0, \hat{\phi}]$ is computed with a gauge-fixing condition $\mathcal{F}^a[a_\mu]$, then $\Gamma[\Phi, \Phi]$ must be computed with the gauge fixing condition $\mathcal{F}^a[a_\mu - \bar{A}]$ in order to ensure that the background-field effective action $\hat{\Gamma}[0, \hat{\phi}]$ and the (standard) effective action $\Gamma[\Phi, \Phi]$ are equal.

One might ask what we gain by the introduction of a background gauge-field, beside the advantages already discussed in Subsec. 2.4.3. The great advantage is that we can choose a gauge-fixing condition $\mathcal{F}^a$ in such a way that the background-field effective action $\hat{\Gamma}[\Phi, \hat{\phi}]$ is a gauge-invariant functional of the background field $\bar{A}$. Let us discuss

this issue more precisely. An appropriate choice is the so-called *background-field gauge condition* [65, 53]

$$\mathcal{F}^a[a_\mu] = D^{ab}_\mu[\bar{A}]a^b_\mu \tag{4.28}$$

with the covariant derivative in the adjoint representation defined as

$$D^{ab}_\mu[A] = \partial_\mu\delta^{ab} - \bar{g}f^{abc}A^c_\mu\,. \tag{4.29}$$

The gauge-fixing condition (4.28) fixes the fluctuation fields a_μ relative to the background fields $\bar{A}_\mu$. Using this condition in the generating functional (4.24), the gauge-fixing action $S_{\rm gf}$ and the ghost action $S_{\rm gh}$ read

$$S_{\rm gf} \overset{(4.28)}{=} -\frac{1}{2\xi}\int d^dx\, a^a_\mu D^{ab}_\mu[\bar{A}]D^{bc}_\nu[\bar{A}]a^c_\nu\,, \tag{4.30}$$

$$S_{\rm gh} = -\int d^dx\bar{c}^a\left\{\frac{\delta F^a}{\delta\epsilon^b}[a+\bar{A}]\right\}c^b = -\frac{1}{\bar{g}}\int d^dx\bar{c}^a D^{ab}_\mu[\bar{A}]D^{bc}_\mu[a+\bar{A}]c^c, \tag{4.31}$$

where we have used that the full gauge field $A_\mu = a_\mu + \bar{A}_\mu$ transforms according to

$$\delta A^a_\mu \equiv \delta(a_\mu+\bar{A}_\mu) = \frac{1}{\bar{g}}D^{ab}_\mu[a+\bar{A}]\epsilon^b\,. \tag{4.32}$$

The prefactor $1/\bar{g}$ in the ghost action is unimportant since it can be factored out of the functional integral (4.24) and absorbed in the physically unimportant normalization factor. For convenience we therefore apply from now on $\bar{g}S_{\rm gh}$ rather than S_{gh} for our calculations. Next we discuss the symmetry properties of the background-field effective $\hat{\Gamma}[\hat{\Phi},\hat{\phi}]$. For this purpose we study how the different contributions of the action, namely the Yang-Mills action, the gauge-fixing action and the ghost action, vary under the symmetries associated with the generators $\mathcal{G}^a_A$, $\mathcal{G}^a_{\rm gh}$ and

$$\bar{\mathcal{G}}^a = D^{ab}_\mu[\bar{A}]\frac{\delta}{\delta\bar{A}^b_\mu}\,. \tag{4.33}$$

The operator $\bar{\mathcal{G}}^a$ is the generator of the so-called *background gauge transformation*, which is an auxiliary symmetry transformation of the auxiliary background-field $\bar{A}$. It is given by

$$\delta\bar{A}^a_\mu = \frac{1}{\bar{g}}D^{ab}_\mu[\bar{A}]\epsilon^b\,. \tag{4.34}$$

The generators $\mathcal{G}^a_A$ and $\mathcal{G}^a_{\rm gh}$ are defined in Eq. (4.12) and (4.20), respectively. The gauge-fixing action $S_{\rm gf}$ and the ghost action $S_{\rm gh}$ change under a variation of the fields according to

$$\left(\mathcal{G}^a_A + \mathcal{G}^a_{\rm gh}\right)S_{\rm gf} = -\bar{\mathcal{G}}^a S_{\rm gf} \quad \text{and} \quad \left(\mathcal{G}^a_A + \mathcal{G}^a_{\rm gh}\right)S_{\rm gh} = -\bar{\mathcal{G}}^a S_{\rm gh}\,. \tag{4.35}$$

From this we conclude that $S_{\rm gf}$ as well as $S_{\rm gh}$ do not vary under the combined transformation $\mathcal{G}^a_A + \mathcal{G}^a_{\rm gh} + \bar{\mathcal{G}}^a$. Since the classical Yang-Mills action $S_{\rm YM}$ is trivially invariant under these combined transformations, we find [65, 53]

$$\left(\mathcal{G}^a_A + \mathcal{G}^a_{\rm gh} + \bar{\mathcal{G}}^a\right) \hat{\Gamma}[\hat{\Phi}, \hat{\phi}] = 0\,. \tag{4.36}$$

So far, the symmetry under the combined transformation $\mathcal{G}^a_A + \mathcal{G}^a_{\rm gh} + \bar{\mathcal{G}}^a$ is only an auxiliary symmetry. However, this symmetry acquires physical significance if we identify the background-field $\hat{\phi}$ with the physical gauge field Φ. When we do this, we can read off from Eq. (4.36) that $\hat{\Gamma}[0, \hat{\phi}]$ is a gauge-invariant functional of the background-field $\bar{A}$ or, in other words, that the standard effective action $\Gamma[\Phi, \Phi]$ is invariant under the physical gauge transformations of the conventional classical field Φ:

$$\left(\mathcal{G}^a_A + \mathcal{G}^a_{\rm gh} + \bar{\mathcal{G}}^a\right) \hat{\Gamma}[\hat{\Phi}, \hat{\phi}]\Big|_{\hat{\Phi}=0} \overset{(4.26)}{=} \left(\mathcal{G}^a_A + \mathcal{G}^a_{\rm gh}\right) \Gamma[\Phi, \Phi] = 0\,. \tag{4.37}$$

The fact that the background-field formalism allows for such a convenient construction of a gauge-invariant effective action is the reason why we use this method for our study of gauge theories within the RG framework in this chapter.

Finally, let us discuss some properties of $\hat{\Gamma}[0, \hat{\phi}] \equiv \Gamma[\Phi, \Phi]$. First, we point out that fluctuations around the background-field $\bar{A}$ are still constrained by standard WTI which are obtained from $\left(\mathcal{G}^a_A + \mathcal{G}^a_{\rm gh} + \bar{\mathcal{G}}^a\right) \hat{\Gamma}[\hat{\Phi}, \hat{\phi}]$ according to Sec. 4.2. The effective action $\hat{\Gamma}[0, \hat{\phi}]$ has a crucial property: Vertices involving fluctuation fields a_μ are only used inside Feynman diagrams, whereas vertices involving background-fields $\bar{A}_\mu$ are used for external lines. Therefore, only propagators of the fluctuation fields appear inside the loops. This is the physical consequence of Eq. (4.37): the background-field propagator is undefined, because $\hat{\Gamma}[0, \hat{\phi}]$ is still invariant under background-field transformations. With regard to our purposes in the subsequent chapters, we remark that a renormalization of the ghost fields as well as the fluctuation fields is not needed since both appear only inside loops. The renormalization of the remaining quantities is given by

$$\left(\bar{A}_\mu\right)_{\rm bare} = Z_{\bar{A}}^{\frac{1}{2}} \bar{A}_\mu\,, \quad \bar{g} = Z_g g \quad \text{and} \quad (\xi)_{\rm bare} = Z_\xi\, \xi\,. \tag{4.38}$$

The fact that $\hat{\Gamma}[0, \hat{\phi}]$ is a gauge-invariant functional of $\bar{A}$ then implies that the renormalized field strength tensor $F_{\mu\nu}$ is identical to the bare field strength, up to a constant. This observation yields a relation between the renormalization constants Z_g and $Z_{\bar{A}}$:

$$Z_g = Z_{\bar{A}}^{-\frac{1}{2}}\,. \tag{4.39}$$

It implies that the product of the background-field strength $\bar{A}$ and the the coupling g is not renormalized, $g\bar{A} = \bar{g}\left(\bar{A}\right)_{\rm bare}$. The relation (4.39) enables us to determine the QCD running-coupling β_{g^2}-function solely from the computation of the background-field two-point function. In Sec. 4.5, we make use of the background-field formalism

for a computation of the running QCD coupling for a wide range of temperatures and scales within the functional RG. At first sight, the running coupling does not seem to be a useful quantity in the nonperturbative domain, since it is dependent on the RG scheme and strongly dependent on the definition. Therefore, we cannot *a priori* associate a universal meaning to the RG flow of the coupling, but we always have to use and interpret it in the light of its definition and the RG scheme. In fact, the background-field formalism provides for a simple non-perturbative definition of the running coupling in terms of the background-field wave function renormalization $Z_{\bar{A},k}$. The running coupling β_{g^2} is related to the anomalous dimension η of the background field via

$$\beta_{g^2} \equiv \partial_t g^2 = (d-4+\eta)g^2 \quad \text{with} \quad \eta = -\frac{1}{Z_{\bar{A},k}}\partial_t Z_{\bar{A},k}\,, \tag{4.40}$$

where we have kept the spacetime dimension d arbitrary. Since the background field can be naturally associated with the vacuum of gluodynamics, we may interpret the so-defined coupling as the response strength of the vacuum to color-charged perturbations.

4.4 RG Flow Equations in Background-Field Gauge

In this section, we show how to apply the background-field formalism for gauge-theories to the functional RG. The starting point for the derivation of the RG flow equation for the background-field effective action $\hat{\Gamma}_{\rm YM}[\hat{\Phi},\hat{\phi}]$ is an appropriate IR- and UV-regularized generating functional $\hat{Z}[J^T,\hat{\phi}]$. In case of gauge theories, this might pose a more difficult problem since such regularizations may violate gauge invariance. However, as already discussed in Subsec. 2.4.2, the IR- and UV- regularizations are only additional sources of gauge-symmetry breaking, since gauge invariance is already violated by the gauge-fixing procedure, see Sec. 4.2. Following the derivation of the flow equation in Sec. 2.4.2 and 2.4.3, we regularize the IR of the path-integral Eq. (4.24) through an insertion of cutoff terms $\Delta S_{k,A}$ and $\Delta S_{k,\rm gh}$ for the gauge fields and the ghost fields, respectively:

$$\Delta S_{k,A} = \frac{1}{2}\int d^dx \overbrace{(A^a_\mu - \bar{A}^a_\mu)}^{=a^a_\mu} R^{ab}_{\bar{A},\mu\nu}(\Delta_A[\bar{A}]) \overbrace{(A^b_\nu - \bar{A}^b_\nu)}^{=a^b_\nu}, \tag{4.41}$$

$$\Delta S_{k,\rm gh} = \int d^dx\, \bar{c}^a R^{ab}_{\rm gh}(\Delta_{\rm gh}[\bar{A}])c^b\,. \tag{4.42}$$

For the moment, we allow general arguments $\Delta_A[\bar{A}]$ and $\Delta_{\rm gh}[\bar{A}]$ which may depend on $\bar{A}$. The coarse-grained effective action $\hat{\Gamma}_k[\hat{\Phi},\hat{\phi}]$ is then obtained by performing a Legendre-transformation of the generating functional $\hat{W}[J^T,\hat{\phi}]$ for connected diagrams:

$$\hat{\Gamma}_k[\hat{\Phi},\hat{\phi}] = -\hat{W}_k[J,\hat{\phi}] + J^T\cdot\hat{\Phi} - \Delta S_k[\hat{\Phi},\hat{\phi}]\,. \tag{4.43}$$

Here we have introduced a matrix-valued regulator $R_k[\bar{A}]$ in field space:

$$R_k[\bar{A}] = \begin{pmatrix} R^{ab}_{A,\mu\nu}(\Delta_A[\bar{A}]) & 0 & 0 \\ 0 & 0 & \left(R^{ab}_{\rm gh}(\Delta_{\rm gh}[\bar{A}])\right)^T \\ 0 & R^{ab}_{\rm gh}(\Delta_{\rm gh}[\bar{A}]) & 0 \end{pmatrix} . \tag{4.44}$$

Using the so-defined matrix and the vectors defined in Eq. (4.22) and (4.25), the cutoff-terms can be written in a compact way:

$$\Delta S_{k,A} + \Delta S_{k,\rm gh} = \frac{1}{2}\hat{\Phi}^T \cdot R_k \cdot \hat{\Phi} \equiv \Delta S_k[\hat{\Phi}, \hat{\phi}] \, . \tag{4.45}$$

In the previous section, we have found that the effective action $\hat{\Gamma}[\hat{\Phi}, \hat{\phi}]$ is invariant under the combined transformation $\mathcal{G}^a_A + \mathcal{G}^a_{\rm gh} + \bar{\mathcal{G}}^a$, see Eq. (4.36). This invariance of the effective action is maintained even in the presence of the regulator term ΔS_k, if the regulator term satisfies

$$\left(\mathcal{G}^a_A + \mathcal{G}^a_{\rm gh} + \bar{\mathcal{G}}^a\right) \Delta S_k[\hat{\Phi}, \hat{\phi}] = 0 \, . \tag{4.46}$$

As has been shown in Ref. [70], the condition (4.46) for the regulator term is fulfilled if the arguments $\Delta_A[\bar{A}]$ and $\Delta_{\rm gh}[\bar{A}]$ of the regulator functions transform as tensors under the background-gauge transformation, i. e. $\bar{\mathcal{G}}^a(x)\Delta^{bc}_i[\bar{A}] = \bar{g} f^{bdc} \Delta^{ad}_i[\bar{A}]\delta(x-y)$. For example, a possible choice for these operators is

$$\Delta^{ab}_{A,\mu\nu}[\bar{A}] = -D^{ab}_\lambda[\bar{A}] D^{bc}_\lambda[\bar{A}] \delta_{\mu\nu} \quad \text{and} \quad \Delta^{ab}_{\rm gh}[\bar{A}] = -D^{ab}_\lambda[\bar{A}] D^{bc}_\lambda[\bar{A}] \, . \tag{4.47}$$

From now on, we assume that the arguments of the regulator functions are chosen in such a way that the constraint (4.46) is fulfilled. Following the steps along the lines of Subsec. 2.4.3, the flow equation for $\hat{\Gamma}[\hat{\Phi}, \hat{\phi}]$ yields

$$\partial_t \hat{\Gamma}_k[\hat{\Phi}, \hat{\phi}] = \frac{1}{2} \, {\rm STr} \left\{ \left[\hat{\Gamma}^{(1,1,0,0)}_k[\hat{\Phi}, \hat{\phi}] + R_k(\Delta[\bar{A}]) \right]^{-1} \left(\partial_t R_k(\Delta[\bar{A}]) \right) \right\} , \tag{4.48}$$

where the super-trace includes a trace over the ghost sector as well, including the corresponding minus sign. We have adopted the short-hand notation for the generalized n-point functions from Subsec. 2.4.3:

$$\hat{\Gamma}^{(i,j,k,l)}_k[\hat{\Phi}, \hat{\phi}] = \overbrace{\left(\frac{\overrightarrow{\delta}}{\delta \hat{\Phi}^T} \cdots \frac{\overrightarrow{\delta}}{\delta \hat{\Phi}^T} \right)}^{i-\text{times}} \overbrace{\left(\frac{\overrightarrow{\delta}}{\delta \hat{\phi}^T} \cdots \frac{\overrightarrow{\delta}}{\delta \hat{\phi}^T} \right)}^{k-\text{times}} \hat{\Gamma}_k[\Phi, \hat{\phi}] \overbrace{\left(\frac{\overleftarrow{\delta}}{\delta \hat{\phi}} \cdots \frac{\overleftarrow{\delta}}{\delta \hat{\phi}} \right)}^{l-\text{times}} \overbrace{\left(\frac{\overleftarrow{\delta}}{\delta \hat{\Phi}} \cdots \frac{\overleftarrow{\delta}}{\delta \hat{\Phi}} \right)}^{j-\text{times}} .$$

As we have discussed in Subsec. (2.4.3), the background-field effective action $\hat{\Gamma}[\hat{\Phi}, \hat{\phi}]$ evaluated at $\hat{\Phi} = 0$ is equivalent to the standard effective action $\Gamma[\Phi, \Phi]$ for $k \to 0$. According to Subsec. (2.4.3), we define

$$\Gamma_k[\Phi] := \hat{\Gamma}_k[0, \hat{\phi}] \, . \tag{4.49}$$

Note that in order to obtain $\Gamma_k[\Phi]$ for a particular value of k, one must first solve the flow equation (4.48) down to this value of k and then one must identify the background-field $\hat{\phi}$ with the field Φ. In this context, we remind the reader that the RHS of the flow equation (4.48) depends on the fluctuation field propagator $\hat{\Gamma}_k^{(1,1,0,0)}[\hat{\Phi},\hat{\phi}]$ and that it is therefore not a functional of $\Gamma_k[\Phi]$, as we have explicitly shown in Eq. (2.56). Consequently, it is not sufficient to study only the symmetries of $\Gamma_k[\Phi]$, but necessary to study also those of $\hat{\Gamma}_k[\hat{\Phi},\hat{\phi}]$, even if we know that $\Gamma_k[\Phi]$ is a gauge-invariant functional, as we will argue next.

Since we assume that Eq. (4.46) is satisfied, we find that $\hat{\Gamma}_k[\hat{\Phi},\hat{\phi}]$ is invariant under the combined transformations $\mathcal{G}_A^a + \mathcal{G}_{\rm gh}^a + \bar{\mathcal{G}}^a$. This implies that $\Gamma_k[\Phi]$ satisfies

$$\left(\mathcal{G}_A^a + \mathcal{G}_{gh}^a\right)\Gamma_k[\Phi] = 0\,. \tag{4.50}$$

Thus $\Gamma_k[\Phi]$ is invariant under physical gauge transformations in the limit $k \to 0$. Physical gauge invariance for finite values of k is encoded in *modified* Ward-Takahashi identities (mWTI) [70], which are given by

$$\begin{aligned}&\left(\mathcal{G}_A^a + \mathcal{G}_{gh}^a\right)\hat{\Gamma}_k[\hat{\Phi},\hat{\phi}]\\ &\quad= \frac{\langle 0|\left(\mathcal{G}_A^a + \mathcal{G}_{gh}^a\right)(S_{\rm gf}+S_{\rm gh})|0\rangle_J}{\langle 0|0\rangle_J} + \frac{\langle 0|\left(\mathcal{G}_A^a + \mathcal{G}_{gh}^a\right)\Delta S_k|0\rangle_J}{\langle 0|0\rangle_J}\,.\end{aligned} \tag{4.51}$$

The first term on the RHS corresponds to the standard WTI in the presence of the regulator scale k, whereas the second arises due to the presence of the regulator terms in the path-integral[5]. From Eq. (4.60), we obtain the standard WTI for $k \to 0$ since the second term on the RHS vanishes in this limit. Moreover, we obtain *background-field* Ward-Takahashi identities (bWTI) by applying $\bar{\mathcal{G}}^a$ to $\hat{\Gamma}_k[\hat{\Phi},\hat{\phi}]$:

$$\bar{\mathcal{G}}^a\hat{\Gamma}_k[\hat{\Phi},\hat{\phi}] = \frac{\langle 0|\bar{\mathcal{G}}^a(S_{\rm gf}+S_{\rm gh})|0\rangle_J}{\langle 0|0\rangle_J} + \frac{\langle 0|\bar{\mathcal{G}}^a\Delta S_k|0\rangle_J}{\langle 0|0\rangle_J}\,. \tag{4.52}$$

Combining the bWTI and the mWTI, we recover the invariance of $\hat{\Gamma}_k[\hat{\Phi},\hat{\phi}]$ under the combined transformations $\mathcal{G}_A^a + \mathcal{G}_{\rm gh}^a + \bar{\mathcal{G}}^a$. Note that this only yields physical gauge invariance of $\Gamma_k[\Phi]$ for $k \to 0$ if the background-field effective action $\hat{\Gamma}_k[\hat{\Phi},\hat{\phi}]$ satisfies the standard WTI in this limit.

Let us now apply our knowledge about the symmetries of $\hat{\Gamma}_k[\hat{\Phi},\hat{\phi}]$ to the flow equation (4.48). As has been shown in Ref. [70], the invariance of $\hat{\Gamma}_k[\hat{\Phi},\hat{\phi}]$ under the transformation $\mathcal{G}_A^a + \mathcal{G}_{\rm gh}^a + \bar{\mathcal{G}}^a$ is sufficient to prove that the flow equation satisfies

$$\left(\mathcal{G}_A^a + \mathcal{G}_{\rm gh}^a + \bar{\mathcal{G}}^a\right)\partial_t\hat{\Gamma}_k[\hat{\Phi},\hat{\phi}] = 0\,, \tag{4.53}$$

implying that

$$\left(\mathcal{G}_A^a + \mathcal{G}_{\rm gh}^a\right)\partial_t\Gamma_k[\Phi] = 0\,. \tag{4.54}$$

[5]It has been explicitly worked out in Ref. [70] that the first term in Eq. (4.60) gives the standard loop contributions to the WTI in Yang-Mills theory.

We conclude from Eq. (4.53) that the full quantum effective action $\hat{\Gamma}_0[\hat{\Phi},\hat{\phi}]$ is invariant under the combined transformations $\mathcal{G}^a_A + \mathcal{G}^a_{\rm gh} + \bar{\mathcal{G}}^a$ and that it satisfies the standard WTI, provided the initial effective action at $k = \Lambda$ is invariant under these transformations[6].

In this work[7], we solve the RG flow defined by Eq. (4.48) approximately by setting $A = \bar{A}$, i. e. $\hat{\Phi} = 0$, right from the beginning. Beside this, we also neglect the difference between the RG flows of the fluctuation and the background field. In the flow equation (4.48), this approximation is reflected in the fact that we identify the propagator $\Gamma_k^{(1,1)}[\Phi]$ with the fluctuation-field propagator (see Eq. (2.56)):

$$\Gamma_k^{(1,1)}[\Phi] \stackrel{!}{=} \hat{\Gamma}_k^{(1,1,0,0)}[0,\Phi]\,. \tag{4.55}$$

In fact, this is in general not the case, as we discussed in Sec. 2.4.3. We refer to [166] for a treatment of this difference. In the following, however, we discuss a strategy developed in [74, 71] for the computation of an approximate solution. The (approximate) RG flow equation under consideration then reads

$$\partial_t\,\Gamma_k[\Phi] = \frac{1}{2}\,\mathrm{STr}\,\left\{\left[\Gamma_k^{(1,1)}[\Phi] + R_k(\Delta[\bar{A}])\right]^{-1}\left(\partial_t R_k(\Delta[\bar{A}])\right)\right\}\,. \tag{4.56}$$

The super-trace includes a trace over the ghost sector as well, with the corresponding minus sign. As the above discussion of symmetries has shown, the property of manifest physical gauge invariance of the solution to this flow equation is still maintained in the approximation of setting $A = \bar{A}$, i. e. $\hat{\Phi} = 0$, even for finite values of k. In this respect, the neglecting of the difference between the RG flows of the fluctuation and the background field is unproblematic. However, as we have already discussed in Subsec. 2.4.3, the flow is no longer *closed* [64] due to the assumption (4.55). In other words, this means an *information loss*, since information required for the next RG step is not completely provided by the preceding step. This is the price to be paid for this approximation. Moreover, this approximation satisfies some but not all constraints imposed by the regulator-modified Ward-Takahashi identities (mWTI). It is instructive to discuss the consequences of setting $\hat{\Phi} = 0$ in Eq. (4.48) explicitly, following Ref. [72, 71]. For this purpose, we assume that the background-field effective action $\hat{\Gamma}_k[\hat{\Phi},\hat{\phi}]$ can be decomposed as follows[8]:

$$\hat{\Gamma}_k[a,c,\bar{c},\bar{A}] = \Gamma_k^{\rm YM}[a+\bar{A}] + \hat{\Gamma}_k^{\rm gf}[a,\bar{A}] + \hat{\Gamma}_k^{\rm gh}[a,c,\bar{c},\bar{A}] + \hat{\Gamma}_k^{\rm gauge}[a,c,\bar{c},\bar{A}]\,, \tag{4.57}$$

[6]Moreover, $\hat{\Gamma}_0[\hat{\Phi},\hat{\phi}]$ satisfies the mWTI on all scales if one can show that it satisfies the mWTI on one particular scale, e. g. at $k = \Lambda$, see Ref. [70].

[7]We also apply the approximations discussed here to our study of the running QCD coupling that incorporates quark degrees of freedom.

[8]This assumption is motivated by the fact that the classical action with the gauge-fixing terms is recovered from $\hat{\Gamma}_k[\hat{\Phi},\hat{\phi}]$ in the limit $k \to \Lambda \to \infty$, see Ref. [72]. Moreover, we have $\hat{\Gamma}_\infty[0,\Phi] = S_{\rm YM}[\Phi]$ in this limit.

where we impose a normalization for $\hat{\Gamma}_k^{\text{gauge}}$

$$\hat{\Gamma}_k^{\text{gauge}}[0,0,0,\bar{A}] = 0\,. \tag{4.58}$$

For better readability, we give the arguments of the (background-field) effective action explicitly rather than in form of a generalized vector in field space, see Eq. (4.22) and (4.25) for our definitions of Φ and $\hat{\phi}$, respectively. Here $\hat{\Gamma}^{\text{gf}}$ and $\hat{\Gamma}^{\text{gh}}$ represent generalized gauge-fixing and ghost contributions, for which we use their classical form in the remainder of this chapter:

$$\hat{\Gamma}_k^{\text{gf}}[a,\bar{A}] = \frac{1}{2\xi}\int_x (D_\mu[\bar{A}]\overbrace{(A-\bar{A})}^{=a_\mu}{}_\mu)^2, \quad \hat{\Gamma}_k^{\text{gh}}[a,\bar{c},c,\bar{A}] = -\int_x \bar{c}D_\mu[\bar{A}]D_\mu[a+\bar{A}]c\,. \tag{4.59}$$

Note that we neglect any non-trivial running in these terms. The gauge-noninvariant remainder of the effective action is summarized in $\hat{\Gamma}_k^{\text{gauge}}$. This includes, e. g., operators parametrizing the non-trivial running in the gauge-fixing and ghost sector. The pure gluonic part Γ_k^{YM} is assumed to be a gauge invariant functional carrying the desired physical information about the quantum theory in the limit $a = c = \bar{c} = 0$, i. e. $A = \bar{A}$. From our decomposition of $\hat{\Gamma}$ in Eq. (4.57), we immediately find that the fluctuation field propagator receives in general a contribution from $\hat{\Gamma}_k^{\text{gauge}}$ even in the limit $a = c = \bar{c} = 0$. In addition, we find that the contribution arising from the gauge-fixing term $\hat{\Gamma}_k^{\text{gf}}$ to the fluctuation field propagator is independent of the fluctuation field a. Neglecting $\hat{\Gamma}_k^{\text{gauge}}$ in Eq. (4.57) then means that we do not take into account that the flow of $\Gamma_k[A = \bar{A}]$ is affected by contributions from $A \neq \bar{A}$. Applying the mWTI, Eq. (4.60), to the decomposed effective action (4.57), we obtain

$$\begin{aligned}\left(\mathcal{G}_A^a + \mathcal{G}_{gh}^a\right)\left(\hat{\Gamma}_k^{\text{gf}} + \hat{\Gamma}_k^{\text{gh}} + \hat{\Gamma}_k^{\text{gauge}}\right) - \frac{\langle 0|\left(\mathcal{G}_A^a + \mathcal{G}_{gh}^a\right)(S_{\text{gf}} + S_{\text{gh}})|0\rangle_J}{\langle 0|0\rangle_J} \\ = \frac{\langle 0|\left(\mathcal{G}_A^a + \mathcal{G}_{gh}^a\right)\Delta S_k|0\rangle_J}{\langle 0|0\rangle_J}\,,\end{aligned} \tag{4.60}$$

where we have used that Γ_k^{YM} is an arbitrary but gauge-invariant functional[9]. We observe that the flow of Γ_k at $A = \bar{A}$ is in general affected by $\hat{\Gamma}_k^{\text{gauge}}$ via the mWTI. Therefore, neglecting of $\hat{\Gamma}_k^{\text{gauge}}$ is in general not consistent with this constraint. In the following, however, we assume that both the information loss and the corrections due to the mWTI are quantitatively negligible for the final result. The advantage of the approximation of using $\Gamma_k[A = \bar{A}] \equiv \hat{\Gamma}[0,0,0,\bar{A}]$ for all k is that we obtain a gauge-invariant approximate solution of the quantum theory[10].

[9] A similar constraint is obtained by applying the bWTI, Eq. (4.52), on the decomposed effective action (4.57).

[10] For recent advances using an alternative approach, which is based on a manifestly gauge invariant regulator, we refer to [57]. Additional proposals for thermal gauge-invariant flows can be found in [167].

For the remainder of this chapter, we optimize our truncated flow by inserting the background-field dependent $\Gamma_k^{(1,1)}[A = \bar{A}]$ in the regulator Eq. (4.56), i. e. we use $\Delta[\bar{A}] = \Gamma_k^{(1,1)}[A]$. Of course, this choice for $\Delta[\bar{A}]$ is consistent with our assumption that Eq. (4.46) is satisfied. Furthermore, it adjusts the regularization to the spectral flow of the fluctuations [71, 64], which leads to a significant improvement since larger classes of diagrams can be resummed in the present truncation scheme, as we have discussed in Subsec. (2.4.3).

4.5 RG Flow of the Running Coupling at Finite Temperature

In this section, we compute the QCD running coupling by applying the background-field formalism to the functional RG. We follow the strategy discussed in the last section. While an investigation of the coupling is interesting in its own right, we will also show in the subsequent sections that it represents a key ingredient to our study of the chiral phase boundary.

4.5.1 Truncated RG flow

Owing to the strong coupling, we cannot expect that low-energy gluodynamics can be described by a small number of gluonic operators. On the contrary, infinitely many operators become RG relevant and will in turn drive the running of the coupling. We span a truncated space of effective action functionals with the ansatz[11]

$$\hat{\Gamma}_k = \Gamma_k^{\mathrm{YM}}[\overbrace{a+\bar{A}}^{=A}] + \hat{\Gamma}_k^{\mathrm{gf}}[a,\bar{A}] + \hat{\Gamma}_k^{\mathrm{gh}}[a,\bar{c},c,\bar{A}] + \hat{\Gamma}_k^{\mathrm{quark}}[a,\bar{\psi},\psi,\bar{A}]\,. \tag{4.61}$$

The terms Γ^{gf} and Γ^{gh} represent gauge-fixing and ghost contributions, which are defined in Eq. (4.59). Our choice for the functional $\Gamma_k^{\mathrm{YM}}[A]$ is only constrained by gauge invariance. The quark contributions are contained in

$$\hat{\Gamma}_k^{\psi}[a,\bar{\psi},\psi,\bar{A}] = \int_x \bar{\psi}(\mathrm{i}\not{D}[a+\bar{A}] + M_{\bar{\psi}\psi})\psi + \Gamma_k^{\text{q-int}}[\bar{\psi},\psi], \tag{4.62}$$

where the last term $\Gamma_k^{\text{q-int}}[\bar{\psi},\psi]$ denotes our ansatz for gluon-induced quark self-interactions. These interactions will be discussed in Sect. 4.6.2. In Eq. (4.62), we have already set the quark wave function renormalization to $Z_\psi = 1$, which is a consequence both of the Landau gauge and our later choice for $\Gamma_k^{\text{q-int}}[\bar{\psi},\psi]$. The pure gluonic subspace $\Gamma_k^{\mathrm{YM}}[A]$ is truncated to an infinite but still tractable set of operators,

$$\Gamma_k^{\mathrm{YM}}[A] = \int_x \mathcal{W}_k(\theta), \quad \theta = \frac{1}{4}F_{\mu\nu}^a F_{\mu\nu}^a. \tag{4.63}$$

[11] In conrast to the previous sections, we give the arguments of the (background-field) effective action explicitly rather in form of a generalized vector in field space.

Expanding the function $\mathcal{W}(\theta) = W_1\theta + \frac{1}{2}W_2\theta^2 + \frac{1}{3!}W_3\theta^3\ldots$, the expansion coefficients W_i denote an infinite set of generalized couplings. Here, W_1 is identical to the desired background-field wave function renormalization, $Z_k \equiv W_1$, which defines the running of the coupling,

$$g^2 = k^{d-4}Z_k^{-1}\bar{g}^2. \tag{4.64}$$

Note that Eq. (4.40) is a consequence of this definition. This truncation corresponds to a gradient expansion in the field strength, in which higher-derivative terms and more complicated color and Lorentz structures are neglected. In this way, the truncation includes arbitrarily high gluonic correlators, projected onto their small-momentum limit and onto the particular color and Lorentz structure arising from powers of F^2. In our truncation, the running of the coupling is successively driven by all generalized couplings W_i.

It is convenient to express the flow equation in terms of dimensionless renormalized quantities

$$\vartheta = g^2k^{-d}Z_k^{-1}\theta \equiv k^{-4}\bar{g}^2\theta, \tag{4.65}$$

$$w(\vartheta) = g^2k^{-d}\mathcal{W}_k(\theta) \equiv k^{-4}Z_k^{-1}\bar{g}^2\mathcal{W}_k(k^4\vartheta/\bar{g}^2). \tag{4.66}$$

Inserting Eq. (4.61) into Eqns. (2.61) and (2.66), we obtain the flow equation for $w(\vartheta)$:

$$\begin{aligned}\partial_t w = -(4-\eta)w + 4\vartheta\dot{w} + \frac{g^2}{2(4\pi)^{\frac{d}{2}}}\int_0^\infty ds\Bigg\{ &-16\sum_{i=1}^{N_c}\sum_{\xi=1}^{N_f}\tilde{h}^\psi(s,\tfrac{m_\xi}{k})f_T^\psi(s,\tfrac{T}{k})f^\psi(sb_i)b_i^{e_d}\\
&+\tilde{h}(s)\Bigg[4\sum_{l=1}^{N_c^2-1}\Big(f_T^A(s\,\dot{w},\tfrac{T}{k})f_1^A(s\,\dot{w}\,b_l) - f_T^A(s,\tfrac{T}{k})f_2^A(sb_l)\Big)b_l^{e_d}\\
&-2f_T^A(s\,\dot{w},\tfrac{T}{k})f_3^A(s\,\dot{w},\frac{\dot{w}}{\dot{w}+2\vartheta\,\ddot{w}})\Bigg] - \Big(\eta\tilde{g}(s) + (\tilde{h}(s)-\tilde{g}(s))\Big(\frac{\partial_t\,\dot{w}-4\vartheta\,\ddot{w}}{\dot{w}}\Big)\Big)\times\\
&\times\Bigg[2\sum_{l=1}^{N_c^2-1}f_T^A(s\,\dot{w},\tfrac{T}{k})f_1^A(s\,\dot{w}\,b_l)b_l^{e_d} - f_T^A(s\,\dot{w},\tfrac{T}{k})f_3^A(s\,\dot{w},\frac{\dot{w}}{\dot{w}+2\vartheta\,\ddot{w}})\Bigg]\\
&-\frac{2(\tilde{h}(s)-\tilde{g}(s))\vartheta}{(\dot{w}+2\vartheta\,\ddot{w})^2}\Big(\ddot{w}\,\partial_t\dot{w} - \dot{w}\,\partial_t\ddot{w} + 4\dot{w}\ddot{w} + 4\vartheta(\dot{w}\dddot{w} - \ddot{w}^2)\Big)f_4^A(s\,\dot{w},\tfrac{T}{k})\Bigg\},\end{aligned} \tag{4.67}$$

where the auxiliary functions f are defined in App. D.1, and we have used the abbreviation $e_d = \frac{d-1}{2}$. The "color magnetic" field components b_i are defined by $b_i = |\nu_i|\sqrt{2\vartheta}$, where ν_i denotes eigenvalues of (n^aT^a) in the fundamental representation; correspondingly, b_l is equivalently defined for the adjoint representation. Furthermore, we have used the short-hand notation $w \equiv w(\vartheta)$ and dots denote derivatives with respect to ϑ. For details on the derivation of Eq. (4.67), we refer the reader to App. G.

In order to extract the flow equation for the running coupling, we expand the function $w(\vartheta)$ in powers of ϑ,

$$w(\vartheta) = \sum_{i=0}^{\infty} \frac{w_i}{i!} \vartheta^i \,, \quad w_1 = 1. \tag{4.68}$$

Note that w_1 is fixed to 1 by definition (4.66). Inserting this expansion into Eq. (4.67), we obtain an infinite tower of first-order differential equations for the coefficients w_i. In the present work, we concentrate on the running coupling and ignore the full form of the function $\mathcal{W}$; hence, we set $w_i \to 0$ for $i \geq 2$ on the RHS of the flow equation as a first approximation, but keep track of the flow of all coefficients w_i. The resulting infinite tower of equations is of the form

$$\partial_t w_i = X_i(g^2, \eta) + Y_{ij}(g^2) \partial_t w_j \,. \tag{4.69}$$

Details on the computation of the functions X_i, Y_{ij} are given in App. G; the function Y_{ij} obeys $Y_{ij} = 0$ for $j > i+1$. Note that we have not dropped the flows of the generalized couplings w_i, namely $\partial_t w_i$, which are a consequence of the spectral adjustment of the flow, see the discussion in Subsec. 2.4.3. This infinite set of equations can be solved iteratively, yielding the anomalous dimension as an infinite power series of g^2

$$\eta = \sum_{m=1}^{\infty} a_m G^m \quad \text{with} \quad G \equiv \frac{g^2}{2(4\pi)^{d/2}} \,. \tag{4.70}$$

The coefficients a_m can be worked out analytically, see App. (G); they depend on the gauge group, the number of quark flavors, their masses, the temperature and the regulator. Equation (4.70) constitutes an asymptotic series, since the coefficients a_m grow at least factorially. This is no surprise, since the expansion (4.68) induces an expansion of the proper-time integrals in Eq. (4.67), for which this is a well-understood property [168]. A good approximation of the underlying finite integral representation of Eq. (4.70) can be deduced from a Borel resummation, including only the leading asymptotic growth of the a_m,

$$\eta \simeq \sum_{m=1}^{\infty} a_m^{\text{l.g.}} G^m \,. \tag{4.71}$$

The leading-growth coefficients are given by a sum of gluon, ghost and quark-gluon contributions,

$$\begin{aligned} a_m^{\text{l.g.}} = 4(-2c_1)^{m-1} \frac{\Gamma(z_d+m)\Gamma(m+1)}{\Gamma(z_d+1)} \Big[& \bar{h}^A_{2m-e_d}(\tfrac{T}{k})(d-2)\frac{2^{2m}-2}{(2m)!}\tau_m^A B_{2m} \\ & - \frac{4}{\Gamma(2m)} \tau_m^A \bar{h}^A_{2m-e_d}(\tfrac{T}{k}) + 4^{m+1} \frac{B_{2m}}{(2m)!} \tau_m^\psi \sum_{i=1}^{N_{\text{f}}} \bar{h}^\psi_{2m-e_d}(\tfrac{m_i}{k}, \tfrac{T}{k}) \Big]. \end{aligned} \tag{4.72}$$

The auxiliary functions c_1, c_2, z_d and the thermal moments $\bar{h}_j$, $\bar{h}_j^\psi$ are defined in App. D.1 and G.3. The group theoretical factors τ_m^A and τ_m^ψ are defined and discussed in App. B.2. The last term in the second line of Eq. (4.72) contains the quark contributions to the anomalous dimension, including a sum over the different quark flavors with mass m_i. The remaining terms are of gluonic origin.

The first term in the second line has to be treated with care, since it arises from the Nielsen-Olesen mode in the propagator [169], which is unstable in the IR. This mode occurs in the perturbative evaluation of gradient-expanded effective actions and signals the instability of chromomagnetic fields with large spatial correlation. At finite temperature, this problem is particularly severe, since such a mode will strongly be populated by thermal fluctuations. This typically spoiling perturbative computations [170].

From the perspective of the flow-equation, this does not cause conceptual problems, since in contrast to the perturbative gradient expansion, no assumption about large spatial correlations of the background field is needed.

For an expansion of the flow equation about the (unknown) true vacuum state, the regulated propagator would be positive definite, $\Gamma_k^{(2)} + R_k > 0$ for $k > 0$. Even without knowing the true vacuum state, it is therefore a viable procedure to include only the positive part of the spectrum of $\Gamma_k^{(2)} + R_k$ in our truncation, since it is an exact operation for stable background fields. At zero temperature, these considerations are redundant, since the unstable mode merely creates imaginary parts that can easily be separated from the flow of the coupling. At finite temperature, we need to remove only the unphysical thermal population of this mode. We do this by using a T-dependent regulator that screens the instability. To ensure an unambiguous regularization, we include the Nielsen-Olesen mode for all $k \geq T$ as it is, dropping possible imaginary parts. For $k < T$, we remove the Nielsen-Olesen mode completely, thus inhibiting its thermal excitation. Of course, a smeared regularization of this mode is also possible, as discussed in App. H. As we show in this appendix, the regularization prescription that we have proposed here is a point of "minimum sensitivity" [44] in a whole class of regulators. This supports our view that our regularization has the least amount of contamination with unphysical thermal population of the Nielsen-Olesen mode.

We outline the resummation of η of Eq. (4.71) in App. G.3. It yields

$$\eta = \eta_1^A + \eta_2^A + \eta^{\mathrm{q}}, \tag{4.73}$$

with gluonic parts η_1^A, η_2^A and the quark contribution to the gluon anomalous dimension[12] η^{q}. Finite integral representations of these functions are given in Eqns. (G.60), (G.66), and (G.67). For pure gluodynamics, η_1^A and η_2^A carry the full information about the running coupling.

In Fig. 4.4, we show the result for the anomalous dimension η as a function of $G = \frac{\alpha_{\mathrm{s}}}{8\pi}$ for $N_{\mathrm{c}} = 3$ and $N_{\mathrm{f}} = 3$ in $d = 4$ dimensions. These results have been obtained

[12]The contribution η^{q} should not be confused with the quark anomalous dimension η_ψ which is zero in our truncation.

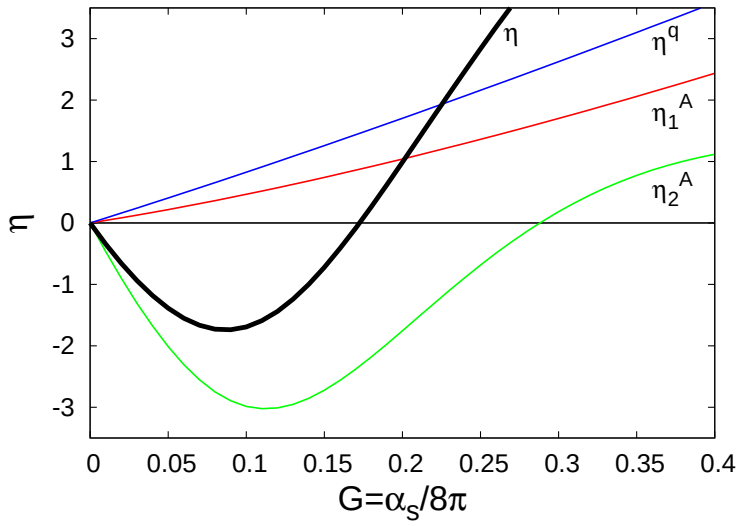

Figure 4.4: Anomalous dimension η as a function of $G = \frac{\alpha_s}{8\pi}$ for $4d$ $SU(N_c = 3)$ theory with $N_f = 3$ massless quark flavors at vanishing temperature. The gluonic parts η_1^A, η_2^A and the quark part η^q contributing to the anomalous dimension η (thick black line) are shown separately. The gluonic parts η_1^A and η_2^A agree with the results found in [71]. The figure shows the results from a calculation with a background field pointing into the 8-direction in color space.

with the exponential regulator, see Eq. (D.19) and Eq. (D.21) in App. D for the gluons and quarks, respectively. For pure gluodynamics (i.e. $N_f = 0$), we find an IR stable fixed point for vanishing temperature,

$$\alpha_* = [\alpha_{*,8}, \alpha_{*,3}] \approx [5.7, 9.7]\,, \tag{4.74}$$

in agreement with the results found in [71]. The (theoretical) uncertainty is due to the fact that we have used a simple approximation for the exact color factors τ_j^A and τ_j^ψ, see App. B.2 for details. This approximation introduces an artificial dependence on the direction of the background field in color space. The extremal cases of this dependence are given by the 3- and 8-direction in the Cartan sub-algebra. The results for these extremal cases span the interval given above for the IR fixed point. Even though this uncertainty is quantitatively large in the pure-glue case, it has little effect on the quantitative results for full QCD, as we will see below.

The inclusion of light quarks yields a smaller value for the infrared fixed point α_*, as can be seen from Fig. 4.4. However, this smaller fixed-point value will only be attained if quarks stay massless or light in the deep IR. If chiral symmetry breaking occurs, the quarks become massive and decouple from the flow, and in consequence the system is expected to approach the pure-glue fixed point. We can read off from Fig. 4.4 that in

any case the inclusion of quarks leads to a smaller coupling compared to the coupling of a pure gluonic system. This happens already in the symmetric regime.

4.5.2 Results for the Running Coupling

For quantitative results with regard to the running coupling, we confine ourselves to $d = 4$ dimensions and to the gauge groups SU(2) and SU(3). Of course, results for arbitrary dimensions with $d > 2$ and other gauge groups can be obtained straightforwardly from our general expressions in App. G.3. For instance, this offers a way to study nonperturbative renormalizability of QCD-like theories in extra dimensions, as initiated in Ref. [171] for pure gauge theories.

To this end, a quantitative evaluation of the coupling flow requires a specification of the regulator shape-function $r(y)$, cf. Eq. (D.19) and Eq. (D.21) in the appendix for the gluons and quarks, respectively. In order to make it easier to establish contact with measured values for the coupling, e.g., at the scale given by Z mass or the τ mass, it is advantageous to choose $r(y)$ in correspondence with a regularization scheme for which the running of the coupling is sufficiently close to the standard $\overline{\text{MS}}$ running in the perturbative domain. Here, it is important to note that already the two-loop β_{g^2} coefficient depends on the regulator. This is due to both the truncation and the mass-dependent regularization scheme. As an example, we give the two-loop β_{g^2} function calculated from Eq. (4.67) for QCD with N_c colors and N_f massless quark flavors in $d = 4$ dimensions:

$$\begin{aligned}\beta(g^2) \;=\; & -\left(\frac{22}{3}\bar{h}^A_{\frac{1}{2}}N_\text{c} - \frac{4}{3}\bar{h}^\psi_{\frac{1}{2}}N_\text{f}\right)\frac{g^4}{(4\pi)^2} - \left(\frac{77N_\text{c}^2\bar{h}^A_{\frac{1}{2}} - 14N_\text{c}N_\text{f}\bar{h}^\psi_{\frac{1}{2}}}{3}\,\bar{g}^A_{\frac{1}{2}}\right. \\ & \left. -\frac{127\tau_2^A\bar{h}^A_{\frac{5}{2}} + N_\text{f}\tau_2^\psi\bar{h}^\psi_{\frac{5}{2}}}{45}\Big(3(N_\text{c}^2-1)(\bar{h}^A_{-\frac{3}{2}} - \bar{g}^A_{-\frac{3}{2}}) + 2(\bar{H}^A_0 - \bar{G}^A_0)\Big)\right)\frac{g^6}{(4\pi)^4} + \dots\,.\end{aligned} \tag{4.75}$$

The thermal moments $\bar{g}_j^{A/\psi}$,$\bar{h}_j^{A/\psi}$, $\bar{G}_j^A$ and $\bar{H}_j^A$ are defined in App. D.1. They specify the regulator dependence of the loop terms and depend on $\frac{T}{k}$. This is visualized in Fig. 4.5. We observe that even the one-loop coefficient is regulator-dependent at finite temperature, but universal and exact at zero temperature, as it should be. The universality and exactness of this coefficient holds, since $\bar{g}^{A/\psi}_{\frac{1}{2}}(\frac{T}{k}=0) = 1$ and $\bar{h}^{A/\psi}_{\frac{1}{2}}(\frac{T}{k}=0) = 1$ for all permissible regulators. Using the exponential regulator, we find

$$\begin{aligned}&\bar{h}^A_{-\frac{3}{2}}(\frac{T}{k}=0) = 2\zeta(3)\,, \quad \bar{g}^A_{-\frac{3}{2}}(\frac{T}{k}=0) = 1\,, \quad \bar{h}^{A/\psi}_{\frac{5}{2}}(\frac{T}{k}=0) = \frac{1}{6}, \\ &\bar{G}^A_0(\frac{T}{k}=0) = \frac{1}{2} \quad \text{and} \quad \bar{H}^A_0(\frac{T}{k}=0) = \zeta(3)\end{aligned} \tag{4.76}$$

for the moments at zero temperature. Using the color factors τ_2^A and τ_2^ψ from App. B.2,

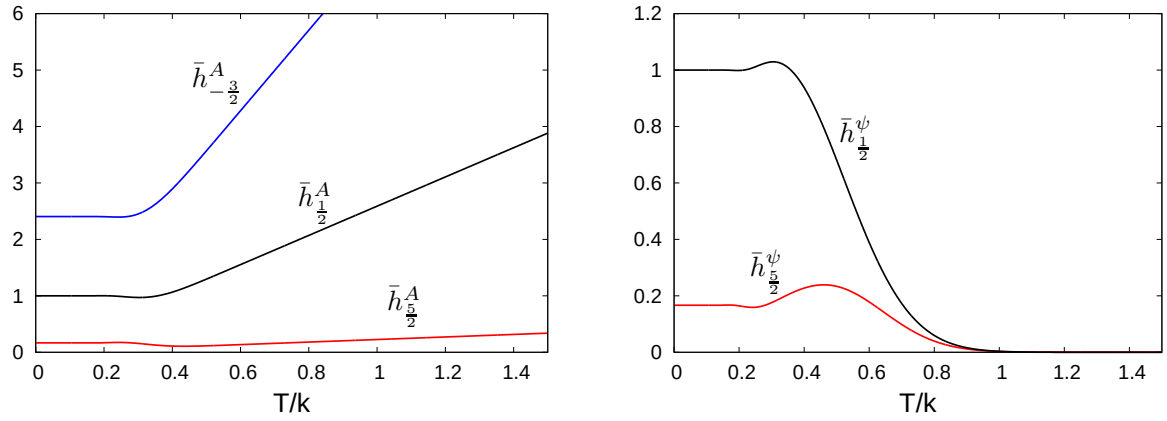

Figure 4.5: Thermal moments as a function of $\frac{T}{k}$ for the exponential regulator. The moments h_i^A as well as h_i^ψ are finite in the limit $\frac{T}{k} \to 0$. The gluonic thermal moments h_i^A grow linearly for increasing $\frac{T}{k}$ due to the presence of a soft Matsubara mode, whereas the fermionic thermal moments h_i^ψ are exponentially supressed for $\frac{T}{k} \to \infty$.

we compare our result to the perturbative two-loop result,

$$\beta_{pert.}(g^2) = -\left(\frac{22}{3}N_\mathrm{c} - \frac{4}{3}N_\mathrm{f}\right)\frac{g^4}{(4\pi)^2} - \left(\frac{68N_\mathrm{c}^3 + 6N_\mathrm{f} - 26N_\mathrm{c}^2N_\mathrm{f}}{3N_\mathrm{c}}\right)\frac{g^6}{(4\pi)^4} + \dots\,, \quad (4.77)$$

and find good agreement to within 99% for the two-loop coefficient for SU(2) and 95% for SU(3) pure gauge theory. Besides this compatibility with the standard $\overline{\mathrm{MS}}$ running, the exponential regulator is also technically and numerically convenient.

The suitability of the regulator for a perturbative calculation is mandatory for a reliable estimate of absolute scales of the final results. The present choice enables us to fix the running coupling to experimental input: as initial condition, we use the value of the coupling measured at the τ mass scale [9], $\alpha_\mathrm{s} = 0.322$, which agrees after RG evolution with the world average of α_s at the Z mass scale. We stress that no other parameter or scale is used as an input.

The global behavior of the running coupling can be characterized in simple terms. Let us first concentrate on pure gluodynamics, setting $N_\mathrm{f} \to 0$ for the moment. At zero temperature, we rediscover the results of [71], which exhibits a standard perturbative behavior in the UV. In the IR, the coupling increases and approaches a stable fixed point g_*^2 which is induced by a second zero of the β_{g^2} function, see Fig. 4.6. The appearance of an IR fixed point in Yang-Mills theories is a well-investigated phenomenon and has also been studied in the Landau gauge, see e. g. Refs. [172, 173, 174, 175, 176, 177]. Here, the IR fixed point is a consequence of a tight link between the fully dressed gluon and ghost propagators at low momenta. This link is visible in a vertex expansion [178]. Most interestingly, this behavior is in accordance with the Kugo-Ojima and Gribov-Zwanziger confinement scenarios [179, 165, 180]. Even though the relation between

the Landau-gauge and the background-gauge IR fixed point is not immediate, it is reassuring that the definition of the running coupling in both frameworks rests on a nonrenormalization property that arises from gauge invariance [181, 65]. Within the present mass-dependent RG scheme, the appearance of an IR fixed point is compatible with the existence of a mass gap: once the scale k has dropped below the lowest physical state in the spectrum, the running of physically relevant couplings is expected to freeze out, since no fluctuations are left to drive any further RG flow. Finally, IR fixed-point scenarios have successfully been applied also in phenomenological studies as well, see e. g. Refs. [182, 183, 184, 185, 186, 187].

For scales $k \gg T$, we find agreement with the perturbative running coupling at zero temperature, as one would naively expect. In the IR, the running is strongly modified: The coupling increases towards smaller scales until it develops a maximum near $k \sim T$. Below, the coupling decreases according to a power law $g^2 \sim k/T$, see Fig. 4.6. The reason for this behavior can be understood within the RG framework: first, the hard gluonic modes decouple from the RG flow at the scale $k \sim T$. At this point, the wavelength of fluctuations with momenta $p^2 < T^2$ is larger than the extent of the compactified Euclidean time direction. Hence these modes become effectively 3-dimensional and their limiting behavior is governed by the spatial $3d$ Yang-Mills theory. However, the decoupling of the hard modes alone cannot explain the decrease of the coupling for scales $k < T$. The second ingredient which is needed is the existence of a non-Gaußian IR fixed point also in the reduced 3-dimensional theory. Indeed, we observe the existence of such a non-Gaußian IR fixed point also in the reduced $3d$ theory, see also Subsec. 4.5.3. A straightforward matching between the $4d$ and $3d$ coupling reveals that the observed power law for the $4d$ coupling is a direct consequence of the strong-coupling IR behavior in the $3d$ theory, $g^2(k \ll T) \approx g^2_{3d,*}\, k/T$. Note that this asymptotic behavior can be deduced analytically from the integral representation of Eq. (4.70), see Subsec. 4.5.3. Again, the IR behavior observed at finite temperature is in accordance with recent results in the Landau gauge [41].

The $3d$ IR fixed point and the perturbative UV-behavior already determine the momentum asymptotics of the running coupling qualitatively. Phenomenologically, the behavior of the coupling in the transition region near its maximum value is most important. Quantitatively, it is provided by the full $4d$ finite-temperature flow equation. In addition to the shift of the position of the maximum with the temperature, we observe a decrease of the maximum value for increasing temperature. On average, the $4d$ coupling gets weaker at higher temperature, in agreement with naive expectations. We emphasize, however, that this behavior results from a nontrivial interplay of various nonperturbative contributions.

Now we turn to the effect of a finite number N_f of massless quark flavors. In Fig. 4.7, we show the running coupling α_s as a function of k for $T = 100$ MeV and for $N_\mathrm{f} = 0, \ldots, 10$. At large scales $k \gg T$, the running of the coupling agrees with the zero-temperature running in the presence of N_f massless quark flavors. Towards smaller scales, the coupling increases less strongly than the coupling of the corresponding SU(3)

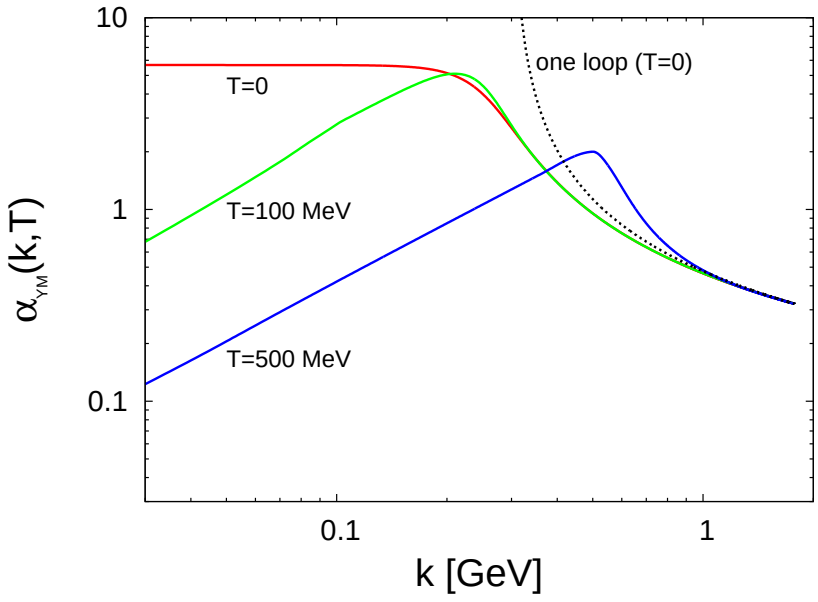

Figure 4.6: Running SU(3) Yang-Mills coupling $\alpha_{\mathrm{YM}}(k,T)$ as a function of k for $T = 0, 100, 500\,\mathrm{MeV}$ compared to the one-loop running at vanishing temperature.

Yang-Mills theory, which is due to fermionic screening. At a scale $k \sim T$, the coupling reaches its maximum value. Below this scale, the quarks decouple from the flow, since they only have hard Matsubara modes. Hence, the coupling universally approaches the result for pure Yang-Mills theory. Furthermore, we observe that for an increasing number of quark flavors, the maximum of the coupling becomes smaller and moves towards smaller scales. Both effects are due to the fact that the anomalous dimension η becomes smaller for an increasing number of quark flavors.

Again, we stress that the results for the coupling with dynamical quarks do not yet account for chiral symmetry breaking, whereby the quarks become massive and decouple from the flow. For temperatures or flavor numbers larger than the corresponding critical value for χSB, our results given so far should be trustworthy on all scales.

4.5.3 Dimensionally reduced high-temperature limit

As discussed above, the running coupling for scales much smaller than the temperature, $k \ll T$, is governed by the IR fixed point of the 3-dimensional theory. More quantitatively, we observe that the flow of the coupling is completely determined by η_1^A for $\frac{T}{k} \gg 1$. As discussed in the previous subsection, the quark contributions decouple from the flow in this limit since they do not have a soft Matsubara mode. Therefore we find an IR fixed point at finite temperature for the $4d$ theory at $g^2 = 0$. In the limit

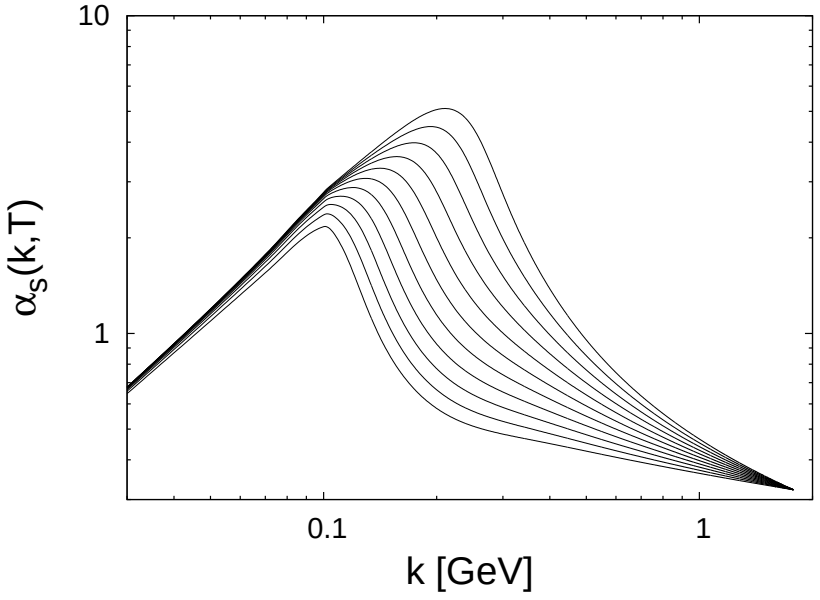

Figure 4.7: Running SU(3) coupling $\alpha_s(k,T)$ as a function of k for $T = 100\,\mathrm{MeV}$ for different number of quark flavors $N_\mathrm{f} = 0, 1, 2, \ldots, 10$ (from top to bottom). For $k \ll T$, the coupling shows *universal* behavior, owing to the attraction of the IR fixed point of the pure glue theory.

$\frac{T}{k} \gg 1$, the anomalous dimension Eq. (4.73) is given by

$$\eta(T \gg k) \approx \eta_1^A(T \gg k) =: \eta_1^\infty(g^2, \tfrac{T}{k}) = \bar{\gamma}_{3d} \left(\tfrac{T}{k}\, g^2\right)^{\frac{5}{4}}, \tag{4.78}$$

where $\bar{\gamma}_{3d}$ is a number which depends on N_c:

$$\bar{\gamma}_{3d} = \frac{32\zeta(\frac{5}{2})(1-2\sqrt{2})\Gamma(\frac{9}{4})\Gamma(\frac{5}{4}+z_4^\infty)\sqrt[4]{c_1^\infty}}{(4\pi)^4\Gamma(\frac{3}{2})\Gamma(z_4^\infty+1)} N_\mathrm{c}\,. \tag{4.79}$$

We refer to App. G.3 for the definition of the constants z_4^∞ and c_1^∞. In the high-temperature limit, we can solve the differential equation (4.40) for g^2 analytically,

$$g^2\Big|_{\frac{T}{k}\gg 1} =: g_\infty^2(\tfrac{k}{T}) = \frac{1}{(\bar{\gamma}_{3d}(\frac{T}{k})^{\frac{5}{4}} - \text{const.})^{\frac{4}{5}}} \approx \bar{\gamma}_{3d}^{-\frac{4}{5}}\, \frac{k}{T} + \mathcal{O}((\tfrac{k}{T})^2)\,. \tag{4.80}$$

The RHS explains the shape of the running coupling for small k/T in Fig. 4.6. The factor $\bar{\gamma}_{3d}^{-\frac{4}{5}}$ is the fixed point value of the dimensionless $3d$ coupling g_{3d}^2, as can be seen from its relation to the dimensionless coupling g^2 in four dimensions:

$$g_{3d}^2 := \frac{T}{k}\, g^2 \quad \to g^2 = \frac{k}{T}\, g_{3d}^2\,. \tag{4.81}$$

Comparing the right-hand side of Eq. (4.80) and (4.81), we find that the fixed point for $N_c = 3$ in three dimensions is given by:

$$\alpha_*^{3d} \equiv \frac{g_{3d,*}^2}{4\pi} = [\alpha_{*,8}^{3d}, \alpha_{*,3}^{3d}] \approx [2.70, 2.77]\,. \tag{4.82}$$

Again, the uncertainty arises from our lack of knowledge about the exact color factors τ_m^A, see App. G.3 and App. B.2.

On the other hand, the fixed point of the 3d theory is determined by the zero of the corresponding β function. In fact, $\eta_1^\infty(g^2, \frac{T}{k})$ is identical to the 3d anomalous dimension $\eta_{3d}(g_{3d}^2)$, as can be deduced from the pure $3d$ theory, and we obtain

$$\partial_t(\tfrac{T}{k} g^2) \equiv \partial_t g_{3d}^2 = (\eta_{3d}(g_{3d}^2) - 1) g_{3d}^2\,, \tag{4.83}$$

as suggested by Eq. (4.40). Since η_{3d} is a monotonously increasing function, we find a $3d$ IR fixed point for $g_{3d,*}^2 = \bar{\gamma}_{3d}^{-\frac{4}{5}}$, which coincides with the result above.

4.6 Fermionic Interactions in QCD

In this section, we discuss the role of four-fermion interactions in QCD within the functional RG. However, before we discuss four-fermion interactions in QCD, we start with a simple truncated NJL-type model in Subsec. 4.6.1 in order to introduce some technical aspects of such a RG study. In addition, a confrontation of the NJL model with our study in Sec. 4.6.2 of four-fermion interactions, which incorporates gauge degrees of freedom, is instructive to point out the substantial differences between both approaches with respect to the mechanisms of chiral symmetry breaking.

4.6.1 A Technical Introduction: The NJL Model

The NJL model at zero temperature and zero fermionic density has been extensively studied with the functional RG in Ref. [188, 189] in particular, the ambiguities arising from Fierz transformations have been explicitly worked out and discussed. In this subsection, we aim to point out the differences in such a study arising from finite temperature and density. For this purpose, we restrict ourselves to a NJL-type model with only one fermion species. Its truncation reads

$$\begin{aligned}\Gamma_{\mathrm{NJL}}\left[\bar{\psi}, \psi\right] &= \int d^4x \Big\{ \bar{\psi}\left[\mathrm{i}\partial\!\!\!/ + \mathrm{i}\mu\gamma_0 + \mathrm{i}m\right]\psi + \frac{1}{2}\bar{\lambda}_\sigma[(\bar{\psi}\psi)^2 - (\bar{\psi}\gamma_5\psi)^2] \\ &\qquad - \frac{1}{2}\bar{\lambda}_V[(\bar{\psi}\gamma_\mu\psi)^2] - \frac{1}{2}\bar{\lambda}_A[(\bar{\psi}\gamma^\mu\gamma_5\psi)^2] \Big\}\,,\end{aligned} \tag{4.84}$$

where we allow for a finite chemical potential μ and an explicit fermion mass term[13]. Furthermore, we consider the four-fermion interactions to be local, i. e. we neglect any

[13] The model is only invariant under chiral $U(1)$-transformations if the mass term vanishes.

non-trivial momentum dependences of the couplings λ_i. We are aware of the fact that this is a crude approximation, but it should be sufficient to detect the critical surface separating the strong and weak coupling regime in the plain spanned by the λ_i. Of course, such a truncation is not sufficient to study the IR properties of the NJL model in the strong-coupling regime. Here the RG flow of the present truncation becomes unstable, as indicated by poles of Landau-type in the couplings λ_i. We have included more four-fermion interactions in our truncation than in the discussion on the origin of the quark-meson model in Sec. 3.4.1. As we argue below, this is necessary because the contributions to the interactions given in the second line of Eq. (4.84) are generated in the RG flow, even if we neglect these interactions in the initial truncation.

For our calculation of the flow equations for the couplings, we apply the following flow equation (see Eq. (2.29)):

$$\partial_t \Gamma_{k,\mathrm{NJL}}[\Phi] = \frac{1}{2}\mathrm{STr}\left\{\left[\Gamma^{(1,1)}_{k,\mathrm{NJL}}[\Phi] + R_k\right]^{-1}\cdot(\partial_t R_k)\right\} \quad \text{with} \quad \Gamma^{(1,1)}_{k,\mathrm{NJL}}[\Phi] = \frac{\overrightarrow{\delta}}{\delta\Phi^T}\Gamma_{k,\mathrm{NJL}}[\Phi]\frac{\overleftarrow{\delta}}{\delta\Phi}.$$

Here Φ represents a vector in field space and is defined by

$$\Phi \equiv \Phi(q) := \begin{pmatrix} \Psi(q) \\ \bar{\Psi}^T(-q) \end{pmatrix} \quad \text{and} \quad \Phi^T \equiv \Phi^T(-q) := \left(\Psi^T(-q), \bar{\Psi}(q)\right) . \tag{4.85}$$

Due to this, $\Gamma^{(1,1)}_{k,\mathrm{NJL}}[\Phi]$ is matrix-valued in field space. Decomposing the inverse regularized propagator on the RHS of the flow equation into a field-independent and a field-dependent part,

$$\Gamma^{(1,1)}_{k,\mathrm{NJL}}[\Phi] + R_k = \mathcal{P}_k + \mathcal{F}_k\,, \tag{4.86}$$

we can expand the flow equation in powers of fields as follows:

$$\begin{aligned} \partial_t \Gamma_{k,\mathrm{NJL}} &= \frac{1}{2}\mathrm{STr}\left\{\tilde{\partial}_t \ln(\mathcal{P}_k + \mathcal{F}_k)\right\} \qquad (4.87)\\ &= \frac{1}{2}\mathrm{STr}\left\{\tilde{\partial}_t\left(\frac{1}{\mathcal{P}_k}\mathcal{F}_k\right)\right\} - \frac{1}{4}\mathrm{STr}\left\{\tilde{\partial}_t\left(\frac{1}{\mathcal{P}_k}\mathcal{F}_k\right)^2\right\} + \frac{1}{6}\mathrm{STr}\left\{\tilde{\partial}_t\left(\frac{1}{\mathcal{P}_k}\mathcal{F}_k\right)^3\right\} \ldots . \end{aligned}$$

Here, $\tilde{\partial}_t$ denotes a formal derivative acting only on the k-dependence of the regulator function R_k. The powers of $\frac{1}{\mathcal{P}_k}\mathcal{F}_k$ can be computed by simple matrix multiplications. The flow equations for the various couplings in a more general truncation than the one given by Eq. (4.84) can now be calculated by comparing the coefficients of the four-fermion operators on the RHS of Eq. (4.87) with the couplings specified in the corresponding truncation. With respect to our truncation (4.84), we observe that only the second term on the RHS contributes to the flow of the four-fermion interactions. In anticipation of the next subsection, where we will couple the fermions additionally to gauge fields via a covariant derivative, we note that we will have to take into account

the contributions arising from the third and fourth term in the expansion as well. These represent contributions from so-called 1PI "triangle"- and "box"-diagrams to the flow of the four-fermion couplings.

Next, we discuss the Lorentz structure of the momentum integrals in the evaluation of the super-trace in the expansion Eq. (4.87). At finite temperature T and chemical potential μ, we encounter two substantially different types of momentum integrals:

$$\begin{aligned} & T\sum_{n=-\infty}^{\infty}\int\frac{d^{d-1}p}{(2\pi)^{(d-1)}}\,\left\{\tilde{p}_\mu^{(\pm)}\tilde{p}_\nu^{(\pm)}+m^2\right\}\mathcal{I}_1\left(\tilde{p}_\lambda^{(\pm)}\tilde{p}_\lambda^{(\pm)},m\right) \\ & =T\sum_{n=-\infty}^{\infty}\int\frac{d^{d-1}p}{(2\pi)^{(d-1)}}\left\{\left[(p_0\pm\mathrm{i}\mu)^2-\frac{\vec{p}^2}{d-1}\right]n_\mu n_\nu+\frac{\vec{p}^2}{d-1}\delta_{\mu\nu}+m^2\right\}\mathcal{I}_1\left(\tilde{p}_\lambda^{(\pm)}\tilde{p}_\lambda^{(\pm)},m\right) \end{aligned} \tag{4.88}$$

and

$$\begin{aligned} & T\sum_{n=-\infty}^{\infty}\int\frac{d^{d-1}p}{(2\pi)^{(d-1)}}\,\left\{\tilde{p}_\mu^{(\pm)}\tilde{p}_\nu^{(\mp)}+m^2\right\}\mathcal{I}_2\left(\tilde{p}_\lambda^{(+)}\tilde{p}_\lambda^{(+)},m\right)\mathcal{I}_2\left(\tilde{p}_\lambda^{(-)}\tilde{p}_\lambda^{(-)},m\right) \\ & =T\sum_{n=-\infty}^{\infty}\int\frac{d^{d-1}p}{(2\pi)^{(d-1)}}\left\{\left[(p_0^2+\mu^2)-\frac{\vec{p}^2}{d-1}\right]n_\mu n_\nu\right. \\ & \qquad\left.+\frac{\vec{p}^2}{d-1}\delta_{\mu\nu}+m^2\right\}\mathcal{I}_2\left(\tilde{p}_\lambda^{(+)}\tilde{p}_\lambda^{(+)},m\right)\mathcal{I}_2\left(\tilde{p}_\lambda^{(-)}\tilde{p}_\lambda^{(-)},m\right), \end{aligned} \tag{4.89}$$

where d counts the number of space-time dimensions, the vector $n_\mu=(1,\vec{0})$ denotes the heat-bath velocity and the four-momenta $\tilde{p}_\mu^{(\pm)}=(\nu_n\pm\mathrm{i}\mu,\vec{p})$ depend on the fermionic Matsubara-frequency $\nu_n=(2n+1)\pi T$. The scalar functions $\mathcal{I}_i$ depend on the squared four-momenta $\tilde{p}_\mu^{(\pm)}$ and the mass m. In order to perform the decomposition of Eqns. (4.88) and (4.89), we have used the heat-bath projectors which are derived and discussed in App. I. We point out that both integrals, Eq. (4.88) and (4.89), reduce to the standard momentum integrals proportional to $\delta_{\mu\nu}$ for vanishing temperature and chemical potential [59]. In the remainder of this work, we take for our calculations of the RG flows of the four-fermion couplings into account only the momentum integrals proportional to $\delta_{\mu\nu}$ on the RHS of Eqns. (4.88) and (4.89). We drop the contributions arising due to the terms proportional to $n_\mu n_\nu$ and m^2. In any case, we will always study the massless limit in this chapter, except for one excursion in Sec. 4.7. Note that we reproduce the correct results for zero temperature and chemical potential even if we neglect the contributions proportional to $n_\mu n_\nu$, since they vanish identically in this limit. The assumption that the neglected contributions are not quantitatively important is non-trivial. However, we have checked numerically that the momentum integrals related to these contributions yield smaller values for $T/k\lesssim 0.6$ and $\mu=0$ than those from the integrals[14] taken into account. This is sufficient for our purposes in Sec. 4.6.2 and 4.7.

[14]The momentum integrals are related to so-called threshold functions, which are discussed in App. D.2.

We can read off from the expansion of the flow equation that contributions to the flow of the four-fermion couplings specified in the second line of Eq. (4.84) are still generated, even if they have been dropped in the truncation: the matrix multiplications on the RHS of Eq. (4.87) mix the contributions from the inverse propagator $\mathcal{P}_k$, which is proportional to γ_μ, with the contributions from the field-dependent part $\mathcal{F}_k$. Suppose for a moment that we use a truncation which consists only of the terms in the first line of Eq. (4.84), then we would nevertheless encounter terms of the form[15]

$$\bar{\lambda}_\sigma^2 \,\mathrm{tr}\left\{\gamma_\mu \psi\bar{\psi}\gamma_\mu\psi\bar{\psi}\right\} = -\bar{\lambda}_\sigma^2(\bar{\psi}\gamma_\mu\psi)(\bar{\psi}\gamma_\mu\psi) \tag{4.90}$$

in the expansion (4.87). This term obviously contributes to the flow of $\bar{\lambda}_V$. Moreover, contributions of this type couple the flow equations of the various four fermion interactions to one another. This observation explains why we need to include the couplings $\bar{\lambda}_V$ and $\bar{\lambda}_A$ in our calculation. Note that the truncation (4.84) is closed, in the sense that no contributions to four-fermion interactions are generated in the RG flow which are not covered by the truncation. This brings us to the problem which arises due to the fact that a particular four-fermion interaction can be expressed by a combination of other four-fermion interactions by means of Fierz transformations. It is well known that it is possible to rewrite the truncation (4.84) by performing Fierz transformations of the four-fermion interactions (see App. C for our conventions for Fierz transformations). It is a temptation to look for a Fierz transformation which transforms away one of the three couplings λ_i. In fact, only two of the three couplings in the present truncation with only one fermion species are independent. This is due to the *Fierz identity* (see App. C)

$$\left[(\bar{\psi}\gamma_\mu\psi)^2 - (\bar{\psi}\gamma_\mu\gamma_5\psi)^2\right] + 2\left[(\bar{\psi}\psi)^2 - (\bar{\psi}\gamma^5\psi)^2\right] = 0. \tag{4.91}$$

Therefore, it is convenient to introduce new couplings $\hat{\lambda}_i$ as

$$\bar{\lambda}_\sigma = \hat{\lambda}_\sigma + 2\gamma\hat{\lambda}_V\,, \quad \bar{\lambda}_V = (1-\gamma)\hat{\lambda}_V\,, \quad \bar{\lambda}_A = \gamma\hat{\lambda}_V\,, \tag{4.92}$$

where γ is an arbitrary parameter. We find $\bar{\lambda}_V - \bar{\lambda}_A + \bar{\lambda}_\sigma = \hat{\lambda}_V + \hat{\lambda}_\sigma$ with this choice for the $\hat{\lambda}_i$. In a study of the NJL model in a mean-field approximation, it is not possible to resolve the ambiguity in the four-fermion interactions [188]. Due to this, mean-field results for the NJL model are always tainted with an uncertainty. In order to carefully remove the so-called *Fierz ambiguity* we follow the strategy of Ref. [188]: first, we insert Eq. (4.84) into the flow equation (4.87). Then we introduce the new couplings defined in Eq. (4.92) into Eq. (4.84) and extract the RG flows for the new four-fermion couplings by comparing the coefficients of the four-fermion operators on the LHS and

[15] At first glance, it seems possible that a term could arise in the calculation with opposite sign to the term in Eq. (4.90), so that both would cancel each other. We are aware of this and stress that Eq. (4.90) should serve only as a motivation. As the full calculation shows (see below), not all terms which couple the RG flows of the different couplings $\bar{\lambda}_i$ drop out in the end.

RHS of the equation. Introducing the dimensionless renormalized couplings $\lambda_i = k^2\hat{\lambda}_i$, we finally obtain the flow equations for λ_σ and λ_V:

$$\begin{aligned}
\beta_\sigma \equiv \partial_t \lambda_{\sigma,k} &= 2\lambda_\sigma - 4\Big[3\lambda_{\sigma,k}^2 + 10\lambda_{\sigma,k}\lambda_{V,k} + 3\lambda_{V,k}^2\Big]\frac{4v_3}{3} L_{1,1}^{(F),4}\left(\tilde{t},\tilde{m},0\right) \\
&\quad +4\Big[\lambda_{\sigma,k}^2 + 2\lambda_{\sigma,k}\lambda_{V,k} - 3\lambda_{V,k}^2\Big]\frac{4v_3}{3} L_{1,1}^{(F),4}\left(\tilde{t},\tilde{m},\tilde{\mu}\right), \\
\beta_V \equiv \partial_t \lambda_{V,k} &= 2\lambda_\sigma - 4\Big[\lambda_{\sigma,k}^2 + 2\lambda_{\sigma,k}\lambda_{V,k} + 5\lambda_{V,k}^2\Big]\frac{4v_3}{3} L_{1,1}^{(F),4}\left(\tilde{t},\tilde{m},0\right) \\
&\quad +4\Big[4\lambda_{V,k}^2\Big]\frac{4v_3}{3} L_{1,1}^{(F),4}\left(\tilde{t},\tilde{m},\tilde{\mu}\right). \qquad (4.93)
\end{aligned}$$

Here we have defined the dimensionless quantities $\tilde{\mu} = \mu/k$, $\tilde{t} = T/k$ and $\tilde{m} = m/k$. The threshold function $L_{1,1}^{(F),4}$, representing the fermionic loop integral, depend on the details of the regularization, see App. D.2. The flow equations agree with the results of Refs. [190, 188] for vanishing temperature and chemical potential[16]. The flow equations for $\lambda_{\sigma,k}$ and $\lambda_{V,k}$ are independent of the parameter γ, which reflects the fact that there is no Fierz ambiguity in the RG flow. Finally, it is worth to be mentioned that the first lines of the flow equations for $\lambda_{\sigma,k}$ and $\lambda_{V,k}$ do not depend on $\tilde{\mu}$ even if we study the NJL model at finite density; this independence of $\tilde{\mu}$ is due to the fact that the integration variables in Eq. (4.88) can be shifted[17].

As a first application, we use the set of flow equations (4.93) to determine the critical surface of the NJL model at zero and finite temperature for vanishing fermion mass m and vanishing density μ. Our study represents a generalization of earlier zero temperature studies, reported in Refs. [190, 188].

Solving the flow equations numerically, we find that the set of possible initial conditions[18] for the flow equations at the scale $k = \Lambda = 1\,\mathrm{GeV}$ can be divided into two subsets for which the NJL model ends up in qualitatively different regimes in the IR, either in a strongly or in a weakly coupled regime. The line separating the two sets of initial conditions is called the critical surface. In Fig. 4.8, we show the critical surfaces for $T = 0$ and $T/\Lambda = 0.2$ which have been obtained with the exponential regulator Eq. (D.21). The names for the two regimes are motivated by the underlying physics. For a given initial condition, there a two possibilities for the system: either the four-fermion couplings approach Gaußian fixed points for $k \to 0$ or the couplings diverge at a finite scale $k = k_{\mathrm{cr}}$. In the former case, the couplings become zero for $k \to 0$ and the NJL reduces to a theory of free fermions. In the latter case, the divergence of the couplings at a finite scale $k = k_{\mathrm{cr}}$ indicates that the four-fermion interactions

[16] In the limit $\mu \to 0$ and $T \to 0$, we have $L_{1,1}^{(F),4}(0,0,0) = \frac{3v_4}{4v_3} l_1^{(F),4}$, where $l_1^{(F),4}$ denotes the standard threshold functions defined in Ref. [59].

[17] We would like to remark two points: first, the shift is performed for the p_0 variable in the continuum limit. Second, this shift is only possible if the integrand is analytic in the complex plane spanned by the real axis and iμ.

[18] Note we have restricted our discussion to positive initial values for the couplings.

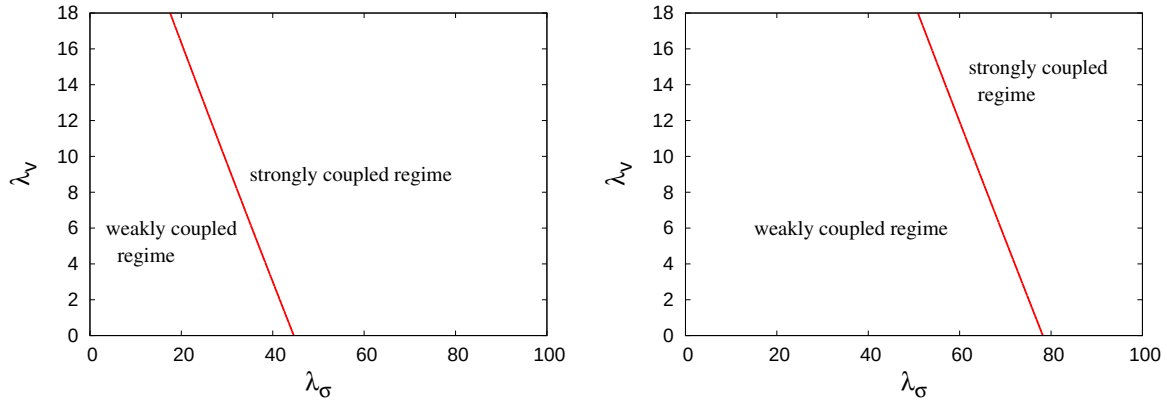

Figure 4.8: "Critical" surface of the NJL model in the plane spanned by the dimensionless couplings λ_σ and λ_V for zero temperature and for $T/\Lambda = 0.2$ (left and right panel, respectively). The red line divides the set of initial conditions for the flows of the coupling at the UV scale $k = \Lambda$ into two subsets for which the NJL model ends up either in a strongly coupled or in a weakly coupled regime. We restrict our discussion to positive initial values for the couplings.

have become large enough to contribute as relevant operators to the flow. This, in turn, indicates the onset of the breaking of the chiral $U(1)$ symmetry of our model, as we have already motivated in our discussion of the relation between the NJL model and the quark-meson model in Subsec. 3.4.1. Hence, the divergence has a physical meaning. This instability of the flow can be cured by including composite operators in the truncation and then applying the so-called rebosonization technique [60, 61]. Such an improvement of the truncation is indispensable if we are interested in the IR properties of the model or the order of the phase transition. However, for a computation of the critical temperature, it is sufficient to detect the divergence in the RG flow. The critical temperature can then be defined as the lowest temperature for which we do not encounter instabilities in the flow.

Usually, the strategy for studying phase transitions in NJL-type models is as follows: first, one chooses some physically motivated initial condition at zero temperature. Then, one uses the *same* initial conditions for a study of the model at finite temperature. For example, choosing $(\lambda_{\sigma,\Lambda} = 75.1, \lambda_{V,\Lambda} = 2.0)$ as initial condition at zero temperature, the system ends up in the strongly coupled regime in the IR. Following the strategy sketched above, we find a critical temperature of $T_{\mathrm{cr}} = 200\,\mathrm{MeV}$. However, we can find infinitely many initial conditions for which we get $T_{\mathrm{cr}} = 200\,\mathrm{MeV}$; all points lying on the critical surface for $T/\Lambda = 0.2$ specify initial conditions at $T = 0$ for which we find $T_{\mathrm{cr}} = 200\,\mathrm{MeV}$. Even worse, the critical temperature depends strongly on the choice of the initial conditions. These ambiguities in the initial conditions and the resulting phase transition temperature are severe drawbacks of NJL-type models. In

the next subsection, we incorporate gauge degrees of freedom into our study of quark interactions. This allows us to get rid of the ambiguities present in the NJL model when we compute the chiral phase transition temperature for QCD in Sec. 4.7.

4.6.2 Chiral Quark Dynamics in QCD

Let us now discuss the chiral quark dynamics in QCD. Dynamical quarks influence the RG flow of QCD through two qualitatively different mechanisms. First, quark fluctuations modify the running coupling directly as discussed above; the non-perturbative contribution in the form of η^{q} in Eq. (4.73) accounts for the screening nature of fermionic fluctuations, following the tendency that is already visible in perturbation theory. Second, gluon exchange between quarks induces quark self-interactions which can become relevant in the strongly-coupled IR. Both the quark and the gluon sector feed back into one another in an involved nonlinear fashion. In general, these nonlinearities have to be taken into account and are apparent in the flow equation. However, we will argue that some intricate nonlinearities drop out or are negligible for the purpose of locating the chiral phase boundary in a first approximation.

From now on, we will be working solely in $d = 4$. For our study of the chiral quark dynamics in QCD, we have to specify our ansatz for the effective action of quark self-interactions $\Gamma_k^{\text{q-int}}[\bar{\psi}, \psi]$, introduced in Eq. (4.62). In a consistent and systematic operator expansion, the lowest nontrivial order is given by [191]

$$\begin{aligned}\Gamma_k^{\psi-\text{int.}}[\bar{\psi},\psi] &= \int_x \frac{1}{2}\Big[\bar{\lambda}_-(\text{V–A}) + \bar{\lambda}_+(\text{V+A}) + \bar{\lambda}_\sigma(\text{S–P}) \\ &\qquad + \bar{\lambda}_{\text{VA}}[2(\text{V–A})^{\text{adj}} + (1/N_{\text{c}})(\text{V–A})]\Big]. \end{aligned} \tag{4.94}$$

The four-fermion interactions appearing here have been classified according to their color and flavor structure. Color and flavor singlets are

$$(\text{V–A}) = (\bar{\psi}\gamma_\mu\psi)^2 + (\bar{\psi}\gamma_\mu\gamma_5\psi)^2, \tag{4.95}$$

$$(\text{V+A}) = (\bar{\psi}\gamma_\mu\psi)^2 - (\bar{\psi}\gamma_\mu\gamma_5\psi)^2, \tag{4.96}$$

where (fundamental) color $(i, j, \dots)$ and flavor $(\chi, \xi, \dots)$ indices are contracted pairwise, e.g., $(\bar{\psi}\psi) \equiv (\bar{\psi}_i^\chi \psi_i^\chi)$. The remaining operators have a non-singlet color or flavor structure,

$$\begin{aligned}(\text{S–P}) &= (\bar{\psi}^\chi\psi^\xi)^2 - (\bar{\psi}^\chi\gamma_5\psi^\xi)^2 \equiv (\bar{\psi}_i^\chi\psi_i^\xi)^2 - (\bar{\psi}_i^\chi\gamma_5\psi_i^\xi)^2, \\ (\text{V–A})^{\text{adj}} &= (\bar{\psi}\gamma_\mu T^a\psi)^2 + (\bar{\psi}\gamma_\mu\gamma_5 T^a\psi)^2, \end{aligned} \tag{4.97}$$

where $(\bar{\psi}^\chi\psi^\xi)^2 \equiv \bar{\psi}^\chi\psi^\xi\bar{\psi}^\xi\psi^\chi$, etc., and $(T^a)_{ij}$ denotes the generators of the gauge group in the fundamental representation.

In the following, we study the four-fermion couplings $\bar{\lambda}_i$ in the point-like limit $\bar{\lambda}(|p_i| \ll k)$. This is a severe approximation in the chirally broken regime where mesons

manifest themselves as momentum singularities of the four-fermion couplings. Nevertheless, the point-like truncation can be a reasonable approximation in the chirally symmetric regime; this has recently been quantitatively confirmed for the zero-temperature chiral phase transition in many-flavor QCD [156], where the regulator independence of universal quantities has been shown to hold remarkably well even in this restrictive truncation. By adopting the same system at finite temperature, we base our truncation on the assumption that quark dynamics both near the finite-temperature phase boundary as well as near the many-flavor phase boundary [152] are driven by qualitatively similar mechanisms.

The set of fermionic self-interactions introduced in Eq. (4.94) forms a complete basis. Any other pointlike four-fermion interaction which is invariant under $\mathrm{SU}(N_\mathrm{c})$ gauge symmetry and $\mathrm{SU}(N_\mathrm{f})_\mathrm{L} \times \mathrm{SU}(N_\mathrm{f})_\mathrm{R}$ flavor symmetry is reducible by means of Fierz transformations, see App. C. Terms accounting for instantons, as $\mathrm{U_A}(1)$-violating interactions, are neglected as well, since we expect them to become relevant only inside the χSB regime or for small N_f. Schematically, the lowest-order $\mathrm{U_A}(1)$-violating term is $\sim (\bar{\psi}\psi)^{N_\mathrm{f}}$, larger N_f correspond to increased irrelevance in the RG sense according to naive power-counting. For $N_\mathrm{f} = 1$, such a term is, of course, important, since it represents a direct fermion mass term; in this case, the chiral transition is expected to be a crossover. Dropping the $\mathrm{U_A}(1)$-violating interactions, we thus confine ourselves to $N_\mathrm{f} \geq 2$.

The flow equations are derived along the lines of Subsec. (4.6.1). Introducing the dimensionless renormalized couplings[19]

$$\lambda_i = k^2 \bar{\lambda}_i \,, \tag{4.98}$$

the flow equations of the four-quark couplings for vanishing chemical potential and N_f quarks with equal masses m read

$$\begin{aligned}
\partial_t \lambda_- \;=\; & 2\lambda_- - \frac{16}{3} v_3 L^{(\mathrm{FB})}_{1,1,1}(\tilde{t}, \tilde{m}, 0, 0) \left[\frac{3}{N_\mathrm{c}} g^2 \lambda_- - 3 g^2 \lambda_{\mathrm{VA}} \right] \\
& - \frac{1}{6} v_3 L^{(\mathrm{FB})}_{1,1,2}(\tilde{t}, \tilde{m}, 0, 0) \left[\frac{12 + 9N_\mathrm{c}^2}{N_\mathrm{c}^2} g^4 \right] - \frac{32}{3} v_3 L^{(\mathrm{F})}_{1,1}(\tilde{t}, \tilde{m}, 0) \Big\{ - N_\mathrm{f} N_\mathrm{c} (\lambda_-^2 + \lambda_+^2) \\
& + \lambda_-^2 - 2(N_\mathrm{c} + N_\mathrm{f}) \lambda_- \lambda_{\mathrm{VA}} + N_\mathrm{f} \lambda_+ \lambda_\sigma + 2 \lambda_{\mathrm{VA}}^2 \Big\},
\end{aligned} \tag{4.99}$$

$$\begin{aligned}
\partial_t \lambda_+ \;=\; & 2\lambda_+ - \frac{16}{3} v_3 L^{(\mathrm{FB})}_{1,1,1}(\tilde{t}, \tilde{m}, 0, 0) \left[- \frac{3}{N_\mathrm{c}} g^2 \lambda_+ \right] - \frac{1}{6} v_3 L^{(\mathrm{FB})}_{1,1,2}(\tilde{t}, \tilde{m}, 0, 0) \left[- \frac{12 + 3N_\mathrm{c}^2}{N_\mathrm{c}^2} g^4 \right] \\
& - \frac{32}{3} v_3 L^{(\mathrm{F})}_{1,1}(\tilde{t}, \tilde{m}, 0) \Big\{ - 3\lambda_+^2 - 2 N_\mathrm{c} N_\mathrm{f} \lambda_- \lambda_+ - 2\lambda_+ (\lambda_- + (N_\mathrm{c} + N_\mathrm{f}) \lambda_{\mathrm{VA}}) \\
& + N_\mathrm{f} \lambda_- \lambda_\sigma + \lambda_{\mathrm{VA}} \lambda_\sigma + \tfrac{1}{4} {\lambda_\sigma}^2 \Big\},
\end{aligned} \tag{4.100}$$

[19] Recall that $Z_\psi = 1$ in our truncation

$$\begin{aligned}\partial_t\lambda_\sigma &= 2\lambda_\sigma - \frac{16}{3}v_3 L^{(\mathrm{FB})}_{1,1,1}(\tilde{t},\tilde{m},0,0)\left[6C_2(N_\mathrm{c})\,g^2\lambda_\sigma - 6g^2\lambda_+\right] \\ &\quad -\frac{1}{3}v_3 L^{(\mathrm{FB})}_{1,1,2}(\tilde{t},\tilde{m},0,0)\Big[-\frac{24-9N_\mathrm{c}^2}{N_\mathrm{c}}\,g^4\Big] - \frac{32}{3}v_3 L^{(\mathrm{F})}_{1,1}(\tilde{t},\tilde{m},0)\Big\{2N_\mathrm{c}\lambda_\sigma^2 \\ &\qquad -2\lambda_-\lambda_\sigma - 2N_\mathrm{f}\lambda_\sigma\lambda_{\mathrm{VA}} - 6\lambda_+\lambda_\sigma\Big\}, \qquad (4.101)\end{aligned}$$

$$\begin{aligned}\partial_t\lambda_{\mathrm{VA}} &= 2\lambda_{\mathrm{VA}} - \frac{16}{3}v_3 L^{(\mathrm{FB})}_{1,1,1}(\tilde{t},\tilde{m},0,0)\left[\frac{3}{N_\mathrm{c}}g^2\lambda_{\mathrm{VA}} - 3g^2\lambda_-\right] \\ &\quad -\frac{1}{6}v_3 L^{(\mathrm{FB})}_{1,1,2}(\tilde{t},\tilde{m},0,0)\left[-\frac{24-3N_\mathrm{c}^2}{N_\mathrm{c}}g^4\right] \\ &\quad -\frac{32}{3}v_3 L^{(\mathrm{F})}_{1,1}(\tilde{t},\tilde{m},0)\Big\{-(N_\mathrm{c}+N_\mathrm{f})\lambda_{\mathrm{VA}}^2 + 4\lambda_-\lambda_{\mathrm{VA}} - \tfrac{1}{4}N_\mathrm{f}\lambda_\sigma^2\Big\}. \qquad (4.102)\end{aligned}$$

Here $C_2(N_\mathrm{c}) = (N_\mathrm{c}^2-1)/(2N_\mathrm{c})$ is a Casimir operator of the gauge group, and $v_3 = 1/(8\pi^2)$. The quantities $\tilde{m}$ and $\tilde{t}$ denote the dimensionless quarks mass m/k and the dimensionless "temperature" T/k. For better readability, we have written all terms dependent on the gauge coupling in square brackets, whereas fermionic self-interactions are grouped inside braces. The threshold functions $L^{(\mathrm{F})}_{1,1}(\tilde{t},\tilde{m},0)$, $L^{(\mathrm{FB})}_{1,1,2}(\tilde{t},\tilde{m},0,0)$ and $L^{(\mathrm{FB})}_{1,1,1}(\tilde{t},\tilde{m},0,0)$ depend on the details of the regularization, see App. D.2. For zero quark mass and vanishing temperature, we recover the equations derived in Refs. [191, 156]. Note that the threshold functions simply reduce to positive numbers in this limit, see, e.g., Eqns. (D.29) and (D.35).[20] For finite quark masses and temperature larger than the regulator scale k, these functions approach zero. This reflects the decoupling of massive modes from the RG flow. Although the flow equations for the four-quark-couplings $\bar{\lambda}_i$ look rather complicated at first glance, we note that the various terms arising on the RHS of the flow equations can be related straightforwardly to one-particle irreducible Feynman-graphs, see Fig. 4.9. As initial conditions for the four-fermion couplings, we use $\bar{\lambda}_i \to 0$ for $k \to \Lambda \to \infty$. This choice ensures that the $\bar{\lambda}_i$ are generated solely by quark-gluon dynamics from first principles for $k < \Lambda$. This point is very important, as it is in contrast to, e.g., the Nambu–Jona-Lasinio model, where the four-fermion couplings serve as independent input parameters which are adjusted in such a way that low-energy observables are reproduced correctly.

Our truncation provides a simple picture for the chiral dynamics, which is illustrated in Fig. 4.10: For vanishing gauge coupling, the flow is solved by vanishing λ_i, which defines the Gaußian fixed point. This fixed point is IR attractive, implying that these self-interactions are RG irrelevant for sufficiently small bare couplings, as they should be. For weak gauge coupling, the RG flow generates quark self-interactions of order $\lambda \sim g^4$, as expected for a perturbative 1PI scattering amplitude. The back-reaction of

[20] Here we ignore a weak dependence of the threshold functions on the anomalous quark and gluon dimensions, which were shown to influence the quantitative results for the present system only on the percent level, if at all [156].

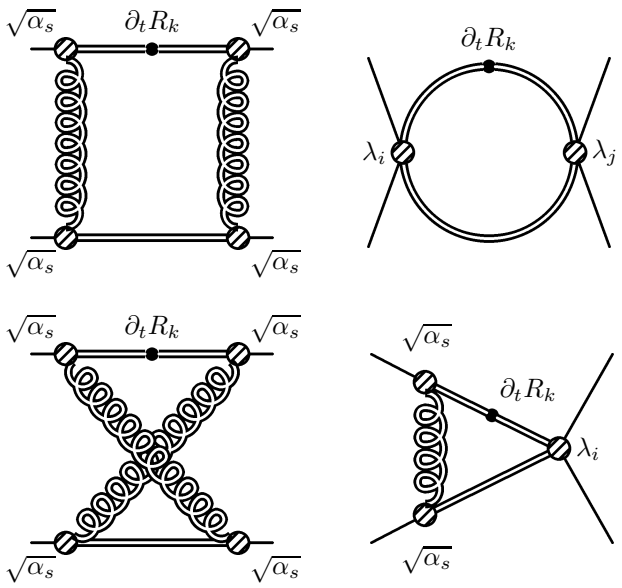

Figure 4.9: Representation of the one-particle irreducible (1PI) graphs which are contained in the RG flow equations for the four-fermion interactions. The double lines represent the fully dressed propagator, and the solid black dots denote the insertion of $\partial_t R_k$ in the loop. The four-fermion couplings λ_i are defined in Eq. (4.94). Diagrams with the same topology but with the regulator insertion attached to other internal lines are present in the RG flow as well.

these self-interactions on the total RG flow is negligible at weak coupling. If the gauge coupling in the IR remains smaller than a critical value $g < g_{\rm cr}$, the self-interactions remain bounded and approach fixed points in the IR. These fixed points can be seen simply as order-g^4 shifted versions of the Gaußian fixed point, modified by the gauge dynamics. At these fixed points, the fermionic subsystem remains in the chirally invariant phase. This is indeed realized at high temperature. If the gauge coupling increases beyond the critical coupling $g > g_{\rm cr}$, the IR fixed points mentioned above are destabilized and the quark self-interactions become critical. This can be visualized with the help of the $\partial_t \lambda_i$ as a function of the λ_i, which is an inverted parabola, see Fig. 4.10. For $g = g_{\rm cr}$, the parabola is pushed below the λ_i axis, such that the (shifted) Gaußian fixed point coincides with the second zero of the parabola. In this case, the gauge-fluctuation-induced $\bar{\lambda}$ have become strong enough to contribute as relevant operators to the RG flow. These couplings now increase rapidly and approach a divergence at a finite scale $k = k_{\chi\rm SB}$. Indeed, this strong increase indicates the formation of chiral quark condensates and therefore the onset of chiral symmetry breaking. We recall the NJL model as an illustration, see Subsecs. 3.4.1 and 4.6.1: There, the mass parameter m^2 of the bosonic fields in the partially bosonized action is inversely proportional to the four-fermion coupling, $\bar{\lambda} \sim 1/m^2$. In addition, we know from such NJL-type models

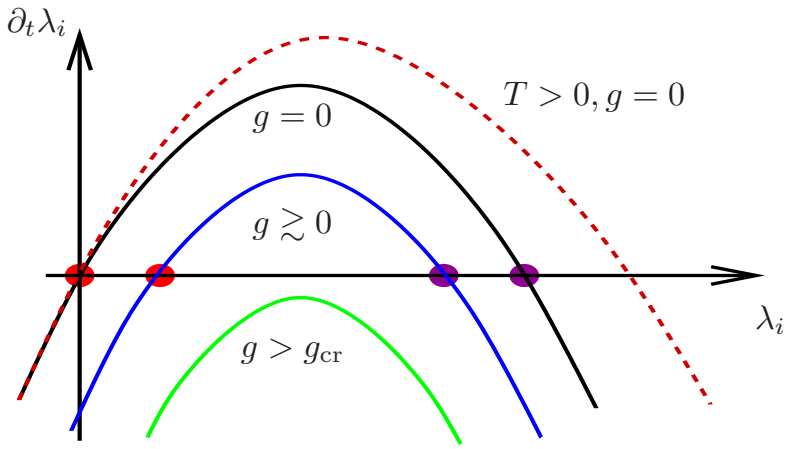

Figure 4.10: Sketch of a typical β function for the fermionic self-interactions λ_i: at zero gauge coupling, $g = 0$ (upper solid curve), the Gaußian fixed point $\lambda_i = 0$ is IR attractive. For small $g \gtrsim 0$ (middle/blue solid curve), the fixed-point positions are shifted on the order of g^4. For gauge couplings larger than the critical coupling $g > g_{\rm cr}$ (lower/green solid curve), no fixed points remain and the self-interactions quickly grow large, signaling χSB. For increasing temperature, the parabolas become broader and higher, owing to thermal fermion masses; this is indicated by the dashed/red line.

that their effective action in the bosonized form corresponds to a Ginzburg-Landau effective potential for the order parameter. In its simplest form, the order parameter is given by the expectation value of a scalar field. Symmetry breaking is then reflected in a non-trivial minimum of this potential. Consequently, the scale $k_{\chi\rm SB}$ at which the four-fermion couplings diverge is a good measure for the chiral symmetry breaking scale. At this scale, the effective potential for the order parameter becomes flat and starts to develop a nonzero vacuum expectation value.

At this point, we have traced the question of the onset of chiral symmetry breaking back to the strength of the coupling g, relative to the critical coupling $g_{\rm cr}$, which is required to trigger χSB. This makes a convenient determination of the chiral phase boundary possible as we will discuss in the next section. Incidentally, the critical coupling $g_{\rm cr}$ itself can be determined by solving the fixed-point equations $\partial_t \lambda_i(\lambda_*) = 0$ algebraically for that value of the coupling, $g = g_{\rm cr}$, where the shifted Gaußian fixed point vanishes. For instance, at zero temperature, the SU(3) critical coupling for the quarks system is $\alpha_{\rm cr} \equiv g_{\rm cr}^2/(4\pi) \simeq 0.8$, see Ref. [61]. This result is only weakly dependent on the number of flavors [156].[21] Since the IR fixed point for the gauge coupling is much larger $\alpha_* > \alpha_{\rm cr}$ (for not too many massless flavors), the QCD vacuum

[21]The critical coupling is a non-universal quantity with a value that depends on the regularization scheme; the value given here for illustration holds for a particular class of regulators in the functional RG scheme that includes the most widely used linear ("optimized") and exponential regulators.

is characterized by chiral symmetry breaking. The same qualitative observations have already been made in Ref. [190] in a similar, though smaller, truncation. We note that the existence of such a critical coupling is also a well-studied phenomenon in Dyson-Schwinger equations [192].

As soon as the the quark sector approaches criticality, its back-reaction onto the gluon sector becomes sizable as well. Here a subtlety of the present formalism becomes important: identifying the fluctuation field with the background field in the RG flow, our approximation generally does not distinguish between the flow of the background-field coupling and that of the fluctuation-field coupling. In our truncation, differences arise from the quark self-interactions. Whereas the running of the background-field coupling is always given by Eq. (4.40), the quark self-interactions can contribute directly to the running of the fluctuation-field coupling in the form of a vertex correction to the quark-gluon vertex. Since the coupling of the fluctuation field is responsible for inducing quark self-interactions, this difference may become important. In Ref. [191], the relevant terms have been derived with the aid of a regulator-dependent Ward-Takahashi identity. The result hence implements an important gauge constraint, leading us to

$$\partial_t g^2 \;=\; \eta\, g^2 - 4v_4 L^{(\mathrm{F})}_{1,1}(\tilde{t},\tilde{m},0)\,\frac{g^2}{1-2v_4 L^{(\mathrm{F})}_{1,1}(\tilde{t},\tilde{m},0)\sum_i c_i\lambda_i}\,\partial_t \sum_i c_i\lambda_i, \quad (4.103)$$

with η provided by Eq. (4.73) in our approximation and

$$c_\sigma = 1+N_\mathrm{f},\;\; c_+ = 0,\;\; c_- = -2,\;\; c_\mathrm{VA} = -2N_\mathrm{f}\,.$$

In principle, the approach to chiral symmetry breaking can now be studied by solving the coupled system of Eqns. (4.99)-(4.103). However, a simpler and, for our purposes, sufficient estimate is provided by the following argument: if the system ends up in the chirally symmetric phase, the λ_i always stay close to the shifted Gaußian fixed point discussed above; apart from a slight variation of this fixed-point position with increasing g^2, the $\partial_t\lambda_i$ flow is small and vanishes in the IR, $\partial_t\lambda_i \to 0$. Therefore, the additional terms in Eq. (4.103) are negligible for all k and drop out in the IR. As a result, the behavior of the running coupling in the chirally symmetric phase is basically determined by η alone, as discussed in the preceding section. In other words, in our truncation the difference between the fluctuation-field coupling and the background-field coupling automatically switches off in the deep IR in the symmetric phase.

Therefore, if the coupling never increases beyond the critical value g^2_cr for any k, as predicted by $\beta_{g^2} \simeq \eta g^2$ alone, the system remains in the chirally symmetric phase. In this case, it will suffice to solve the g^2 flow and to compare it with g^2_cr, which can be deduced from a purely algebraic solution of the fixed-point equations, $\partial_t\lambda_i(\lambda_*) = 0$.

If the coupling approaches g_cr for some finite scale k_cr, as predicted by $\beta_{g^2} \simeq \eta g^2$, the quark sector becomes critical and all couplings start to grow rapidly. To the present level of accuracy, this serves as an indication for the onset of chiral symmetry

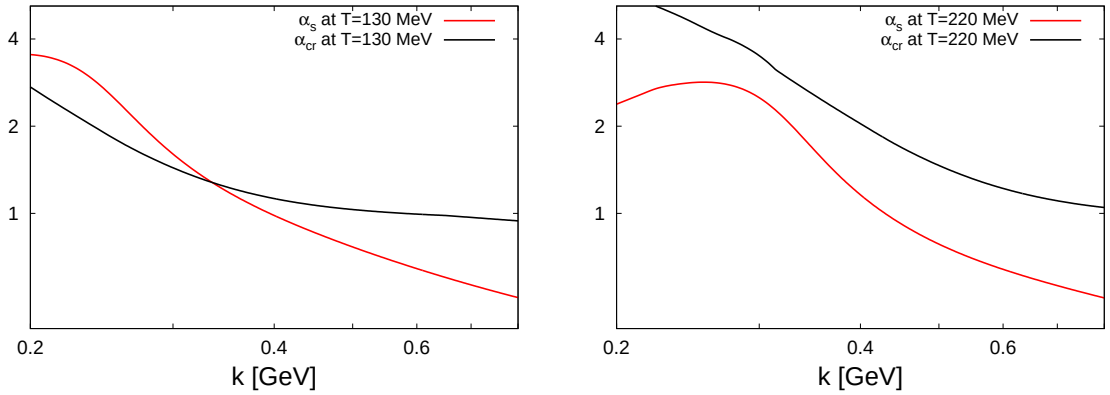

Figure 4.11: Running QCD coupling $\alpha_{\rm s}(k,T)$ for $N_{\rm f}=2$ massless quark flavors and $N_{\rm c}=3$ colors and the critical value of the running coupling $\alpha_{\rm cr}(k,T)$ as a function of k for $T=130\,\text{MeV}$ (left panel) and $T=220\,\text{MeV}$ (right panel). The existence of the $(\alpha_{\rm s},\alpha_{\rm cr})$ intersection point in the left panel indicates that the χSB quark dynamics can become critical for $T=130\,\text{MeV}$.

breaking. Of course, if the gauge coupling dropped quickly for decreasing k, the quark sector could, in principle, become subcritical again. However, this might happen only for a marginal range of $g^2\simeq g^2_{\rm cr}$, if at all. For even larger values of the gauge coupling, the flow towards the regime with broken chiral symmetry is unavoidable.

Inside the regime with broken chiral symmetry, the induced quark masses cause also a back-reaction of the quarks onto the gluonic flow by decoupling the quark fluctuations, i.e., $\eta^{\rm q}$ in Eq. (4.73) approaches zero. However, the present truncation does not allow us to explore the properties of the sector with broken chiral symmetry; for this, the introduction of effective mesonic degrees of freedom along the lines of Ref. [61, 60] is most useful and will be employed in future work.

4.7 The Chiral Phase Boundary of QCD

In this section, we use the insights that we attained into the chiral quark dynamics for a study of the chiral phase boundary of QCD. As elucidated in the previous section, the breaking of chiral symmetry is triggered if the gauge coupling g^2 increases beyond $g^2_{\rm cr}$, thus signaling criticality of the quark sector. We will study the dependence of the chiral symmetry status on two parameters: the temperature T and the number of (massless) flavors $N_{\rm f}$. As already discussed in Sect. 4.5, the increase of the running coupling in the IR is weakened on average for both larger T and larger $N_{\rm f}$. In addition, $g_{\rm cr}$ also depends on T and $N_{\rm f}$, even though the $N_{\rm f}$ dependence is rather weak.

The temperature dependence of $g_{\rm cr}$ has a physical interpretation: at finite T, all quark modes acquire thermal masses, which leads to a quark decoupling for $k\lesssim T$. Hence stronger interactions are required to excite critical quark dynamics. Technically,

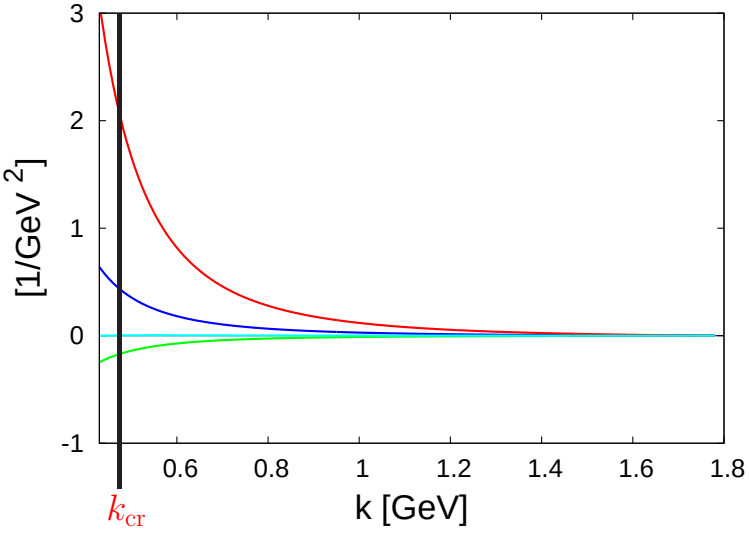

Figure 4.12: The figure shows the dimensionful four-fermion couplings $\bar{\lambda}_i$ as a function of the regulator scale k at vanishing temperature for $N_{\rm f} = 2$ massless quark flavors; from top to bottom: $\bar{\lambda}_\sigma$ (red line), $\bar{\lambda}_-$ (blue line), $\bar{\lambda}_{\rm VA}$ (turquoise line) and $\bar{\lambda}_+$ (green line). The black, vertical line depicts the value of the scale $k_{\rm cr}$, where the quark dynamics become critical.

this T/k dependence is a direct consequence of the T/k dependence of the threshold functions $L^{(\rm F)}_{1,1}(\tilde{t}, \tilde{m}, 0)$, $L^{(\rm FB)}_{1,1,2}(\tilde{t}, \tilde{m}, 0, 0)$ and $L^{(\rm FB)}_{1,1,1}(\tilde{t}, \tilde{m}, 0, 0)$ in Eqns. (4.99) - (4.102). Since the threshold functions decrease with increasing temperature, the λ_i parabolas shown in Fig. 4.10 become broader with a larger value at the maximum. Hence, the annihilation of the Gaußian fixed point achieved by pushing the parabola below the λ_i axis requires a larger $g_{\rm cr}$.

At zero temperature and for small $N_{\rm f}$, the IR fixed point of the running coupling is far larger than $g^2_{\rm cr}$, hence the QCD vacuum is in the phase with borken chiral symmetry. For increasing temperature, the temperature dependence of the coupling and that of $g^2_{\rm cr}$ compete with each other. This is illustrated in Fig. 4.11, where we show the running coupling $\alpha_{\rm s} \equiv \frac{g^2}{4\pi}$ and its critical value $\alpha_{\rm cr} \equiv \frac{g^2_{cr}}{4\pi}$ for $T = 130\,\text{MeV}$ and $T = 220\,\text{MeV}$ as a function of the regulator scale k. The intersection point $k_{\rm cr}$ between both curves marks the scale where the quark dynamics become critical. Below the scale $k_{\rm cr}$, the system runs quickly into the regime with broken chiral symmetry. A corresponding RG flow of the dimensional four-fermion coupling $\bar{\lambda}_i$ for the case of chiral symmetry breaking at vanishing temperature is shown in Fig. 4.12. Although the divergence itself is not shown in the figure, below the scale $k_{\rm cr}$ the couplings approach a divergence at a finite scale $k_{\chi\rm SB}$ which indicates the onset of chiral symmetry breaking (see also the discussion in the previous section).

We estimate the critical temperature $T_{\rm cr}$ as the lowest temperature for which no intersection point between $\alpha_{\rm s}$ and $\alpha_{\rm cr}$ occurs.[22] We find

$$T_{\rm cr}(N_{\rm f}=2) \approx 172 \, {}^{+40}_{-34} \, \text{MeV} \qquad \text{and} \qquad T_{\rm cr}(N_{\rm f}=3) \approx 148 \, {}^{+32}_{-31} \, \text{MeV} \tag{4.104}$$

for two and three massless quark flavors, respectively. These values are in good agreement with lattice QCD simulations, cf. Ref. [15] and Tab. 3.4 in Chap. 3. The errors arise from the experimental uncertainties on $\alpha_{\rm s}$ [9]. The theoretical error, due to the uncertainty in the color-factor, turns out to be subdominant by a large degree, see Fig. 4.13. Dimensionless ratios of observables are less contaminated by this uncertainty of $\alpha_{\rm s}$. For instance, the relative difference for $T_{\rm cr}$ for $N_{\rm f}=2$ and 3 flavors is

$$\Delta := \frac{T_{\rm cr}^{N_{\rm f}=2} - T_{\rm cr}^{N_{\rm f}=3}}{(T_{\rm cr}^{N_{\rm f}=2} + T_{\rm cr}^{N_{\rm f}=3})/2} = 0.150 \, , \tag{4.105}$$

in reasonable agreement with the lattice value of ~ 0.12 [15].[23]

Before we continue with the discussion of the phase boundary in the plane spanned by the temperature and the number of massless quark flavors, we briefly comment on the current quark mass dependence of $T_{\rm cr}$ for $N_{\rm f}=2$ and $N_{\rm f}=3$. For simplicity, we assume degenerate quark masses. In contrast to our study of this dependence with the quark-meson model in Sec. 3.6, we find that $T_{\rm cr}$ is almost independent of the current quark mass m, provided $m < 10\,\text{MeV}$:

$$T_{\rm cr}(m) \approx T_{\rm cr}(0) \quad \text{for} \quad (m < 10\,\text{MeV}) \, . \tag{4.106}$$

Increasing the quark masses to higher values, we observe a weakly increasing value for $T_{\rm cr}$. As we have discussed in Sec. 3.4.3, a current quark mass of $m \approx 10\,\text{MeV}$ is associated with a pion mass $m_\pi \approx 200\,\text{MeV}$. From a linear extrapolation of the lattice data [15], we get the following relative deviation of the phase transition temperature from its value for $N_{\rm f}=2$ in the chiral limit:

$$\left. \frac{T_{\rm cr}(m) - T_{\rm cr}(0)}{T_{\rm cr}(0)} \right|_{m_\pi \approx 200\,\text{MeV}} \approx 0.04 \, . \tag{4.107}$$

From this, we conclude that our result for the mass dependence of the phase transition temperature is consistent with the lattice data, in contrast to our findings for

[22] Strictly speaking, this simplified analysis yields a sufficient but not a necessary criterion for chiral-symmetry restoration. In this sense, our estimate for $T_{\rm cr}$ is an upper bound for the true $T_{\rm cr}$. Small corrections to this estimate could arise if the quark dynamics become uncritical again. This could be caused by a strong decrease of the gauge coupling towards the IR, as discussed in the preceding section.

[23] Even this comparison is potentially contaminated by fixing the scales in the two theories with different flavor content in different ways. While lattice simulations generically keep the string tension fixed, we determine all scales by fixing α at the τ mass scale, cf. the discussion below.

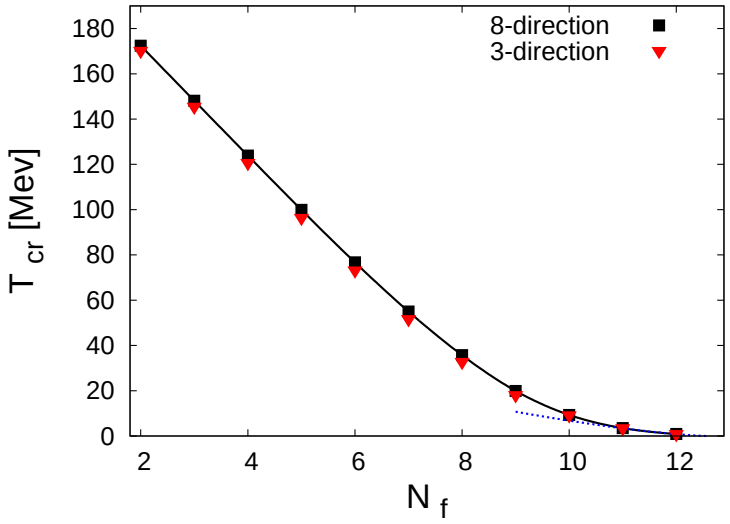

Figure 4.13: Chiral-phase-transition temperature $T_{\rm cr}$ versus the number of massless quark flavors $N_{\rm f}$ for $N_{\rm f} \geq 2$. The flattening at $N_{\rm f} \gtrsim 10$ is a consequence of the IR fixed-point structure. The dotted line depicts the analytic estimate near $N_{\rm f}^{\rm cr}$ which follows from the fixed-point scenario (cf. Eq. (4.114) below). Squares and triangles correspond to calculations with a background field in the 8- and 3-direction of the Cartan, respectively. The theoretical uncertainty which is given by the difference between both curves is obviously negligible in full QCD.

the quark-meson model in Sec. 3.6. Thus, our study indicates that the quark-meson model in its original form without gauge degrees of freedom does not capture the chiral quark dynamics in QCD near the critical temperature completely. Two comments concerning our present study are in order: first, there is no unique definition of the critical temperature if chiral symmetry is explicitly broken by quark mass terms. For our determination of $T_{\rm cr}(m)$, we apply the same definition as in the chiral limit, thus assuming that it is compatible with the standard definition of $T_{\rm cr}$ on the lattice via the chiral susceptibility. Second, our present study of the mass dependence of the critical temperature by means of quarks and gluons has one particular shortcoming: our truncation for the four-fermion interactions, Eq. (4.94), does not represent a complete basis any longer if we allow for finite current quark masses. In this case the RG flow generates contributions which are not invariant under chiral transformations. On the one hand, we neglect the influence of the non-invariant terms in the RG flow, since such terms are not covered by our truncation. On the other hand, these contributions are suppressed as m^2/k^2 relative to the chirally symmetric contributions in the flow, as we have shown in Eq. (4.88) and (4.89). Therefore we assume that our results for small quark masses are not too strongly affected by neglecting the symmetry-breaking operators in our truncation.

The weak dependence of our results on m is not unexpected when we consider the threshold functions $l_{1,1}^{(\mathrm{F})}(\tilde{t},\tilde{m},0)$, $l_{1,1,2}^{(\mathrm{FB})}(\tilde{t},\tilde{m},0,0)$ and $l_{1,1,1}^{(\mathrm{FB})}(\tilde{t},\tilde{m},0,0)$, that represent the regularized loop integrals in the flow equations (4.99)-(4.102). The fermionic propagators in these integrals are essentially given by

$$(2n+1)^2\pi^2T^2+\vec{p}^2+m^2 \quad \text{with} \quad (n\in\mathbb{N})\,. \tag{4.108}$$

We immediately read off that the fermionic propagators are almost unaffected by the mass m, provided $m \ll T$. It is remarkable that our simple, truncated flow already provides a simple picture for the weak mass dependence for the critical temperature which yields consistent results for the quark mass dependence of the critical temperature.

Let us now discuss the phase boundary for massless quark flavors. For the case of several massless quark flavors N_{f}, the critical temperature is plotted in Fig. 4.13. We observe an almost linear decrease of the critical temperature for increasing N_{f} with a slope of $\Delta T_{\mathrm{cr}} = T(N_{\mathrm{f}}) - T(N_{\mathrm{f}}+1) \approx 24\,\mathrm{MeV}$. In addition, we find a critical number of quark flavors, $N_{\mathrm{f}}^{\mathrm{cr}} \simeq 12.5$, above which no chiral phase transition occurs. This result for $N_{\mathrm{f}}^{\mathrm{cr}}$ agrees with other studies based on the two-loop β-function [152]. However, the precise value of $N_{\mathrm{f}}^{\mathrm{cr}}$ has to be considered with some skepticism: for instance, in a perturbative framework, $N_{\mathrm{f}}^{\mathrm{cr}}$ is sensitive to the three-loop coefficient which can bring $N_{\mathrm{f}}^{\mathrm{cr}}$ down to $N_{\mathrm{f}}^{\mathrm{cr}} \simeq 10$ [156]. In our nonperturbative approach, the truncation error can induce similar uncertainties; in fact, it is reassuring that our prediction for $N_{\mathrm{f}}^{\mathrm{cr}}$ lies in the same ball park as the perturbative estimates, even though the details of the corresponding β_{g^2} function are very different. This suggests that our truncation error for $N_{\mathrm{f}}^{\mathrm{cr}}$ is also of order $\mathcal{O}(1)$. We expect that a more reliable estimate can be obtained even within our truncation by using an optimized regulator function [88, 63].

A remarkable feature of the T-N_{f} phase diagram of Fig. 4.13 is the shape of the phase boundary, in particular the flattening near $N_{\mathrm{f}}^{\mathrm{cr}}$. In fact, this shape can be understood from analytical arguments which reveal a direct connection between two universal quantities: the phase boundary and the IR critical exponent of the running coupling.

Before we outline the arguments in detail, let us start with an important caveat: varying the number of massless quark flavors N_{f}, unlike varying the temperature T, corresponds to an unphysical deformation of a physical system. Whereas the deformation itself is unambiguously defined, the comparison of the physical theory with the deformed theory (or between two deformed theories) is not unique. A meaningful comparison requires to identify one particular parameter or one particular scale in both theories. In our case, we keep the running coupling at the τ mass scale always fixed to $\alpha(m_\tau) = 0.322$. Obviously, the couplings in the two theories are different on all other scales, as are generally all dimensionful quantities, such as Λ_{QCD}. There is, of course, no generic choice for fixing the corresponding theories relative to one another. Nevertheless, we believe that our choice is particularly useful, since the τ mass scale is close to the transition between perturbative and nonperturbative regimes. In this

sense, a meaningful comparison between the theories can be made in both regimes, without being too much afflicted by the choice of the fixing condition.

Let us now study the shape of the phase boundary for small N_f. Once the coupling is fixed to $\alpha(m_\tau) = 0.322$, no free parameter is left. As a crude approximation, the mass scale of all dimensionful IR observables such as the critical temperature T_cr is set by the scale k_co where the running gauge coupling undergoes the crossover from small to nonperturbatively large couplings (for instance, one can define the crossover scale k_co from the inflection point of the running coupling in Fig. 4.6). As an even cruder estimate, let us approximate k_co by the position of the Landau pole of the perturbative one-loop running coupling.[24] The latter can be derived from the one-loop relation

$$\frac{1}{\alpha(k)} = \frac{1}{\alpha(m_\tau)} + 4\pi b_0 \ln\frac{k}{m_\tau}, \quad b_0 = \frac{1}{8\pi^2}\left(\frac{11}{3}N_\mathrm{c} - \frac{2}{3}N_\mathrm{f}\right). \tag{4.109}$$

Defining k_co by using the Landau-pole scale, $1/\alpha(k_\mathrm{co}) = 0$, and estimating the order of the critical temperature by $T_\mathrm{cr} \sim k_\mathrm{co}$, we obtain

$$T_\mathrm{cr} \sim m_\tau \, \mathrm{e}^{-\frac{1}{4\pi b_0 \alpha(m_\tau)}} \simeq m_\tau \, \mathrm{e}^{-\frac{6\pi}{11 N_\mathrm{c} \alpha(m_\tau)}} \left(1 - \epsilon N_\mathrm{f} + \mathcal{O}((\epsilon N_\mathrm{f})^2)\right), \tag{4.110}$$

where $\epsilon = \frac{12\pi}{121 N_\mathrm{c}^2 \alpha(m_\tau)} \simeq 0.107$ for $N_\mathrm{c} = 3$. This simple estimate hence predicts a linear decrease of the phase boundary $T_\mathrm{cr}(N_\mathrm{f})$ for small N_f which is confirmed by the full solution plotted in Fig. 4.13. Actually, this estimate is also quantitatively accurate, since it predicts a relative difference for T_cr for N_f=2 and 3 flavors of $\Delta \simeq 0.146$, which is in very good agreement with the full result given in Eq. (4.105). We conclude that the shape of the phase boundary for small N_f is basically determined by fermionic screening.

For larger N_f, the above estimate cannot be used any longer, because neither one-loop perturbation theory nor the N_f expansion are justified. However, a different analytic argument can be made. For $N_\mathrm{f} \approx N_\mathrm{f}^\mathrm{cr}$, fermionic screening of color charges keeps the coupling small. Therefore the running coupling has to come close to its maximal value in order to be strong enough to drive the quark sector to criticality. This maximal value is, of course, close to the IR fixed point value α_* attained for $T = 0$. Even though at finite temperature the coupling is eventually governed by the $3d$ fixed point, which implies a linear decrease with k, the status of chiral symmetry breaking will still be dictated by the maximum coupling value, which roughly corresponds to the $T = 0$ fixed point. In the fixed-point regime, we can approximate the β_{g^2} function by a linear expansion about the fixed-point value,

$$\beta_{g^2} \equiv \partial_t g^2 = -\Theta\,(g^2 - g_*^2) + \mathcal{O}((g^2 - g_*^2)^2), \tag{4.111}$$

where the universal critical exponent Θ denotes the first expansion coefficient. We know that $\Theta < 0$, since the fixed point is IR attractive. For vanishing temperature, we find an approximately linear dependence of Θ on N_f, cf. Tab. 4.1.

[24] Actually, this is a reasonable estimate, since the N_f dependence of k_co, which is all that matters in the following, is close to the perturbative behavior.

$N_{\rm f}$	0	4	5	6	7	8	9	10	11	12	13
$-\Theta$	6.39	5.50	4.99	4.41	3.82	3.19	2.58	1.97	1.42	0.95	0.57

Table 4.1: The critical exponent Θ for different values of $N_{\rm f}$ at vanishing temperature.

The solution of Eq. (4.111) for the running coupling in the fixed-point regime reads

$$g^2(k) = g_*^2 - \left(\frac{k}{k_0}\right)^{-\Theta}, \tag{4.112}$$

where the scale k_0 is implicitly defined by a suitable initial condition to be set in the fixed-point regime. In the following, we keep k_0 fixed. It provides all dimensionful scales in the following and is related to the initial τ mass scale by RG evolution. Our criterion for the occurence of chiral symmetry breaking is that $g^2(k)$ exceeds $g_{\rm cr}^2$ for some value of $k = k_{\rm cr}$. We expect that this scale $k_{\rm cr}$ is generically somewhat larger than the temperature, since for all k smaller than T the coupling decreases again due to the $3d$ fixed point.[25] This allows us to ignore the temperature dependence of the running coupling g^2 and of the critical coupling $g_{\rm cr}$ as a rough approximation, since the T dependence of the threshold functions is rather weak for $T \lesssim k$. From Eq. (4.112) and the condition $g^2(k_{\rm cr}) = g_{\rm cr}^2$, we derive the estimate

$$k_{\rm cr} \simeq k_0 \, (g_*^2 - g_{\rm cr}^2)^{-\frac{1}{\Theta}}. \tag{4.113}$$

The scale $k_{\rm cr}$ plays the same role as the crossover scale $k_{\rm co}$ in the small-$N_{\rm f}$ argument given above: it sets the scale for $T_{\rm cr} \sim k_{\rm cr}$, with a proportionality coefficient provided by the solution of the full flow. To conclude the line of arguments: we note that the IR fixed-point value g_*^2 depends roughly linearly on $N_{\rm f}$, since the quark contribution to the coupling flow given by $\eta^{\rm q}$ is linear in $N_{\rm f}$. From Eq. (4.113), we thus find the relation

$$T_{\rm cr} \sim k_0 |N_{\rm f} - N_{\rm f}^{\rm cr}|^{-\frac{1}{\Theta}}, \tag{4.114}$$

which is expected to hold near $N_{\rm f}^{\rm cr}$ for $N_{\rm f} \leq N_{\rm f}^{\rm cr}$. Here Θ should be evaluated at $N_{\rm f}^{\rm cr}$.[26] Relation (4.114) is an analytic prediction for the shape of the chiral phase boundary in the T-$N_{\rm f}$ plane of QCD. Remarkably, it relates two universal quantities to one another: the phase boundary and the IR critical exponent.

This relation can be checked with a fit of the full numerical result parametrized by the RHS of Eq. (4.114). In fact, the fit result, $\Theta_{\rm fit} \simeq -0.71$, determined from the phase boundary agrees with the direct determination of the critical exponent from the

[25] Indeed, this assumption is justified, since we find in the full calculation that $k_{\rm cr} \gg T$ for large $N_{\rm f}$ and for temperatures in the vicinity of the critical temperature $T_{\rm cr}$.

[26] Accounting for the $N_{\rm f}$ dependence of Θ by an expansion around $N_{\rm f}^{\rm cr}$ yields mild logarithmic corrections to Eq. (4.114).

β_{g^2} function at zero temperature, $\Theta(N_{\rm f}^{\rm cr} \simeq 12.5) \simeq -0.71$. The fit is depicted by the dashed line in Fig. 4.13. In particular, the fact that $|\Theta| < 1$ near $N_{\rm f}^{\rm cr}$ explains the flattening of the phase boundary near the critical number of flavors.

Qualitatively, relation (4.114) is a consequence of the IR fixed-point scenario predicted by our truncated flow equation. We emphasize, however, that the quantitative results for universal quantities such as Θ are likely to be affected by truncation errors. These can be reduced by an optimization of the present flow; we expect from preliminary regulator studies that more reliable estimates of Θ yield smaller absolute values and, thus, a more pronounced flattening of the phase boundary.

We know that the relation (4.114) is difficult to test, for instance, in lattice QCD simulations: neither the fixed-point scenario in the deep IR nor large flavor numbers are easily accessible, even though there are promising investigations that have collected evidence for the IR fixed-point scenario in the Landau gauge [193, 194] (see also [195, 196, 197]) as well as the existence of a critical flavor number [151]. Given the conceptual simplicity of the fixed-point scenario in combination with χSB, further lattice studies are certainly desirable.

4.8 Conclusions

We have obtained new non-perturbative results for the chiral phase boundary of QCD in the plane spanned by the temperature and the number of massless quark flavors. To our knowledge, this is the first determination of the full chiral phase boundary in QCD. For a small number of quark flavors, where lattice simulations are available, we found remarkable agreement of our values for the critical temperature with the results obtained from lattice simulations.

Our work is based on the functional RG, which yields a flow equation for the effective average action of QCD. We have studied this effective action from first principles in a systematic and consistent operator expansion. We consider the truncated expansion as a minimal approximation of the effective action that is capable of accessing the non-perturbative IR domain and addressing the dynamics of chiral symmetry breaking at zero as well as finite temperature.

In the gluon sector, this truncation results in a stable flow of the gauge coupling, which runs into a fixed point in the IR at zero temperature. This is in agreement with the results of Ref. [71] for the pure glue sector. As a physically non-trivial new result, we find that the $3d$ analogue of this IR fixed point governs the flow of the gauge coupling at finite temperature for scales $k \ll T$. Our truncation in the quark sector facilitates a description of critical dynamics with a gluon-driven approach to chiral symmetry breaking. The resulting picture for chiral symmetry breaking is comparatively simple: in order to penetrate the phase boundary between the chirally symmetric and chirally broken regime, the coupling is required to exceed a critical value $g_{\rm cr}$. This allows us to trace back the question of the onset of chiral symmetry breaking to the strength of

the strong running coupling relative to this critical value. Whether or not this critical value is reached depends on the RG flow of the strong coupling. The fixed points of the coupling in the deep IR generically put an upper bound on the maximal value of the coupling. This value depends on the external parameters such as temperature and the number of quark flavors. Even though the underlying mechanism for chiral symmetry breaking is remarkably simple, the interplay between the gluon and quark sectors in general, and between the strong coupling and the critical coupling in particular, is highly nonlinear, since both sectors induce back-reactions onto one another in a manner that is quantitatively captured by the flow equation.

The phase boundary in the T-$N_{\rm f}$ plane, spanned by the temperature and the number of massless quark flavors, exhibits a characteristic shape which can be understood analytically in terms of simple physical mechanisms: for small $N_{\rm f}$, we observe a linear decrease of $T_{\rm cr}$ as a function of $N_{\rm f}$ which is a direct consequence of the color-screening properties of light fermions. Our study confirms also the existence of a critical flavor number, $N_{\rm f}^{\rm cr} \approx 12$, above which the system remains in the chirally symmetric phase even at zero temperature, and even though the theory is still asymptotically free for $N_{\rm f}$ not too much larger than $N_{\rm f}^{\rm cr}$. Although the screening property of the fermions is ultimately responsible for the existence of a critical flavor number $N_{\rm f}^{\rm cr}$, the shape of the phase boundary for $N_{\rm f} \lesssim N_{\rm f}^{\rm cr}$ cannot be explained by this property alone. In this region, the critical temperature is very small, and thus the system is probed in the deep IR. We have shown that this connection becomes most obvious in a remarkable relation between the shape of the phase boundary for $N_{\rm f} \lesssim N_{\rm f}^{\rm cr}$ and the IR critical exponent Θ of the running coupling at zero temperature. In particular, the flattening of the phase boundary in this regime is a direct consequence of $|\Theta|$ being smaller than 1. Since both the shape of the phase boundary and the critical exponent are universal quantities, their relation is a generic, testable prediction of our analysis. This prediction can be tested directly by other nonperturbative approaches, e. g. lattice simulations[27] or DSE.

Our present study already provides results for the quark-mass dependence of the chiral phase transition temperature. Even if our truncation does not contain quark self-interactions that violate chiral symmetry, we have argued that our study is still trustworthy for small quark masses. We found a quark mass dependence which is consistent with the results from lattice QCD and thereby seems to exclude the quark-meson model in its original form without gauge degrees of freedom as an appropriate model for an accurate description of the chiral phase boundary of QCD at finite temperature. Further generalizations in this direction will aim at a more accurate study of the effect of finite quark masses; the formalism for this has largely been developed in this work. Owing to the mechanism of fermionic decoupling, we expect that the largest modifications will arise from a realistic strange quark mass which is of the order of the characteristic scales such as $T_{\rm cr}$ or the scale of χSB.

[27] We know that it may be numerically expensive to test this prediction in lattice simulations.

Let us now give a critical discussion of the reliability of our results in the light of our underlying truncation. First of all, it is impossible to study the flow of the most general effective action, consisting of all operators that are compatible with the symmetries of the theory. Therefore we must truncate the action to a subset of operators, which is not necessarily finite. Nevertheless, such an approximation of the full theory can also describe non-perturbative physics reliably, provided the relevant degrees of freedom in the form of RG relevant operators are kept in the ansatz for the effective action. We know that this is obviously the most problematic part, since it requires a lot of physical insight to make the correct physical choice. A first but highly nontrivial check of any solution to the flow equation is provided by a stability analysis of its RG flow, since insufficient truncations generically exhibit IR instabilities of Landau-pole type. The truncation in the quark sector that supports potential critical dynamics is an obvious example for this. The approximation can become (more) controlled if the inclusion of higher-order operators does not lead to serious modifications of the results. In the quark sector, it can indeed be verified easily that the contribution of many higher-order operators such as $(\bar{\psi}\psi)^4$ or mixed gluonic-fermionic operators is generically suppressed by the one-loop structure of the flow equation or the fixed-point argument given below Eq. (4.103). This holds at least in the symmetric regime, which is sufficient to trace out the phase boundary. The Landau-pole type instability in the RG flow has a physically meaning since it is related to the onset of chiral symmetry breaking. This instability can be cured by including composite operators in the truncation, yielding a stable flow even in the deep IR, as has been shown for one-flavor QCD at zero temperature [61]. The inclusion of such operators in the truncation is indispensable if we are interested in the deep IR or in a study of the order of the phase transition. However, in this work, we have restricted our study to a determination of the chiral phase boundary by approaching it from the chiral symmetric regime. In this case, it is sufficient to locate the instability of the present truncation. In contrast to the fermionic sector, we are not aware of similar arguments for the gluonic sector; here, higher-order expansions involving, e.g., $(F_{\mu\nu}\widetilde{F}^{\mu\nu})^2$ or operators with covariant derivatives or ghost fields eventually have to be used to verify the expansion scheme. At finite temperature, the difference between so-called electric and magnetic sectors can become important, as mediated by operators involving the heat-bath four-velocity u_μ, e.g., $(F_{\mu\nu}u_\nu)^2$. In view of results obtained in the Landau gauge [172], the inclusion of ghost contributions in the gauge sector appears important, if not indispensable, for a description of color confinement. A posteriori, our truncation can be verified by a direct comparison with lattice results, which shows satisfactory agreement.

As we have discussed in Subsec. 2.4.2, a stability analysis of results from RG flows can also be obtained by varying the regulator. Since universal quantities are independent of the regulator in the exact theory, any such regulator dependence of the truncated system is a measure for the reliability of the truncation. For our underlying truncation in the quark sector, such an analysis has been performed at zero temperature in Ref. [156], showing a surprisingly weak dependence on the regulator which

strongly supports the choice of the truncation. By contrast, we do not expect such a regulator independence to hold in the truncated gluonic sector. If so, it is advisable to improve results for universal quantities towards their physical values. This can indeed be done by using stability criteria for the flow equation which have led to optimization schemes [88, 63, 198]. As has been pointed out for scalar field theories in Ref. [198], the use of such optimized regulators gives better results for dimensionless quantities, e.g. the relative shift (4.105) in the transition temperature or the IR critical exponent Θ. An optimization of the regulator for the present study is subject of a current work [199].

Chapter 5

Summary and Outlook

We have studied the chiral dynamics of QCD in a finite Euclidean volume and at finite temperature within a non-perturbative RG framework based on a simple flow equation for the effective action. This flow equation makes an interpolation possible between the classical action and the full quantum effective action of a given theory. The RG flow equation for this effective action provides a powerful but easy to handle machinery for studying all kinds of quantum field theories non-perturbatively. We have argued that such an approach is complementary to the one taken in lattice QCD simulations since it has its advantages exactly at those points where the lattice approach has its shortcomings. For example, the chiral limit is accessible or the fact that quantum field theories can be studied in finite as well as in infinite volume. On the other hand, it is impossible to study the RG flow of the most general effective action of a given theory. A suitable truncation of the effective action to a subset of operators is therefore required. However, this limitation can be turned into an advantage since it provides the opportunity for a systematic and consistent expansion of a quantum field theory. The relevant mechanisms for a phenomenon can be worked out by a careful cross-check of the results obtained from a given truncation with results from other non-perturbative approaches such as lattice simulations.

In Chap. 3, we have studied finite-volume effects in low-energy observables of QCD by means of the quark-meson model. The quark-meson model is an effective low-energy model for the description of dynamical chiral symmetry breaking in QCD. It contains mesonic and quark degrees of freedom, but does not contain any gluonic degrees of freedom, and it is not confining. It relies on the fact that the low-energy limit of QCD can be described well in terms of weakly interacting pions. However, due to the missing gluonic degrees of freedom, the quark-meson model in its present form is obviously not sufficient for bridging the gap between the low- and high-energy limit of QCD, since the high-energy limit is best described in terms of quarks and gluons. Nevertheless the model provides a reliable description for the low-energy limit and should thus be trustworthy for a study of QCD for volume sizes that are not too small

or temperatures that are not too high. If the volume is too small or the temperature too high, a description of QCD by means of the quark-meson model is naturally bound to fail due to the lack of gauge degrees of freedom.

We have shown that the qualitative behavior of the pion mass and the pion decay constant as a function of the volume size depends on the the choice of the quark boundary conditions in spatial directions. The reason for this can be immediately traced back to the existence of zero-momentum modes for the quarks in case of periodic boundary conditions. The most important result of our study is that we have found agreement between our results obtained for anti-periodic boundary conditions for the quarks with the results from chiral perturbation theory. On the other hand, our results are qualitatively in accordance with lattice QCD studies, provided we choose periodic boundary conditions for the quarks in spatial direction. Of course, this agreement with lattice studies is not unexpected since the quarks are usually implemented with periodic boundary conditions on the lattice. However, the dependence of low-energy observables on the volume size obtained from periodic quark boundary conditions differs significantly from those that we have obtained for anti-periodic boundary conditions. The difference between both is most pronounced for intermediate volume sizes, $V^{1/3} \sim 1-2$ fm, and becomes negligible for large volumes, $V^{1/3} \gtrsim 4\,\mathrm{fm}$. Since current lattice simulations use lattices of a size for which the effects arising due to the choice of the boundary conditions are mostly pronounced, we conclude that lattice simulations have not yet reached the point where chiral perturbation theory can be used for extrapolations to the infinite volume limit, at least for the low-energy observables. Currently, we have included the RG flow of the wave-function renormalization in a finite-volume study of a scalar $O(N)$ model [200]. Such a study can provide important information about finite-size scaling and, in particular, about scaling functions which are important for a reliable extrapolation of lattice results to the infinite-volume limit.

In addition, we have also studied the chiral phase transition in finite and infinite volume in Chap. 3 with the quark-meson model. From our results for the dependence of the transition temperature on the (current) quark mass in finite and infinite volume, we conclude that the weak dependence of the phase transition on the quark mass found in lattice studies cannot be explained with the quark-meson model. What is more, we have also excluded that this weak dependence is a finite-volume effect. On the contrary, we have found that the dependence of the phase transition temperature in finite volume becomes even stronger than in the infinite volume limit. These findings confirm the conjecture mentioned above that the quark-meson in its original form without gauge degrees of freedom cannot correctly capture all the dynamics at high temperatures, in particular near the phase boundary. Extensions of the quark-meson model which might cure this lack of the model are currently researched [148, 61, 150].

In Chap. 4, we have studied a first-principles approach to chiral symmetry breaking in QCD in terms of microscopic degrees of freedom, namely in terms of quarks and gluons. First, we have computed the running coupling of Yang-Mills theory and of QCD

for all temperatures and scales, extending previous work at zero temperature [71]. In this study, we have found a non-trivial IR fixed point in $3d$ Yang-Mills theory. At scales larger than a particular temperature, the flow of the coupling is in agreement with the zero-temperature result. Following the RG flow towards lower scales, we encounter a maximum in the value of the coupling at a scale which is of the order of the temperature. Finally, the coupling decreases for scales lower than the temperature where the RG flow is governed by the spatial $3d$ Yang-Mills theory. We have argued that the decrease in this regime can be traced back to the existence of the above-mentioned non-trivial IR fixed point in the underlying $3d$ Yang-Mills theory. From the phenomenological point of view, the behavior of the coupling for intermediate momenta in the transition region is most important. The behavior of the coupling influences physical observables especially near its maximum. With increasing temperature the position of the maximum shifts to higher momentum scales, and the value at the maximum decreases. On average, the system becomes less strongly coupled for higher temperature, in agreement with naive expectations from a temperature-dependent effective coupling. This behavior influences, e. g., the scattering cross-section of a quark with the particles in the quark-gluon plasma. In a current study [201], the running coupling, including its modification due to finite temperature, is used in a computation of the energy loss of an incident quark in the quark-gluon plasma.

In this work, we have applied the running coupling computed in Chap. 4 to a study of the chiral phase boundary. For this purpose, we have included quark self-interactions in our truncation of the effective action. We have used the lowest non-trivial choice for the quark self-interactions in a consistent and systematic operator expansion. We stress that our truncation of the quark self-interactions forms a complete basis in the sense that any other gauge- and chirally symmetric point-like four-quark interaction can be reduced in terms of the operators which we included. In our approach, we have been able to provide a simple picture of the chiral dynamics of QCD in the vicinity of the finite-temperature phase boundary. We have computed a critical value for the gauge coupling which must be exceeded in order to reach the regime with broken chiral symmetry. The existence of such a critical value enabled us to trace back the question of the onset of chiral symmetry breaking to the strength of the running coupling relative to its critical value. We have then applied our findings to a study of the chiral phase boundary of QCD. The critical temperature in this context has been defined as the lowest temperature for which the running coupling does not exceed its critical value. Our results for the critical temperature for a small number of massless quark flavors are in good agreement with the results from lattice QCD simulations. At this point, we stress that no other parameter except for the running coupling at the τ-mass scale has been used as an input. A generalization of our study to an arbitrary number of massless quark flavors allowed us to compute the phase boundary of QCD in the plane of temperature and flavor number. Our results show that the phase boundary is characterized by a linear decrease of the critical temperature for small number of quark flavors, owing to the screening nature of the quarks. For a large number of quark

flavors, our study confirms the existence of a critical number $N_{\rm f}^{\rm cr}$ of massless quark flavors above which QCD is still asymptotically free, but no chiral symmetry breaking occurs. Additionally, we have found that the chiral phase boundary is characterized by a flattening near $N_{\rm f}^{\rm cr}$. We have shown that there is an intriguing direct relation between the characteristic flattening of the chiral phase boundary near $N_{\rm f}^{\rm cr}$ and the infrared fixed point structure of QCD.

The fact that our study relies on only one input parameter demonstrates nicely how powerful our approach is. It serves as a promising starting point for further phenomenological studies of QCD. An extension of the present work to finite density seems to be a natural first step and should provide information about the QCD phase boundary for small chemical potentials; work in this direction has been already started [202]. Further extensions of our study should include mesonic operators which can be treated with RG rebosonization techniques [60, 61]. This would not only provide access to the broken phase and a study of mesonic properties but also permit a study of the order of the phase transition.

In conclusion, we have demonstrated the efficacy of RG methods for an investigation of QCD. With our determination of the transition temperature independent of lattice simulations, we believe that we have made a valuable contribution to the continually improving knowledge of QCD. However, as we mentioned above, a lot of work is still in progress and much remains to be done.

Appendix A

Notations and Conventions

In App. A.1, we give the relation between the the physical units used in this work and the corresponding units of the SI system. Our conventions concerning Euclidean space-time are found in App. A.2. In this context, we discuss also the relation between quantum field theory and statistical physics. Our abbreviations are summarized in App. A.3.

A.1 Units

Throughout this work we set $\hbar = c = k_B = 1$. As a consequence of this convention, the SI units for length (Meter, m) and temperature (Kelvin, K) are related to the energy unit MeV as follows

$$1\ \mathrm{m} = 10^{15}\ \mathrm{fm} \approx 5.1 \times 10^{12}\ \frac{1}{\mathrm{MeV}} \qquad \text{and} \qquad 1\ \mathrm{K} \approx 8.6 \times 10^{-11}\ \mathrm{MeV}\,. \tag{A.1}$$

A.2 Euclidean Space-Time

A.2.1 Minkowski- and Euclidean Space-Time

The coordinates in Euclidean space-time and Minkowski space-time are related by

$$x_{M,0} = -\mathrm{i}x_0 \tag{A.2}$$

$$g^{\mu\nu}x_{M,\mu}x_{M,\nu} = x_0^2 - \vec{x}_M^2 = x_0^2 + \vec{x}^2 \equiv g^{\mu\nu}x_\mu x_\nu = -x^2\,, \tag{A.3}$$

where $\mu, \nu = 1, \ldots, d$ and correspondingly for the momenta. In this Subsection, we add an index "M" to the coordinates in Minkowski space-time. The metric tensor in (flat) Euclidean space-time is given by the Kronecker-Delta, $g^{\mu\nu} = \delta^{\mu\nu}$, whereas we have the metric tensor $g_M^{\mu\nu} = \mathrm{diag}(+, -, -, \ldots, -)$ in (flat) Minkowski space-time. When we treat fermions, we deal with the Dirac operator $\mathrm{i}\partial\!\!\!/$ which is defined as

$$\mathrm{i}\partial\!\!\!/ = \mathrm{i}\gamma_\mu\partial_\mu\,, \tag{A.4}$$

where the γ_μ denote hermitean γ-matrices in Euclidean space-time. We refer to App. C for our conventions for γ-matrices. In order to have a hermitean Dirac-operator $\mathrm{i}\partial\!\!\!/$ in Euclidean space-time, we make use of the fact that the fermion fields ψ and $\bar{\psi}$ are independent variables in the path-integral. Therefore we can relate the fermion fields in Euclidean space-time to their Minkowski counterparts ψ_M and $\bar{\psi}_M$ through

$$\psi = \psi_M \quad \text{and} \quad \bar{\psi} = \mathrm{i}\bar{\psi}_M \,. \tag{A.5}$$

For this reason, the mass terms of the fermion fields are always dressed with the imaginary unit-factor "i" throughout this work.

A.2.2 Quantum Field Theory and Statistical Physics

Let us now discuss briefly the relation between quantum field theory and statistical physics, cf. [159, 54]. In statistical physics, it is convenient to use the grand canonical partition function Z for a theoretical description of thermal systems:

$$Z = \mathrm{Tr}\, e^{-\beta(\hat{H}-\mu_i\hat{N}_i)} = \sum_n \langle n|\, e^{-\beta(\hat{H}-\mu_i\hat{N}_i)}\, |n\rangle \;, \tag{A.6}$$

where $\hat{H}$ denotes the Hamilton operator of the system and $\hat{N}$ denotes the particle number operator. The temperature T enters the definition of the grand canonical partition function Z via the factor $\beta = 1/T$. Since the grand canonical partition function contains the full information of the physical system, which is described by the Hamilton operator $\hat{H}$, we can compute all thermodynamical quantities from it. Comparing Eq. (A.6) with the generating functional[1] Z in Euclidean space-time,

$$Z \propto \int D\phi\, e^{-S[\phi]+\int d^4x\{J\phi\}} \,, \tag{A.7}$$

we observe that both expressions are similar from the mathematical point of view. For example, the source term J corresponds to an external magnetic field applied to a spin system in statistical physics. However, in order to treat thermal systems within a path-integral approach, we have to use the following generating functional:

$$Z \propto \int_{\text{periodic}} D\phi\, e^{-S[\phi]+\int d^4x J\phi} \,. \tag{A.8}$$

The index "periodic" indicates that the functional integration must be performed under the constraint $\phi(0,\vec{x}) = \phi(\beta,\vec{x})$. In statistical physics, the explicit dependence on the external perturbation of a system, such as the magnetic field in a spin-system, is eliminated through a Legendre transformation of the free energy $F = -\ln Z$, which yields

[1] For convenience, we restrict the discussion to single-component scalar field theory. The generalization to fermion fields and vector fields is straightforward.

the so-called Gibbs energy. The stable ground state of the system is then obtained by minimizing the Gibbs energy. In our discussion of the effective action in Sec. 2.4.2, we have shown that the generating functional W of the connected Green's functions is related to the generating functional Z via $W = \ln Z$. Thus W corresponds to the free energy in statistical physics. Moreover, we have shown that the effective action Γ is obtained through a Legendre transformation of the generating functional W. Thus we find that the effective action corresponds to the Gibbs energy in statistical physics.

Since we consider quantum field theories at finite temperature in this work, it is important to keep in mind these relations between the field-theoretical quantities and their statistical counterparts.

A.3 Abbreviations

1PI	one particle irreducible
bWTI	background-field Ward-Takahashi identity
chPT	Chiral Perturbation Theory
DSE	Dyson Schwinger Equation(s)
FRG	Functional Renormalization Group
IR	Infrared
LHS	Left Hand Side
LPA	Local Potential Approximation
mWTI	modified Ward-Takahashi identity
QCD	Quantum Chromodynamics
QED	Quantum Electrodynamics
RG	Renormalization Group
RHS	Right Hand Side
UV	Ultraviolet
WTI	Ward-Takahashi identity

Appendix B

Color Algebra

In this appendix, we give our conventions for the generators of the $SU(N_c)$ Lie-groups and discuss some details on the evaluation of the color traces which we encounter in the calculation of the strong coupling.

B.1 The Group $SU(N_c)$

Our studies in Chap. 4 are not restricted to Yang-Mills theory or QCD with $N_c = 2$ or $N_c = 3$ colors. In the derivation of the RG flow equations, we have allowed for an arbitrary number of colors N_c. The underlying group $SU(N_c)$ of unitary matrices U of rank N_c with determinant $\det U = 1$ has $N_c^2 - 1$ generators T^a which obey the commutation relations

$$\left[T^a, T^b\right] = \mathrm{i} f^{abc} T^c \,, \tag{B.1}$$

where f^{abc} are the (anti-symmetric) structure constants of the group, and a, b, c take the values $1, \ldots, N_c^2 - 1$. The normalization of the generators is given by

$$\mathrm{Tr}\left\{T^a T^b\right\} = \frac{1}{2}\delta^{ab} \,. \tag{B.2}$$

Moreover, the generators fulfill

$$\sum_a (T^a)_{\alpha\beta}(T^a)_{\gamma\delta} = \frac{1}{2}\delta_{\alpha\delta}\delta_{\beta\gamma} - \frac{1}{2N_c}\delta_{\alpha\beta}\delta_{\gamma\delta} \tag{B.3}$$

and

$$\sum_a \left\{ (T^a)_{\alpha\beta}(T^a)_{\gamma\delta} + \frac{1}{N_c}(T^a)_{\alpha\delta}(T^a)_{\beta\gamma} \right\} = \frac{N_c^2 - 1}{2N_c^2}\delta_{\alpha\delta}\delta_{\beta\gamma} \,. \tag{B.4}$$

For $SU(2)$, the generators are related to the Pauli matrices τ^a via $T^a = \frac{1}{2}\tau^a$ and the structure constants f^{abc} are given by the (standard) totally antisymmetric tensor ϵ^{abc}. The generators for the group $SU(3)$ can be expressed in terms of the Gell-Mann matrices λ^a via $T^a = \frac{1}{2}\lambda^a$.

B.2 Color Traces for the Calculation of the Strong Coupling

The leading growth coefficients $a_m^{\text{l.g.}}$ given in Eq. (4.72) depend on the color factors τ_i^A and τ_i^ψ in Eq. (4.72). These factors carry the information of the underlying $SU(N_\text{c})$ gauge group. The gluonic factors τ_i^A appearing in the leading growth coefficients and thus in the flow equation for the strong coupling have been discussed in Refs. [74, 71, 171]. Let us summarize these discussions, before we discuss the color factors τ_i^ψ of the quark sector.

Gauge group information enters the flow of the coupling via color traces over products of field strength tensors and gauge potentials. For our calculation, it suffices to consider a pseudo-abelian background field $\bar{A}$ which points into a constant color direction n^a. In this case, the color traces reduce to

$$n^{a_1} n^{a_2} \dots n^{a_{2i}} \, \text{tr}_\text{c}[T^{(a_1} T^{a_2} \dots T^{a_{2i})}] \,, \tag{B.5}$$

where the parentheses at the color indices denote symmetrization. These factors are not independent of the direction of n^a, but the LHS of the flow equation is independent of it. Note that the LHS of the flow equation is a function of $\frac{1}{4} F^a_{\mu\nu} F^a_{\mu\nu} \to \frac{1}{2} B^2$ which is independent of n^a. For this reason, we only need that part of the symmetric invariant tensor $\text{tr}_\text{c}[T^{(a_1} \dots T^{a_{2i})}]$ which is proportional to the trivial one,

$$\text{tr}_\text{c}[T^{(a_1} T^{a_2} \dots T^{a_{2i})}] = \tau_i \, \delta_{(a_1 a_2} \dots \delta_{a_{2i-1} a_{2i})} + \dots \,. \tag{B.6}$$

Here, we have neglected further nontrivial symmetric invariant tensors. This is justified since these neglected terms do not contribute to the flow of $\mathcal{W}_k(\theta)$, but to that of other operators which do not belong to our truncation. For the gauge group SU(2), there are no further symmetric invariant tensors in Eq. (B.6), implying

$$\tau_i^{\text{SU(2)}} = 2, \quad i = 1, 2, \dots \,. \tag{B.7}$$

However, for higher gauge groups, the complications mentioned above arise. Therefore we do not evaluate the τ_i^A's from Eq. (B.6) directly; instead, we use the fact that the color unit vector n^a can always be rotated into the Cartan sub-algebra. We choose the two color vectors n^a which give the extremal values for the whole trace of Eq. (B.5). For $SU(3)$, these extremal values are obtained by choosing a color vector n^a pointing into the 3- and 8-direction in color space, respectively:

$$\tau_{i,3}^{A,\text{SU(3)}} = 2 + \frac{1}{4^{i-1}}, \quad \tau_{i,8}^{A,\text{SU(3)}} = 3 \left(\frac{3}{4}\right)^{i-1} \,. \tag{B.8}$$

Let us now discuss the color factors τ_j^ψ of the quark sector. The considerations for the gluonic factors τ_j^A also hold for the contributions of the flow equation which arise from

the fermionic part of our truncation Eq. (4.61) and (4.62). Choosing a color vector n^a pointing into the 3- or 8-direction and taking into account that quarks live in the fundamental representation, we obtain the color factors for $SU(3)$:

$$\tau_{i,3}^{\psi,\mathrm{SU(3)}} = 2\left(\frac{1}{4}\right)^i, \quad \tau_{i,8}^{\psi,\mathrm{SU(3)}} = 2\left(\frac{1}{12}\right)^i + \left(\frac{1}{3}\right)^i \quad i = 1, 2, \dots \ . \tag{B.9}$$

Note that all complications are absent for SU(2) and we find $\tau_i^{\psi,\mathrm{SU(2)}} = \tau_{i,3}^{\psi,\mathrm{SU(3)}}$.

It is this uncertainty introduced by the artificial n^a dependence of the color factors which is responsible for the uncertainties of our results for the critical temperature and the fixed point values in three and four dimensions.

Appendix C

Dirac Algebra and Fierz Identities

C.1 Clifford Algebra

We work exclusively in Euclidean space-time in this work, see App. A for details. Whenever we treat fermions, we restrict our discussion to $d = 4$ space-time dimensions. The Dirac algebra is then defined through

$$\begin{aligned} \{\gamma^\mu, \gamma^\nu\} &= \gamma^\mu\gamma^\nu + \gamma^\nu\gamma^\mu = 2\delta^{\mu\nu}\mathbf{1}, \\ (\gamma^\mu)^\dagger &= \gamma^\mu, \\ \gamma^5 &= \gamma^1\gamma^2\gamma^3\gamma^0, \\ \sigma^{\mu\nu} &= \frac{i}{2}[\gamma^\mu, \gamma^\nu] = \frac{i}{2}(\gamma^\mu\gamma^\nu - \gamma^\nu\gamma^\mu). \end{aligned} \tag{C.1}$$

An explicit representation for the γ-matrices is given by,

$$\gamma^\mu = \begin{pmatrix} 0 & -i\sigma^\mu \\ i\sigma^\mu & 0 \end{pmatrix}, \quad \gamma^5 = \begin{pmatrix} \mathbf{1} & 0 \\ 0 & -\mathbf{1} \end{pmatrix}, \tag{C.2}$$

where $\sigma^\mu = (i\mathbf{1}, \sigma^i)$. The matrices σ^i denote the well-known Pauli-matrices

$$\sigma^1 = \begin{pmatrix} 0 & 1 \\ 1 & 0 \end{pmatrix}, \quad \sigma^2 = \begin{pmatrix} 0 & -i \\ i & o \end{pmatrix}, \quad \sigma^3 = \begin{pmatrix} 1 & 0 \\ 0 & -1 \end{pmatrix}. \tag{C.3}$$

and $\mathbf{1}$ is here the 2×2 unit matrix. It is convenient to introduce the projection operators $P_{\mathrm{L,R}} = \frac{1\pm\gamma^5}{2}$ for the chiral components and to work in a chiral basis for the fermion fields,

$$\psi = \begin{pmatrix} \psi_\mathrm{L} \\ \psi_\mathrm{R} \end{pmatrix} \quad \text{and} \quad \bar\psi = (\bar\psi_\mathrm{R}, \bar\psi_\mathrm{L}), \tag{C.4}$$

where ψ and $\bar\psi$ are anti-commuting Grassmann variables and should be considered as independent.

C.2 Fierz Transformations

Defining $O_{\rm S} = \mathbf{1}_d$, $O_{\rm V} = \gamma_\mu$, $O_{\rm T} = \frac{1}{\sqrt{2}}\sigma_{\mu\nu}$, $O_{\rm A} = \gamma_\mu\gamma_5$ and $O_{\rm P} = \sigma_5$ we obtain the following Fierz identities,

$$(\bar\psi_a O_{\rm X}\psi_b)(\bar\psi_c O_{\rm X}\psi_d) = \sum_{\rm Y} C_{\rm XY}(\bar\psi_a O_{\rm Y}\psi_d)(\bar\psi_c O_{\rm Y}\psi_b), \tag{C.5}$$

where X,Y = S,V,T,A,P and

$$C_{\rm XY} = \frac{1}{4}\begin{pmatrix} -1 & -1 & -1 & 1 & -1 \\ -4 & 2 & 0 & 2 & 4 \\ -6 & 0 & 2 & 0 & -6 \\ 4 & 2 & 0 & 2 & -4 \\ -1 & 1 & -1 & -1 & -1 \end{pmatrix}. \tag{C.6}$$

In Subsec. 4.6.1 we study a NJL model at finite temperature and density with only one fermionic species. In this special case, the combination $(\bar\psi O_{\rm V}\psi)^2 + (\bar\psi O_{\rm A}\psi)^2$ is invariant under Fierz-transformations. Due to the relation

$$(\bar\psi O_{\rm V}\psi)^2 - (\bar\psi O_{\rm A}\psi)^2 + 2[(\bar\psi O_{\rm S}\psi)^2 - (\bar\psi O_{\rm P}\psi)] = 0\,, \tag{C.7}$$

we can transform the combination $(\bar\psi O_{\rm V}\psi)^2 - (\bar\psi O_{\rm A}\psi)^2$ completely into scalar and pseudoscalar channels.

Considering the case of several flavors and colors, the Fierz transformations turn singlets into non-singlets and vice versa. This can be used to reduce the number of possible couplings. In Subsec. 4.6.2, we study a truncation of the effective action which includes four four-fermion couplings and which is invariant under $SU(N_c)$ gauge and $SU(N_f)_L \times SU(N_f)_R$ chiral transformations. We have pointed out that our choice of the four-fermion couplings represents a complete basis in the sense that any other point-like four-fermion interaction, which is invariant under $SU(N_c)$ gauge and $SU(N_f)_L \times SU(N_f)_R$ chiral-transformations, is reducible in terms of this basis. Let us sketch the line of arguments which allows us to write down an ansatz consisting of only four (independent) four-fermion couplings: We have five Lorentz-invariant structures $O_{\rm S}$, $O_{\rm V}$, $O_{\rm T}$, $O_{\rm A}$ and $O_{\rm P}$. Since $O_{\rm T}$ breaks chiral symmetry for any possible combination of color and flavor indices, we are left with four possible couplings. Moreover, even the four fermion interactions generated by $O_{\rm S}$ and $O_{\rm P}$ separately break the chiral symmetry. However, it is possible to construct a potentially chirally symmetric interaction by combing both interactions in an appropriate way, namely $(\bar\psi O_{\rm S}\psi)(\bar\psi O_{\rm S}\psi) - (\bar\psi O_{\rm P}\psi)(\bar\psi O_{\rm P}\psi)$. Thus, we are left with three possible interactions. Now we have to take into account that each of these remaining couplings can be present in a flavor and color singlet structure as well as in a flavor and color non-singlet structure. This increases the number of couplings by a factor of four. Due to the (Dirac) Fierz identities given above, we can then reduce the number of couplings

by a factor of two. Thus, we are left with six four-fermion couplings. Finally, the constraint, which is given by the $SU(N_f)_L \times SU(N_f)_R$ invariance, reduces the number of (independent) four-fermion couplings to four.

Appendix D

Thermal Moments and Threshold Functions

D.1 Thermal Moments

In this section, we give the definitions of the various auxiliary functions and the *thermal moments* which we have introduced in the derivation of the flow equation of the strong coupling in Sec. (4.5.1). Moreover, we specify the regulator shape functions that we have used throughout Chap. (4). The auxiliary functions f, which are first introduced in Eq. (4.67), are defined as

$$f_T^A(u,v) = 2\sqrt{4\pi}v \sum_{q=-\infty}^{\infty} \int_0^\infty dx\, \mathrm{e}^{-(2\pi v x)^2 u} \cos(2\pi q x)\,, \tag{D.1}$$

$$f_T^\psi(u,v) = 2\sqrt{4\pi}v \sum_{q=-\infty}^{\infty} (-1)^q \int_0^\infty dx\, \mathrm{e}^{-(2\pi v x)^2 u} \cos(2\pi q x)\,, \tag{D.2}$$

$$f^\psi(u) = \frac{1}{2}\frac{1}{u^{e_d}} u \coth(u), \tag{D.3}$$

$$f_1^A(u) = \frac{1}{u^{e_d}}\left(e_d \frac{u}{\sinh u} + 2u \sinh u\right), \tag{D.4}$$

$$f_2^A(u) = \frac{1}{2}\frac{1}{u^{e_d}}\frac{u}{\sinh u}\,, \tag{D.5}$$

$$f_3^A(u) = \frac{1}{u^{e_d}}(1-v)\,, \tag{D.6}$$

$$f_4^A(u,v) = 2\sqrt{4\pi}v \sum_{q=-\infty}^{\infty} \int_0^\infty dx (2\pi v x)^{d-1} \Gamma\big(-e_d, (2\pi v x)^2 u\big) \cos(2\pi q x). \tag{D.7}$$

Here, the sum over q arises from the application of Poisson's Formula to the (usual) sum over Matsubara modes. These functions are needed for the construction of the *thermal moments* $\bar{h}_j^\psi$ $\bar{h}_j^A$, $\bar{g}_j^A$, $\bar{H}_j^A$ and $\bar{G}_j^A$ which carry the regulator dependence of the

flow equation of the strong coupling via Eqs. (2.55), (2.59), (2.60), (2.69), (2.70) and which are given by

$$\bar{h}_j^{\psi} := \bar{h}_j^{\psi}\big(\tilde{m}, v\big) = \int_0^{\infty} ds\, \widetilde{h}^{\psi}(s, \tilde{m}) s^j f_T^{\psi}\big(s, v\big)\,, \tag{D.8}$$

$$\bar{h}_j^{A} := \bar{h}_j^{A}\big(v\big) = \int_0^{\infty} ds\, \widetilde{h}(s) s^j f_T^{A}\big(s, v\big)\,, \tag{D.9}$$

$$\bar{g}_j^{A} := \bar{g}_j^{A}\big(v\big) = \int_0^{\infty} ds\, \widetilde{g}(s) s^j f_T^{A}\big(s, v\big)\,, \tag{D.10}$$

$$\bar{H}_j^{A} := \bar{H}_j^{A}\big(v\big) = \int_0^{\infty} ds\, \widetilde{h}(s) s^j f_4^{A}\big(s, v\big)\,, \tag{D.11}$$

$$\bar{G}_j^{A} := \bar{G}_j^{A}\big(v\big) = \int_0^{\infty} ds\, \widetilde{g}(s) s^j f_4^{A}\big(s, v\big)\,, \tag{D.12}$$

where $\tilde{m}$ denotes a dimensionless quark mass parameter. It is also possible to express the thermal moments in momentum space with the aid of the regulator functions $h(y)$ and $g(y)$, which are defined in Eq. (2.55). In order to obtain the representations for $\bar{h}_j^{A/\psi}$ and $\bar{g}_j^{A}$, we introduce

$$\frac{s^{b+1}}{\Gamma(b+1)} \int_0^{\infty} du\, u^b \mathrm{e}^{-su} = 1 \qquad (b > -1) \tag{D.13}$$

in Eqs. (D.9), (D.10) and (D.8) and use Eq. (D.1) and (D.2), respectively:

$$\bar{h}_j^{\psi} = \frac{2}{\Gamma(b+1)\sqrt{\pi}} \sum_{q=-\infty}^{\infty} (-1)^q \int_0^{\infty} dx\, \cos\Big(q\frac{x}{v}\Big)\Big(-\frac{d}{dy}\Big)^{j+b+1} \int_0^{\infty} du\, u^b h^{\psi}(y{+}u{+}x^2, \tilde{m})\Big|_{y=0}\,, \tag{D.14}$$

$$\bar{h}_j^{A} = \frac{2}{\Gamma(b+1)\sqrt{\pi}} \sum_{q=-\infty}^{\infty} \int_0^{\infty} dx\, \cos\Big(q\frac{x}{v}\Big)\Big(-\frac{d}{dy}\Big)^{j+b+1} \int_0^{\infty} du\, u^b h(y{+}u{+}x^2)\Big|_{y=0}\,, \tag{D.15}$$

$$\bar{g}_j^{A} = \frac{2}{\Gamma(b+1)\sqrt{\pi}} \sum_{q=-\infty}^{\infty} \int_0^{\infty} dx\, \cos\Big(q\frac{x}{v}\Big)\Big(-\frac{d}{dy}\Big)^{j+b+1} \int_0^{\infty} du\, u^b g(y{+}u{+}x^2)\Big|_{y=0}\,. \tag{D.16}$$

Note that b is an arbritrary parameter which can, e.g., be used to avoid fractional derivatives. By applying Poisson's formula to the (usual) Matsubara sum, we have obtained the sum over q which has good convergence properties for $k \gtrsim T$. Moreover, we use the moments $\bar{H}_j^{A}$ and $\bar{G}_j^{A}$ for $j = 0$ in App. G.3 where we give a detailed derivation of the anomalous dimensions of the strong coupling. Integrating Eq. (D.11) and (D.12) by parts and using Eq. (D.7) and (D.13), we obtain

$$\bar{H}_0^{A} = \frac{2}{\Gamma(b+1)\sqrt{\pi}} \sum_{q=-\infty}^{\infty} \int_0^{\infty} dx\, \cos\Big(q\frac{x}{v}\Big)\, \Big(-\frac{d}{dy}\Big)^{b-e_d} \int_0^{\infty} du\, \frac{u^b}{u+x^2} h(y{+}u{+}x^2)\Big|_{y=0}\,, \tag{D.17}$$

$$\bar{G}_0^A = \frac{2}{\Gamma(b+1)\sqrt{\pi}} \sum_{q=-\infty}^{\infty} \int_0^\infty dx\, \cos\left(q\frac{x}{v}\right) \left(-\frac{d}{dy}\right)^{b-e_d} \int_0^\infty du\, \frac{u^b}{u+x^2} g(y+u+x^2)\Big|_{y=0} . \tag{D.18}$$

Throughout Chap. (4) we use the exponential regulator. For the gluon and ghost fields, this regulator is given by

$$R_k(\Delta) = \Delta\, r\left(\tfrac{\Delta}{k^2}\right) \quad \text{with} \quad r(y) = \frac{1}{\mathrm{e}^y - 1}\,, \tag{D.19}$$

and the functions $h(y)$ and $g(y)$ read [71]

$$h(y) = \frac{y}{\mathrm{e}^y - 1} \quad \text{and} \quad g(y) = \mathrm{e}^{-y}\,. \tag{D.20}$$

For the fermionic fields, the exponential regulator reads

$$R_k^\psi(\mathrm{i}\bar{\not{p}}) = \mathrm{i}\bar{\not{p}}\, r_\psi\left(\tfrac{(\mathrm{i}\bar{\not{p}})^2}{k^2}\right) \quad \text{with} \quad r_\psi(y) = \frac{1}{\sqrt{1-\mathrm{e}^{-y}}} - 1\,, \tag{D.21}$$

and the functions $h^\psi(y, \frac{m}{k})$ and $g^\psi(y, \frac{m}{k})$ are given by

$$h^\psi(y,\tilde{m}) = \frac{y^2}{(\mathrm{e}^y-1)(y+\tilde{m}^2(1-\mathrm{e}^{-y}))} \quad \text{and} \quad g^\psi(y,\tilde{m}) = \frac{y(1-\mathrm{e}^{-y})(1-\sqrt{1-\mathrm{e}^{-y}})}{y+\tilde{m}^2(1-\mathrm{e}^{-y})}\,. \tag{D.22}$$

The thermal moments used in this work are now completely determined by inserting Eqs. (D.20) and (D.22) into Eqs. (D.14)-(D.18).

D.2 Threshold Functions for the Functional RG

In Subsecs. 4.6.1 and 4.6.2, the regulator dependence of the flow equations of the four-fermion interactions is controlled by (dimensionless) threshold functions which arise from Feynman graphs, incorporating fermionic and/or bosonic fields. Let us first introduce the so-called dimensionless regularized bosonic (p_B) and fermionic (p_ψ) momenta, which carry the information on the corresponding regulator shape-function [59]:

$$r_\psi(y_\psi) = \sqrt{\frac{p_\psi(y_\psi)}{y_\psi}} - 1 \qquad \text{and} \qquad r(y_B) = \frac{p_B(y_B)}{y_B} - 1\,. \tag{D.23}$$

Here, y_B and y_ψ are dimensionless quantities. It is convenient to define the following fermionic (ψ) and bosonic (B) kernels:

$$\mathcal{P}_1^\psi(\tilde{y}_\psi, w) = \frac{1+r_\psi(\tilde{y}_B)}{p_\psi(\tilde{y}_\psi)+w}\,, \qquad \mathcal{P}_2^\psi(\tilde{y}_\psi, w) = \tilde{\partial}_t\, \mathcal{P}_1^\psi(\tilde{y}_\psi, w)\,, \tag{D.24}$$

$$\mathcal{P}_1^B(\tilde{y}_B, w) = \frac{1}{p_B(\tilde{y}_B)+w}\,, \qquad \mathcal{P}_2^B(\tilde{y}_B, w) = -2\left(p_B(\tilde{y}_B) - \tilde{y}_B\, \frac{\partial p_B(\tilde{y}_B)}{\partial \tilde{y}_B}\right), \tag{D.25}$$

where the dimensionless momenta $\tilde{y}_\psi^{(\pm)} = (\tilde{\nu}_n \pm \mathrm{i}\tilde{\mu})^2 + y$ and $\tilde{y}_B = \tilde{\omega}_n^2 + y$ depend on the dimensionless fermionic Matsubara frequency $\tilde{\nu}_n = (2n+1)\pi\tilde{t}$ and the dimensionless bosonic Matsubara frequency $\tilde{\omega}_n = (2n+1)\pi\tilde{t}$, respectively. Additionally, y_ψ depends on the dimensionless fermionic chemical potential $\tilde{\mu} = \mu/k$. The Matsubara frequencies are related to the temperature T and the regulator scale k through $\tilde{t} = T/k$. The dimensionless quantity w is related to a mass m of the fermions and bosons via $w = (\frac{m}{k})^2$, respectively. The formal derivative $\tilde{\partial}_t$ acts[1] only on the k-dependence of the regulator function r_ψ.

The purely fermionic threshold functions are defined by

$$L_{1,1}^{(F),d}\left(\tilde{t}, w, \tilde{\mu}\right) = -\frac{\tilde{t}}{2} \sum_{n=-\infty}^{\infty} \int_0^\infty dy\, y^{\frac{d-1}{2}} \Big[\mathcal{P}_1^\psi\left(\tilde{y}_\psi^{(+)}, w\right) \mathcal{P}_2^\psi\left(\tilde{y}_\psi^{(-)}, w\right) + \mathcal{P}_2^\psi\left(\tilde{y}_\psi^{(+)}, w\right) \mathcal{P}_1^\psi\left(\tilde{y}_\psi^{(-)}, w\right) \Big] . \quad \text{(D.26)}$$

For example, one have to deal with this threshold function if one only takes the term proportional to $\delta_{\mu\nu}$ in the decompositions Eqns. (I.11)-(I.14) into account. Although we have not used them in this work, we give also the purely fermionic threshold functions which arise due to terms proportional to m^2, μ^2 and $p_0^2 = \nu_n^2$ in the decompositions Eqns. (I.11)-(I.14), see also Eqns. (4.88) and (4.89). The threshold function that arises due to the terms proporional to m^2 or μ^2 is defined as

$$M_{1,1}^{(F),d}\left(\tilde{t}, w, \tilde{\mu}\right) = -\frac{\tilde{t}}{2} \sum_{n=-\infty}^{\infty} \int_0^\infty dy\, y^{\frac{d-3}{2}} \Big[\mathcal{P}_1^\psi\left(\tilde{y}_\psi^{(+)}, w\right) \mathcal{P}_2^\psi\left(\tilde{y}_\psi^{(-)}, w\right) + \mathcal{P}_2^\psi\left(\tilde{y}_\psi^{(+)}, w\right) \mathcal{P}_1^\psi\left(\tilde{y}_\psi^{(-)}, w\right) \Big] . \quad \text{(D.27)}$$

Finally, we find a threshold function due to the terms proportions to $p_0^2 = \nu_n^2$ in the decomposition. It is given by

$$N_{1,1}^{(F),d}\left(\tilde{t}, w, \tilde{\mu}\right) = -\frac{\tilde{t}}{2} \sum_{n=-\infty}^{\infty} \tilde{\nu}_n^2 \int_0^\infty dy\, y^{\frac{d-3}{2}} \Big[\mathcal{P}_1^\psi\left(\tilde{y}_\psi^{(+)}, w\right) \mathcal{P}_2^\psi\left(\tilde{y}_\psi^{(-)}, w\right) + \mathcal{P}_2^\psi\left(\tilde{y}_\psi^{(+)}, w\right) \mathcal{P}_1^\psi\left(\tilde{y}_\psi^{(-)}, w\right) \Big] . \quad \text{(D.28)}$$

For $w = 0$, $\tilde{\mu} = 0$ and $\tilde{t} = 0$, the fermionic threshold functions $L_{1,1}^{(F)}(0,0,0)$, $M_{1,1}^{(F)}(0,0,0)$ and $N_{1,1}^{(F)}(0,0,0)$ reduce to real numbers. For example, using the exponential regulator Eq. (D.21), we find

$$L_{1,1}^{(F),4}(0,0,0) = \frac{3}{16} = \frac{3v_4}{4v_3}\, l_1^{(F),4}(0,0)\,, \quad \text{(D.29)}$$

[1] This is a derivative with respect to $t = \ln(k/\Lambda)$, not to be confused with the dimensionless quantity $\tilde{t} = T/k$.

in $d=4$ dimensions. Here, $l_1^{(F),4}$ denotes the standard threshold functions which are defined in Ref. [59]. The factor v_d^{-1} is proportional to the volume of the d dimensional unit ball:

$$v_d^{-1} = 2^{d+1}\pi^{\frac{d}{2}}\Gamma\left(\frac{d}{2}\right) . \tag{D.30}$$

Note that a simple relation, such as Eq. (D.29), between $l_1^{(F),4}$ and $L_{1,1}^{(F),4}$ exists only in the limit $w \to 0$, $\tilde{\mu} \to 0$ and $\tilde{t} \to 0$. For any finite value of either w, $\tilde{\mu}$ or $\tilde{t}$, a simple relation between $l_1^{(F),4}$ and $L_{1,1}^{(F),4}$ does not exist.

Let us now turn to the discussion of the threshold functions $L_{1,1,n}^{(FB),d}(\tilde{t}, w_1, \tilde{\mu}, w_2)$, $M_{1,1,n}^{(FB),d}(\tilde{t}, w_1, \tilde{\mu}, w_2)$ and $N_{1,1,n}^{(FB),d}(\tilde{t}, w_1, \tilde{\mu}, w_2)$ which ultimately arise from 1PI graphs with two fermionic internal lines and n bosonic internal lines. According to the purely fermionic case, we define the threshold functions $L_{1,1,n}^{(FB),d}$, $M_{1,1,n}^{(FB),d}$ and $N_{1,1,n}^{(FB),d}$:

$$\begin{aligned}
&L_{1,1,n}^{(FB),d}\left(\tilde{t}, w_1, \tilde{\mu}, w_2\right) = \\
&\quad -\frac{\tilde{t}}{2}\sum_{n=-\infty}^{\infty}\int_0^\infty dy\, y^{\frac{d-1}{2}}\Big[\mathcal{P}_1^\psi\left(\tilde{y}_\psi^{(+)}, w_1\right)\mathcal{P}_2^\psi\left(\tilde{y}_\psi^{(-)}, w_1\right)\left(\mathcal{P}_1^B\left(\tilde{y}_B, w_2\right)\right)^n \\
&\qquad\qquad +\mathcal{P}_2^\psi\left(\tilde{y}_\psi^{(+)}, w_1\right)\mathcal{P}_1^\psi\left(\tilde{y}_\psi^{(-)}, w_1\right)\left(\mathcal{P}_1^B\left(\tilde{y}_B, w_2\right)\right)^n \\
&\qquad -n\,\mathcal{P}_1^\psi\left(\tilde{y}_\psi^{(+)}, w_1\right)\mathcal{P}_1^\psi\left(\tilde{y}_\psi^{(-)}, w_1\right)\left(\mathcal{P}_1^B\left(\tilde{y}_B, w_2\right)\right)^{n+1}\mathcal{P}_2^B\left(\tilde{y}_B, w_2\right)\Big] .
\end{aligned} \tag{D.31}$$

$$\begin{aligned}
&M_{1,1,n}^{(FB),d}\left(\tilde{t}, w_1, \tilde{\mu}, w_2\right) = \\
&\quad -\frac{\tilde{t}}{2}\sum_{n=-\infty}^{\infty}\int_0^\infty dy\, y^{\frac{d-3}{2}}\Big[\mathcal{P}_1^\psi\left(\tilde{y}_\psi^{(+)}, w_1\right)\mathcal{P}_2^\psi\left(\tilde{y}_\psi^{(-)}, w_1\right)\left(\mathcal{P}_1^B\left(\tilde{y}_B, w_2\right)\right)^n \\
&\qquad\qquad +\mathcal{P}_2^\psi\left(\tilde{y}_\psi^{(+)}, w_1\right)\mathcal{P}_1^\psi\left(\tilde{y}_\psi^{(-)}, w_1\right)\left(\mathcal{P}_1^B\left(\tilde{y}_B, w_2\right)\right)^n \\
&\qquad -n\,\mathcal{P}_1^\psi\left(\tilde{y}_\psi^{(+)}, w_1\right)\mathcal{P}_1^\psi\left(\tilde{y}_\psi^{(-)}, w_1\right)\left(\mathcal{P}_1^B\left(\tilde{y}_B, w_2\right)\right)^{n+1}\mathcal{P}_2^B\left(\tilde{y}_B, w_2\right)\Big] .
\end{aligned} \tag{D.32}$$

$$\begin{aligned}
&N_{1,1,n}^{(FB),d}\left(\tilde{t}, w_1, \tilde{\mu}, w_2\right) = \\
&\quad -\frac{\tilde{t}}{2}\sum_{n=-\infty}^{\infty}\tilde{\nu}_n^2\int_0^\infty dy\, y^{\frac{d-3}{2}}\Big[\mathcal{P}_1^\psi\left(\tilde{y}_\psi^{(+)}, w_1\right)\mathcal{P}_2^\psi\left(\tilde{y}_\psi^{(-)}, w_1\right)\left(\mathcal{P}_1^B\left(\tilde{y}_B, w_2\right)\right)^n \\
&\qquad\qquad +\mathcal{P}_2^\psi\left(\tilde{y}_\psi^{(+)}, w_1\right)\mathcal{P}_1^\psi\left(\tilde{y}_\psi^{(-)}, w_1\right)\left(\mathcal{P}_1^B\left(\tilde{y}_B, w_2\right)\right)^n \\
&\qquad -n\,\mathcal{P}_1^\psi\left(\tilde{y}_\psi^{(+)}, w_1\right)\mathcal{P}_1^\psi\left(\tilde{y}_\psi^{(-)}, w_1\right)\left(\mathcal{P}_1^B\left(\tilde{y}_B, w_2\right)\right)^{n+1}\mathcal{P}_2^B\left(\tilde{y}_B, w_2\right)\Big] .
\end{aligned} \tag{D.33}$$

For $w_1 = w_2 = 0$, $\tilde{\mu} = 0$ and $\tilde{t} = 0$, these functions reduce to simple numbers. Using the exponential regulator, we find the following values for the threshold functions $L_{1,1,1}^{(FB),4}$

and $L^{(FB),4}_{1,1,2}$ in $d=4$ dimensions:

$$L^{(FB),4}_{1,1,1}(0,0,0,0) = \frac{3}{16} = \frac{3v_4}{4v_3}\, l^{(FB),4}_{1,1}(0,0,0) \tag{D.34}$$

$$L^{(FB),4}_{1,1,2}(0,0,0,0) = \frac{9}{16}\ln(\tfrac{4}{3}) = \frac{3v_4}{4v_3}\, l^{(FB),4}_{1,2}(0,0,0)\,. \tag{D.35}$$

The standard threshold functions $l^{(FB),4}_{1,1}$ and $l^{(FB),4}_{1,2}$ denote the standard threshold functions which are defined in Ref. [59]. Again, there exists no relation between the functions $L^{(FB),4}_{1,1,n}$ and $l^{(F),4}_{1,n}$ for finite value of w_1, w_2, $\tilde{\mu}$ or $\tilde{t}$.

For $\tilde{t} \to \infty$ or $w_i \to \infty$, the threshold functions $L^{(F),d}_{1,1}$ and $L^{(FB),d}_{1,1,n}$ approach zero. For finite $\tilde{t}$, w_i and $\tilde{mu}$, the threshold functions can easily be evaluated numerically.

D.3 Threshold Functions for the Proper-Time RG

In Sec. 3.4.2, we have introduced the following auxiliary (dimensionless) functions for the fermionic (F) and bosonic (B) degrees of freedom:

$$\Theta^{(F)}_{ap}(a,\omega,t) = \int_0^\infty ds\, s^a \mathrm{e}^{-\frac{s\omega}{4\pi}} \vartheta_{ap}(st^2)\Big(\vartheta_{ap}(s)\Big)^3, \tag{D.36}$$

$$\Theta^{(F)}_{p}(a,\omega,t) = \int_0^\infty ds\, s^a \mathrm{e}^{-\frac{s\omega}{4\pi}} \vartheta_{ap}(st^2)\Big(\vartheta_{p}(s)\Big)^3, \tag{D.37}$$

$$\Theta^{(B)}_{p}(a,\omega,t) = \int_0^\infty ds\, s^a \mathrm{e}^{-\frac{s\omega}{4\pi}} \vartheta_{p}(st^2)\Big(\vartheta_{p}(s)\Big)^3. \tag{D.38}$$

Here, ϑ_p and ϑ_{ap} are Jacobi-Elliptic-Theta functions defined as [203]

$$\vartheta_{ap}(x) = \sum_{n=-\infty}^{\infty} \mathrm{e}^{-x\pi(n+\frac{1}{2})^2} = x^{-\frac{1}{2}} + 2\sum_{q=1}^{\infty}(-1)^q x^{-\frac{1}{2}} \mathrm{e}^{-\frac{\pi q^2}{x}}\,, \tag{D.39}$$

$$\vartheta_{p}(x) = \sum_{n=-\infty}^{\infty} \mathrm{e}^{-x\pi n^2} = x^{-\frac{1}{2}} + 2\sum_{q=1}^{\infty} x^{-\frac{1}{2}} \mathrm{e}^{-\frac{\pi q^2}{x}}\,. \tag{D.40}$$

Note that the representation of the flow equation (3.17) in terms of these functions accelerates the numerical calculations by a factor of about a hundred, compared to the representation used in Refs. [84, 85]. The first representation in Eq. (D.39) and (D.40) is the standard Matsubara summation of the momenta for anti-periodic (ap) boundary conditions and periodic (ap) boundary conditions, respectively. The second representation on the right hand side in Eq. (D.39) and (D.40) is obtained by applying Poisson's formula to the first representation. One can use this representation to separate the zero-temperature and/or infinite-volume contributions of the flow equation. For illustration, we discuss how the flow equation for the meson potential (3.18) in infinite

volume at zero temperature can be derived from the corresponding finite-volume flow equation (3.17). Using the approximation $\vartheta_{ap}(s) = \vartheta_p(s) \approx s^{-\frac{1}{2}}$ in Eqs. (D.36), (D.37), and (D.38), we obtain the threshold functions at zero-temperature and infinite-volume:

$$\Theta^{(F)}_{ap}(a,\omega,t) = \Theta^{(F)}_{p}(a,\omega,t) = \Theta^{(B)}_{p}(a,\omega,t) \approx \frac{1}{t}\frac{\Gamma(a-1)}{\omega^{a-1}}\,. \tag{D.41}$$

Indeed, inserting this in Eq. (3.17), we obtain the flow equation (3.18) for infinite volume and zero temperature.

Appendix E

Implementation of Explicit Symmetry Breaking

We show that our postulated ansatz (3.24) for the meson potential is sufficient to capture all contributions in the RG flow which arise due to the explicit symmetry breaking through the current quark mass m_c. For convenience, we consider the infinite-volume flow equation (3.18) of the meson potential with the cutoff-function parameter $a = 2$. However, the generalization of our considerations to the flow equation for finite volumes and/or other values of a is straightforward. Neglecting the mesonic contributions to the flow equation, we are left with the terms arising from the fermions:

$$k\frac{\partial}{\partial k}U_k^F(\sigma,\vec{\pi}^2) \;=\; -\frac{N_c}{4\pi^2}\frac{k^6}{k^2+M_q^2}\,, \tag{E.1}$$

where N_c gives the number of colors. The only source of explicitly symmetry breaking in the flow equation is contained in the constituent quark mass M_q through its dependence on the current quark mass m_c. By expanding around the minimum of the potential, we have shown in Eq. (3.23) that the quark mass can be written as

$$M_q^2 \;=\; g^2[(\sigma_0+m_c)^2+2m_c(\sigma-\sigma_0)+(\sigma^2+\vec{\pi}^2-\sigma_0^2)]\,. \tag{E.2}$$

Note that we have rescaled m_c by a factor of g for convenience. When we expand the denominator in the flow equation (E.1) in the deviation of the fields from the vacuum expectation value, the result contains only those terms which we postulated in our

ansatz for the potential:

$$
\begin{aligned}
k\frac{\partial}{\partial k}U_k^F(\sigma,\vec{\pi}^2) \;=\; & -\frac{1}{4\pi^2}N_c\frac{k^6}{k^2+g^2(\sigma_0+m_c)^2}\times \\
& \times\Bigg\{(\sigma^2+\vec{\pi}^2-\sigma_0^2)\;\left[-\frac{g^2}{k^2+g^2(\sigma_0+m_c)^2}\right] \\
& +(\sigma^2+\vec{\pi}^2-\sigma_0^2)^2\left[\left(\frac{g^2}{k^2+g^2(\sigma_0+m_c)^2}\right)^2\right] \\
& +(\sigma-\sigma_0)\;\left[-2m_c\left(\frac{g^2}{k^2+g^2(\sigma_0+m_c)^2}\right)\right] \\
& +(\sigma-\sigma_0)^2\left[4m_c^2\left(\frac{g^2}{k^2+g^2(\sigma_0+m_c)^2}\right)^2\right] \\
& +(\sigma-\sigma_0)(\sigma^2+\vec{\pi}^2-\sigma_0^2)\;2\;\left[-2m_c\left(\frac{g^2}{k^2+g^2(\sigma_0+m_c)^2}\right)^2\right] \\
& +\ldots\Bigg\}. \qquad \text{(E.3)}
\end{aligned}
$$

All remaining terms are of higher order in $(\sigma-\sigma_0)$ or $(\sigma^2+\vec{\pi}^2-\sigma_0^2)$ or any combination thereof. In the chiral limit, $m_c \to 0$, we find that the only terms, which remain in the expansion, contain solely powers of $(\sigma^2+\vec{\pi}^2-\sigma_0^2)=(\phi^2-\sigma_0^2)$; all other terms vanish. Thus the potential reduces to the standard form in this limit.

Appendix F

One-Loop Calculation of the Meson Masses

In Subsec. 3.6.2, we have computed the meson masses in finite volume as a function of the temperature. In order to gain a better understanding of the slope of the meson masses in the symmetric phase as a function of the temperature, we have compared the results obtained from the RG flow equation of the meson potential (3.17) to the one-loop result for the masses of the scalar fields in an $O(4)$-model. In this appendix, we discuss the details of the one-loop calculation.

We have given the simplest, non-trivial truncation for the effective action of an $O(4)$-model in Eq. (3.44). Let us generalize our considerations to an $O(N)$-model with the effective action

$$\Gamma[\phi] = \int d^4x \left\{ \frac{1}{2}(\partial_\mu \phi)^2 + \frac{1}{2} m^2 \phi^2 + \frac{\lambda}{4}\phi^4 \right\}, \tag{F.1}$$

where, in contrast to the effective action (3.44), ϕ is now an N dimensional vector in field space. In order to compute the finite-temperature and finite-volume corrections to the masses of this model in one-loop approximation, it is convenient to use the RG flow equations which we have already derived in Subsec. 3.4.2. Indeed, the RG flow equation for the potential of an $O(N)$-model in a finite volume can be straightforwardly deduced from Eq. (3.17) by neglecting the quark contributions and by taking into account that we have now $N-1$ Goldstone modes and one radial mode:

$$k\frac{\partial}{\partial k} U_k(\phi^2, T, L) = \frac{T}{L^3} \frac{(kL)^{2(a+1)}}{(4\pi)^{a+1}\Gamma(a+1)} \sum_{j=1}^{N} \Theta_p^{(B)}\left(a, (k^2 + M_j^2(\phi^2))L^2, TL\right). \tag{F.2}$$

Here L denotes the length of the 3-dimensional box in space directions, and L_t denotes the length of the box in the Euclidean time direction. Recall that the extent of the Euclidean time direction L_t and the temperature T are related by $L_t = 1/T$. The threshold function $\Theta_p^{(B)}$ is defined and discussed in App. D.3. The masses of the radial

mode and the Goldstone modes are given by $M_1^2(\phi) = m^2 + 3\lambda\phi^2$ and $M_j^2(\phi) = m^2 + \lambda\phi^2$ for $j = 2, ..., N$, respectively. Since we are only interested in the behavior of the meson masses above the phase transition temperature, we can assume that the masses depend only on ϕ^2. In an accurate RG study of the $O(N)$-model in a finite volume [200], it is indispensable to allow for an explicit symmetry breaking, in a similar way as in our RG study of the quark-meson model in finite volume in Chap. 3.

In order to calculate the masses of the scalar fields, we make use of the fact that the threshold function $\Theta_p^{(B)}$ is defined in terms of integrals over Jacobi-Elliptic-Theta functions, see App. D.3. This allows us to isolate the divergent part of the effective potential in the limit $\Lambda \to \infty$, which is contained in the infinite volume contribution. Writing the threshold function $\Theta_p^{(B)}$ in terms of the second representation of the Jacobi-Elliptic-Theta function in Eq. (D.40), we can divide the flow equation for the effective potential in three contributions,

$$k\frac{\partial U^{1\mathrm{L}}}{\partial k} = k\frac{\partial U_\infty^{1\mathrm{L}}(T\to 0, L\to\infty)}{\partial k} + k\frac{\partial U_1^{1\mathrm{L}}(T, L\to\infty)}{\partial k} + k\frac{\partial U_2^{1\mathrm{L}}(T, L)}{\partial k}\,. \tag{F.3}$$

The effective potential in one-loop approximation $U^{1\mathrm{L}}$ can be extracted from the flow equation (F.2), when we omit a possible dependence of the masses M_i on the regulator scale k. The potential is then obtained by a straightforward integration of the flow equation (F.2) from the UV cutoff scale $k = \Lambda$ to $k = 0$. The first term on the RHS of Eq. (F.3) is divergent in the limit $\Lambda \to \infty$, whereas the other terms remain finite in this limit. In the following, we do not consider the contributions from the divergent part $U_\infty^{1\mathrm{L}}$, since we are only interested in the finite-temperature and finite-volume corrections to the mass.

Let us start with the calculation of the mass correction due to the volume-independent contribution $U_1^{1\mathrm{L}}(T) = U_1^{1\mathrm{L}}(T, L\to\infty)$. The integration of the corresponding term in Eq. (F.3) from $k = \Lambda \to \infty$ to $k = 0$ yields

$$U_1^{1\mathrm{L}}(T) = -\frac{1}{(4\pi)^2}\sum_{j=1}^{N}\sum_{q=1}^{\infty}\int_0^\infty \frac{ds}{s^3}\exp\Big(-\frac{q^2}{4sT^2} - sM_j^2(\phi^2)\Big)\,. \tag{F.4}$$

Note that the expression is independent of the parameter a which specifies the cutoff function. In order to calculate the mass correction in the symmetric phase, we have to take the second derivative of $U_1^{1\mathrm{L}}(T)$ with respect to the field ϕ and evaluate the resulting expression at $\phi = 0$:

$$\delta m_1^2(T) = \frac{\partial^2}{\partial\phi^2}U_1^{1\mathrm{L}}(T)\bigg|_{\phi=0} = \frac{2(N+2)\lambda}{(2\pi)^2}mT\sum_{q=1}^{\infty}\frac{1}{q}K_1\Big(\frac{qm}{T}\Big)\,. \tag{F.5}$$

Here we have used the integral representation of the modified Bessel functions [203]:

$$2\Big(\frac{x}{2}\Big)^\nu K_\nu(x) = \int_0^\infty ds s^{\nu-1}\mathrm{e}^{-s-\frac{x^2}{4s}}\,. \tag{F.6}$$

For $T \gg m$, we use

$$K_1(x) \approx \frac{1}{x} \quad (x \ll 1)\,, \tag{F.7}$$

and obtain the simple expression

$$\delta m_1^2(T) \approx \frac{(N+2)\lambda}{12}\, T^2 \tag{F.8}$$

for the correction $\delta m_1^2(T)$, which agrees with the result found in Ref. [29].

Now we turn to the calculation of the mass correction due to the contribution $U_2^{1\mathrm{L}}(T,L)$. For our purposes in Subsec. 3.6.2, it is convenient to use the Poisson-representation for the spatial contributions and the usual Matsubara sum for the thermal contribution. Performing the integration from $k=\Lambda$ to $k=0$ in Eq. (F.3), the contribution from $U_2^{1\mathrm{L}}(T,L)$ to the potential in the limit $\Lambda \to \infty$ reads

$$U_2^{1\mathrm{L}}(T,L) = -\frac{T}{2(4\pi)^{\frac{3}{2}}} \sum_{j=1}^{N} \sum_{n=-\infty}^{\infty} {\sum_{\{l_i\}}}' \int_0^\infty \frac{ds}{s^{\frac{5}{2}}} \exp\Big(- s(M_j^2(\phi^2) + 4\pi^2 n^2 T^2) - \frac{\vec{l}^{\,2} L^2}{4s} \Big)\,. \tag{F.9}$$

The vector $\vec{l}$ is defined as $\vec{l} = \{l_1, l_2, l_3\}$, and the prime indicates that the term with $\vec{l} = 0$, corresponding to the infinite-volume contribution, is excluded from the summation. The sum over n runs over the thermal Matsubara modes. We point out that $U_2^{1\mathrm{L}}$ is independent of the cutoff-function parameter a. Taking the second derivative with respect to the fields ϕ and evaluating at $\phi = 0$, we obtain the corresponding mass correction

$$\begin{aligned} &\delta m_2^2(T,L) \\ &= \frac{(N+2)\lambda T L^{-\frac{1}{2}}}{(2\pi)^{\frac{3}{2}}} \sum_{n=-\infty}^{\infty} {\sum_{\{l_i\}}}' \left(\frac{m^2 + 4\pi^2 n^2 T^2}{\vec{l}^{\,2}} \right)^{\frac{1}{4}} K_{\frac{1}{2}} \Big(\sqrt{\vec{l}^{\,2}((mL)^2 + 4\pi^2 n^2 (TL)^2)} \Big)\,. \end{aligned} \tag{F.10}$$

We used again the integral representation of the modified Bessel functions Eq. (F.6). Finally, we show that this contribution becomes proportional to the temperature T for $TL \gg 1$. Using the asymptotic expansion of the Bessel-functions for large arguments, which is given by

$$K_\nu(x) \approx \sqrt{\frac{\pi}{x}} \mathrm{e}^{-x} \quad (x \gg 1)\,, \tag{F.11}$$

the mass correction $\delta m_2^2(T,L)$ for $TL \gg 1$ reads

$$\delta m_2^2(T,L) \approx \frac{3(N+2)\lambda}{2\sqrt{2}\pi} \frac{T}{L} \sum_{n=-\infty}^{\infty} {\sum_{\{l_i\}}}' \frac{1}{\sqrt{\vec{l}^{\,2}}} \exp\left(-\sqrt{\vec{l}^{\,2}\left((mL)^2 + 4\pi^2 n^2 (TL)^2\right)} \right). \tag{F.12}$$

From this, we find that the contributions from the non-vanishing thermal Matsubara-modes drop exponentially in the limit $TL \to \infty$, whereas the contribution from the zeroth thermal Matsubara-mode ($n = 0$) remains finite and is proportional to the temperature T. For $TL \gg 1$, the mass-correction $\delta m_2^2(T, L)$ is thus sub-leading, compared to the contribution $\delta m_1^2(T)$.

Appendix G

Computation of the Coupling Flow

We summarize details of the computation of the flow equation for the running QCD coupling. In App. G.1, we discuss the decomposition of the inverse propagator which is obtained from the truncation (4.61), following the strategy of Refs. [72, 74]. In App. G.2, we discuss the expansion of the flow equation (4.67), which ultimately leads to the flow equation for the running QCD coupling. The resummation of the anomalous dimension in App. G.3 is performed along the lines of Ref. [71, 171]. However, we generalize the strategy to arbitrary regulator functions and dimensions as well as to finite temperature.

G.1 Decomposition of the Inverse Propagator

In this part of the appendix, we discuss the decomposition of the second functional derivative of the truncation (4.61) from which we have derived the flow equation (4.67).

The derivation of the flow equation (4.67) is based on the fact that it is sufficient to consider a covariantly constant magnetic background field in order to project the flow equation (4.56) onto the truncation (4.61). A convenient choice for such a covariantly constant color magnetic field is

$$\bar{A}^z_\mu(x) = n^z \mathsf{A}_\mu(x)\,, \qquad \mathsf{F}_{\mu\nu} = \partial_\mu \mathsf{A}_\nu - \partial_\nu \mathsf{A}_\mu = B\epsilon^\perp_{\mu\nu} = \text{const.}\,. \tag{G.1}$$

Here n^z is a constant unit vector in color space, $n^2 = 1$. The "Abelian" gauge field and the corresponding field strength are given by $\mathsf{A}_\mu(x)$ and $\mathsf{F}_{\mu\nu}$, respectively. The antisymmetric tensor $\epsilon^\perp$ specifies the direction of the magnetic field; we choose $\epsilon^\perp_{12} = -\epsilon^\perp_{21} = 1$. Thus our present choice for $\mathsf{A}_\mu(x)$ corresponds to a constant magnetic field B along the 3-direction. In the following we make also the additional assumption that the field strength $F_{\mu\nu}$ is covariantly constant, i. e.

$$[D_\mu[A], F_{\mu\nu}] = 0\,. \tag{G.2}$$

The covariant derivative $D_\mu[A]$ in the adjoint representation is defined in Eq. (4.29). Indeed, the choice Eq. (G.1) obeys the condition (G.2).

For the moment, we neglect the contributions from the quarks in Eq. (4.61) and restrict the discussion to the terms arising due to the gauge fields and the ghosts. Taking the second derivative of the corresponding terms in the truncation (4.61) with respect to the fluctuation field, we obtain

$$\left(\hat{\Gamma}_A^{(1,1,0,0)}[a,\bar{A}]\right)^{yz}_{\mu\nu} = \mathcal{W}_k'(\theta)(\mathcal{D}_T[A]-\mathcal{D}_L[A])^{yz}_{\mu\nu} + \mathcal{W}_k''(\theta)\mathcal{S}^{yz}_{\mu\nu}[A] + \frac{1}{\xi_k}(\mathcal{D}_L[\bar{A}])^{yz}_{\mu\nu}\,, \quad \text{(G.3)}$$

and

$$\left(\hat{\Gamma}_{\text{gh.}}^{(1,1,0,0)}[a,\bar{c},c,\bar{A}]\right)^{yz} = -D[\bar{A}]^{yw}_{\lambda} D[A]^{wz}_{\lambda}\,, \quad \text{(G.4)}$$

where $\bar{g}$ is the (bare) gauge coupling and ξ_k is the gauge-fixing parameter. The fluctuation field a and the field A are related by $A = a + \bar{A}$. The Greek letters denote Lorentz indices, whereas the Roman letters denote color indices[1]. For convenience, we have introduced the operator θ which is connected with the field strength $F_{\mu\nu}$ by

$$\theta = \frac{1}{4}F^z_{\mu\nu}F^{\mu\nu}_z \overset{A=\bar{A}}{=} \frac{1}{2}B^2\,. \quad \text{(G.5)}$$

The various operators in Eq. (G.3) are defined as

$$(\mathcal{D}_T)^{yz}_{\mu\nu} = (-D[A]^{yw}_{\lambda} D[A]^{wz}_{\lambda}\delta_{\mu\nu} - 2\bar{g} f^{yzw} F^w_{\mu\nu})\,, \quad \text{(G.6)}$$

$$(\mathcal{D}_L)^{yz}_{\mu\nu} = -D[A]^{yw}_{\mu} D[A]^{wz}_{\nu}\,, \quad \text{(G.7)}$$

$$\mathcal{S}^{yz}_{\mu\nu} = F^a_{\mu\rho}F^b_{\sigma\nu}D[A]^{ya}_{\rho}D[A]^{bz}_{\sigma}\,. \quad \text{(G.8)}$$

Finally, the primes in Eq. (G.3) denote derivatives with respect to θ. Note that $\hat{\Gamma}_k^{(1,1,0,0)}$ is matrix-valued in field space. Here the operators $\hat{\Gamma}_A^{(1,1,0,0)}$ and $\hat{\Gamma}_{\text{gh.}}^{(1,1,0,0)}$ represent the gluonic and ghost submatrix of $\hat{\Gamma}_A^{(1,1,0,0)}$.

We remind the reader of the fact that the effective action $\hat{\Gamma}_k[0,0,0,\bar{A}=A]$ is a gauge-invariant functional of A from which we can extract $\mathcal{W}_k$. Thus it is sufficient to consider $\hat{\Gamma}_k^{(1,1,0,0)}[0,\bar{A}=A]$ from now on. Following the strategy discussed in Subsec. 2.4.3 and Sec. 4.4, we define $\Gamma_k[A] := \hat{\Gamma}_k[0,0,0,A]$ and identify $\Gamma_k^{(1,1)}[A]$ with $\hat{\Gamma}_k^{(1,1,0,0)}[0,0,0,A=\bar{A}]$. This allows us to use the flow equation (2.61) to compute the flow equation for $\mathcal{W}_k$.

In order to obtain the flow equation for $\mathcal{W}_k$, we have to compute traces over color and Lorentz indices. Let us first discuss the tools which are needed to decompose $\Gamma_k^{(1,1)}[A]$ in such a way that the traces can be computed most easily. Due to the fact that we are considering covariantly constant fields (see Eq. (G.1) and (G.2)), we find that the operators $\mathcal{D}_L$ and $\mathcal{D}_T$ commute. As a consequence, we can introduce the projection operators[2]

$$P_L = \mathcal{D}_T^{-1}\mathcal{D}_L\,, \qquad P_T = 1 - P_L\,, \quad \text{(G.9)}$$

[1] Recall that the gluons live in the adjoint representation.

[2] For vanishing gauge field A_μ, these operators reduce to the well-known longitudinal and transversal projectors $(P_T)_{\mu\nu}[A=0] = \delta_{\mu\nu} - \partial_\mu\partial_\nu/\partial^2$ and $(P_L)_{\mu\nu}[A=0] = \partial_\mu\partial_\nu/\partial^2$.

which satisfy $P_{T,L}^2 = P_{T,L}, P_T + P_L = 1$ and $P_T P_L = 0 = P_L P_T$. The operators P_L and P_T obey the following commutation relation

$$[P_L, \theta] = 0 = [P_T, \theta]\,. \tag{G.10}$$

Due to our choice (G.1) for the background field, we can define a set of projectors which act solely in color space and project on the spaces perpendicular and parallel to the direction given by n^a, respectively. These projectors are given by

$$P_\perp^{yz} = \delta^{yz} - n^y n^z \quad \text{and} \quad P_\parallel^{yz} = n^y n^z\,, \tag{G.11}$$

and satisfy $P_{\perp,\parallel}^2 = P_{\perp,\parallel}, P_\perp + P_\parallel = 1$ and $P_\perp P_\parallel = 0 = P_\parallel P_\perp$. Note that the projectors $P_{\perp,\parallel}$ and $P_{T,L}$ commute:

$$[P_{\perp,\parallel}, P_{T,L}] = 0\,. \tag{G.12}$$

Moreover, we find that the covariant derivative (4.29) evaluated for the background field (G.1) reads

$$D[\bar{A}]_\mu^{yw} = \partial_\mu \delta^{yw} + \bar{g} f^{yzw} n^z \mathsf{A}_\mu\,. \tag{G.13}$$

Due to the antisymmetry property of the structure constants we then obtain

$$\begin{aligned} \left[P_{\perp,\parallel}, D_\mu\right] &= 0\,, & \left[P_{\perp,\parallel}, D^2\right] &= 0\,, \\ \left[P_{\perp,\parallel}, \mathcal{D}_T\right] &= 0\,, & \left[P_{\perp,\parallel}, \mathcal{D}_L\right] &= 0\,, \\ \left[P_{\perp,\parallel}, \mathsf{F}_{\mu\nu}\right] &= 0\,, \end{aligned} \tag{G.14}$$

and

$$P_\parallel A_\mu = 0\,, \quad P_\parallel D_\mu = P_\parallel \partial_\mu\,, \quad P_\parallel (\mathcal{D}_T)_{\mu\nu} = -\partial^2 \delta_{\mu\nu} P_\parallel\,. \tag{G.15}$$

The operator $\mathcal{S}$ factorizes according to

$$\mathcal{S}_{\mu\nu}^{yz} = P_{||}^{yz} s_{\mu\nu}\,, \qquad s_{\mu\nu} \;=\; \mathsf{F}_{\mu\rho}\mathsf{F}_{\sigma\nu}\partial^\rho\partial^\sigma\,. \tag{G.16}$$

Thus the operators $D^2, \mathcal{D}_L$ and $\mathcal{D}_T$ commute with the operator $\mathcal{S}$. Furthermore, we find the commutation relations

$$\Big[P_T[A=0], s\Big] = s \quad \text{and} \quad \Big[P_L[A=0], s\Big] = 0\,. \tag{G.17}$$

Finally, it is convenient to introduce a projector $P_{\text{gh.}}$ which trivially projects on the ghost sector.

By means of the projectors $P_{L,T}$ and $P_{\perp,\parallel}$ and $P_{\text{gh.}}$, we can now decompose $\Gamma_k^{(1,1)}[A]$ as follows

$$\begin{aligned} \Gamma_k^{(1,1)}[A] \;=\; & P_{||} P_T \Gamma_{||,T}^{(1,1)} P_{||} P_T + P_{||} P_L \Gamma_{||,L}^{(1,1)} P_{||} P_L + P_\perp P_T \Gamma_{\perp,T}^{(1,1)} P_\perp P_T \\ & + P_\perp P_L \Gamma_{\perp,L}^{(1,1)} P_\perp P_L + P_{\text{gh.}} \Gamma_{\text{gh.}}^{(1,1)} P_{\text{gh.}}\,, \end{aligned} \tag{G.18}$$

with

$$\left(\Gamma^{(1,1)}_{||,T}\right)_{\mu\nu} = -\partial^2 W_k' \delta_{\mu\nu} + W_k'' s_{\mu\nu}\,, \tag{G.19}$$

$$\Gamma^{(1,1)}_{||,L} = -\frac{1}{\xi_k}\partial^2\,, \tag{G.20}$$

$$\left(\Gamma^{(1,1)}_{\perp,T}\right)^{yz}_{\mu\nu} = [W_k' \mathcal{D}_T]^{yz}_{\mu\nu}\,, \tag{G.21}$$

$$\left(\Gamma^{(1,1)}_{\perp,L}\right)^{yz}_{\mu\nu} = \frac{1}{\xi_k}\,[\mathcal{D}_T]^{yz}_{\mu\nu}\,, \tag{G.22}$$

$$\left(\Gamma^{(1,1)}_{\text{gh.}}\right)^{yz} = -(D^2)^{yz}\,. \tag{G.23}$$

As we have discussed in the main text, we improve the regulator function by adjusting the regulator to the spectral flow of $\Gamma_k^{(1,1)}$. In doing this, we integrate over shells of eigenvalues of $\Gamma_k^{(1,1)}$ rather than ordinary canonical momentum shells. On the one hand, this stabilizes the RG flow, and on the other hand, it allows us to satisfy the symmetry constraint given by Eq. (4.46). Since the various terms on the RHS of Eq. (G.18) annihilate each other, e. g.

$$\left(P_{||}P_T\Gamma^{(1,1)}_{||,T}P_{||}P_T\right)\left(P_{||}P_L\Gamma^{(1,1)}_{||,L}P_{||}P_L\right) = 0\,, \tag{G.24}$$

we can also decompose the regulator function R_k:

$$\begin{aligned} R_k(\Gamma_k^{(1,1)}) = {} & P_{||}P_T R_k(\Gamma^{(1,1)}_{||,T})P_{||}P_T + P_{||}P_L R_k(\Gamma^{(1,1)}_{||,L})P_{||}P_L + P_\perp P_T R_k(\Gamma^{(1,1)}_{\perp,T})P_\perp P_T \\ & + P_\perp P_L R_k(\Gamma^{(1,1)}_{\perp,L})P_\perp P_L + P_{\text{gh.}} R_k(\Gamma^{(1,1)}_{\text{gh.}})P_{\text{gh.}} \end{aligned} \tag{G.25}$$

Finally, we have to choose a matrix $\mathcal{Z}_k$ in the definition (2.49) of the regulator function. A choice for the matrix entries of $\mathcal{Z}_k$, which establishes manifest RG invariance of the flow equation, is given by the wave function renormalizations of the corresponding fields. For the longitudinal gluon components, such a choice implies that the matrix entry $(\mathcal{Z}_k)_{\text{L}}$ is proportional to the inverse gauge-fixing parameter ξ_k. As a result, this renders the truncated flow independent of ξ_k, and we can implicitly choose the Landau gauge $\xi_k \equiv 0$ which is known to be an RG fixed point [55, 68]. For the transversal gluon components we choose Z_k which is related to the running coupling through Eq. (4.64). For the ghost sector, we choose $Z_{\text{gh.}} = 1$. Consequently, the matrix $\mathcal{Z}_k$ can be written in terms of the projectors defined above:

$$\mathcal{Z}_k = Z_k P_T[\bar{A}] + \frac{1}{\xi_k} P_L[\bar{A}] + P_{\text{gh.}}\,. \tag{G.26}$$

Inserting the decomposition (G.18) into the flow equation (2.61), the traces can be worked out straightforwardly and we finally obtain the contributions from the ghost and the gluons to the flow equation (4.67).

Let us briefly discuss the contribution of the quarks to the flow equation (4.67) which arise from the term bilinear in the quark fields in the truncation (4.61). As we have discussed in Subsec. 2.4.3, we need $(\hat{\Gamma}_\psi^{(1,1,0,0)}-\mathrm{i}M)(\hat{\Gamma}_\psi^{(1,1,0,0)}-\mathrm{i}M)^\dagger$ rather than $\hat{\Gamma}_\psi^{(1,1,0,0)}$:

$$(\hat{\Gamma}_\psi^{(1,1,0,0)}-\mathrm{i}M)(\hat{\Gamma}_\psi^{(1,1,0,0)}-\mathrm{i}M)^\dagger = \begin{pmatrix} (\mathrm{i}\not{D})(\mathrm{i}\not{D})^\dagger & 0 \\ 0 & (\mathrm{i}\not{D})^\dagger(\mathrm{i}\not{D}) \end{pmatrix} . \tag{G.27}$$

Evaluating Eq. (G.27) for $A = \bar{A}$, we find the following expression for the diagonal elements:

$$(\mathrm{i}\not{D})(\mathrm{i}\not{D})^\dagger = -D^2 + \frac{1}{2}\bar{g}\sigma_{\mu\nu}\mathsf{F}_{\mu\nu} , \tag{G.28}$$

where $\sigma_{\mu\nu}$ is defined in App. C. Note that the quarks live in the fundamental representation. Inserting Eq. (G.27) into the flow equation (4.67), the quark contributions to the flow equation (4.67) can be computed.

G.2 Flow Equations for the Operators $(F_{\mu\nu}F_{\mu\nu})^n$

Here we discuss the expansion of the flow equation (4.67) which is required for the computation of the anomalous dimension in Sect. 4.5.

In the following we expand the various functions in the flow equation (4.67) in powers of the renormalized dimensionless squared field strength ϑ. As we will see, such an expansion is related to an expansion in powers of the proper-time variable s. Due to the fact that we first expand the integrands of the various proper-time integrals in Eq. (4.67) and then perform the integration over s, the resulting series will be asymptotic[3], involving strongly increasing coefficients.

As discussed in the main text, we neglect all w_i in the expansion of $w_k(\vartheta) = \vartheta + w_2\frac{1}{2}\vartheta^2 + w_3\frac{1}{6}\vartheta^3 \ldots$. The expansions of the auxiliary functions $f^A_{1,2,3}$ and f^ψ as defined in Eqns. (D.3)-(D.6) are then given by (recall $b_l = |\nu_l|\sqrt{2\vartheta}$):

$$\begin{aligned} 2\sum_{l=1}^{N_c^2-1} f_1^A(s\dot{w}_k b_l)\, b_l^{(d-1)/2}\Big|_{w_i\to 0} &= -(d-1)\sum_{i=0}^{\infty}\frac{2^i(2^{2i}-2)}{(2i)!}\,\tau_i\, B_{2i}\, s^{2i-(d-1)/2}\,\vartheta^i \\ &\quad +4\sum_{i=0}^{\infty}\frac{2^i}{(2i-1)!}\,\tau_i\, s^{2i-(d-1)/2}\,\vartheta^i , \end{aligned} \tag{G.29}$$

$$2\sum_{l=1}^{N_c^2-1} f_2^A(sb_l)\, b_l^{(d-1)/2} = -\sum_{i=0}^{\infty}\frac{2^i(2^{2i}-2)}{(2i)!}\,\tau_i^A\, B_{2i}\, s^{2i-(d-1)/2}\,\vartheta^i , \tag{G.30}$$

[3]We note that the interchange of integration and expansion does not necessarily result in an asymptotic series. However, in our study the result of this procedure represents an asymptotic series.

$$f_3^A\Big(s\dot{w}, \frac{\dot{w}}{\dot{w}+2\vartheta\ddot{w}}\Big)\Big|_{w_i\to 0} \;=\; f_3^A(s,1) = 0\,, \tag{G.31}$$

$$4\sum_{l=1}^{N_c} f^\psi(sb_l)\, b_l^{(d-1)/2}\Big|_{w_i\to 0} \;=\; \sum_{i=0}^{\infty} \frac{2^{3i+1}}{(2i)!}\,\tau_i^\psi\, B_{2i}\, s^{2i-(d-1)/2}\,\vartheta^i\,, \tag{G.32}$$

where B_i denotes the Bernoulli numbers, and we define $1/(-1)! = 0$. The color factors τ_i^A and τ_i^ψ are defined in App. B.2. These factors are related to the group theoretical factors $\sum_{l=1}^{N_c^2-1}(\nu_l^2)^i$ and $\sum_{l=1}^{N_c}(\nu_l^2)^i$ that occur in the expansions for the functions of $f^A_{1,2,3}$ and f^ψ, respectively. Note that the ν_l are the eigenvalues of (n^aT^a) in the adjoint representation for the functions $f^A_{1,2,3}$, whereas the ν_l are the eigenvalues of (n^aT^a) in the fundamental representation for the function f^ψ. Finally, we obtain a contribution from the last line of Eq. (4.67):

$$\begin{aligned}\frac{2\vartheta}{(\dot{w}+2\vartheta\,\ddot{w})^2}\Big(\,\ddot{w}\,\partial_t\dot{w} - \dot{w}\,\partial_t\ddot{w} + 4\dot{w}\ddot{w} + 4\vartheta(\dot{w}\dddot{w} - \ddot{w}^2)\Big) f_4^A(s\,\dot{w}, \tfrac{T}{k})\Big|_{w_i\to 0} \\ = -\sum_{i=1}^{\infty}\frac{2i}{i!}\,\vartheta^i f_4^A(s,\tfrac{T}{k})\,\partial_t w_{i+1}\,,\end{aligned} \tag{G.33}$$

where the auxiliary function f_4^A is defined in Eq. (D.7).

Now we turn to the computation of the functions Y_{ij} and X_i in Eq. (4.69), which define the flow equations for the generalized couplings w_i in the present truncation. Before we continue with the derivation of the flow equation, we rewrite Eq. (4.69). Since we have $w_1 = 1$ by definition (see Eq. (4.66)), we find $\partial_t w_1 = 0$. Moreover, we observe that the RHS of Eq. (4.67) depends only linearly on η. Introducing a infinitely dimensional vector $\vec{w}_t$ through

$$\vec{w}_t = \begin{pmatrix} -\eta \\ \partial_t w_2 \\ \partial_t w_3 \\ \vdots \end{pmatrix}\,, \tag{G.34}$$

we can rewrite Eq. (4.69) in the present truncation (recall $w_i = 0$ for $i \geq 2$) as follows

$$w_{t,i} = G\tilde{X}_i \,+\, G\tilde{Y}_{ij}\, w_{tj}\,. \tag{G.35}$$

Here we have factored out a factor $G := \frac{g^2}{2(4\pi)^{d/2}} = \frac{\alpha_s}{8\pi}$. Thus the new auxiliary functions $\tilde{X}_i$ and $\tilde{Y}_{ij}$ are independent of the coupling g^2. In order to compute the anomalous dimension η, we have to compute first the new auxiliary functions $\tilde{X}_i$ and $\tilde{Y}_{ij}$. The explicit representation of $\tilde{Y}_{ij}$ and $\tilde{X}_i$ can be found by inserting the expansions (G.29)-(G.33) into the flow equation (4.67) and then performing the integration over the

proper-time variable s:

$$\begin{aligned}\tilde{X}_i &= -2^{i+1}\,\tau_i^A\,\bar{h}^A_{2i-\frac{d-1}{2}}(\tfrac{T}{k})\,i!\left((d-2)\tfrac{(2^{2i}-2)}{(2i)!}\,B_{2i}-\tfrac{4}{(2i-1)!}\right)\\ &\quad -8\,i!\frac{2^{3i}}{(2i)!}B_{2i}\tau_i^\psi\sum_{j=1}^{N_{\rm f}}\bar{h}^\psi_{2i-\frac{d-1}{2}}(\tfrac{m_j}{k},\tfrac{T}{k})\,, \qquad \text{(G.36)}\\ \tilde{Y}_{ij} &= \tilde{A}_{ij}+\tilde{B}_{ij}+\tilde{C}_{ij}\,. \qquad \text{(G.37)}\end{aligned}$$

The auxiliary matrices A, B, C are given by

$$\tilde{A} = \begin{cases}\tilde{A}_{i1}=0\\ \tilde{A}_{ij}=0 \text{ for } j>i+1\\ \tilde{A}_{ij}=\frac{i!}{(j-1)!}\left[2^n\tau_n^A\left(\bar{h}^A_{2n-\frac{d-1}{2}}-\bar{g}^A_{2n-\frac{d-1}{2}}\right)\left((d-1)\frac{2^{2n}-2}{(2n)!}B_{2n}-\frac{4}{(2n-1)!}\right)\right]_{n=1+i-j}\end{cases} \qquad \text{(G.38)}$$

$$\tilde{B} = \begin{cases}\tilde{B}_{ij}=0 \text{ for } j>1\\ \tilde{B}_{i1}=-2^i\tau_i^A\bar{g}^A_{2i-\frac{d-1}{2}}\,i!\left((d-1)\frac{2^{2i}-2}{(2i)!}B_{2i}-\frac{4}{(2i-1)!}\right)\end{cases} \qquad \text{(G.39)}$$

$$\tilde{C} = \begin{cases}\tilde{C}_{ij}=0 \text{ for } j\neq i+1\\ \tilde{C}_{i,i+1}=-2i\,(\bar{H}_0^A-\bar{G}_0^A)\end{cases}\,. \qquad \text{(G.40)}$$

The thermal moments $\bar{h}_j^A$, $\bar{g}_j^A$, $\bar{h}_j^\psi$, $\bar{H}_0^A$ and $\bar{G}_0^A$ arise due to the proper-time integration, see Eqns. (D.8)-(D.12) for their definitions. Note that $\tilde{Y}_{ij}$ is independent of the quark contributions in the present truncation.

The anomalous dimension in now obtained by solving the infinite set of equations Eq. (G.35). Let us write Eq. (G.35) in form of a matrix equation (recall also the discussion in Sec. (2.4.3)):

$$\vec{w}_t=G\vec{\tilde{X}}+G\,\tilde{Y}\cdot\vec{w}_t \qquad\Longrightarrow\qquad \vec{w}_t=G\left(1-G\,\tilde{Y}\right)^{-1}\cdot\vec{\tilde{X}}\,. \qquad \text{(G.41)}$$

From this representation, we find the following equation for η:

$$\eta\equiv-w_{t,1}=\sum_{m=1}^{\infty}a_m G^m \quad\text{with}\quad a_m:=-(\tilde{Y}^{m-1})_{1j}\tilde{X}_j\,. \qquad \text{(G.42)}$$

Using this equation, we can now compute straighforwardly the QCD β_{g^2} function to any finite order in perturbation theory within our truncation. In Sec. 4.5.2, we have used Eq. (G.42) for a calculation of the two-loop β_{g^2} function. However, Eq. (G.42) represent an asymptotic series; for the exponential regulator (D.19) used in this work, the coefficients a_m grow even more strongly than factorials and alternate in sign. The reason for this behavior can be traced back to the fact that we have interchanged integration and expansion in our derivation of equation Eq. (G.42) from the flow equation (4.67). Note that the RHS of Eq. (4.67) is finite. Thus we have to reconstruct

a well-defined integral representation out of the asymptotic series Eq. (G.42). In this work, we reconstruct such a representation by taking only the leading growth of the series coefficients into account. It has been shown for various examples that this already leads to a good approximation of the underlying integral representation [204]. For a particular m, we can isolate the leading growth $a_m^{\text{l.g.}}$ in the term that contains $\tilde{X}_m$:

$$a_1^{\text{l.g.}} = -\tilde{X}_1, \quad a_2^{\text{l.g.}} = -\tilde{Y}_{12}\tilde{X}_2, \quad a_m^{\text{l.g.}} = -\tilde{Y}_{12}\tilde{Y}_{23}\tilde{Y}_{34}\ldots\tilde{Y}_{m-1,m}\tilde{X}_m\,. \tag{G.43}$$

Inserting Eqns. (G.40)-(G.40) into Eq. (G.43), we find the leading-growth coefficients given in Eq. (4.72). In App. G.3, we discuss the resummation of the anomalous dimension by means of these leading growth coefficients.

G.3 Resummation of the Anomalous Dimension

In Sec. 4.5, we have computed and discussed the RG flow of the running QCD coupling. Here, we present details for the resummation of the series expansion of the anomalous dimension η,

$$\eta \simeq \sum_{m=1}^{\infty} a_m^{\text{l.g.}} G^m\,. \tag{G.44}$$

The leading growth (l.g.) coefficients $a_m^{\text{l.g.}}$ read

$$\begin{aligned} a_m^{\text{l.g.}} = a_m^A + a_m^{\text{q}} = 4(-2c_1)^{m-1}\frac{\Gamma(z_d+m)\Gamma(m+1)}{\Gamma(z_d+1)}\Big[\bar{h}^A_{2m-e_d}(\tfrac{T}{k})(d-2)\frac{2^{2m}-2}{(2m)!}\tau_m^A B_{2m} \\ - \frac{4}{\Gamma(2m)}\tau_m^A\bar{h}^A_{2m-e_d}(\tfrac{T}{k}) + 4^{m+1}\frac{B_{2m}}{(2m)!}\tau_m^{\psi}\sum_{i=1}^{N_{\text{f}}}\bar{h}^{\psi}_{2m-e_d}(\tfrac{m_i}{k},\tfrac{T}{k})\Big]\,, \end{aligned} \tag{G.45}$$

where B_{2m} are the Bernoulli numbers [203] and z_d is defined as

$$z_d := (d-1)(N_{\text{c}}^2-1)c_2\,. \tag{G.46}$$

The temperature and regulator-dependent functions c_1 and c_2 are given by

$$c_1 = 2\big(\bar{H}_0^A(\tfrac{T}{k}) - \bar{G}_0^A(\tfrac{T}{k})\big)\,, \tag{G.47}$$

$$c_2 = \frac{\bar{h}^A_{-e_d}(\tfrac{T}{k}) - \bar{g}^A_{-e_d}(\tfrac{T}{k})}{c_1}\,. \tag{G.48}$$

Note that $c_1 > 0$ and $c_2 > 0$ for $\frac{T}{k} \geq 0$. In the limits $\frac{T}{k} \to 0$ and $\frac{T}{k} \to \infty$, c_1 and c_2 are given by

$$\lim_{\frac{T}{k}\to 0} c_1 = c_1^0 = \frac{4}{d}\Big(\frac{d}{2}\zeta\Big(1+\frac{d}{2}\Big) - 1\Big)\,, \tag{G.49}$$

$$\lim_{\frac{T}{k}\to 0} c_2 = c_2^0 = \frac{d}{4}\,, \tag{G.50}$$

$$\lim_{\frac{T}{k}\to \infty} \tfrac{k}{T} c_1 = c_1^\infty = 2\sqrt{4\pi}\Big(\zeta\Big(1+e_d\Big) - \frac{2}{d-1}\Big)\,, \tag{G.51}$$

$$\lim_{\frac{T}{k}\to \infty} c_2 = c_2^\infty = \frac{e_d\zeta(1+e_d)-1}{2(\zeta(1+e_d)-\frac{2}{d-1})}\,, \tag{G.52}$$

where we have used Eq. (D.9)-(D.18) for the exponential regulator (D.19) and $\zeta(x)$ denotes the Riemann Zeta function.

In the following we perform the resummation of η along the lines of Ref. [71]: We split the anomalous dimension Eq. (4.70) into three contributions,

$$\eta = \eta_1^A + \eta_2^A + \eta^{\mathrm{q}}\,, \tag{G.53}$$

where η_1^A corresponds to the resummation of the term $\sim \tau_m^A B_{2m}$ in Eq. (G.45) and η_2^A to the resummation of the term containing the Nielsen-Olesen unstable mode ($\sim 1/\Gamma(2m)$), representing the leading and subleading growth, respectively. The remaining contributions, which include the quark effects, are contained in η^{q}.

For the moment, we confine ourselves to $SU(N_c = 2)$ for which the group theoretical factors are $\tau_m^A = N_c$ and $\tau_m^\psi = N_{\mathrm{c}}\,(1/4)^m = 2\,(1/4)^m$ (see App. B.2 for details), but we artificially retain the N_{c} dependence in all terms in order to simplify the generalization to gauge groups of higher rank.

We start with the resummation of η_1^A: For this purpose, we use the standard integral representation of the Γ functions [203],

$$\Gamma(z_d+m)\Gamma(m+1) = \int_0^\infty ds_1 \int_0^\infty ds_2\, s_1 s_2^{z_d} (s_1 s_2)^{m-1} \mathrm{e}^{-(s_1+s_2)} = \int_0^\infty dp\, \tilde{K}_{z_d-1}(p)\, p^{m-1}, \tag{G.54}$$

where we have introduced the modified Bessel function

$$\tilde{K}_{z_d-1}(s) = 2 s^{\frac{1}{2}(z_d+1)} K_{z_d-1}(2\sqrt{s})\,. \tag{G.55}$$

Furthermore, we use the series representation of the Bernoulli numbers [203],

$$\frac{B_{2m}}{(2m)!} = 2\frac{(-1)^{m-1}}{(2\pi)^{2m}} \sum_{l=1}^{\infty} \frac{1}{l^{2m}}\,. \tag{G.56}$$

Using Eq. (G.54) and (G.56), it is possible to rewrite η_1^A as follows

$$\eta_1^A = \frac{4(d-2)N_c G}{\pi^2\Gamma(z_d+1)} \sum_{m=1}^{\infty}\sum_{l=1}^{\infty} \frac{1}{l^2} \int_0^\infty dp\, \tilde{K}_{z_d-1}(p)\, \bar{h}^A_{2m-e_d}(\tfrac{T}{k}) \Big[2\Big(\frac{2Gpc_1}{\pi^2 l^2}\Big)^{m-1} - \Big(\frac{Gpc_1}{2\pi^2 l^2}\Big)^{m-1}\Big] . \tag{G.57}$$

In order to perform the summation over m, we define

$$\begin{aligned} S_b^A(q,v) =& \sum_{l=1}^{\infty}\frac{1}{l^2}\sum_{m=1}^{\infty}\Big(\frac{q}{l^2}\Big)^{m-1}\bar{h}^A_{2m-e_d}(v) \\ =& \frac{2}{\sqrt{\pi}}\sum_{l=1}^{\infty}\sum_{m=0}^{\infty}\sum_{n=-\infty}^{\infty}\int_0^\infty dx\cos\Big(\frac{nx}{v}\Big)\int_0^\infty dt\,\frac{\mathrm{e}^{-t}}{l^2}\int_0^\infty ds\,\tilde{h}(s)\frac{s^{2-e_d}}{(2m)!}\Big(\frac{st\sqrt{q}}{l}\Big)^{2m}\mathrm{e}^{-sx^2} \\ =& \frac{1}{\Gamma(b+1)\sqrt{q\pi}}\sum_{n=-\infty}^{\infty}\int_0^\infty dx\,\cos\Big(\frac{nx}{v}\Big)\int_0^\infty dt\,\mathrm{Li}_1\Big(\mathrm{e}^{-\frac{t}{\sqrt{q}}}\Big)\,\sigma_b^A(x^2,t)\,, \end{aligned} \tag{G.58}$$

where we have used Eqns. (D.9), (D.1) and (D.13). The auxiliary function σ_b^A is defined as

$$\sigma_b^A(x,t) = \Big(-\frac{d}{dy}\Big)^{b+3-e_d}\int_0^\infty du\,u^b\Big[h(y+u+x^2-t)+h(y+u+x^2+t)\Big]\Big|_{y=0} . \tag{G.59}$$

With the aid of Eq. (G.58), we obtain the final expression for η_1^A,

$$\eta_1^A = \frac{4(d-2)N_c G}{\pi^2\Gamma(z_d+1)}\int_0^\infty dp\,\tilde{K}_{z_d-1}(p)\,\Big[2S_b^A\Big(\frac{2Gpc_1}{\pi^2},\frac{T}{k}\Big) - S_b^A\Big(\frac{Gpc_1}{2\pi^2},\frac{T}{k}\Big)\Big] , \tag{G.60}$$

which can straightforwardly be evaluated numerically.

Next we turn to the calculation of η_2^A, the subleading-growth part of η. Here, a careful treatment of the zeroth Matsubara frequency which contains the Nielsen-Olesen mode is necessary. For this purpose we transform the modified moments $\bar{h}_j^A$ in Eq. (D.15) into a sum over Matsubara frequencies and insert a regulator function $\mathcal{P}\big(\frac{T}{k}\big)$ for the unstable mode,

$$\bar{h}_j^{A,reg}(v) = \sqrt{4\pi}v\sum_{n=-\infty}^{\infty}\int_0^\infty ds\,\widetilde{h}(s)s^j\mathrm{e}^{-s\widetilde{\mathcal{P}}_n(v)} . \tag{G.61}$$

Here, we have introduced

$$\widetilde{\mathcal{P}}_n(v) = \begin{cases} (2\pi n v)^2 & (n\neq 0) \\ \mathcal{P}(v) & (n=0) \end{cases} . \tag{G.62}$$

The function $\mathcal{P}(v)$ specifies the regularization of the Nielsen-Olesen mode and is defined in Eq. (H.3); the hard Matsubara modes ($n \neq 0$) remain unmodified.

Now we rewrite η_2^A by means of Eq. (G.54),

$$\eta_2^A = -\frac{16N_cG}{\Gamma(z_d+1)} \sum_{m=1}^{\infty} \frac{1}{\Gamma(2m)} \int_0^\infty dp\, \tilde{K}_{z_d-1}(p)\, \bar{h}^{A,reg}_{2m-e_d}(\tfrac{T}{k}) \Big(-2Gpc_1 \Big)^{m-1} . \quad \text{(G.63)}$$

For what follows, it is convenient to introduce an auxiliary function $T^A(q)$ which is defined as

$$\begin{aligned} T_b^A(q,v) =& \sum_{m=1}^{\infty} \frac{1}{\Gamma(2m)} \Big(-q \Big)^{m-1} \bar{h}^{A,reg}_{2m-e_d}(v) \\ =& \frac{\sqrt{\pi}v}{\Gamma(b+1)} \sum_{n=-\infty}^{\infty} \int_0^1 dt \int_0^\infty du\, u^b \int_0^\infty ds \tilde{h}(s) s^{b+3-e_d} \mathrm{e}^{-s(u+\widetilde{\mathcal{P}}_n(v))} \Big[\mathrm{e}^{-st\sqrt{-q}} + \mathrm{e}^{st\sqrt{-q}} \Big] \\ =& \frac{\sqrt{\pi}v}{\Gamma(b+1)} \sum_{n=-\infty}^{\infty} \vartheta_b^A(\widetilde{\mathcal{P}}_n(v), q) \,, \end{aligned} \quad \text{(G.64)}$$

Here, we have used Eqns. (G.61) and (D.13). Furthermore, we have defined the auxiliary function ϑ_b^A:

$$\vartheta_b^A(x,q) = \Big(-\frac{d}{dy} \Big)^{b+3-e_d} \int_0^1 dt \int_0^\infty du\, u^b \Big[h(y+u+x-t\sqrt{-q}) + h(y+u+x+t\sqrt{-q}) \Big] \Big|_{y=0} . \quad \text{(G.65)}$$

Applying Eq. (G.64) to Eq. (G.63), we finally obtain

$$\eta_2^A = -\frac{16N_cG}{\Gamma(z_d+1)} \int_0^\infty dp\, \tilde{K}_{z_d-1}(p)\, T_b^A\Big(2Gpc_1, \frac{T}{k}\Big) . \quad \text{(G.66)}$$

This expression can straightforwardly be evaluated numerically.

The calculation of the contribution η^{q} of the quarks to the gluon anomalous dimension can be performed along the lines of the calculation of η_1^A. We obtain

$$\eta^{\mathrm{q}} = \frac{8N_cG}{\pi^2\Gamma(z_d+1)} \sum_{i=1}^{N_f} \int_0^\infty dp\, \tilde{K}_{z_d-1}(p)\, S_b^\psi\Big(\frac{pGc_1}{2\pi^2}, \frac{T}{k}, \frac{m_i}{k}\Big) . \quad \text{(G.67)}$$

The auxiliary function $S_b^\psi(q,\tilde{m})$ is given by

$$S_b^\psi(q,v,\tilde{m}) = \frac{1}{\Gamma(b+1)\sqrt{4\pi q}} \sum_{n=-\infty}^{\infty} (-1)^n \int_0^\infty dx \cos\Big(\frac{nx}{v}\Big) \int_0^\infty dt \mathrm{Li}_1\Big(\mathrm{e}^{-\frac{t}{\sqrt{q}}}\Big) \sigma_b^\psi(u,x^2,t,\tilde{m}), \quad \text{(G.68)}$$

where $\sigma_b^\psi(u,x,t,\tilde{m})$ is defined as

$$\begin{aligned} \sigma_b^\psi(u,x,t,\tilde{m}) =& \Big(-\frac{d}{dy} \Big)^{b+3-e_d} \int_0^\infty du\, u^b \Big[h_s^\psi\Big(\sqrt{y+u+x-t}, \tilde{m}\Big) \\ &+ h_s^\psi\Big(\sqrt{y+u+x+t}, \tilde{m}\Big) + h_s^\psi\Big(-\sqrt{y+u+x-t}, \tilde{m}\Big) + h_s^\psi\Big(-\sqrt{y+u+x+t}, \tilde{m}\Big) \Big] \Big|_{y=0} . \end{aligned} \quad \text{(G.69)}$$

The regulator function occurs in the function $h_s^\psi(\sqrt{y},\tilde{m})$, which is related to $h^\psi(y,\tilde{m})$ defined in Eq. (D.22) by

$$h_s^\psi(\sqrt{y},\tilde{m}) \equiv h^\psi(y,\tilde{m})\,. \tag{G.70}$$

Note that there is one essential difference between the resummation of $\eta_{1/2}^A$ and that of η^q: the regulator shape-function $r(y)$ can be expanded in powers of y, while the corresponding function $r_\psi(y)$ for the quark fields should have a power series in $\sqrt{y}$. This is a consequence of chiral symmetry [59] and justifies the notation $h_s^\psi(\sqrt{y},\tilde{m})$.

We stress that all integral representations in Eqs. (G.60), (G.66) and (G.67) are finite and can be evaluated numerically. For $d = 4$ and in the limit of vanishing temperature, $T \to 0$, the results agree with those of Ref. [71].

In the remainder of this section we discuss how the results obtained above for $SU(2)$ can be generalized to higher gauge groups. Since we do not have the explicit representation of the color factors $\tau_m^{A/\psi}$ for gauge groups with $N_\mathrm{c} \geq 3$ at hand, we have to scan the Cartan subalgebra for the extremal values of the color factors τ_m^A and τ_m^ψ. As discussed in App. B.2, these extremal values of τ_m^A and τ_m^ψ can be calculated straightforwardly. Inserting the extremal values into Eq. (G.45), we find that the anomalous dimension for $SU(3)$ can be written in terms of the formulas already calculated for $SU(2)$ as

$$\eta_3^{\mathrm{SU(3)}} = \frac{2}{3}\Big[\eta_1^A + \eta_2^A\Big]_{N_\mathrm{c}\to 3} + \frac{1}{3}\Big[\eta_1^A + \eta_2^A\Big]_{N_\mathrm{c}\to 3, c_1 \to c_1/4} + \frac{2}{3}\eta^\psi\Big|_{N_\mathrm{c}\to 3}\,, \tag{G.71}$$

$$\eta_8^{\mathrm{SU(3)}} = \Big[\eta_1^A + \eta_2^A\Big]_{N_\mathrm{c}\to 3, c_1 \to 3c_1/4} + \frac{2}{9}\eta^\psi\Big|_{N_\mathrm{c}\to 3, c_1 \to c_1/3} + \frac{4}{9}\eta^\psi\Big|_{N_\mathrm{c}\to 3, c_1 \to 4c_1/3}. \tag{G.72}$$

The notation here serves as a recipe for replacing N_c and c_1, defined in Eq. (G.47), on the right-hand sides of Eqns. (G.60), (G.66) and (G.67). Note that the replacement of N_c results also in a modification of the function z_d, which is defined in Eq. (G.46). However, c_2, which appears in the definition of z_d, remains unchanged for all gauge groups and depends only on the dimension d.

Appendix H

Regulator Dependence from the Unstable Mode

In this part of the appendix, we discuss the regulator dependence of the critical temperature $T_{\rm cr}$ that arises from the details of projecting out the unstable Nielsen-Olesen mode. We already pointed out in Subsec. 4.5.1 that removing the tachyonic part of the unstable mode corresponds to an exact operation on the space of admissible stable background fields. With regard to our purposes, it even suffices to remove only the thermal excitations of the tachyonic part of the mode. This is due to the fact that the imaginary part arising from quantum fluctuations can easily be identified and dropped; in the context of a non-perturbative RG study, this has already been shown in Ref. [71]. Now let us take a less strict point of view in the sense that we allow for a smeared regularization of this mode in a whole class of regulators. The true physical result will not depend on this part of the regularization. Therefore we can identify the optimal (truncated) result with a stationary point in the space of regulators, using the "principle of minimum sensitivity", cf. Ref. [44]. In order to prevent the thermal population of the Nielsen-Olesen mode $E^{\rm NO}$, it is sufficient to regularize only the soft part (zero Matsubara frequency) of this mode as follows:

$$\frac{\mathrm{E}^{\rm NO}_{\rm soft} + R_k}{k^2} \quad \longrightarrow \quad \mathcal{P}(\tfrac{T}{k}) + \frac{\mathrm{E}^{\rm NO}_{\rm soft} + R_k}{k^2}\,. \tag{H.1}$$

The function $\mathcal{P}(\frac{T}{k})$ has to satisfy the following constraints:

$$\lim_{T/k\to 0} \mathcal{P}(\tfrac{T}{k}) = 0 \qquad \text{and} \qquad \lim_{T/k\to\infty} \mathcal{P}(\tfrac{T}{k}) \to \infty\,. \tag{H.2}$$

As a convenient example, we choose

$$\mathcal{P}(\tfrac{T}{k}) \equiv \mathcal{P}_m(\tfrac{T}{k}) = (\tfrac{T}{k})^m \qquad \text{with} \qquad m > 0\,. \tag{H.3}$$

Our regulator-optimization condition is given by the demand that $T_{\rm cr}$ should be stationary with respect to a variation of the optimal regulator function. Calculating $T_{\rm cr}$

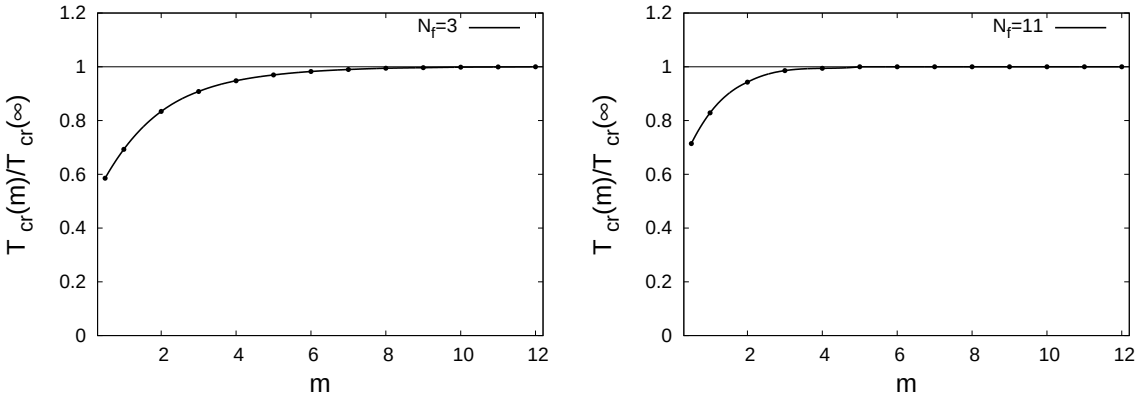

Figure H.1: The figure shows the dependence of the critical temperature $T_{\rm cr}$ on the smeared regularization of the Nielsen-Olesen mode. The regulators are labeled by m, see also Eq. (H.3). The left and the right panel show the results for $N_{\rm c}$ with $N_{\rm f} = 3$ and $N_{\rm f} = 11$ massless quark flavors, respectively. The limit $m \to \infty$ can be identified with the stationary point, and thus the optimal regulator in the class of considered regulators. This justifies constructively the procedure used in the main text which was derived from general considerations.

as a function of the parameter m, the optimization condition for the regulator function translates into

$$\left.\frac{\partial T_{cr}}{\partial m}\right|_{m=\bar{m}} \stackrel{!}{=} 0\,. \tag{H.4}$$

The solution $m = \bar{m}$ of this equation defines the desired optimized regulator.

As an example, we show $T_{\rm cr}(m)/T_{\rm cr}(\infty)$ as a function of m for $N_{\rm c} = 3$ with $N_{\rm f} = 3$ and with $N_{\rm f} = 11$ quark flavors in Fig. H.1. The figure illustrates nicely our finding that the optimized regulator is given by $m \to \infty$ for all $N_{\rm c}$ and $N_{\rm f}$. This represents an independent and constructive justification of the regularization used in the Chap. 4, corresponding to the choice $m \to \infty$.

Appendix I

Heat-Bath Projectors for Finite Temperature and Density

When we calculate the flow equations for the four-fermion interactions in Subsec. 4.6.1 and Subsec. 4.6.2, we encounter momentum integrals of the following form:

$$T \sum_{n=-\infty}^{\infty} \int \frac{d^{d-1}p}{(2\pi)^{(d-1)}} \tilde{p}_\mu^{(\pm)} \tilde{p}_\nu^{(\pm)} \mathcal{I}_1 \left(\tilde{p}_\lambda^{(\pm)} \tilde{p}_\lambda^{(\pm)} \right) \tag{I.1}$$

and

$$T \sum_{n=-\infty}^{\infty} \int \frac{d^{d-1}p}{(2\pi)^{(d-1)}} \tilde{p}_\mu^{(\pm)} \tilde{p}_\nu^{(\mp)} \mathcal{I}_2 \left(\tilde{p}_\lambda^{(+)} \tilde{p}_\lambda^{(+)} \right) \mathcal{I}_2 \left(\tilde{p}_\lambda^{(\mp)} \tilde{p}_\lambda^{(-)} \right) . \tag{I.2}$$

Here, d counts the number of space-time dimensions. We assume that the functions $\mathcal{I}_1$ and $\mathcal{I}_2$ drop exponentially for large momenta and that they depend only on Lorentz-scalars[1].

Note that we allow for an additional dependence of these functions on a mass parameter m in in Eqs. (4.88) and (4.89). For simplicity, we drop the dependence on m here, since it is not relevant for what follows. The d-dimensional momenta $\tilde{p}_\mu^{(\pm)}$ are defined as

$$\tilde{p}_\mu^{(\pm)} = (\overbrace{\nu_n \pm \mathrm{i}\mu}^{=\tilde{p}_0^{(\pm)}}, \vec{p}) \, , \tag{I.3}$$

where $\nu_n = (2n+1)\pi T$ denotes the n-th fermionic Matsubara-frequency. Note that $\vec{p}$ is a $(d-1)$-dimensional vector. The chemical potential of the fermions is given by μ. In order to perform the momentum integration, it is convenient to decompose the

[1] We encounter contributions with both fermionic and bosonic internal lines in the calculation of the flow equations in Subsec. 4.6.2. In this case, the functions $\mathcal{I}_1$ and $\mathcal{I}_2$ have an additional dependence on $p_\mu p_\mu = \omega_n^2 + \vec{p}^2$, where ω_n denotes the n-th bosonic Matsubara-frequency.

non-trivial tensor structure in Eqs. (I.1) and (I.2) by means of an appropriate basis. For this purpose, we define the following operators:

$$
\begin{aligned}
(P_A)_{\mu\nu} &= n_\mu n_\nu \,, && \text{(I.4)}\\
(P_B)_{\mu\nu} &= \delta_{\mu\nu} - n_\mu n_\nu \,, && \text{(I.5)}\\
(P_C^{(\pm)})_{\mu\nu} &= \frac{1}{|\vec{p}|}\left(n_\mu \tilde{p}_\nu^{(\pm)} - n_\mu n_\nu \tilde{p}_0^{(\pm)}\right) \,, && \text{(I.6)}\\
(P_D^{(\mp)})_{\mu\nu} &= \frac{1}{|\vec{p}|}\left(\tilde{p}_\mu^{(\mp)} n_\nu - n_\mu n_\nu \tilde{p}_0^{(\mp)}\right) \,. && \text{(I.7)}
\end{aligned}
$$

The vector $n_\mu = (1, \vec{0})$ denotes the heat-bath velocity. From the definitions of the operators P_A, P_B, $P_C^{(\pm)}$ and $P_D^{(\mp)}$, we obtain immediately

$$
\begin{aligned}
\mathrm{Tr} P_A P_B &= \mathrm{Tr} P_B P_C^{(\pm)} = \mathrm{Tr} P_A P_C^{(\pm)} = \mathrm{Tr} P_B P_D^{(\mp)} = \mathrm{Tr} P_C^{(\pm)} P_C^{(\pm)} \\
&= \mathrm{Tr} P_D^{(\mp)} P_D^{(\mp)} \mathrm{Tr} P_A P_C^{(\pm)} = \mathrm{Tr} P_C^{(\pm)} P_C^{(\pm)} = \mathrm{Tr} P_D^{(\mp)} P_D^{(\mp)} = 0 \,, \qquad \text{(I.8)}
\end{aligned}
$$

and

$$
\mathrm{Tr} P_A P_A = \mathrm{Tr} P_C^{(\pm)} P_D^{(\mp)} = 1 \,, \qquad \mathrm{Tr} P_B P_B = (d-1) \,. \qquad \text{(I.9)}
$$

Now it is a straightforward task to show that the following set of operators represents a complete orthonormal tensor basis:

$$
\mathcal{B} = \left\{ P_A, \frac{1}{\sqrt{d-1}} P_B, \frac{1}{\sqrt{2}}\left(P_C^{(\pm)} + P_D^{(\mp)}\right), \frac{\mathrm{i}}{\sqrt{2}}\left(P_C^{(\pm)} - P_D^{(\mp)}\right) \right\} . \qquad \text{(I.10)}
$$

Using the operators P_A, P_B, $P_C^{(\pm)}$ and $P_D^{(\mp)}$, or equivalently the basis $\mathcal{B}$, the tensors in Eqs. (I.1) and (I.2) can be decomposed as follows:

$$
\begin{aligned}
\tilde{p}_\mu^{(+)} \tilde{p}_\nu^{(-)} &= \tilde{p}_0^{(+)} \tilde{p}_0^{(-)} (P_A)_{\mu\nu} + \frac{\vec{p}^2}{d-1}(P_B)_{\mu\nu} + \tilde{p}_0^{(+)} |\vec{p}| (P_C^{(+)})_{\mu\nu} + \tilde{p}_0^{(-)} |\vec{p}| (P_D^{(-)})_{\mu\nu} \,, && \text{(I.11)}\\
\tilde{p}_\mu^{(-)} \tilde{p}_\nu^{(+)} &= \tilde{p}_0^{(-)} \tilde{p}_0^{(+)} (P_A)_{\mu\nu} + \frac{\vec{p}^2}{d-1}(P_B)_{\mu\nu} + \tilde{p}_0^{(-)} |\vec{p}| (P_C^{(+)})_{\mu\nu} + \tilde{p}_0^{(+)} |\vec{p}| (P_D^{(-)})_{\mu\nu} \,, && \text{(I.12)}\\
\tilde{p}_\mu^{(+)} \tilde{p}_\nu^{(+)} &= \tilde{p}_0^{(+)} \tilde{p}_0^{(+)} (P_A)_{\mu\nu} + \frac{\vec{p}^2}{d-1}(P_B)_{\mu\nu} + \tilde{p}_0^{(+)} |\vec{p}| (P_C^{(+)})_{\mu\nu} + \tilde{p}_0^{(+)} |\vec{p}| (P_D^{(+)})_{\mu\nu} \,, && \text{(I.13)}\\
\tilde{p}_\mu^{(-)} \tilde{p}_\nu^{(-)} &= \tilde{p}_0^{(-)} \tilde{p}_0^{(-)} (P_A)_{\mu\nu} + \frac{\vec{p}^2}{d-1}(P_B)_{\mu\nu} + \tilde{p}_0^{(-)} |\vec{p}| (P_C^{(-)})_{\mu\nu} + \tilde{p}_0^{(-)} |\vec{p}| (P_D^{(-)})_{\mu\nu} \,. && \text{(I.14)}
\end{aligned}
$$

We observe that the terms proportional to $P_C^{(\pm)}$ and proportional to $P_D^{(\mp)}$ are only linear in the spatial momenta $\tilde{p}_i$. Therefore these terms drop out when we perform the momentum integration. Taking this into account, the decompositions, which we have given in Eqs. (4.88) and (4.89), are finally obtained by reinserting the definitions of the operators P_A and P_B into the relations (I.11)-(I.14).

Bibliography

[1] M. Gell-Mann, *Symmetries of baryons and mesons*, Phys. Rev. **125**, 1067–1084 (1962).

[2] M. Gell-Mann, *A Schematic model of baryons and mesons*, Phys. Lett. **8**, 214–215 (1964).

[3] H. Fritzsch, M. Gell-Mann, and H. Leutwyler, *Advantages of the color octet gluon picture*, Phys. Lett. **B47**, 365–368 (1973).

[4] Y. Nambu, *Strings, monopoles, and gauge fields*, Phys. Rev. **D10**, 4262 (1974).

[5] W. A. Bardeen and R. B. Pearson, *Local gauge invariance and the bound state nature of hadrons*, Phys. Rev. **D14**, 547 (1976).

[6] O. W. Greenberg and C. A. Nelson, *Color models of hadrons*, Phys. Rept. **32**, 69–121 (1977).

[7] J. Gasser and H. Leutwyler, *Chiral perturbation theory to one loop*, Ann. Phys. **158**, 142 (1984).

[8] M. Gell-Mann and M. Levy, *The axial vector current in beta decay*, Nuovo Cim. **16**, 705 (1960).

[9] S. Bethke, *alpha(s) at Zinnowitz 2004*, Nucl. Phys. Proc. Suppl. **135**, 345–352 (2004), hep-ex/0407021.

[10] H. D. Politzer, *Reliable perturbative results for strong interactions?*, Phys. Rev. Lett. **30**, 1346–1349 (1973).

[11] D. J. Gross and F. Wilczek, *Ultraviolet behavior of non-abelian gauge theories*, Phys. Rev. Lett. **30**, 1343–1346 (1973).

[12] S. Scherer, *Quark-Gluon Plasma im Computer (in German)*, talk given at the HHLR user colloquium, Darmstadt (2003) .

[13] E. V. Shuryak and I. Zahed, *Rethinking the properties of the quark gluon plasma at T approx. T(c)*, Phys. Rev. **C70**, 021901 (2004), hep-ph/0307267.

[14] E. V. Shuryak, *What RHIC experiments and theory tell us about properties of quark-gluon plasma?*, Nucl. Phys. **A750**, 64–83 (2005), hep-ph/0405066.

[15] F. Karsch, E. Laermann, and A. Peikert, *Quark mass and flavor dependence of the QCD phase transition*, Nucl. Phys. **B605**, 579–599 (2001), hep-lat/0012023.

[16] Z. Fodor and S. D. Katz, *Lattice determination of the critical point of QCD at finite T and mu*, JHEP **03**, 014 (2002), hep-lat/0106002.

[17] P. de Forcrand and O. Philipsen, *The QCD phase diagram for small densities from imaginary chemical potential*, Nucl. Phys. **B642**, 290–306 (2002), hep-lat/0205016.

[18] C. R. Allton et al., *The equation of state for two flavor QCD at non-zero chemical potential*, Phys. Rev. **D68**, 014507 (2003), hep-lat/0305007.

[19] F. Karsch, E. Laermann, and C. Schmidt, *The chiral critical point in 3-flavor QCD*, Phys. Lett. **B520**, 41–49 (2001), hep-lat/0107020.

[20] R. V. Gavai and S. Gupta, *The critical end point of QCD*, Phys. Rev. **D71**, 114014 (2005), hep-lat/0412035.

[21] V. Laliena, *Searching for the critical endpoint in QCD with two quark flavors*, hep-lat/0509153.

[22] M. D'Elia, A. Di Giacomo, and C. Pica, *Two flavor QCD and confinement*, hep-lat/0503030.

[23] U. W. Heinz and M. Jacob, *Evidence for a new state of matter: An assessment of the results from the CERN lead beam programme*, nucl-th/0002042.

[24] P. Braun-Munzinger, D. Magestro, K. Redlich, and J. Stachel, *Hadron production in Au Au collisions at RHIC*, Phys. Lett. **B518**, 41–46 (2001), hep-ph/0105229.

[25] P. Braun-Munzinger, K. Redlich, and J. Stachel, *Particle production in heavy ion collisions*, nucl-th/0304013.

[26] P. Braun-Munzinger, J. Stachel, and C. Wetterich, *Chemical freeze-out and the QCD phase transition temperature*, Phys. Lett. **B596**, 61–69 (2004), nucl-th/0311005.

[27] U. W. Heinz, *Thermalization at RHIC*, AIP Conf. Proc. **739**, 163–180 (2005), nucl-th/0407067.

[28] J. Berges and K. Rajagopal, *Color superconductivity and chiral symmetry restoration at nonzero baryon density and temperature*, Nucl. Phys. **B538**, 215–232 (1999), hep-ph/9804233.

[29] L. Dolan and R. Jackiw, *Symmetry behavior at finite temperature*, Phys. Rev. **D9**, 3320–3341 (1974).

[30] I. Montvay and G. Munster, *Quantum fields on a lattice*, Cambridge, UK: Univ. Pr. (1994) 491 p. (Cambridge monographs on mathematical physics).

[31] W. Greiner, S. Schramm, and E. Stein, *Quantum chromodynamics*, Berlin, Germany: Springer (2002) 551 p.

[32] K. G. Wilson, *Confinement of quarks*, Phys. Rev. **D10**, 2445–2459 (1974).

[33] F. Karsch and E. Laermann, *Thermodynamics and in-medium hadron properties from lattice QCD*, hep-lat/0305025.

[34] Y. Shamir, *Lattice Chiral Fermions*, Nucl. Phys. Proc. Suppl. **47**, 212–227 (1996), hep-lat/9509023.

[35] J. S. Schwinger, *On the Green's functions of quantized fields. 1*, Proc. Nat. Acad. Sci. **37**, 452–455 (1951).

[36] F. J. Dyson, *The S matrix in quantum electrodynamics*, Phys. Rev. **75**, 1736–1755 (1949).

[37] J. Zinn-Justin, *Quantum field theory and critical phenomena*, Int. Ser. Monogr. Phys. **113**, 1–1054 (2002).

[38] H. Terao, *ERG and Schwinger-Dyson equations: Comparison in formulations and applications*, Int. J. Mod. Phys. **A16**, 1913–1926 (2001), hep-ph/0101107.

[39] R. Alkofer and L. von Smekal, *The infrared behavior of QCD Green's functions: Confinement, dynamical symmetry breaking, and hadrons as relativistic bound states*, Phys. Rept. **353**, 281 (2001), hep-ph/0007355.

[40] A. Maas, J. Wambach, B. Gruter, and R. Alkofer, *High-temperature limit of Landau-gauge Yang-Mills theory*, Eur. Phys. J. **C37**, 335–357 (2004), hep-ph/0408074.

[41] A. Maas, J. Wambach, and R. Alkofer, *The high-temperature phase of Landau-gauge Yang-Mills theory*, Eur. Phys. J. **C42**, 93–107 (2005), hep-ph/0504019.

[42] A. Maas, *Gluons at finite temperature in Landau gauge Yang-Mills theory*, Mod. Phys. Lett. **A20**, 1797–1811 (2005), hep-ph/0506066.

[43] C. S. Fischer, *Infrared properties of QCD from Dyson-Schwinger equations*, J. Phys. **G32**, R253–R291 (2006), hep-ph/0605173.

[44] P. M. Stevenson, *Optimized perturbation theory*, Phys. Rev. **D23**, 2916 (1981).

[45] S. Pokorski, *Gauge field theories*, Cambridge, Uk: Univ. Pr. (1987) 394 P. (Cambridge Monographs On Mathematical Physics).

[46] K. G. Wilson and J. B. Kogut, *The Renormalization group and the epsilon expansion*, Phys. Rept. **12**, 75–200 (1974).

[47] F. J. Wegner and A. Houghton, *Renormalization group equation for critical phenomena*, Phys. Rev. **A8**, 401–412 (1973).

[48] J. Polchinski, *Renormalization and effective Lagrangians*, Nucl. Phys. **B231**, 269–295 (1984).

[49] T. R. Morris, *The Exact renormalization group and approximate solutions*, Int. J. Mod. Phys. **A9**, 2411–2450 (1994), hep-ph/9308265.

[50] C. Wetterich, *Exact evolution equation for the effective potential*, Phys. Lett. **B301**, 90–94 (1993).

[51] S.-B. Liao, *On connection between momentum cutoff and the proper time regularizations*, Phys. Rev. **D53**, 2020–2036 (1996), hep-th/9501124.

[52] U. Ellwanger, M. Hirsch, and A. Weber, *The heavy quark potential from Wilson's exact renormalization group*, Eur. Phys. J. **C1**, 563–578 (1998), hep-ph/9606468.

[53] L. F. Abbott, *Introduction to the background field method*, Acta Phys. Polon. **B13**, 33 (1982).

[54] M. E. Peskin and D. V. Schroeder, *An Introduction to quantum field theory*, Reading, USA: Addison-Wesley (1995) 842 p.

[55] U. Ellwanger, M. Hirsch, and A. Weber, *Flow equations for the relevant part of the pure Yang-Mills action*, Z. Phys. **C69**, 687–698 (1996), hep-th/9506019.

[56] M. Bonini, M. D'Attanasio, and G. Marchesini, *BRS symmetry for Yang-Mills theory with exact renormalization group*, Nucl. Phys. **B437**, 163–186 (1995), hep-th/9410138.

[57] T. R. Morris, *A gauge invariant exact renormalization group. II*, JHEP **12**, 012 (2000), hep-th/0006064.

[58] S. Arnone, T. R. Morris, and O. J. Rosten, *A generalised manifestly gauge invariant exact renormalisation group for SU(N) Yang-Mills*, hep-th/0507154.

[59] D. U. Jungnickel and C. Wetterich, *Effective action for the chiral quark-meson model*, Phys. Rev. **D53**, 5142–5175 (1996), hep-ph/9505267.

[60] H. Gies and C. Wetterich, *Renormalization flow of bound states*, Phys. Rev. **D65**, 065001 (2002), hep-th/0107221.

[61] H. Gies and C. Wetterich, *Universality of spontaneous chiral symmetry breaking in gauge theories*, Phys. Rev. **D69**, 025001 (2004), hep-th/0209183.

[62] H. Gies and C. Wetterich, *Renormalization flow from UV to IR degrees of freedom*, Acta Phys. Slov. **52**, 215–220 (2002), hep-ph/0205226.

[63] J. M. Pawlowski, *Aspects of the functional renormalisation group*, hep-th/0512261.

[64] D. F. Litim and J. M. Pawlowski, *Completeness and consistency of renormalisation group flows*, Phys. Rev. **D66**, 025030 (2002), hep-th/0202188.

[65] L. F. Abbott, *The background field method beyond one loop*, Nucl. Phys. **B185**, 189 (1981).

[66] D. F. Litim and J. M. Pawlowski, *Wilsonian flows and background fields*, Phys. Lett. **B546**, 279–286 (2002), hep-th/0208216.

[67] D. F. Litim and J. M. Pawlowski, *Renormalisation group flows for gauge theories in axial gauges*, JHEP **09**, 049 (2002), hep-th/0203005.

[68] D. F. Litim and J. M. Pawlowski, *Flow equations for Yang-Mills theories in general axial gauges*, Phys. Lett. **B435**, 181–188 (1998), hep-th/9802064.

[69] D. F. Litim and J. M. Pawlowski, *On gauge invariant Wilsonian flows*, hep-th/9901063.

[70] F. Freire, D. F. Litim, and J. M. Pawlowski, *Gauge invariance and background field formalism in the exact renormalisation group*, Phys. Lett. **B495**, 256–262 (2000), hep-th/0009110.

[71] H. Gies, *Running coupling in Yang-Mills theory: A flow equation study*, Phys. Rev. **D66**, 025006 (2002), hep-th/0202207.

[72] M. Reuter and C. Wetterich, *Effective average action for gauge theories and exact evolution equations*, Nucl. Phys. **B417**, 181–214 (1994).

[73] H. Gies and J. Jaeckel, *Renormalization flow of QED*, Phys. Rev. Lett. **93**, 110405 (2004), hep-ph/0405183.

[74] M. Reuter and C. Wetterich, *Gluon condensation in nonperturbative flow equations*, Phys. Rev. **D56**, 7893–7916 (1997), hep-th/9708051.

[75] J. Braun, H. Gies, and H. J. Pirner, *RG flow of the Polyakov-loop potential: First status report*, AIP Conf. Proc. **775**, 162–172 (2005).

[76] J. Braun and H. Gies, *Running coupling at finite temperature and chiral symmetry restoration in QCD*, hep-ph/0512085.

[77] J. Braun and H. Gies, *Chiral phase boundary of QCD at finite temperature*, JHEP **06**, 024 (2006), hep-ph/0602226.

[78] B.-J. Schaefer and H.-J. Pirner, *The equation of state of quarks and mesons in a renormalization group flow picture*, Nucl. Phys. **A660**, 439–474 (1999), nucl-th/9903003.

[79] O. Bohr, B. J. Schaefer, and J. Wambach, *Renormalization group flow equations and the phase transition in O(N) models*, Int. J. Mod. Phys. **A16**, 3823–3852 (2001), hep-ph/0007098.

[80] J. Meyer, K. Schwenzer, H.-J. Pirner, and A. Deandrea, *Renormalization group flow in large N(c)*, Phys. Lett. **B526**, 79–89 (2002), hep-ph/0110279.

[81] B.-J. Schaefer and J. Wambach, *The phase diagram of the quark meson model*, Nucl. Phys. **A757**, 479–492 (2005), nucl-th/0403039.

[82] J. Braun, K. Schwenzer, and H.-J. Pirner, *Linking the quark meson model with QCD at high temperature*, Phys. Rev. **D70**, 085016 (2004), hep-ph/0312277.

[83] A. Bonanno and M. Reuter, *Proper time flow equation for gravity*, JHEP **02**, 035 (2005), hep-th/0410191.

[84] J. Braun, B. Klein, and H. J. Pirner, *Volume dependence of the pion mass in the quark-meson model*, Phys. Rev. **D71**, 014032 (2005), hep-ph/0408116.

[85] J. Braun, B. Klein, and H. J. Pirner, *Influence of quark boundary conditions on the pion mass in finite volume*, Phys. Rev. **D72**, 034017 (2005), hep-ph/0504127.

[86] J. Braun, B. Klein, H. J. Pirner, and A. H. Rezaeian, *Volume and quark mass dependence of the chiral phase transition*, Phys. Rev. **D73**, 074010 (2006), hep-ph/0512274.

[87] D. F. Litim and J. M. Pawlowski, *Predictive power of renormalisation group flows: A comparison*, Phys. Lett. **B516**, 197–207 (2001), hep-th/0107020.

[88] D. F. Litim, *Optimised renormalisation group flows*, Phys. Rev. **D64**, 105007 (2001), hep-th/0103195.

[89] D. F. Litim, *Optimisation of the exact renormalisation group*, Phys. Lett. **B486**, 92–99 (2000), hep-th/0005245.

[90] D. Becirevic and G. Villadoro, *Impact of the finite volume effects on the chiral behavior of f(K) and B(K)*, Phys. Rev. **D69**, 054010 (2004), hep-lat/0311028.

[91] A. Ali Khan et al., *The nucleon mass in N(f) = 2 lattice QCD: Finite size effects from chiral perturbation theory*, Nucl. Phys. **B689**, 175–194 (2004), hep-lat/0312030.

[92] M. Guagnelli et al., *Finite size effects of a pion matrix element*, Phys. Lett. **B597**, 216–221 (2004), hep-lat/0403009.

[93] D. Arndt and C. J. D. Lin, *Heavy meson chiral perturbation theory in finite volume*, Phys. Rev. **D70**, 014503 (2004), hep-lat/0403012.

[94] M. Procura, T. R. Hemmert, and W. Weise, *Nucleon mass, sigma term and lattice QCD*, Phys. Rev. **D69**, 034505 (2004), hep-lat/0309020.

[95] S. R. Beane and M. J. Savage, *Baryon axial charge in a finite volume*, Phys. Rev. **D70**, 074029 (2004), hep-ph/0404131.

[96] M. E. Berbenni-Bitsch et al., *Random-matrix universality in the small-eigenvalue spectrum of the lattice Dirac operator*, Nucl. Phys. Proc. Suppl. **63**, 820–822 (1998), hep-lat/9709102.

[97] G. Colangelo and C. Haefeli, *An asymptotic formula for the pion decay constant in a large volume*, Phys. Lett. **B590**, 258–264 (2004), hep-lat/0403025.

[98] G. Colangelo and S. Dürr, *The pion mass in finite volume*, Eur. Phys. J. **C33**, 543–553 (2004), hep-lat/0311023.

[99] J. Gasser and H. Leutwyler, *Light quarks at low temperatures*, Phys. Lett. **B184**, 83 (1987).

[100] J. Gasser and H. Leutwyler, *Thermodynamics of chiral symmetry*, Phys. Lett. **B188**, 477 (1987).

[101] J. Gasser and H. Leutwyler, *Spontaneously broken symmetries: effective Lagrangians at finite volume*, Nucl. Phys. **B307**, 763 (1988).

[102] H. Leutwyler and A. Smilga, *Spectrum of Dirac operator and role of winding number in QCD*, Phys. Rev. **D46**, 5607–5632 (1992).

[103] V. Bernard, T. R. Hemmert, and U.-G. Meissner, *Cutoff schemes in chiral perturbation theory and the quark mass expansion of the nucleon mass*, Nucl. Phys. **A732**, 149–170 (2004), hep-ph/0307115.

[104] V. Bernard, T. R. Hemmert, and U.-G. Meissner, *Chiral extrapolations and the covariant small scale expansion*, Phys. Lett. **B622**, 141–150 (2005), hep-lat/0503022.

[105] G. Colangelo, S. Dürr, and C. Haefeli, *Finite volume effects for meson masses and decay constants*, hep-lat/0503014.

[106] P. F. Bedaque, H. W. Griesshammer, and G. Rupak, *A nucleon in a tiny box*, hep-lat/0407009.

[107] D. B. Leinweber, D. H. Lu, and A. W. Thomas, *Nucleon magnetic moments beyond the perturbative chiral regime*, Phys. Rev. **D60**, 034014 (1999), hep-lat/9810005.

[108] W. Detmold, W. Melnitchouk, J. W. Negele, D. B. Renner, and A. W. Thomas, *Chiral extrapolation of lattice moments of proton quark distributions*, Phys. Rev. Lett. **87**, 172001 (2001), hep-lat/0103006.

[109] S. Aoki et al., *Light hadron spectroscopy with two flavors of O(a)-improved dynamical quarks*, Phys. Rev. **D68**, 054502 (2003), hep-lat/0212039.

[110] B. Orth, T. Lippert, and K. Schilling, *Finite-size effects in lattice QCD with dynamical Wilson fermions*, hep-lat/0503016.

[111] A. Ali Khan et al., *Light hadron spectroscopy with two flavors of dynamical quarks on the lattice*, Phys. Rev. **D65**, 054505 (2002), hep-lat/0105015.

[112] L. Jendges, B. Klein, H. J. Pirner, and K. Schwenzer, *Chiral expansion from renormalization group flow equations*, hep-ph/0608056.

[113] D. U. Jungnickel and C. Wetterich, *The linear meson model and chiral perturbation theory*, Eur. Phys. J. **C2**, 557–567 (1998), hep-ph/9704345.

[114] N. Goldenfeld, *Lectures on phase transitions and the renormalization group*, Reading, USA: Addison-Wesley (1992) 394 p. (Frontiers in physics, 85).

[115] Z. Fodor and S. D. Katz, *Critical point of QCD at finite T and mu, lattice results for physical quark masses*, JHEP **04**, 050 (2004), hep-lat/0402006.

[116] C. R. Allton et al., *The QCD thermal phase transition in the presence of a small chemical potential*, Phys. Rev. **D66**, 074507 (2002), hep-lat/0204010.

[117] O. Philipsen, *The QCD phase diagram at zero and small baryon density*, hep-lat/0510077.

[118] P. de Forcrand and O. Philipsen, *The QCD phase diagram for three degenerate flavors and small baryon density*, Nucl. Phys. **B673**, 170–186 (2003), hep-lat/0307020.

[119] C. R. Allton et al., *Thermodynamics of two flavor QCD to sixth order in quark chemical potential*, Phys. Rev. **D71**, 054508 (2005), hep-lat/0501030.

[120] R. D. Pisarski and F. Wilczek, *Remarks on the chiral phase transition in chromodynamics*, Phys. Rev. **D29**, 338–341 (1984).

[121] S. A. Gottlieb et al., *Thermodynamics of lattice QCD with two light quark flavours on a 16**3 x 8 lattice. II*, Phys. Rev. **D55**, 6852–6860 (1997), hep-lat/9612020.

[122] C. Bernard et al., *QCD thermodynamics with three flavors of improved staggered quarks*, Phys. Rev. **D71**, 034504 (2005), hep-lat/0405029.

[123] J. Berges, D. U. Jungnickel, and C. Wetterich, *Two flavor chiral phase transition from nonperturbative flow equations*, Phys. Rev. **D59**, 034010 (1999), hep-ph/9705474.

[124] A. Dumitru, D. Roder, and J. Ruppert, *The quark-mass dependence of T(c) in QCD: Working up from m = 0 or down from m = infinity?*, Phys. Rev. **D70**, 074001 (2004), hep-ph/0311119.

[125] M. Lüscher, *Volume dependence of the energy spectrum in massive quantum field theories. 1. stable particle states*, Commun. Math. Phys. **104**, 177 (1986).

[126] S. Aoki et al., *Finite size effects of hadron masses in lattice QCD: A Comparative study for quenched and full QCD simulations*, Phys. Rev. **D50**, 486–494 (1994).

[127] S. Aoki et al., *Finite size effect of hadron masses with Kogut-Susskind quarks*, Nucl. Phys. Proc. Suppl. **34**, 363–365 (1994), hep-lat/9311049.

[128] S. R. Sharpe, *Quenched chiral logarithms*, Phys. Rev. **D46**, 3146–3168 (1992), hep-lat/9205020.

[129] C. W. Bernard and M. F. L. Golterman, *Chiral perturbation theory for the quenched approximation of QCD*, Phys. Rev. **D46**, 853–857 (1992), hep-lat/9204007.

[130] Y. Nambu and G. Jona-Lasinio, *Dynamical model of elementary particles based on an analogy with superconductivity. I*, Phys. Rev. **122**, 345–358 (1961).

[131] T. Kugo, *Eichtheorie (in German)*, Berlin, Heidelberg: Springer (1997).

[132] G. Papp, B. J. Schaefer, H. J. Pirner, and J. Wambach, *On the convergence of the expansion of renormalization group flow equation*, Phys. Rev. **D61**, 096002 (2000), hep-ph/9909246.

[133] J. D. Walecka, *Theoretical nuclear and subnuclear physics*, Oxford Stud. Nucl. Phys. **16**, 1–610 (1995).

[134] J. Braun, *Dynamics of the linear σ-model at finite temperature, density and volume*, Diploma thesis (in German), University of Heidelberg (2004).

[135] C. R. Allton et al., *Effects of non-perturbatively improved dynamical fermions in QCD at fixed lattice spacing*, Phys. Rev. **D65**, 054502 (2002), hep-lat/0107021.

[136] C. Aubin et al., *Light pseudoscalar decay constants, quark masses, and low energy constants from three-flavor lattice QCD*, Phys. Rev. **D70**, 114501 (2004), hep-lat/0407028.

[137] Y. Aoki et al., *Domain wall fermions with improved gauge actions*, Phys. Rev. **D69**, 074504 (2004), hep-lat/0211023.

[138] Y. Aoki et al., *Lattice QCD with two dynamical flavors of domain wall fermions*, hep-lat/0411006.

[139] M. Fukugita, H. Mino, M. Okawa, G. Parisi, and A. Ukawa, *Origin of the finite size effect for the QCD hadron masses*, Nucl. Phys. Proc. Suppl. **30**, 365–368 (1993).

[140] S. P. Klevansky, *The Nambu-Jona-Lasinio model of quantum chromodynamics*, Rev. Mod. Phys. **64**, 649–708 (1992).

[141] A. Ali Khan et al., *Phase structure and critical temperature of two flavor QCD with renormalization group improved gauge action and clover improved Wilson quark action*, Phys. Rev. **D63**, 034502 (2001), hep-lat/0008011.

[142] V. G. Bornyakov et al., *Critical temperature in QCD with two flavors of dynamical quarks*, Proc. Sci. **LAT2005**, 157 (2005), hep-lat/0509122.

[143] D. F. Litim and J. M. Pawlowski, *Non-perturbative thermal flows and resummations*, hep-th/0609122.

[144] J.-P. Blaizot, A. Ipp, R. Mendez-Galain, and N. Wschebor, *Perturbation theory and non-perturbative renormalization flow in scalar field theory at finite temperature*, hep-ph/0610004.

[145] F. Karsch and E. Laermann, *Susceptibilities, the specific heat and a cumulant in two flavor QCD*, Phys. Rev. **D50**, 6954–6962 (1994), hep-lat/9406008.

[146] S. Aoki et al., *Scaling study of the two-flavor chiral phase transition with the Kogut-Susskind quark action in lattice QCD*, Phys. Rev. **D57**, 3910–3922 (1998), hep-lat/9710048.

[147] C. W. Bernard et al., *Scaling tests of the improved Kogut-Susskind quark action*, Phys. Rev. **D61**, 111502 (2000), hep-lat/9912018.

[148] K. Fukushima, *Chiral effective model with the Polyakov loop*, Phys. Lett. **B591**, 277–284 (2004), hep-ph/0310121.

[149] P. N. Meisinger and M. C. Ogilvie, *Chiral Symmetry Restoration and Z_N Symmetry*, Phys. Lett. **B379**, 163–168 (1996), hep-lat/9512011.

[150] C. Ratti and W. Weise, *Thermodynamics of two-colour QCD and the Nambu Jona-Lasinio model*, Phys. Rev. **D70**, 054013 (2004), hep-ph/0406159.

[151] Y. Iwasaki, K. Kanaya, S. Sakai, and T. Yoshie, *Quark confinement and number of flavors in strong coupling lattice QCD*, Phys. Rev. Lett. **69**, 21–24 (1992).

[152] T. Banks and A. Zaks, *On the phase structure of vector - like gauge theories with massless fermions*, Nucl. Phys. **B196**, 189 (1982).

[153] T. Appelquist, J. Terning, and L. C. R. Wijewardhana, *The Zero Temperature Chiral Phase Transition in SU(N) Gauge Theories*, Phys. Rev. Lett. **77**, 1214–1217 (1996), hep-ph/9602385.

[154] V. A. Miransky and K. Yamawaki, *Conformal phase transition in gauge theories*, Phys. Rev. **D55**, 5051–5066 (1997), hep-th/9611142.

[155] T. Schafer and E. V. Shuryak, *Instantons in QCD*, Rev. Mod. Phys. **70**, 323–426 (1998), hep-ph/9610451.

[156] H. Gies and J. Jaeckel, *Chiral phase structure of QCD with many flavors*, Eur. Phys. J. **C46**, 433–438 (2006), hep-ph/0507171.

[157] E. Shuryak, *Why does the quark gluon plasma at RHIC behave as a nearly ideal fluid?*, Prog. Part. Nucl. Phys. **53**, 273–303 (2004), hep-ph/0312227.

[158] E. V. Shuryak, *Theory of hadronic plasma*, Sov. Phys. JETP **47**, 212–219 (1978).

[159] J. I. Kapusta, *Quantum chromodynamics at high temperature*, Nucl. Phys. **B148**, 461–498 (1979).

[160] P. Arnold and C.-X. Zhai, *The Three loop free energy for pure gauge QCD*, Phys. Rev. **D50**, 7603–7623 (1994), hep-ph/9408276.

[161] A. D. Linde, *Infrared problem in thermodynamics of the Yang-Mills gas*, Phys. Lett. **B96**, 289 (1980).

[162] E. Braaten and R. D. Pisarski, *Simple effective Lagrangian for hard thermal loops*, Phys. Rev. **D45**, 1827–1830 (1992).

[163] M. Laine, *What is the simplest effective approach to hot QCD thermodynamics?*, hep-ph/0301011.

[164] M. Bonini, M. D'Attanasio, and G. Marchesini, *Perturbative renormalization and infrared finiteness in the Wilson renormalization group: The Massless scalar case*, Nucl. Phys. **B409**, 441–464 (1993), hep-th/9301114.

[165] V. N. Gribov, *Quantization of non-Abelian gauge theories*, Nucl. Phys. **B139**, 1 (1978).

[166] J. M. Pawlowski, *On Wilsonian flows in gauge theories*, Int. J. Mod. Phys. **A16**, 2105–2110 (2001).

[167] M. D'Attanasio and M. Pietroni, *Gauge-invariant renormalization group at finite temperature*, Nucl. Phys. **B498**, 443–466 (1997), hep-th/9611038.

[168] G. V. Dunne and T. M. Hall, *Borel summation of the derivative expansion and effective actions*, Phys. Rev. **D60**, 065002 (1999), hep-th/9902064.

[169] N. K. Nielsen and P. Olesen, *An unstable Yang-Mills mode*, Nucl. Phys. **B144**, 376 (1978).

[170] W. Dittrich and V. Schanbacher, *Effective QCD Lagrangian at finite temperature*, Phys. Lett. **B100**, 415 (1981).

[171] H. Gies, *Renormalizability of gauge theories in extra dimensions*, Phys. Rev. **D68**, 085015 (2003), hep-th/0305208.

[172] L. von Smekal, R. Alkofer, and A. Hauck, *The infrared behavior of gluon and ghost propagators in Landau gauge QCD*, Phys. Rev. Lett. **79**, 3591–3594 (1997), hep-ph/9705242.

[173] D. Atkinson and J. C. R. Bloch, *QCD in the infrared with exact angular integrations*, Mod. Phys. Lett. **A13**, 1055–1062 (1998), hep-ph/9802239.

[174] C. Lerche and L. von Smekal, *On the infrared exponent for gluon and ghost propagation in Landau gauge QCD*, Phys. Rev. **D65**, 125006 (2002), hep-ph/0202194.

[175] C. S. Fischer and R. Alkofer, *Infrared exponents and running coupling of SU(N) Yang-Mills theories*, Phys. Lett. **B536**, 177–184 (2002), hep-ph/0202202.

[176] J. M. Pawlowski, D. F. Litim, S. Nedelko, and L. von Smekal, *Infrared behaviour and fixed points in Landau gauge QCD*, Phys. Rev. Lett. **93**, 152002 (2004), hep-th/0312324.

[177] C. S. Fischer and H. Gies, *Renormalization flow of Yang-Mills propagators*, JHEP **10**, 048 (2004), hep-ph/0408089.

[178] R. Alkofer, C. S. Fischer, and F. J. Llanes-Estrada, *Vertex functions and infrared fixed point in Landau gauge SU(N) Yang-Mills theory*, Phys. Lett. **B611**, 279–288 (2005), hep-th/0412330.

[179] T. Kugo and I. Ojima, *Local covariant operator formalism of nonabelian gauge theories and quark confinement problem*, Prog. Theor. Phys. Suppl. **66**, 1 (1979).

[180] D. Zwanziger, *Non-perturbative Faddeev-Popov formula and infrared limit of QCD*, Phys. Rev. **D69**, 016002 (2004), hep-ph/0303028.

[181] J. C. Taylor, *Ward identities and charge renormalization of the Yang-Mills field*, Nucl. Phys. **B33**, 436–444 (1971).

[182] Y. L. Dokshitzer, A. Lucenti, G. Marchesini, and G. P. Salam, *On the universality of the Milan factor for 1/Q power corrections to jet shapes*, JHEP **05**, 003 (1998), hep-ph/9802381.

[183] E. Eichten et al., *The spectrum of charmonium*, Phys. Rev. Lett. **34**, 369–372 (1975).

[184] G. Grunberg, *Fixing the conformal window in QCD*, Phys. Rev. **D65**, 021701 (2002), hep-ph/0009272.

[185] D. V. Shirkov and I. L. Solovtsov, *Analytic model for the QCD running coupling with universal alpha(s)-bar(0) value*, Phys. Rev. Lett. **79**, 1209–1212 (1997), hep-ph/9704333.

[186] S. J. Brodsky, S. Menke, C. Merino, and J. Rathsman, *On the behavior of the effective QCD coupling alpha(tau)(s) at low scales*, Phys. Rev. **D67**, 055008 (2003), hep-ph/0212078.

[187] A. Deur, V. Burkert, J. P. Chen, and W. Korsch, *Experimental determination of the effective strong coupling constant*, hep-ph/0509113.

[188] J. Jaeckel and C. Wetterich, *Flow equations without mean field ambiguity*, Phys. Rev. **D68**, 025020 (2003), hep-ph/0207094.

[189] J. Jaeckel, *Effective actions for strongly interacting fermionic systems*, hep-ph/0309090.

[190] K.-I. Aoki, K. Morikawa, J.-I. Sumi, H. Terao, and M. Tomoyose, *Analysis of the Wilsonian effective potentials in dynamical chiral symmetry breaking*, Phys. Rev. **D61**, 045008 (2000), hep-th/9908043.

[191] H. Gies, J. Jaeckel, and C. Wetterich, *Towards a renormalizable standard model without fundamental Higgs scalar*, Phys. Rev. **D69**, 105008 (2004), hep-ph/0312034.

[192] V. A. Miransky, *Dynamics of spontaneous chiral symmetry breaking and continuum limit in quantum electrodynamics*, Nuovo Cim. **A90**, 149–170 (1985).

[193] P. J. Silva and O. Oliveira, *On the infrared gluon propagator*, hep-lat/0511043.

[194] E. M. Ilgenfritz, M. Muller-Preussker, A. Sternbeck, and A. Schiller, *Gauge-variant propagators and the running coupling from lattice QCD*, hep-lat/0601027.

[195] A. Cucchieri, *Infrared behavior of the gluon propagator in lattice Landau gauge*, Phys. Lett. **B422**, 233–237 (1998), hep-lat/9709015.

[196] F. D. R. Bonnet, P. O. Bowman, D. B. Leinweber, A. G. Williams, and J. M. Zanotti, *Infinite volume and continuum limits of the Landau-gauge gluon propagator*, Phys. Rev. **D64**, 034501 (2001), hep-lat/0101013.

[197] I. L. Bogolubsky, G. Burgio, M. Muller-Preussker, and V. K. Mitrjushkin, *Landau gauge ghost and gluon propagators in SU(2) lattice gauge theory: Gribov ambiguity revisited*, hep-lat/0511056.

[198] D. F. Litim, *Universality and the renormalisation group*, JHEP **07**, 005 (2005), hep-th/0503096.

[199] J. Braun, H. Gies, and J. M. Pawlowski, (forthcoming).

[200] J. Braun and B. Klein, (forthcoming).

[201] J. Braun and H.-J. Pirner, (forthcoming).

[202] J. Braun, H. Gies, and J. M. Pawlowski, (forthcoming).

[203] G. I. S. and R. I. M., *Table of integrals, series, and products*, 6th ed., Jeffrey, Alan (ed.), Academic Press, San Diego (2000).

[204] J. C. Le Guillou (editor) and J. Zinn-Justin (editor), *Large order behavior of perturbation theory*, Amsterdam, Netherlands: North-Holland (1990) 580 p. (Current physics - sources and comments.

Thank you very much!

First of all, I would like to thank my supervisor Prof. Dr. Hans-Jürgen Pirner for giving me the opportunity to become a doctoral student in his group. I am very thankful for uncountable illuminating discussions with him and his strong support throughout my diploma and doctoral studies. Moreover, I am much obliged to him for encouraging me to visit the New York state university (Stony Brook) in spring 2006.

I am deeply grateful to my second supervisor Dr. habil. Holger Gies for collaboration, for being such a great teacher, for his ongoing optimism and for encouraging me throughout my doctoral studies. Moreover, I would like to thank him for providing me the opportunity to participate in the ERG conference on Lefkada.

Special thanks go to Dr. Bertram Klein for a very careful proofreading of this thesis and for many suggestions and for uncountable discussions. Moreover, I am grateful for the collaboration on finite-volume effects in QCD. I would like to thank him also for organizing dinners in the evening.

I appreciate many discussions and collaboration with Dr. habil. Jan Pawlowski.

It is a pleasure for me to thank Dr. Achim Schwenk for the opportunities he has offered to me.

I would like to thank Prof. Dr. Bengt Friman for his interest in my work and for supporting my participation in the school on "Renormalization Group and Effective Field Theory Approaches to Many-Body Systems" in Trento.

Thanks go to Daniel Grünewald for his help on computer problems.

I would like to thank the *Gesselschaft für Schwerionenforschung* (GSI) Darmstadt for financial support during my doctoral studies. Furhermore, I acknowledge financial support from the Deutsche Forschungsgemeinschaft (DFG) for participations in conferences.

I am deeply grateful to Sabrina Lohner for all the wonderful moments with her, for supporting me and believing in me and especially for her love.

Last but not least, I would like to thank my parents for supporting me all the time. Without their support my studies in physics would have never been possible!